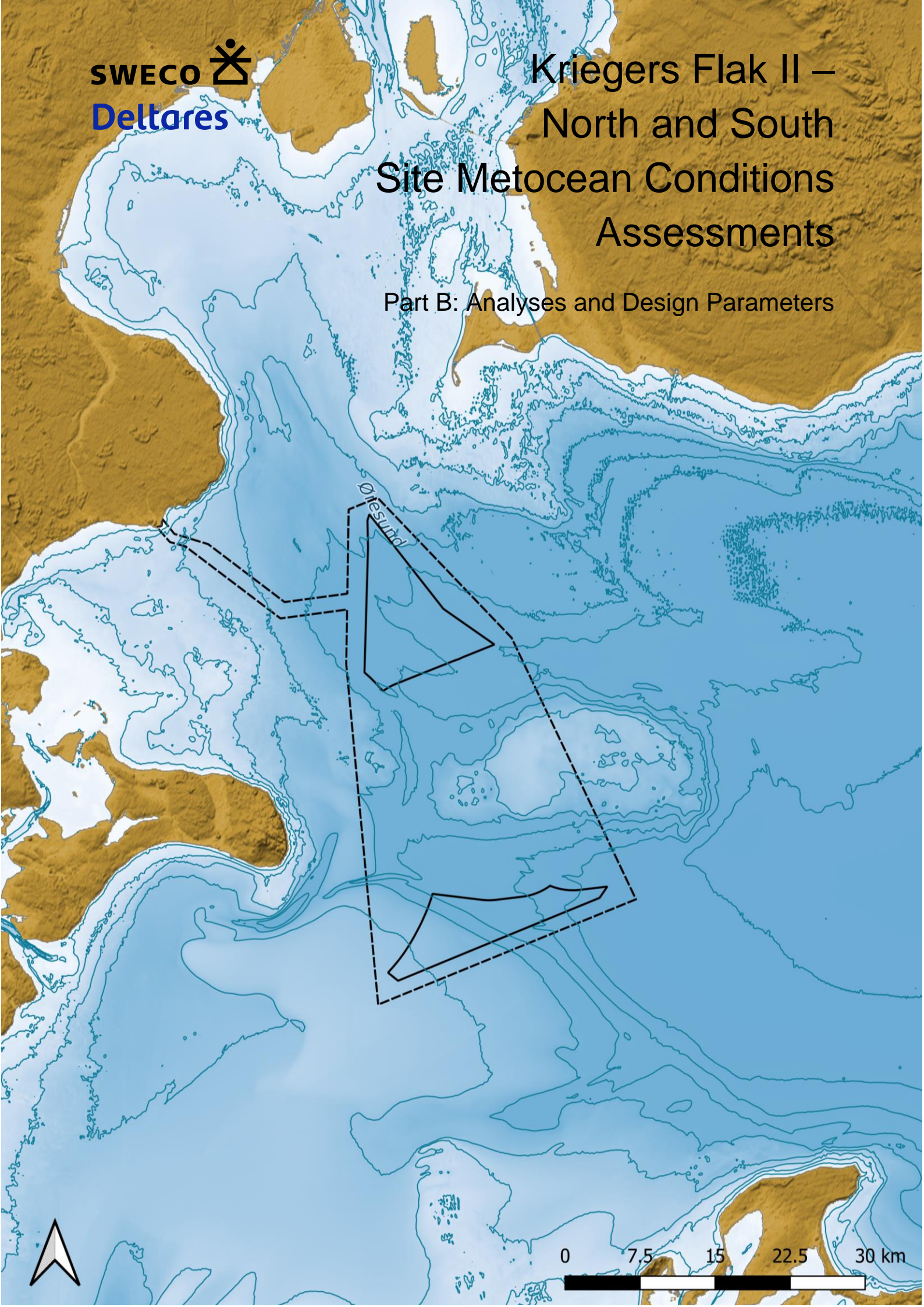


# Kriegers Flak II – North and South Site Metocean Conditions Assessments

Part B: Analyses and Design Parameters



---

## Change list

Ver	Date	Description of the change	Author	Reviewed	Approved by
0	2024-07-12	New Document	Magnus Maribo	Per Kofoed Rasmussen	Anders Helkjær
1	2024-08-30	Update with HD data	Magnus Maribo	Per Kofoed Rasmussen	Anders Helkjær
2	2024-10-15	Updated with clients comments	Magnus Maribo	Per Kofoed Rasmussen	Anders Helkjær

**Project Name** Site MetOcean Conditions Assessment  
**Project Manager** Anders Helkjær, [anders.helkjaer@sweco.dk](mailto:anders.helkjaer@sweco.dk), +4527233341  
**Client** Energinet Eltransmission A/S  
**Author** Magnus Maribo Vinter  
**Controlled by** Per Kofoed Rasmussen  
**Approved by** Anders Helkjær  
**Date** 2024-10-15  
**Ver** 2  
**Document number** 41011329B  
**Document reference** 41011329B\_KFII\_PartB\_Analyses\_and\_Design\_Parameters

# Table of contents

1	Summary .....	14
2	Introduction .....	16
3	Data basis .....	18
3.1	Reference Locations .....	18
3.2	Historical extreme events .....	19
3.2.1	Storm frequency in Denmark .....	20
3.2.2	Assessment of the 45-year hindcast period .....	21
3.2.3	Very extreme historical events .....	22
3.2.4	Easterly storms .....	22
3.2.5	Extreme events 1979-2023 .....	23
3.2.6	Conclusion .....	23
4	Wind Conditions .....	25
4.1	Normal wind conditions .....	25
4.1.1	Wind speed at reference height .....	26
4.1.2	Wind speed at hub height .....	29
5	Water levels .....	33
5.1	Normal water level conditions .....	33
5.1.1	Timeseries .....	33
5.1.2	Tidal levels .....	34
5.1.3	Histogram .....	35
5.1.4	Monthly statistics .....	36
5.2	Extreme water level conditions .....	36
5.2.1	Extreme high-water levels .....	37
5.2.2	Extreme residual high-water levels .....	38
5.2.3	Extreme low-water levels .....	38
5.2.4	Extreme residual low-water levels .....	39
5.2.5	Maps of Extreme high-water levels .....	40
5.2.6	Maps of Extreme low-water levels .....	43
6	Current conditions .....	47
6.1	Normal current conditions .....	47
6.1.1	Timeseries .....	48
6.1.2	Current roses .....	49
6.1.3	Histogram .....	51
6.1.4	Monthly statistics .....	52
6.1.5	Directional statistics .....	54
6.1.6	Vertical profiles of current speed, temperature, and salinity .....	55
6.1.7	Maps of $C_s$ .....	57
6.2	Extreme current conditions unscaled .....	64
6.2.1	Extreme total current speed at near surface .....	64
6.2.2	Extreme total current speed at mid-depth .....	68
6.2.3	Extreme total current speed at near bed .....	71
6.2.4	Maps of extreme current speed at 3 levels .....	75
6.3	Extreme current conditions scaled .....	82
7	Wave conditions .....	84
7.1	Normal wave conditions .....	84
7.1.1	Timeseries .....	85

7.1.2	Wave roses .....	87
7.1.3	Histogram .....	90
7.1.4	Monthly statistics .....	91
7.1.5	Directional statistics .....	92
7.1.6	Correlation between wave height and period ...	93
7.1.7	Maps of $H_{m0}$ .....	93
7.2	Extreme wave conditions unscaled .....	95
7.2.1	Extreme $H_{m0}$ .....	96
7.2.2	Extreme $H_{max}$ .....	103
7.2.3	Extreme $C_{max}$ .....	106
7.3	Extreme wave conditions scaled .....	107
7.4	Wave Spectrum .....	107
7.4.1	Directional Spreading .....	108
8	Scatter Distributions .....	111
8.1.1	Wind-wave misalignment .....	111
8.1.2	Scatter distribution of wave height and water level .....	113
9	Reference Sea States .....	116
9.1	Normal Sea State .....	116
9.2	Severe sea state .....	117
9.3	Extreme sea state .....	121
10	Other atmospheric and oceanographic conditions .....	122
10.1	Air temperature, pressure, humidity, and solar radiation	122
10.2	Lightning .....	126
10.3	Salinity, seawater temperature and density .....	127
10.3.1	Salinity .....	127
10.3.2	Seawater temperature .....	130
10.3.3	Density .....	133
10.4	Marine growth .....	136
11	Bibliography .....	139
	Appendix A .....	141
	Appendix B .....	142

## List of Figures

Figure 2-1 Overview of the windfarm area Kriegers Flak II. The dashed line indicates the full data delivery area, and the hatched areas indicate the OWFs. ....	16
Figure 3-1 Overview of the reference locations within each OWF. The dashed line indicates the full data delivery area, and the full line indicate the OWFs. Contour lines are seabed levels in metres below MSL. ....	19
Figure 3-2 Observed Class 2, 3 and 4 storms in Denmark, 1891 – 2021 (130 years), from [3]. ....	21
Figure 3-3 Scatter plot of simulated wind direction versus the wind speed, associated with the 220 highest $H_{m0}$ events underlying the EVA of $H_{m0}$ at KFIIS-1. ....	23
Figure 4-1 Time series of $U_{10mag}$ at KFIIS-1. ....	26
Figure 4-2 Rose plot of $U_{10mag}$ , sorted by $U_{10dir}$ , at KFIIS-1. ....	27
Figure 4-3 Scatter of $U_{10mag}$ and $U_{10dir}$ at KFIIS-1. ....	27
Figure 4-4 Probability plot of $U_{10mag}$ at KFIIS-1. ....	28
Figure 4-5 Time series of $U_{150mag}$ at KFIIS-1. ....	29
Figure 4-6 Rose plot of $U_{150mag}$ , sorted by $U_{150dir}$ , at KFIIS-1. ....	30
Figure 4-7 Scatter of $U_{150mag}$ and $U_{150dir}$ at KFIIS-1. ....	30
Figure 4-8 Probability plot of $U_{150mag}$ at KFIIS-1. ....	31
Figure 5-1 Time series of water level at KFIIS-1. ....	34
Figure 5-2 Histogram of the water level, WL, at KFIIS-1. ....	36
Figure 5-3 Monthly statistics of the water level, WL, at KFIIS-1. ....	36
Figure 5-4 Marginal EVA of total high-water level, WL, at KFIIS-1. ....	37
Figure 5-5 Marginal EVA of residual high-water level, $WL_r$ , at KFIIS-1. ....	38
Figure 5-6 Marginal EVA of low-water level, $WL_{low}$ , at KFIIS-1. Note that the low water levels are positive on the figure. ....	39
Figure 5-7 Marginal EVA of residual low-water level, $WL_{r,low}$ , at KFIIS-1. Note that the low water levels are positive on the figure. ....	40
Figure 5-8 Spatial variation across the data delivery area of KFII of total water level, WL, for return periods of 1 years. The colour map shows the water level, and the contours show water depths. ....	41
Figure 5-9 Spatial variation across the data delivery area of KFII of total water level, WL, for return periods of 5 years. The colour map shows the water level, and the contours show water depths. ....	41
Figure 5-10 Spatial variation across the data delivery area of KFII of total water level, WL, for return periods of 10 years. The colour map shows the water level, and the contours show water depths. ....	42
Figure 5-11 Spatial variation across the data delivery area of KFII of total water level, WL, for return periods of 25 years. The colour map shows the water level, and the contours show water depths. ....	42
Figure 5-12 Spatial variation across the data delivery area of KFII of total water level, WL, for return periods of 50 years. The colour map shows the water level, and the contours show water depths. ....	43
Figure 5-13 Spatial variation across the data delivery area of KFII of total water level, $WL_{low}$ , for return periods of 1 years. The colour map shows the low water level, and the contours show water depths. ....	44
Figure 5-14 Spatial variation across the data delivery area of KFII of total water level, $WL_{low}$ , for return periods of 5 years. The colour map shows the low water level, and the contours show water depths. ....	44

Figure 5-15 Spatial variation across the data delivery area of KFII of total water level,  $WL_{low}$ , for return periods of 10 years. The colour map shows the low water level, and the contours show water depths. .... 45

Figure 5-16 Spatial variation across the data delivery area of KFII of total water level,  $WL_{low}$ , for return periods of 25 years. The colour map shows the low water level, and the contours show water depths. .... 45

Figure 5-17 Spatial variation across the data delivery area of KFII of total water level,  $WL_{low}$ , for return periods of 50 years. The colour map shows the low water level, and the contours show water depths. .... 46

Figure 6-1 Time series of  $CS_{stot}$  at KFIS-1..... 48

Figure 6-2 Time series of  $CS_{mtot}$  at KFIS-1..... 49

Figure 6-3 Time series of  $CS_{btot}$  at KFIS-1. .... 49

Figure 6-4 Rose plot of  $CS_{stot}$  at KFIS-1. .... 50

Figure 6-5 Rose plot of  $CS_{mtot}$  at KFIS-1. .... 50

Figure 6-6 Rose plot of  $CS_{btot}$  at KFIS-1..... 51

Figure 6-7 Probability plot of  $CS_{stot}$  at KFIS-1..... 51

Figure 6-8 Probability plot of  $CS_{mtot}$  at KFIS-1..... 52

Figure 6-9 Probability plot of  $CS_{btot}$  at KFIS-1. .... 52

Figure 6-10 Monthly statistics of  $CS_{stot}$  at KFIS-1..... 53

Figure 6-11 Monthly statistics of  $CS_{mtot}$  at KFIS-1. .... 53

Figure 6-12 Monthly statistics of  $CS_{btot}$  at KFIS-1..... 54

Figure 6-13 Directional statistics of  $CS_{stot}$ , sorted by  $CD_{stot}$ , at KFIS-1. .... 54

Figure 6-14 Directional statistics of  $CS_{mtot}$ , sorted by  $CD_{mtot}$ , at KFIS-1..... 55

Figure 6-15 Directional statistics of  $CS_{btot}$ , sorted by  $CD_{btot}$ , at KFIS-1. .... 55

Figure 6-16 Profiles of current speed, Sea water temperature and salinity for each season winter, spring, summer, and fall. .... 56

Figure 6-17 Profiles of current speed, Sea water temperature and salinity for each month. .... 57

Figure 6-18 Spatial variation of moments of  $CSs$  across the data delivery area,  $m=1$  ..... 58

Figure 6-19 Spatial variation of moments of  $CSs$  across the data delivery area,  $m=2$ ..... 58

Figure 6-20 Spatial variation of moments of  $CSs$  across the data delivery area,  $m= 4$ ..... 59

Figure 6-21 Spatial variation of moments of  $CSs$  across the data delivery area,  $m=5$ ..... 59

Figure 6-22 Spatial variation of moments of  $CSm$  across the data delivery area,  $m=1$ ..... 60

Figure 6-23 Spatial variation of moments of  $CSm$  across the data delivery area,  $m=2$ ..... 60

Figure 6-24 Spatial variation of moments of  $CSm$  across the data delivery area,  $m=4$ ..... 61

Figure 6-25 Spatial variation of moments of  $CSm$  across the data delivery area,  $m=5$ ..... 61

Figure 6-26 Spatial variation of moments of  $CSb$  across the data delivery area,  $m=1$  ..... 62

Figure 6-27 Spatial variation of moments of  $CSb$  across the data delivery area,  $m=2$ ..... 62

Figure 6-28 Spatial variation of moments of  $CSb$  across the data delivery area,  $m=4$ ..... 63

Figure 6-29 Spatial variation of moments of  $CSb$  across the data delivery area,  $m=5$ ..... 63

Figure 6-30 Marginal Omni-directional EVA estimates of  $CS_{stot}$  at KFIS-1. .... 64

Figure 6-31 Marginal directional EVA estimates of  $CS_{stot}$  for  $CD_{stot}$  [°N-going to] sectors every 22.5° for KFIIS-1. Weibull LS,  $\lambda = 1$ . Confidence limits 2.5% - 97.5%..... 66

Figure 6-32 Marginal directional EVA estimates of  $CS_{stot}$  for  $CD_{stot}$  [°N-going to] sectors every 22.5° for KFIIS-1. Weibull LS,  $\lambda = 1$ . Confidence limits 2.5% - 97.5%..... 67

Figure 6-33 Marginal omni-directional EVA estimates of  $CS_{mtot}$  at KFIIS-1. .... 68

Figure 6-34 Marginal directional EVA estimates of  $CS_{mtot}$  for  $CD_{mtot}$  [°N-going to] sectors every 22.5° for KFIIS-1. Weibull LS,  $\lambda = 1$ . Confidence limits 2.5% - 97.5%..... 70

Figure 6-35 Marginal directional EVA estimates of  $CS_{mtot}$  for  $CD_{mtot}$  [°N-going to] sectors every 22.5° for KFIIS-1. Weibull LS,  $\lambda = 1$ . Confidence limits 2.5% - 97.5%..... 71

Figure 6-36 Marginal omni-directional EVA estimates of  $CS_{btot}$  at KFIIS-1. .... 72

Figure 6-37 Marginal directional EVA estimates of  $CS_{btot}$  for  $CD_{btot}$  [°N-going to] sectors every 22.5° for KFIIS-1. Weibull LS,  $\lambda = 1$ . Confidence limits 2.5% - 97.5%..... 73

Figure 6-38 Marginal directional EVA estimates of  $CS_{btot}$  for  $CD_{btot}$  [°N-going to] sectors every 22.5° for KFIIS-1. Weibull LS,  $\lambda = 1$ . Confidence limits 2.5% - 97.5%..... 74

Figure 6-39 Spatial variation across the data delivery area of KFII of  $CS_{stot}$  for return periods of 1 years. The colour map shows the current speed, and the contours show water depths..... 75

Figure 6-40 Spatial variation across the data delivery area of KFII of  $CS_{stot}$  for return periods of 5 years. The colour map shows the current speed, and the contours show water depths..... 76

Figure 6-41 Spatial variation across the data delivery area of KFII of  $CS_{stot}$  for return periods of 10 years. The colour map shows the current speed, and the contours show water depths..... 76

Figure 6-42 Spatial variation across the data delivery area of KFII of  $CS_{stot}$  for return periods of 25 years. The colour map shows the current speed, and the contours show water depths..... 77

Figure 6-43 Spatial variation across the data delivery area of KFII of  $CS_{stot}$  for return periods of 50 years. The colour map shows the current speed, and the contours show water depths..... 77

Figure 6-44 Spatial variation across the data delivery area of KFII of  $CS_{mtot}$  for return periods of 1 years. The colour map shows the current speed, and the contours show water depths..... 78

Figure 6-45 Spatial variation across the data delivery area of KFII of  $CS_{mtot}$  for return periods of 5 years. The colour map shows the current speed, and the contours show water depths..... 78

Figure 6-46 Spatial variation across the data delivery area of KFII of  $CS_{mtot}$  for return periods of 10 years. The colour map shows the current speed, and the contours show water depths..... 79

Figure 6-47 Spatial variation across the data delivery area of KFII of  $CS_{mtot}$  for return periods of 25 years. The colour map shows the current speed, and the contours show water depths..... 79

Figure 6-48 Spatial variation across the data delivery area of KFII of  $CS_{mtot}$  for return periods of 50 years. The colour map shows the current speed, and the contours show water depths..... 80

Figure 6-49 Spatial variation across the data delivery area of KFII of  $CS_{btot}$  for return periods of 1 years. The colour map shows the current speed, and the contours show water depths..... 80

Figure 6-50 Spatial variation across the data delivery area of KFII of  $CS_{btot}$  for return periods of 5 years. The colour map shows the current speed, and the contours show water depths..... 81

Figure 6-51 Spatial variation across the data delivery area of KFII of  $CS_{btot}$  for return periods of 10 years. The colour map shows the current speed, and the contours show water depths..... 81

Figure 6-52 Spatial variation across the data delivery area of KFII of  $CS_{btot}$  for return periods of 25 years. The colour map shows the current speed, and the contours show water depths..... 82

Figure 6-53 Spatial variation across the data delivery area of KFII of  $CS_{btot}$  for return periods of 50 years. The colour map shows the current speed, and the contours show water depths..... 82

Figure 7-1 Timeseries of  $H_{m0}$  and  $T_p$  at KFIIS-1..... 86

Figure 7-2 Timeseries of  $T_{m02}$ ,  $T_{m10}$ ,  $T_{m01}$  at KFIIS-1..... 87

Figure 7-3 Rose plot of  $H_{m0}$ , sorted by MWD, at KFIIS-1..... 88

Figure 7-4 Rose plot of  $T_p$ , sorted by MWD, at KFIIS-1..... 89

Figure 7-5 Probability plot of  $H_{m0}$  at KFIIS-1..... 90

Figure 7-6 Probability plot of  $T_p$  at KFIIS-1..... 90

Figure 7-7 Monthly statistics of  $H_{m0}$  at KFIIS-1..... 91

Figure 7-8 Monthly statistics of  $T_p$  at KFIIS-1..... 91

Figure 7-9 Directional statistics of  $H_{m0}$  sorted by MWD at KFIIS-1..... 92

Figure 7-10 Directional statistics of  $T_p$  sorted by MWD at KFIIS-1..... 92

Figure 7-11  $T_p$  based on the mean of  $H_{m0}$  at KFIIS-1 for omni..... 93

Figure 7-12 Spatial variation of moments of  $H_{m0}$  across the data delivery area,  $m=1$ ..... 94

Figure 7-13 Spatial variation of moments of  $H_{m0}$  across the data delivery area,  $m=2$ ..... 94

Figure 7-14 Spatial variation of moments of  $H_{m0}$  across the data delivery area,  $m=4$ ..... 95

Figure 7-15 Spatial variation of moments of  $H_{m0}$  across the data delivery area,  $m=5$ ..... 95

Figure 7-16 Extreme  $H_{m0}$  for omni at KFIIS-1..... 96

Figure 7-17 Extreme  $H_{m0}$  for MWD directional sectors at KFIIS-1 (56.4251°E, 11.6797°N, Seabed level=-27.61mMSL, 1979-01-01 to 2023-12-31;  $\Delta t=1h$ ). Weibull LS,  $\lambda = 1$ . Confidence limits 2.5% -97.5%. ..... 98

Figure 7-18 Extreme  $H_{m0}$  for MWD directional sectors at KFIIS-1 (56.4251°E, 11.6797°N, Seabed level=-27.61mMSL, 1979-01-01 to 2023-12-31;  $\Delta t=1h$ ). Weibull LS,  $\lambda = 1$ . Confidence limits 2.5% -97.5%. ..... 99

Figure 7-19 Spatial variation across the data delivery area of KFII of  $H_{m0}$  for return periods of 50 years. The colour map shows the wave height, and the contours show water depths..... 100

Figure 7-20 Spatial variation across the data delivery area of KFII of  $H_{m0}$  for return periods of 25 years. The colour map shows the wave height, and the contours show water depths..... 101

Figure 7-21 Spatial variation across the data delivery area of KFII of  $H_{m0}$  for return periods of 10 years. The colour map shows the wave height, and the contours show water depths..... 101

Figure 7-22 Spatial variation across the data delivery area of KFII of  $H_{m0}$  for return periods of 5 years. The colour map shows the wave height, and the contours show water depths..... 102

Figure 7-23 Spatial variation across the data delivery area of KFII of  $H_{m0}$  for return periods of 1 year. The colour map shows the wave height, and the contours show water depths..... 102



Figure 7-24 Relationship between the extreme wave height with a return period of 50 years and the depth at MSL at each model grid point in KFII. ....	103
Figure 7-25 Comparison of hindcast (mean wave spectrum) and JONSWAP spectra for $H_{m0} = 4.0-4.5$ m at KFIIS-1. ....	108
Figure 7-26 Wave directional standard deviation as a function $H_{m0}$ . ....	109
Figure 7-27 Relationship between directional standard deviation and Spreading factor applied in ISO 19901-1:2015. ....	109
Figure 8-1 Scatter of MWD and $U_{150dir}$ at KFIIS-1. ....	111
Figure 8-2 Scatter of $U_{150mag}$ and $U_{150dir} - MWD$ . ....	112
Figure 8-3 Scatter of $H_{m0}$ and WL at KFIIS-1. Plots for all directions of MWD are in the appendices. ....	114
Figure 9-1 NSS for omni with fit. Fits and coefficients for all directional sectors are presented in the appendices. ....	116
Figure 9-2 IFORM contour for SSS with a 50-year return period for $H_{m0}$ and $U_{150mag}$ at KFIIS-1. The blue line shows the marginal 50-year return period $H_{m0}$ . ....	117
Figure 9-3 Exponentiated Weibull fit for sections of $H_{m0}$ data binned by 2 m/s intervals of $U_{150mag}$ . ....	119
Figure 9-4 Exponentiated Weibull fit for sections of $H_{m0}$ data binned by 2 m/s intervals of $U_{150mag}$ . ....	120
Figure 10-1 Monthly statistics of air temperature at 2 m above sea level. ....	122
Figure 10-2 Monthly statistics of pressure at 2 m above sea level. ....	123
Figure 10-3 Monthly statistics of relative humidity at 2 m above sea level. ....	123
Figure 10-4 Monthly statistics of downward solar radiation. ....	124
Figure 10-5 Monthly statistics of lightning counts at the data delivery area. ...	126
Figure 10-6 Plot of monthly statistics of $Sal_s$ , at KFIIS-1. ....	128
Figure 10-7 Plot of monthly statistics of $Sal_m$ , at KFIIS-1. ....	129
Figure 10-8 Plot of monthly statistics of $Sal_b$ , at KFIIS-1. ....	130
Figure 10-9 Plot of monthly statistics of $T_{sw,s}$ , at KFIIS-1. ....	131
Figure 10-10 Plot of monthly statistics of $T_{sw,m}$ , at KFIIS-1. ....	132
Figure 10-11 Plot of monthly statistics of $T_{sw,b}$ , at KFIIS-1. ....	133
Figure 10-12 Plot of monthly statistics of $D_{sw,s}$ , at KFIIS-1. ....	134
Figure 10-13 Plot of monthly statistics of $D_{sw,m}$ , at KFIIS-1. ....	135
Figure 10-14 Plot of monthly statistics of $D_{sw,b}$ , at KFIIS-1. ....	136
Figure 11-1 Sensitivity of 50 year marginal $H_{m0}$ EVA to distribution, threshold, and fitting. Inter-event time 72h. ....	142

## List of Tables

Table 1-1 Extreme design conditions for 50-year return period at KFIIS-1 (unscaled).....	14
Table 1-2 Extreme design conditions for 50-year return period current conditions at KFIIS -1 (unscaled). .....	15
Table 1-3 Extreme design conditions for 50-year return period water level conditions at KFIIS -1. ....	15
Table 3-1 List of the reference locations for the area for KFII with name, location, and depth. ....	19
Table 3-2 Number of storms observed by DMI between 1891 and 2024 [2].....	21
Table 4-1 Metadata of the wind dataset .....	25
Table 4-2 Wind variables of the data set .....	25
Table 4-3 Table of $U_{10mag}$ and $U_{10dir}$ in percentage, at KFIIS-1.....	28
Table 4-4 Probability table of $U_{10mag}$ , at KFIIS-1.....	29
Table 4-5 Table of $U_{150mag}$ and $U_{150dir}$ in percentage, at KFIIS-1. ....	31
Table 4-6 Probability table of $U_{150mag}$ , at KFIIS-1. ....	32
Table 5-1 Metadata of the water level dataset. ....	33
Table 5-2 Wave variables of the water level dataset.....	33
Table 5-3 Tidal levels at KFII. ....	35
Table 5-4 Estimates of total water level, WL, at KFIIS-1.....	37
Table 5-5 Estimates of residual high-water level, $WL_r$ , at KFIIS-1. ....	38
Table 5-6 Estimates of low water level, $WL_{low}$ , at KFIIS-1.....	39
Table 5-7 Estimates of residual low water level, $WL_{r,low}$ , at KFIIS-1.....	40
Table 6-1 Metadata of the wave dataset. ....	47
Table 6-2 Total current variables of the hydrodynamic dataset .....	47
Table 6-3 Summary of current speed at 3 depths at KFIIS-1.....	48
Table 6-4 Oceanographic variables of the hydrodynamic dataset .....	56
Table 6-5 Marginal directional EVA estimates of $CS_{stot}$ at KFIIS-1. ....	65
Table 6-6 Marginal directional EVA estimates of $CS_{mtot}$ at KFIIS-1.....	69
Table 6-7 Marginal directional EVA estimates of $CS_{btot}$ at KFIIS-1. ....	72
Table 7-1 Metadata of the wave dataset. ....	84
Table 7-2 Wave variables of the wave dataset.....	84
Table 7-3 Overview of simple statistics for wave variables data period 1979-01-01 to 2023-12-31 at KFIIS-1.....	85
Table 7-4 Table of $H_{m0}$ and MWD in percentage, at KFIIS-1. ....	88
Table 7-5 Table of $T_p$ and MWD in percentage, at KFIIS-1.....	89
Table 7-6 Marginal directional EVA estimates of $H_{m0}$ , at KFIIS-1. ....	97
Table 7-7 Peak wave period associated with the extreme $H_{m0}$ at KFIIS-1 based on mean correlation between $H_{m0}$ and $T_p$ .....	97
Table 7-8 Marginal directional estimates of $H_{max}$ , at KFIIS-1. ....	104
Table 7-9 Mode wave period associated with the maximum wave height at KFIIS-1.....	105
Table 7-10 Wave period (low) associated with the maximum wave height at KFIIS-1.....	105
Table 7-11 Wave period (high) associated with the maximum wave height at KFIIS-1.....	106
Table 7-12 Marginal directional extreme estimates of $C_{max_1}$ , at KFIIS-1. ....	107
Table 8-1 Table of $U_{150dir}$ and MWD in percentage, at KFIIN-1. Total number of events=394464. ....	111
Table 8-2 Table of $U_{150mag}$ and $U_{150dir}$ —MWD in percentage, at KFIIS-1.....	113
Table 8-3 Table of $H_{m0}$ and WL in percentage, at KFIIS-1.....	115

Table 9-1 SSS from the 50-year return period environmental contour for $H_{m0}$ and $U_{150mag}$ .....	118
Table 9-2 ESS for 50-year return period at KFIIS-1 (unscaled) .....	121
Table 9-3 ESS for 1-year return period at KFIIS-1 (unscaled) .....	121
Table 10-1 Monthly statistics for air temperature at 2 m above sea level at KFIIS-1 .....	124
Table 10-2 Monthly statistics for pressure at KFIIS-1 at 2 m above sea level at KFIIS-1 .....	125
Table 10-3 Monthly statistics for relative humidity at KFIIS-1 .....	125
Table 10-4 Annual and monthly statistics for downward solar radiation at KFIIS-1 .....	125
Table 10-5 Seasonal variation of lightning strike across the data delivery area. ....	127
Table 10-6 Oceanographic variables of the hydrodynamic dataset .....	127
Table 10-7 Table with monthly statistics of $Sal_s$ , at KFIIS-1 .....	128
Table 10-8 Table with monthly statistics of $Sal_m$ , at KFIIS-1 .....	129
Table 10-9 Table with monthly statistics of $Sal_b$ , at KFIIS-1 .....	130
Table 10-10 Table with monthly statistics of $T_{sw,s}$ , at KFIIS-1 .....	131
Table 10-11 Table with monthly statistics of $T_{sw,m}$ , at KFIIS-1 .....	132
Table 10-12 Table with monthly statistics of $T_{sw,b}$ , at KFIIS-1 .....	133
Table 10-13 Table with monthly statistics of $D_{sw,s}$ , at KFIIS-1 .....	134
Table 10-14 Table with monthly statistics of $D_{sw,m}$ , at KFIIS-1 .....	135
Table 10-15 Table with monthly statistics of $D_{sw,b}$ , at KFIIS-1 .....	136

## Nomenclature

Variable	Abbreviation	Unit
<b>Atmosphere</b>		
Wind speed @ 10 m height	$U_{10mag}$	m/s
Wind direction @ 10 m height	$U_{10dir}$	°N (clockwise from)
Wind speed @ 150 m height	$U_{150mag}$	m/s
Wind direction @ 150 m height	$U_{150dir}$	°N (clockwise from)
Air pressure @ mean sea level	P	Pa
Air temperature @ 2 m height	$T_{2m}$	°C
Relative humidity @ 2 m height	RH	-
Surface solar radiation	SSR	J/m <sup>2</sup>
<b>Ocean</b>		
Water level	WL	mMSL
Current speed	CS	m/s
Current direction	CD	°N (clockwise to)
Sea surface temperature	SST	°C
Water temperature @ {x} m depth	$T_{sw\{x\}}$	°C
Water Salinity	Salinity	PSU (practical salinity unit)
<b>Waves</b>		
Significant wave height	$H_{m0}$	m
Maximum wave height	$H_{max}$	m
Maximum wave crest height	$C_{max}$	m
Peak wave period	$T_p$	s
Wave energy period	$T_{mm10}$	s
Mean wave period	$T_{m01}$	s
Zero-crossing wave period	$T_{m02}$	s
Wave period associated with the maximum wave height	$T_{Hmax}$	s
Peak wave direction	PWD	°N (clockwise from)
Mean wave direction	MWD	°N (clockwise from)
Direction standard deviation	DSpr	°
<b>Definitions</b>		
Coordinate System	WGS84 EPSG 4326 (unless specified differently)	
Direction	Clockwise from North	

Wind	°N coming from
Current	°N going to
Waves	°N coming from
Time	Times are relative to UTC
Vertical Datum	MSL (unless specified differently)

Abbreviations	
2D	2-dimensional
3D	3-dimensional
DMI	Danish Meteorological Institute
DNV	Det Norske Veritas
ECMWF	European Centre for Medium-Range Weather Forecasts
ERA5	ECMWF Re-analysis v5
ESS	Extreme Sea State
EVA	Extreme Value Analysis
FEED	Front-End Engineering Design
IEC	International Electrotechnical Commission
ISO	International Organization for Standardization
KFII	Kriegers Flak II
mMSL	Metres above Mean Sea Level
MSL	Mean Sea Level
NSS	Normal Sea State
OWF	Offshore Wind Farm
POT	Peak Over Threshold
SSS	Severe Sea State
UTC	Coordinated Universal Time
WGS84	World Geodetic System 1984

# 1 Summary

This report presents the results of MetOcean site conditions assessment study focusing on analysis of design parameters for the Kriegers Flak II OWF.

The report analyses a hindcast modelling period covering 45 years, from January 1<sup>st</sup> 1979, to December 31<sup>st</sup> 2023. This hindcast data is used to estimate operational and extreme hydrographic conditions for the FEED design of the OWF. The selected period includes several extreme storm events with varying direction, duration, and extreme peak values of wind, water level, waves, and currents. Additionally, the report analyses other atmospheric and oceanographic conditions such as air temperature, pressure, humidity, solar radiation, lightning strikes, seawater temperature, salinity, and marine growth. Six reference locations within the OWF area are chosen to capture the variation across the site.

Data is categorized by spatial, temporal, and spectral dimensions and is delivered in two packages: one for detailed analysis at reference locations and another for a fine-gridded overview across the entire data delivery area. The data is presented in various formats, such as time series, wind roses, scatter plots, and histograms. The document presents data for one point but with appendices with additional data for all points.

Below are the most important extreme design parameters summarized. The report contains also design parameters for operational conditions. It is noted that all Extreme Value Analysis results presented in the relevant sections of this report (ie. sections 6.2, 7.2 and 9.3) are unscaled, in other words raw results from the EVA without scaling with regards to directionality. Scaled results according to DNV-RP-C205 where consistency between directional extremes and Omni for all return periods are ensured can be found in the appendices, see section 6.3 and 7.3 for details on the scaling.

Table 1-1 Extreme design conditions for 50-year return period at KFIIS-1 (unscaled).

Parameter	MWD [°N-from]																
	0.0	22.5	45.0	67.5	90.0	112.5	135.0	157.5	180.0	202.5	225.0	247.5	270.0	292.5	315.0	337.5	Omni
$H_{m0}$ [m]	3.0	3.1	3.5	4.6	5.0	3.8	2.6	2.8	3.0	3.3	5.2	5.6	4.4	3.9	3.7	3.1	5.8
$T_p$ [s]	6.2	6.1	7.8	8.6	8.8	7.9	6.8	6.1	6.3	6.8	8.3	8.5	7.4	7.0	7.0	6.7	9.0
$H_{max}$ [m]	5.8	6.1	6.8	8.9	9.8	7.4	5.2	5.4	5.8	6.4	10.1	11.0	8.6	7.6	7.2	6.1	11.2
$T_{Hmax,ass,low}$ [s]	6.1	6.3	6.6	7.6	8.0	6.9	5.8	5.9	6.1	6.4	8.1	8.4	7.5	7.0	6.8	6.3	8.5
$T_{Hmax,ass,high}$ [s]	7.9	8.1	8.5	9.8	10.3	8.9	7.4	7.6	7.9	8.3	10.4	10.8	9.6	9.0	8.8	8.1	11.0
$C_{max}$ [m]	3.4	3.6	3.8	5.1	5.7	4.2	2.9	3.1	3.4	3.7	6	6.6	5.1	4.5	4.2	3.5	6.7

Table 1-2 Extreme design conditions for 50-year return period current conditions at KFIIS -1 (unscaled).

Parameter	CD [°N-going]																
	0.0	22.5	45.0	67.5	90.0	112.5	135.0	157.5	180.0	202.5	225.0	247.5	270.0	292.5	315.0	337.5	Omni
CS <sub>stot</sub> [m/s]	1.3	1.3	1.4	1.4	1.3	1.1	1	1	0.9	1	1.3	1.7	1.7	1.3	1.4	1.2	1.7
CS <sub>mtot</sub> [m/s]	0.7	0.8	0.8	0.8	0.8	0.7	0.6	0.6	0.6	0.6	0.8	1	1	0.8	0.8	0.8	1
CS <sub>btot</sub> [m/s]	0.4	0.4	0.4	0.4	0.5	0.5	0.6	0.6	0.4	0.5	0.4	0.3	0.3	0.3	0.3	0.3	0.6

Table 1-3 Extreme design conditions for 50-year return period water level conditions at KFIIS -1.

Parameter	Omni
WL [mMSL]	1.6
WL <sub>r</sub> [mMSL]	1.4
WL <sub>low</sub> [mMSL]	-1.8
WL <sub>r,low</sub> [mMSL]	-1.9

## 2 Introduction

The Danish Energy Agency has tasked Energinet with undertaking site MetOcean conditions assessments for the development of the offshore wind farm area Kriegers Flak II. The offshore wind farm is to be in The Baltic Sea east of the Danish Island Møn. An overview is shown on Figure 2-1.

The site MetOcean conditions assessments will form part of the larger site conditions assessment work and will be a part of the technical basis for the public tender on the development of offshore wind farms within the areas. The site MetOcean conditions assessment is considered suitable for the Front-End Engineering and Design (FEED) of offshore WTG and other support structures for the offshore wind farm.



Figure 2-1 Overview of the windfarm area Kriegers Flak II. The dashed line indicates the full data delivery area, and the hatched areas indicate the OWFs.

The full study consists of several deliverables in which this report, Part B, is one of several:

- Part A: Measurements and Hindcast Data Basis (report).
- Part B: Analyses and Design Parameters (this report).
- Long-term hindcast data (digital time series).
- Measurement data (digital time series).



- Reverification of Hindcast Data (report).

The study refers to the following standards and guidelines:

- DNV-RP-C205:2021-09
- DNV-ST-0437:2024-05
- IEC 61400-3-1:2019
- ISO 19901-1:2015

## 3 Data basis

The data basis for the analysis is based on Part A: Measurements and Hindcast Data Basis [1]. Along the report is hindcast data for the selected reference locations within the OWF. For more information of this matter please consult Part A.

The digital data deliveries are split into different parts due to their native dimensions. Their native dimensions are given based on spatial, temporal, and spectral discretization. Within the spatial dimension is latitude, longitude, and depth, within the temporal dimension is time and within the spectral dimension is frequency and direction.

The wind and wave data is grouped into a single file due to their similarity in dimensions. The rest of the atmospheric data is grouped into a single file describing the OWF area. The wave spectrum is grouped into a single file due to its unique spectral dimensions. Likewise, the water level and current data is grouped into a single file due to their variation across the depth.

The data is delivered in two different packages. One for the reference locations used for detailed analysis and one fine gridded across the full data delivery area. The reference locations are named based on this key:

`{area}_{reference location name}_{latitude}_{longitude}_{type}_{timespan}.nc`

The individual reference locations in the data delivery area are named based on this key:

`{area}_{latitude}_{longitude}_{type}_{timespan}.nc`

The main body of this report presents results at reference location KFIS-1, while results at all reference locations are given in the appendices which are attached to this report. The appendices contain all tables and figures presented below.

### 3.1 Reference Locations

For KFII offshore wind farm areas six reference locations have been chosen. The reference locations are to capture the variation across the area. The reference locations are chosen based on variations in  $H_{m0}$ ,  $T_p$  and CS with most attention towards their maximum value and the 95<sup>th</sup> percentile in the time domain. The six chosen reference locations are listed in Table 3-1, and showed in the overview map, Figure 3-1.

Table 3-1 List of the reference locations for the area for KFII with name, location, and depth.

Reference location	Latitude WGS84 [°N]	Longitude WGS84 [°E]	Seabed level [mMSL]
KFIIS-1	54.9197	12.9998	-39.71
KFIIS-2	54.9200	12.7802	-31.4
KFIIS-3	54.8498	12.7096	-18.43
KFIIN-1	55.1252	12.8199	-32.02
KFIIN-2	55.2345	12.6905	-23.69
KFIIN-3	55.0940	12.6997	-29.66

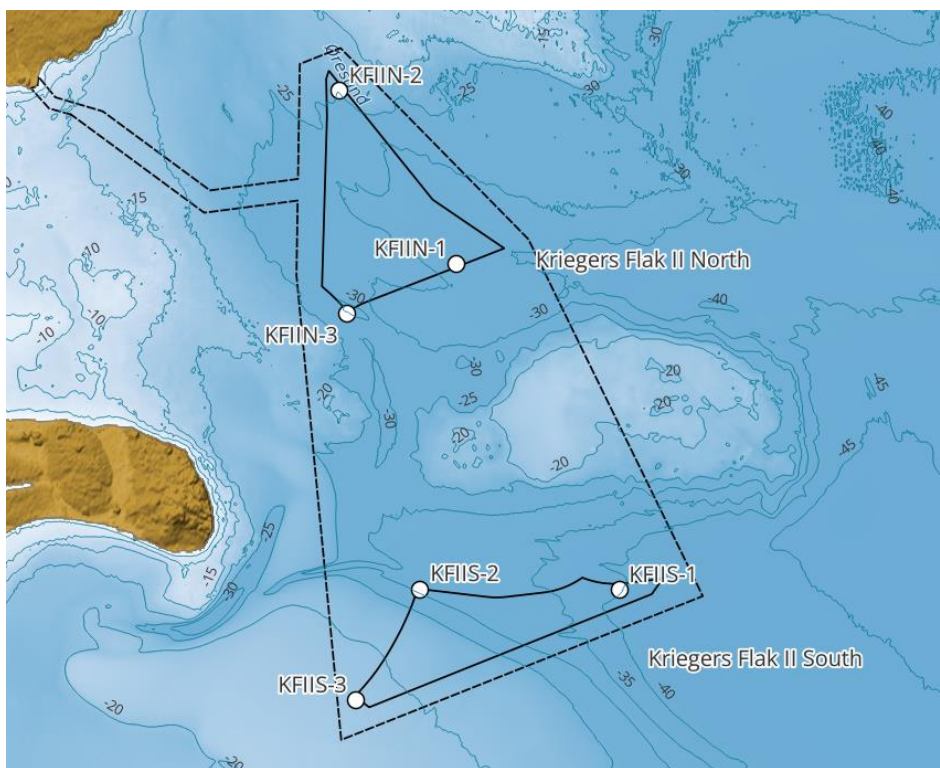


Figure 3-1 Overview of the reference locations within each OWF. The dashed line indicates the full data delivery area, and the full line indicate the OWFs. Contour lines are seabed levels in metres below MSL.

## 3.2 Historical extreme events

The hindcast modelling is elaborated and presented in Part A: Measurements and Hindcast Data Basis [1]. The data is based on a hydrodynamic simulation of relevant hydrographic variables covering the period 1 January 1979 – 1 January 2024, ie. a period with a total duration of 45 years.

The extreme hydrographic conditions as elaborated and presented in this Part B report, see Chapter 5, 6 and 7, have been estimated by carrying out EVA analyses of the relevant data in the 45-year period.

The selected 45-year simulation period includes several extreme storm events, with varying direction, duration and extreme peak values of wind, water level, waves and currents.

A hindcast period of 45-year duration will normally be considered sufficiently long for the elaboration of extreme design values, especially for the actual project with a requirement of estimations of values with return periods up to maximum 50 years only, i.e. the required return period for estimation of extreme values is only a few years longer than the duration of the hindcast simulation.

However, a review of historical records of storm events might potentially reveal that the selected 45-year hindcast period, forming the basis for the EVA analyses, is not fully statistically representative for long-term conditions. This is assessed in this section.

### 3.2.1 Storm frequency in Denmark

The Danish Meteorological Institute (DMI) currently assesses storms and storm patterns in Denmark, dividing storms into 4 categories:

- Class 1 – Average wind speeds in the range, 20.8-24.5 m/s
- Class 2 – Average wind speeds in the range, 24.5-26.5 m/s
- Class 3 – Average wind speeds in the range, 26.6-28.5 m/s
- Class 4 – Average wind speeds of 28.5 m/s or above

Some storms are national (covering > 30% of coastal areas), while others are regional storms affecting only parts (10-30% of Danish coastal areas). A storm may not be classified as a storm by DMI, if it only affects less than 10% of the coastal areas. Figure 3-2 shows the timing of all Class 2, 3 and 4 storms occurred in Denmark in the period, 1891 – 2021 (130 years), as observed by DMI. The actual hindcast simulation period, 1979-2023, is also shown in Figure 3-2.

In [2] DMI presents a list of all storms observed in Denmark in the period, 1891 – 2024, including Class 1 events also and the main wind direction for each storm. Table 3-2 presents the number of storms observed within each storm Class in the entire period, 1891-2023, however distinguished between the period, 1891-1978 (88 years) and 1979-2023 (45 years). The DMI list of storms does not provide any information on specific area(s) affected by each storm on the list. At a given point the actual number of storms in the period is probably smaller than reflected by Figure 3-2 and Table 3-2.

It is noted that the required design return period is up to a 50-year return period event, therefore a 133-year record of storms is considered sufficient for this analysis. Furthermore, the older the events the larger the uncertainty on the event, particularly when evaluating extreme current and wave conditions. In [2] it is informed that the classification of storms has become more accurate the last 20 years.

Going through the record of Class 2, 3 and 4 storm events illustrated in Figure 3-2 and Table 3-2 covering the period 1891-2021, it appears that most of these storms are associated with winds from westerly directions, especially for Class 3 and 4 storms with only one Class 3 and none Class 4 storms from easterly directions within the entire 130-year period. This is also illustrated by Figure 4-7 showing a scatter plot of simulated wind directions versus wind speeds for the

45-year hindcast period, with apparent relatively small wind speeds from easterly directions, see also below section 3.2.5.

It shall be noted that while the illustration in Figure 3-2 is based on wind observations only, the occurrence of extreme waves, currents and water levels in Danish waters are normally well-correlated to extreme wind speeds. With respect to extreme water levels, current and waves it shall, however, also be noted that the actual path of the low pressure, wind direction, and storm duration do also play a significant role for the development of extreme conditions.

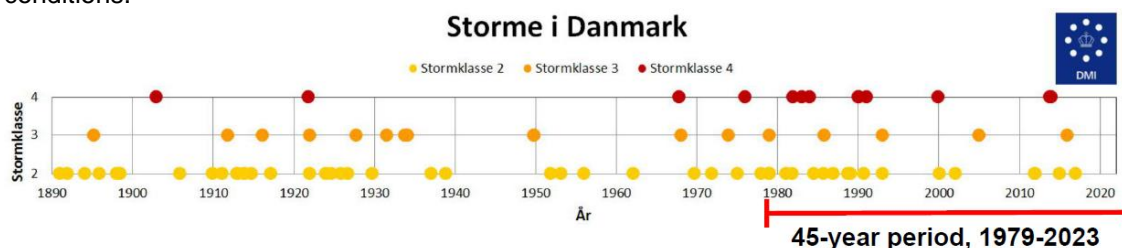


Figure 3-2 Observed Class 2, 3 and 4 storms in Denmark, 1891 – 2021 (130 years), from [3].

Table 3-2 Number of storms observed by DMI between 1891 and 2024 [2].

\* By DMI listed as a snow storm without wind direction, the majority likely to be easterly.

Storm Class	Number of storms observed				
	w/o direction	1891-1978 (88 years)		1979-2023 (45 years)	
		Easterly	Westerly	Easterly	Westerly
1 (>20.8 m/s)	17*	7	46	2	39
2 (>24.5 m/s)	2*	3	27	1	19
3 (>26.5 m/s)	-	1	11	0	4
4 (>28.5 m/s)	-	0	4	0	9

### 3.2.2 Assessment of the 45-year hindcast period

From Figure 3-2 and Table 3-2 it is clear that within the 45-year hindcast period, storms of Class 2 and 3 are in general represented well within the period, while it appears that Class 4 are over-represented within the hindcast period, compared to the full 130-year period considered in [3]. This may be a result of the random, stochastic nature of extreme storm events. However, this might potentially also be a result of climate change, but it is beyond the scope of this report to evaluate this further.

The 45-year hindcast period includes two of the most prominent Class 4 hurricanes ever recorded in the North Sea and Denmark, namely the storms on 24 November 1981 and 3 December 1999. However, while the inner Danish waters were affected by extreme wind speeds during these two storms, the associated storm surges mainly hit the west coast of Denmark and not the Kattegat region. Extreme water levels in the Kattegat region were generated during the storms on 1 November 2006 and 5-6 December 2013 (Bodil), during

which two storms, also within the 45-year hindcast period, the highest water levels ever observed in the Kattegat region have been recorded, see [4].

On 20 October 2023 an easterly storm generated storm surge levels in the western Baltic Sea region, including coastal areas near Kriegers Flak II OWF's, of a size not observed since 1904, ie. 120 years ago.

Generally, the strongest and most extreme currents in Kattegat and inner Danish waters occur in events with a high-water level difference between Kattegat and the western part of the Baltic Sea. With respect to south-going currents these are associated with extreme high water in Kattegat, hence also included in the hindcast period.

For the 133-year period, 1891 – 2023, DMI has observed a total number of 13 Class 4 storms in Denmark, while 9 of these fall within the 45-year hindcast period, see Table 3-2, in which the number of storms in each Class is presented, distinguishing between the period 1891-1978 and the hindcast period, 1979-2023.

The general assessment of the chosen 45-year hindcast period is therefore that the Class 4 storms appear to be over-represented compared to long-term conditions, and the most extreme water levels with return periods in the order of 100 years are also observed within the hindcast period.

Therefore, the use of the chosen 45-year period is considered conservative for derivation of metocean variables with a 50-year return period.

### 3.2.3 Very extreme historical events

The above assessments of historical events are based on data records going 133 years back, starting in 1891. Going further back in history, observations of very extreme events are mainly based on storm surges, due to their very significant impact on coasts, damage on buildings and loss of lives.

The available observations of storm surges show that the 45-year hindcast period includes the most extreme high water levels observed within a 130-year period in the Kattegat region, see above section 3.2.2., which are associated with extreme inflow of water into the western Baltic Sea, also having an impact on the current pattern in the Kriegers Flak area.

For the western Baltic Sea region there are observations of storm surges, which significantly exceed records within the 133-year period. Notably, the easterly storm event on 13 November 1872 and also one on 10 January 1694 can be mentioned. However, central estimates of their statistical return period are in the order of 1,000 and 250 years respectively, and for estimation of values with a 50-year return period it is considered acceptable not to consider these very extreme historical events further.

### 3.2.4 Easterly storms

Easterly winds rarely exceed a wind speed of 24.5 m/s, to be classified as a Class 2 storm or above, which appears in Table 3-2. Of all Class 2 storms observed by DMI less than 10% are of easterly origin. Only one easterly Class 3 storm has been observed, while no easterly Class 4 storms have been observed in the entire period, 1891 - 2024.

Even the easterly storm on 20 October 2023, generating 100-year storm surges in the western part of the Baltic Sea (along southern and southeastern Danish

coasts), is only classified as a Class 1 storm by DMI, with an average wind speed of 20.8 m/s or above, in DMI's list of Danish storms [2]. In addition, the hindcast simulation has on 15 February 1979 one more easterly storm at the reference points in the Kriegers Flak area, which qualifies as a Class 1 storm according to the DMI criteria, but which has not been listed as a Class 1 storm by DMI.

### 3.2.5 Extreme events 1979-2023

For the reference point, KFIIS-1, Figure 3-2 presents a scatter plot of the simultaneous simulated values of wind direction vs. wind speed, associated with the simulated values of  $H_{m0}$  underlying the EVA analysis of  $H_{m0}$  for this reference point. It is clear that easterly storms have relatively low wind speeds. Although easterly winds generally have relatively low speeds at KFIIS-1, they do generate relatively high wave heights, as they are associated with long free fetches towards east.

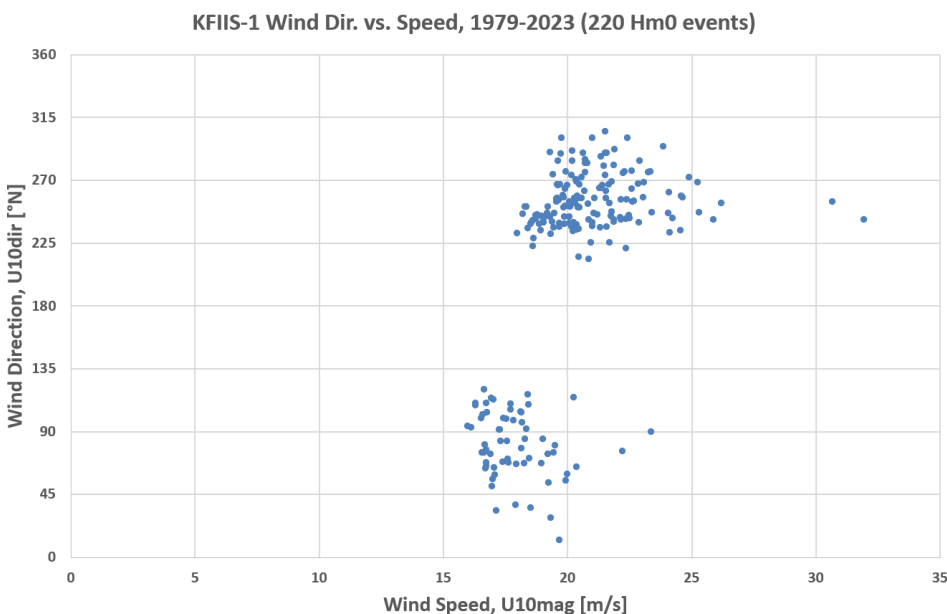


Figure 3-3 Scatter plot of simulated wind direction versus the wind speed, associated with the 220 highest  $H_{m0}$  events underlying the EVA of  $H_{m0}$  at KFIIS-1.

### 3.2.6 Conclusion

The conclusion is that the 45-year hindcast period is assessed to have a sufficient number of storm events from westerly directions, to be used for reliable estimates of extreme values of hydrographic variables up to 50-year recurrency intervals for the KFIIN and KFIIS offshore wind farms areas.

For easterly directions the period 1979-2023 seems to have an underrepresentation of easterly storms, in terms of wind speed, compared to 1891-1978, see Table 3-2. Thus there is an indication that 50 year extreme current, water level and wave conditions during easterly storms may be slightly underestimated when only considering the wind speed as the driving parameter. However extreme current, water level and wave conditions are also dependent

on low pressure, wind direction, and storm duration, as well as bathymetry and potential climate effects. Keeping these uncertainties in mind and considering that both model hindcast and measurement data used for model calibration contains an extreme water level event generated by an easterly storm (20-21 October 2023) with an estimated return period of 100 years, it is assessed to be reasonable to apply the 45 years hindcast modelling for reliable estimates of extreme values of hydrographic variables up to 50-year recurrence intervals for the KFIIN and KFIIS offshore wind farms areas.



## 4 Wind Conditions

**This section presents a summary of the modelled wind data, followed by a presentation of normal wind conditions.**

Note that wind data is included only to assess the misalignment relative to waves and for descriptions of sea states. Other wind conditions are addressed in a separate wind study assessing the wind conditions within the OWF area. This report only briefly describes the wind to give a general understanding of the site-specific conditions.

The wind data is adopted from [1] and consists of ERA5 [5] data during the period 1979 – 2024 (45 years). The ERA5 data is available at a 0.25° grid and used to run the wave model. The wind is interpolated from the ERA5 data from its native resolution (0.25° and 1 hour) to the mesh and output time step of the wave model of this study (~300 m and 1 hour). The wind dataset is combined with the wave dataset due to their common dimensions. Table 3.1 summarises the metadata.

Table 4-1 Metadata of the wind dataset

Name	Value
<b>Start Date [UTC]:</b>	1979-01-01 00:00:00
<b>End Date [UTC]:</b>	2023-12-31 23:00:00
<b>Time Step [s]</b>	3600

The data is calibrated with local measurements, details are available in [1]. The data set is considered representative of a 1-hour averaging period for both 10mMSL and 150mMSL height. The 150mMSL height is referred to as hub height.

The wind analyses cover the entire period and are presented in windspeed bins of 1.0 m/s and directional bins of 22.5° at both 10mMSL and 150mMSL height.

Table 4-2 presents the variables of the dataset, including the bin sizes applied in the analyses of the normal conditions.

Table 4-2 Wind variables of the data set

Variable name	Abbrev.	Unit	Bin size
<b>Wind speed at 10 mMSL</b>	U <sub>10mag</sub>	m/s	1.0
<b>Wind speed at 150 mMSL</b>	U <sub>150mag</sub>	m/s	1.0
<b>Wind direction at 10 mMSL</b>	U <sub>10dir</sub>	°N-from	22.5
<b>Wind direction at 150 mMSL</b>	U <sub>150dir</sub>	°N-from	22.5

### 4.1 Normal wind conditions

The normal wind conditions are presented both reference at 10mMSL and hub height at 150mMSL at the three reference locations in terms of:

- Time series

- Windrose
- Scatter plot
- Statistics – monthly and directional
- Histogram

#### 4.1.1 Wind speed at reference height

The sections present the wind speed at reference height at 10mMSL.

##### 4.1.1.1 Timeseries

Figure 4-1 shows a time series of wind speed at reference height at KFIIS-1 during the 45-year hindcast period. The mean wind speed is 7.7 m/s, and the maximum wind speed is 26.2 m/s.

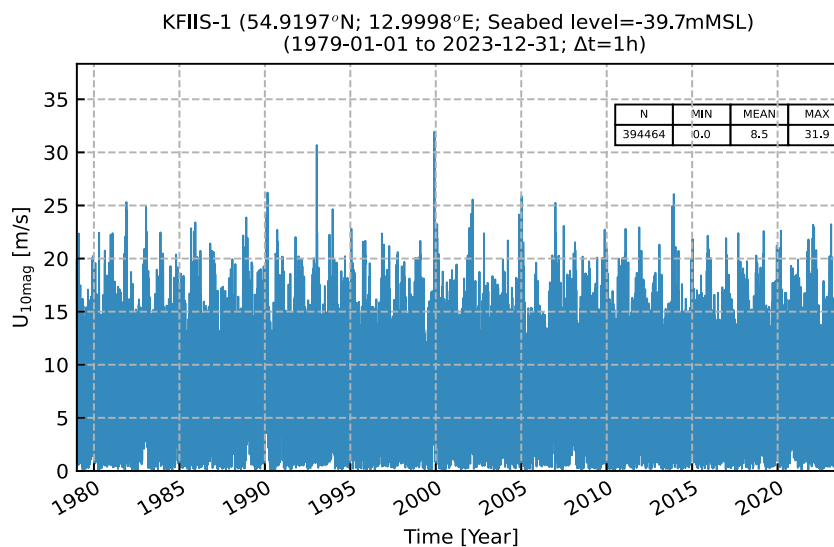


Figure 4-1 Time series of  $U_{10mag}$  at KFIIS-1.

##### 4.1.1.2 Windrose

Figure 4-2 shows a wind rose at KFIIS-1, showing the dominant wind coming from the west. Figure 4-2 shows the scatter plot of the wind speed and the wind direction at KFIIS-1. This aligns with the wind rose that the most frequent and dominant direction is west.

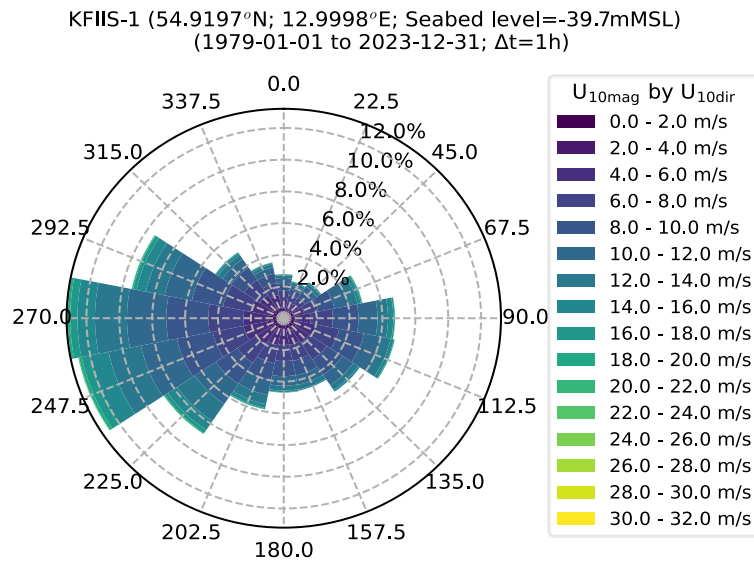


Figure 4-2 Rose plot of U<sub>10mag</sub>, sorted by U<sub>10dir</sub>, at KFIIS-1.

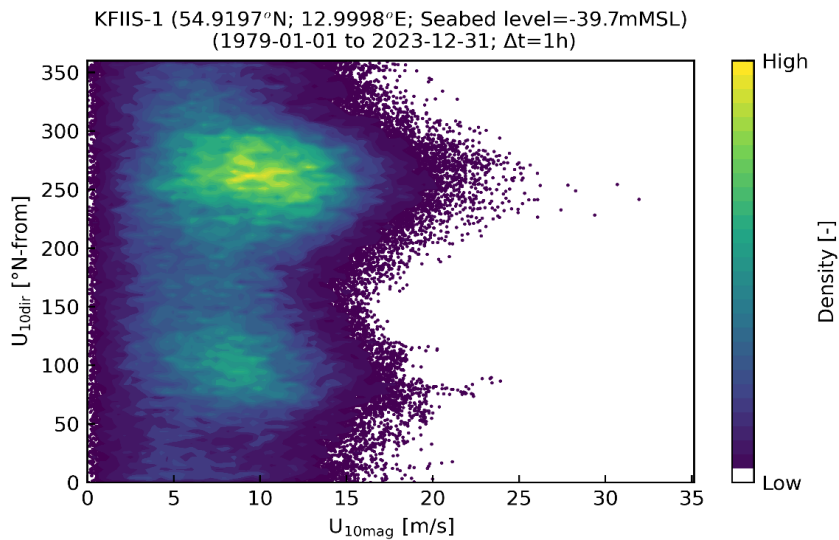


Figure 4-3 Scatter of U<sub>10mag</sub> and U<sub>10dir</sub> at KFIIS-1.

Table 4-3 Table of  $U_{10mag}$  and  $U_{10dir}$  in percentage, at KFIIS-1.

$U_{10mag}$ [m/s]	$U_{10dir}$ [°N-from]																
	0.0	22.5	45.0	67.5	90.0	112.5	135.0	157.5	180.0	202.5	225.0	247.5	270.0	292.5	315.0	337.5	Omni
0.0 - 2.0	0.17	0.15	0.16	0.16	0.18	0.20	0.21	0.21	0.21	0.22	0.23	0.22	0.22	0.20	0.19	0.19	3.1
2.0 - 4.0	0.46	0.39	0.37	0.45	0.54	0.66	0.65	0.59	0.60	0.62	0.71	0.82	0.73	0.60	0.55	0.52	9.3
4.0 - 6.0	0.58	0.49	0.53	0.66	0.93	1.14	1.00	0.91	0.88	0.90	1.09	1.46	1.50	1.26	1.01	0.77	15.1
6.0 - 8.0	0.56	0.44	0.50	0.86	1.33	1.43	1.27	1.03	1.02	1.16	1.36	1.91	2.14	1.71	1.16	0.79	18.7
8.0 - 10.0	0.45	0.38	0.47	1.01	1.56	1.52	1.15	0.93	0.95	1.11	1.57	2.22	2.56	1.93	0.94	0.61	19.4
10.0 - 12.0	0.31	0.27	0.37	0.88	1.16	1.08	0.79	0.61	0.60	0.94	1.53	2.23	2.39	1.69	0.63	0.40	15.9
12.0 - 14.0	0.18	0.19	0.21	0.55	0.64	0.58	0.36	0.29	0.30	0.59	1.30	2.01	1.95	1.15	0.32	0.19	10.8
14.0 - 16.0	0.05	0.05	0.09	0.20	0.32	0.20	0.12	0.07	0.10	0.24	0.68	1.18	1.06	0.59	0.14	0.10	5.2
16.0 - 18.0	0.01	0.02	0.03	0.08	0.09	0.05	0.01	0.01	0.03	0.07	0.22	0.48	0.44	0.22	0.06	0.02	1.8
18.0 - 20.0	0.00	0.00	0.01	0.03	0.01	0.01	0.00	0.00	0.00	0.02	0.06	0.16	0.15	0.07	0.02	0.00	0.5
20.0 - 22.0	0.00	0.00	0.00	0.00	0.00	0.00	0.00	0.00	0.00	0.00	0.01	0.04	0.05	0.02	0.00	0.00	0.1
22.0 - 24.0	0.00	0.00	0.00	0.00	0.00	0.00	0.00	0.00	0.00	0.00	0.01	0.01	0.02	0.00	0.00	0.00	0.0
24.0 - 26.0	0.00	0.00	0.00	0.00	0.00	0.00	0.00	0.00	0.00	0.00	0.00	0.00	0.00	0.00	0.00	0.00	0.0
26.0 - 28.0	0.00	0.00	0.00	0.00	0.00	0.00	0.00	0.00	0.00	0.00	0.00	0.00	0.00	0.00	0.00	0.00	0.0
28.0 - 30.0	0.00	0.00	0.00	0.00	0.00	0.00	0.00	0.00	0.00	0.00	0.00	0.00	0.00	0.00	0.00	0.00	0.0
30.0 - 32.0	0.00	0.00	0.00	0.00	0.00	0.00	0.00	0.00	0.00	0.00	0.00	0.00	0.00	0.00	0.00	0.00	0.0
All	2.8	2.4	2.7	4.9	6.8	6.9	5.6	4.7	4.7	5.9	8.8	12.7	13.2	9.4	5.0	3.6	####

### 4.1.1.3 Histogram

The histogram Figure 4-4 provides a visual representation of the binned wind speeds at the reference height at 10mMSL. The 30% quantile is 6.28 m/s, the 50% quantile is 8.39 m/s, and the 70% quantile is 10.51 m/s.

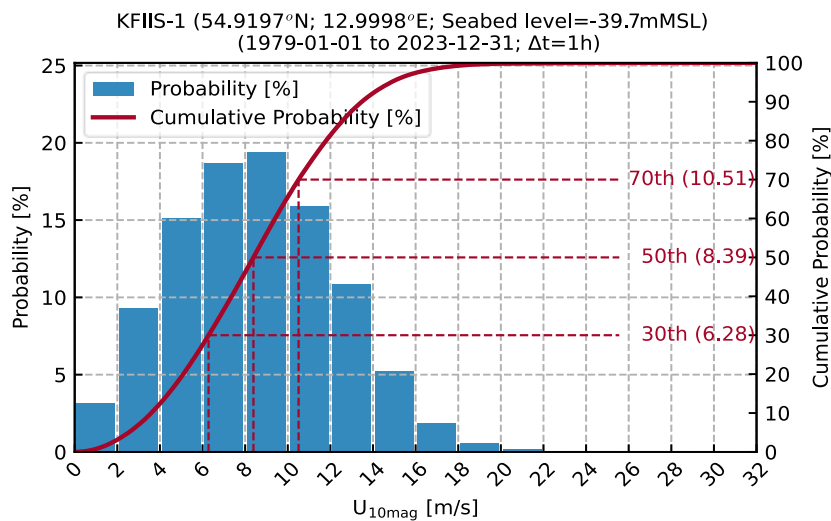


Figure 4-4 Probability plot of  $U_{10mag}$  at KFIIS-1.

The seasonal variation across  $U_{10mag}$  is shown in Table 4-4. At KFIIS-1 the largest winds are expected during winter.

Table 4-4 Probability table of  $U_{10mag}$ , at KFIIS-1.

Season	$U_{10mag}$ [m/s]		
Month	30%-tile	50%-tile	70%-tile
Jan	7.7	10.0	12.2
Feb	7.2	9.5	11.7
Mar	6.6	8.7	10.7
Apr	5.5	7.4	9.4
May	5.2	7.0	8.9
Jun	5.1	6.9	8.8
Jul	5.3	7.1	9.0
Aug	5.4	7.2	9.1
Sep	6.2	8.3	10.4
Oct	7.2	9.3	11.5
Nov	7.2	9.5	11.8
Dec	7.4	9.9	12.1

#### 4.1.2 Wind speed at hub height

The sections present the wind speed at hub height at 150mMSL.

##### 4.1.2.1 Timeseries

Figure 4-5 shows a time series of wind speed at hub height at KFIIS-1 during the 45-year hindcast period. The mean wind speed is 9.2 m/s, and the maximum wind speed is 34.3 m/s.

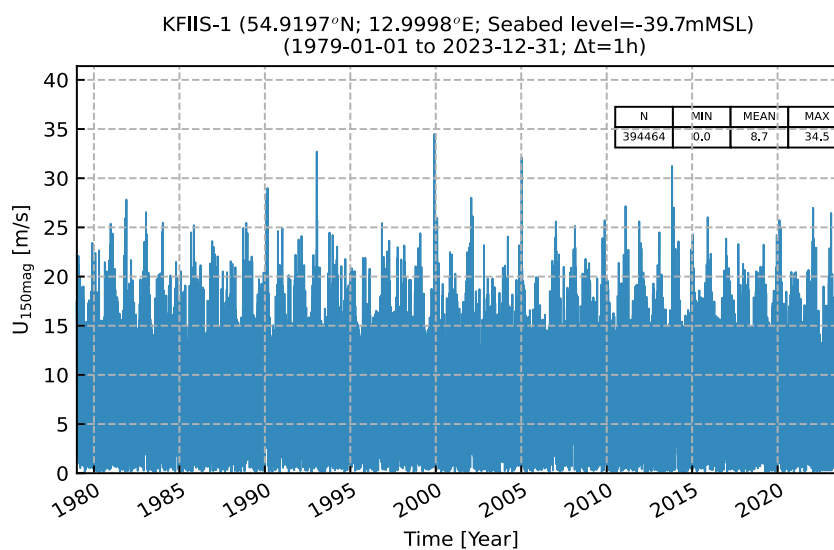


Figure 4-5 Time series of  $U_{150mag}$  at KFIIS-1.

### 4.1.2.2 Windrose

Figure 4-6 shows a wind rose at KFIIS-1, showing the dominant wind coming from the west. Figure 4-7 shows the scatter plot of the wind speed and the wind direction at KFIIS-1. This aligns with the wind rose that the most frequent and dominant direction is west.

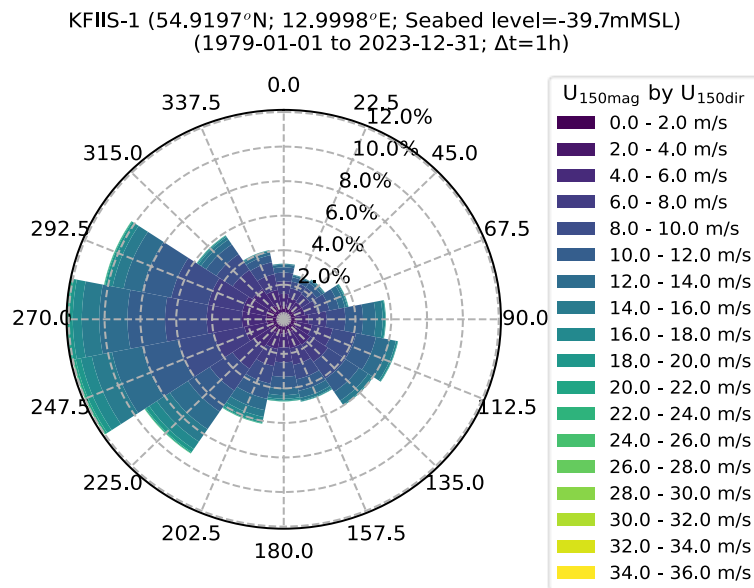


Figure 4-6 Rose plot of  $U_{150mag}$ , sorted by  $U_{150dir}$ , at KFIIS-1.

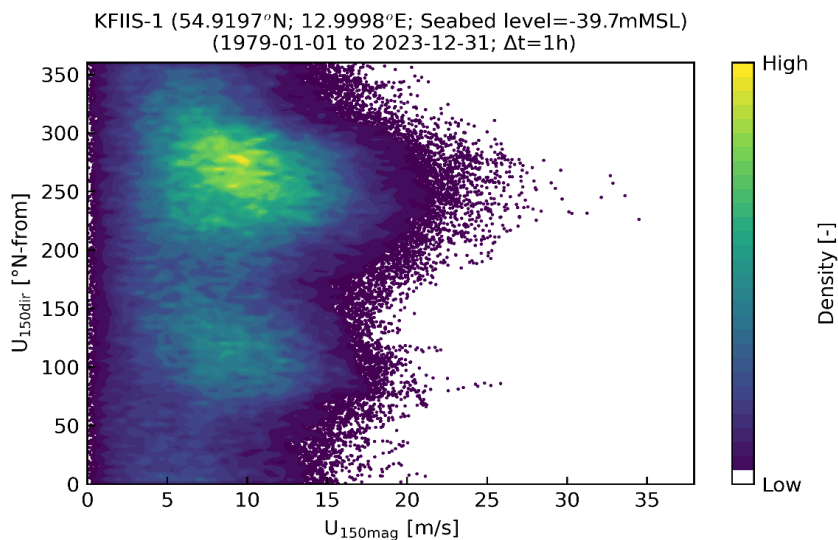


Figure 4-7 Scatter of  $U_{150mag}$  and  $U_{150dir}$  at KFIIS-1.

Table 4-5 Table of  $U_{150mag}$  and  $U_{150dir}$  in percentage, at KFIIS-1.

$U_{150mag}$ [m/s]	$U_{150dir}$ [°N-from]																
	0.0	22.5	45.0	67.5	90.0	112.5	135.0	157.5	180.0	202.5	225.0	247.5	270.0	292.5	315.0	337.5	Omni
0.0 - 2.0	0.22	0.21	0.20	0.21	0.20	0.19	0.20	0.20	0.20	0.23	0.22	0.22	0.23	0.25	0.23	0.23	3.4
2.0 - 4.0	0.56	0.50	0.48	0.46	0.49	0.54	0.61	0.60	0.62	0.64	0.68	0.72	0.73	0.74	0.71	0.62	9.7
4.0 - 6.0	0.69	0.59	0.52	0.54	0.69	0.87	0.97	0.91	0.81	0.88	1.10	1.30	1.37	1.36	1.17	0.88	14.7
6.0 - 8.0	0.73	0.54	0.55	0.71	1.00	1.18	1.19	0.98	0.86	1.01	1.44	1.75	1.97	1.95	1.32	0.93	18.1
8.0 - 10.0	0.50	0.39	0.46	0.68	1.05	1.33	1.17	0.85	0.84	1.03	1.52	2.03	2.33	2.10	1.10	0.70	18.1
10.0 - 12.0	0.30	0.26	0.31	0.54	0.99	1.13	0.91	0.67	0.67	0.90	1.47	2.02	2.10	1.67	0.69	0.42	15.0
12.0 - 14.0	0.15	0.11	0.15	0.34	0.70	0.77	0.62	0.42	0.39	0.67	1.22	1.72	1.57	1.05	0.34	0.17	10.4
14.0 - 16.0	0.05	0.04	0.07	0.13	0.39	0.37	0.28	0.17	0.21	0.40	0.87	1.16	0.97	0.63	0.18	0.08	6.0
16.0 - 18.0	0.01	0.01	0.02	0.06	0.15	0.10	0.06	0.05	0.10	0.25	0.51	0.62	0.50	0.30	0.08	0.04	2.8
18.0 - 20.0	0.00	0.00	0.00	0.02	0.03	0.03	0.01	0.02	0.04	0.11	0.22	0.29	0.21	0.13	0.03	0.01	1.1
20.0 - 22.0	0.00	0.00	0.00	0.01	0.01	0.00	0.00	0.00	0.02	0.03	0.07	0.12	0.08	0.05	0.01	0.00	0.4
22.0 - 24.0	0.00	0.00	0.00	0.00	0.00	0.00	0.00	0.00	0.00	0.01	0.02	0.04	0.04	0.01	0.00	0.00	0.1
24.0 - 26.0	0.00	0.00	0.00	0.00	0.00	0.00	0.00	0.00	0.00	0.00	0.01	0.01	0.02	0.00	0.00	0.00	0.0
26.0 - 28.0	0.00	0.00	0.00	0.00	0.00	0.00	0.00	0.00	0.00	0.00	0.00	0.00	0.01	0.00	0.00	0.00	0.0
28.0 - 30.0	0.00	0.00	0.00	0.00	0.00	0.00	0.00	0.00	0.00	0.00	0.00	0.00	0.00	0.00	0.00	0.00	0.0
30.0 - 32.0	0.00	0.00	0.00	0.00	0.00	0.00	0.00	0.00	0.00	0.00	0.00	0.00	0.00	0.00	0.00	0.00	0.0
32.0 - 34.0	0.00	0.00	0.00	0.00	0.00	0.00	0.00	0.00	0.00	0.00	0.00	0.00	0.00	0.00	0.00	0.00	0.0
34.0 - 36.0	0.00	0.00	0.00	0.00	0.00	0.00	0.00	0.00	0.00	0.00	0.00	0.00	0.00	0.00	0.00	0.00	0.0
All	3.2	2.6	2.8	3.7	5.7	6.5	6.0	4.9	4.8	6.2	9.3	12.0	12.1	10.2	5.9	4.1	100

### 4.1.2.3 Histogram

The histogram on Figure 4-8 provides a visual representation of the binned wind speeds at the hub height at 150mMSL. The 30% quantile is 6.26 m/s, the 50% quantile is 8.44 m/s, and the 70% quantile is 10.74 m/s.

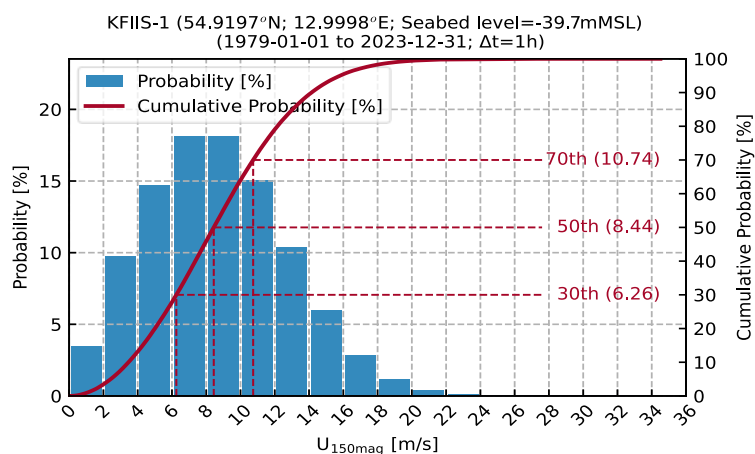


Figure 4-8 Probability plot of  $U_{150mag}$  at KFIIS-1.

The seasonal variation across  $U_{150\text{mag}}$  is shown on Table 4-6. At KFIS-1 the largest wind speeds are expected during winter.

Table 4-6 Probability table of  $U_{150\text{mag}}$ , at KFIS-1.

Season	$U_{150\text{mag}}$ [m/s]		
	30%-tile	50%-tile	70%-tile
Jan	7.7	10.1	12.7
Feb	7.2	9.7	12.3
Mar	6.9	9.2	11.6
Apr	5.7	7.8	10.1
May	5.3	7.4	9.5
Jun	5.2	7.1	9.0
Jul	5.3	7.1	9.0
Aug	5.4	7.2	9.1
Sep	6.2	8.3	10.4
Oct	7.2	9.4	11.6
Nov	7.2	9.5	11.8
Dec	7.4	9.9	12.4



## 5 Water levels

This section presents a summary of the water level data basis established in [6], followed by a presentation of normal and extreme water level conditions at the KFII area.

The total Water Level was separated, by a decomposition done by harmonic analysis, into a tidal and a residual water level component [6]. Table 5-1 summarises the metadata of the dataset.

Table 5-1 Metadata of the water level dataset.

Name	Value
<b>Start Date [UTC]:</b>	1979-01-01 00:00:00
<b>End Date [UTC]:</b>	2023-12-31 23:00:00
<b>Time Step [s]</b>	3600

The water level data is relative to mean sea level (MSL).

The water level analyses are presented in bins of 0.1 m. Table 4.2 presents the water level variables of the dataset, including the bin sizes applied in figures and tables throughout this report. For each variable a derived variable for the tidal component and the residual component exists, denoted with suffix  $t$  and  $r$  respectively.

Table 5-2 Wave variables of the water level dataset

Variable name	Abbrev.	Unit	Bin size
<b>Water Level</b>	WL	mMSL	0.1
<b>Water Level - Tide</b>	WL <sub>t</sub>	mMSL	0.1
<b>Water Level - Residual</b>	WL <sub>r</sub>	mMSL	0.1

In this chapter mainly the Water Level (WL) is presented, In the appendices the full statistics of the tide and residual components can be found.

### 5.1 Normal water level conditions

The normal water level conditions are presented in terms of:

- Time series
- Tidal levels
- Histograms
- Monthly statistics

#### 5.1.1 Timeseries

Figure 5-1 shows a time series of the water level at KFIS-1 during the 45-year period. The decomposition of water levels is explained in part A [6]. The tidal levels are given in section 5.1.2.

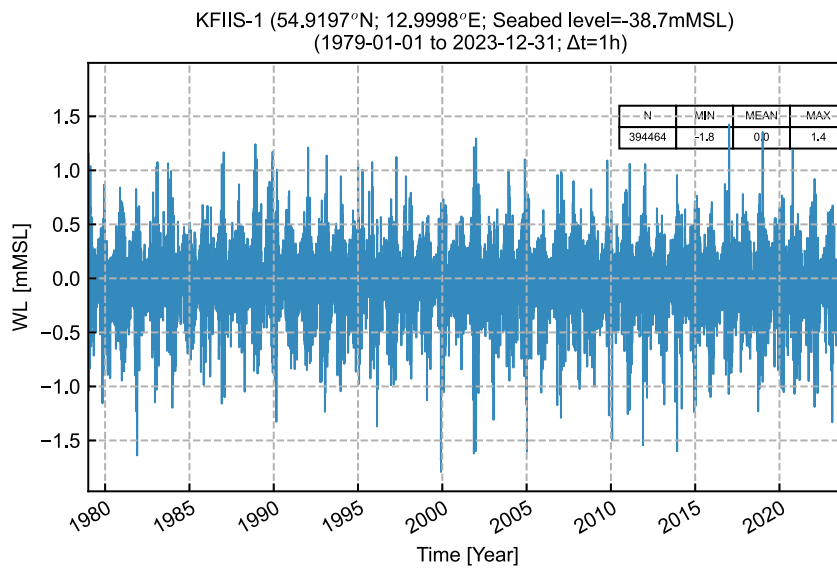


Figure 5-1 Time series of water level at KFIIS-1.

### 5.1.2 Tidal levels

To quantify the tidal levels at KFII the astronomical water levels (tidal levels) are provided below.

Figure 5-1 shows the time series of the total, astronomical tidal and residual water level KFIIS-1, while Table 5-3 summarises the astronomical water levels.

The astronomical water levels are defined as (<https://ntslf.org/tgi/definitions>):

- HAT: Maximum predicted tidal WL.
- MHWS: Average of the two successive high waters reached during the 24 hours when the tidal range is at its greatest (spring tide).
- MHWN: Average of the two successive high waters reached during the 24 hours when the tidal range is at its lowest (neap tide).
- MLWN: Average of the two successive low waters reached during the 24 hours when the tidal range is at its lowest (neap tide).
- MLWS: Average of the two successive low waters reached during the 24 hours when the tidal range is at its greatest (spring tide).
- LAT: Minimum predicted tidal WL.

Table 5-3 Tidal levels at KFI.

Tidal level	Abbrev.	KFIIS -1	KFIIS -2	KFIIS -3	KFIIN -1	KFIIN -2	KFIIN -3	Unit
Highest astronomical tide	HAT	0.13	0.14	0.13	0.13	0.14	0.13	mMSL
Mean high water springs	MHWS	0.06	0.06	0.06	0.06	0.06	0.06	mMSL
Mean high water neaps	MHWN	0.04	0.04	0.04	0.04	0.04	0.04	mMSL
Mean sea level	MSL	0	0	0	0	0	0	mMSL
Mean low water neaps	MLWN	-0.05	-0.05	-0.04	-0.05	-0.05	-0.04	mMSL
Mean low water springs	MLWS	-0.07	-0.08	-0.07	-0.07	-0.08	-0.07	mMSL
Lowest astronomical tide	LAT	-0.17	-0.18	-0.17	-0.17	-0.18	-0.17	mMSL

### 5.1.3 Histogram

Figure 5-2 shows a histogram of total water level at KFIIS-1.

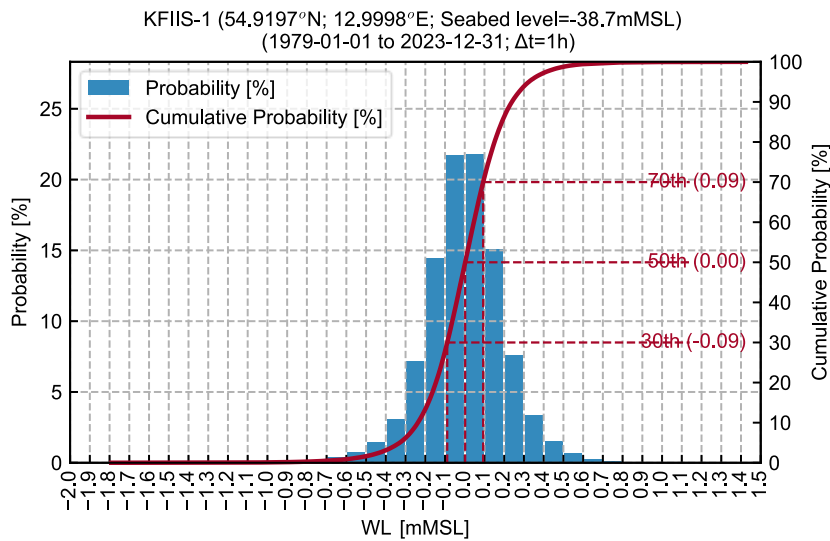


Figure 5-2 Histogram of the water level, WL, at KFIIS-1.

### 5.1.4 Monthly statistics

Figure 5-3 shows the monthly statistics of the water level at KFIIS-1. The variation in the monthly mean water level is small, about 0.2 m during the year. The highest (+1.6 mMSL) as well as the lowest (-1.6 mMSL) water levels occur during winter.

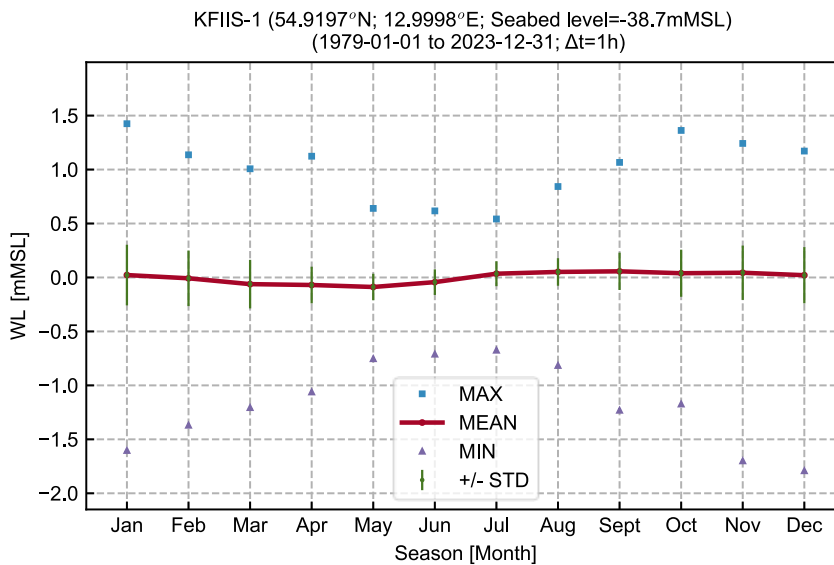


Figure 5-3 Monthly statistics of the water level, WL, at KFIIS-1.

## 5.2 Extreme water level conditions

Extreme water level conditions are established using Extreme Value Analysis. The analysis is based on its performance and sensitivity to selection of distribution, threshold selection method,  $\lambda$ -value evaluation, and fitting

estimator. A description of the methodology and the selection of settings is available in Appendix B.

For both the low- and high-water levels, the 3-parameter Weibull distribution was fitted by the least square method to 45 peak events ( $\lambda=1$ ) for high water and 180 peak events ( $\lambda=4$ ) for low water separated by at least 72 hours. It is noted that the average relative error on the residual low water level in the EVA does not stabilize until after 3 events per year, therefore 4 events have been preferred. It is noted, however, that the actual effect on the estimated quantiles is very low for the range of 1-4 events, thus using 1 or 4 events will not significantly impact results.

### 5.2.1 Extreme high-water levels

The extreme total high water level fit for the 45-year hindcast period is shown on Figure 5-4. Values for selected return periods are additionally shown in Table 5-4. The Weibull distribution fitted with the least squares method is shown along the upper 97.5% and lower 2.5% confidence interval. The fitted distribution aligns well to the hindcast data points, also at the tail, and all events are within the confidence levels. The 50-year total high-water level is 1.6 mMSL.

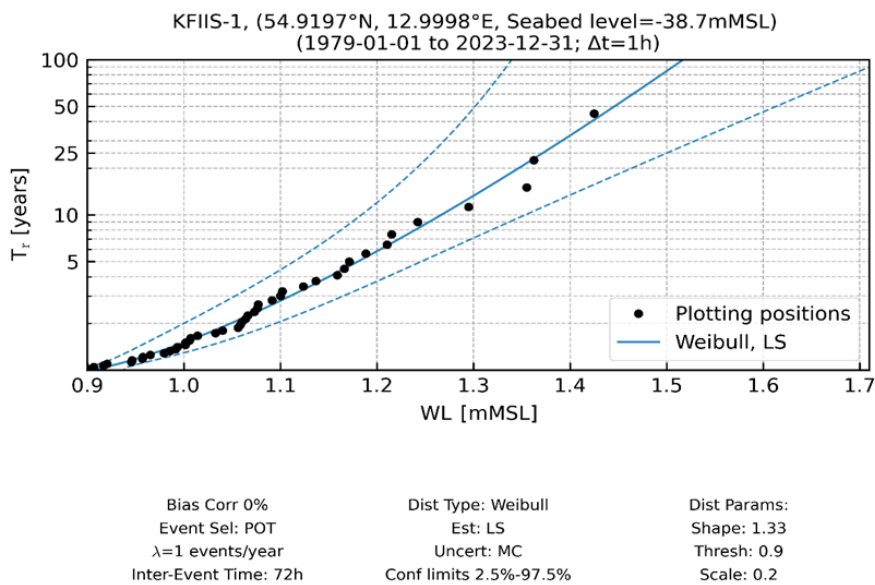


Figure 5-4 Marginal EVA of total high-water level, WL, at KFIIS-1.

Table 5-4 Estimates of total water level, WL, at KFIIS-1.

	WL [mMSL]					
	Quantile	T <sub>r</sub> 1	T <sub>r</sub> 5	T <sub>r</sub> 10	T <sub>r</sub> 25	T <sub>r</sub> 50
Omni	2.5%-tile	0.8	1.1	1.2	1.2	1.3
	50%-tile	0.9	1.2	1.3	1.4	1.4
	97.5%-tile	0.9	1.2	1.4	1.5	1.6

### 5.2.2 Extreme residual high-water levels

The extreme residual high water level fit for the 45-year hindcast period is shown on Figure 5-5. Values for selected return periods are additionally shown in Table 5-5. The Weibull distribution fitted with the least squares method is shown along the upper 97.5% and lower 2.5% confidence interval. The fitted distribution aligns well to the hindcast data points, also at the tail, and all events are within the confidence levels. The 50-year residual high-water level is 1.4 mMSL.

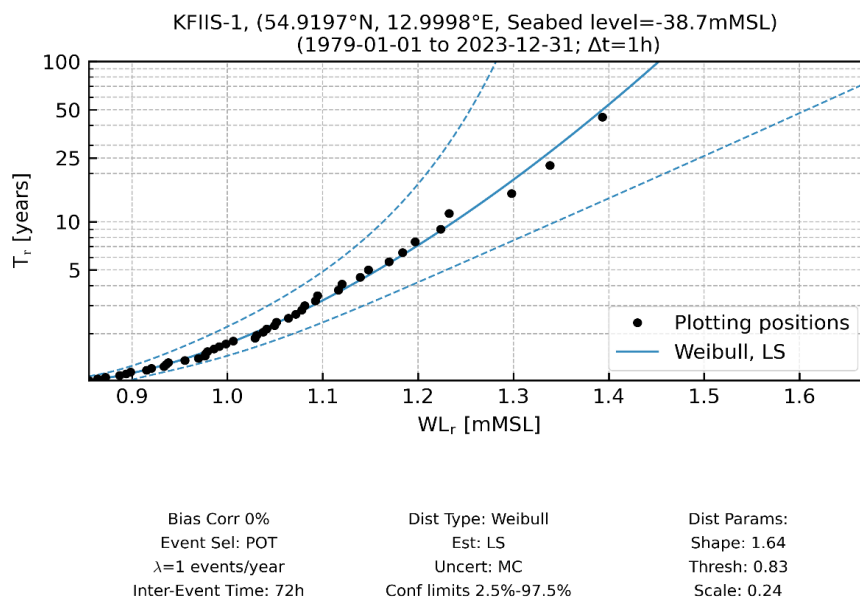


Figure 5-5 Marginal EVA of residual high-water level,  $WL_r$ , at KFIIS-1.

Table 5-5 Estimates of residual high-water level,  $WL_r$ , at KFIIS-1.

	$WL_r$ [mMSL]					
	Quantile	$T_r$ 1	$T_r$ 5	$T_r$ 10	$T_r$ 25	$T_r$ 50
Omni	2.5%-tile	0.8	1.1	1.2	1.2	1.3
	50%-tile	0.8	1.2	1.2	1.3	1.4
	97.5%-tile	0.9	1.2	1.3	1.5	1.6

### 5.2.3 Extreme low-water levels

The extreme low water level fit for the 45-year hindcast period is shown on Figure 5-6. Note that the low water levels are positive on the figure. Values for selected return periods are additionally shown in Table 5-6. The Weibull distribution fitted with the least squares method is shown along the upper 97.5% and lower 2.5% confidence interval. The fitted distribution aligns well to the hindcast data points, also at the tail, and all events are within the confidence levels. The 50-year total low-water level is -1.8 mMSL.

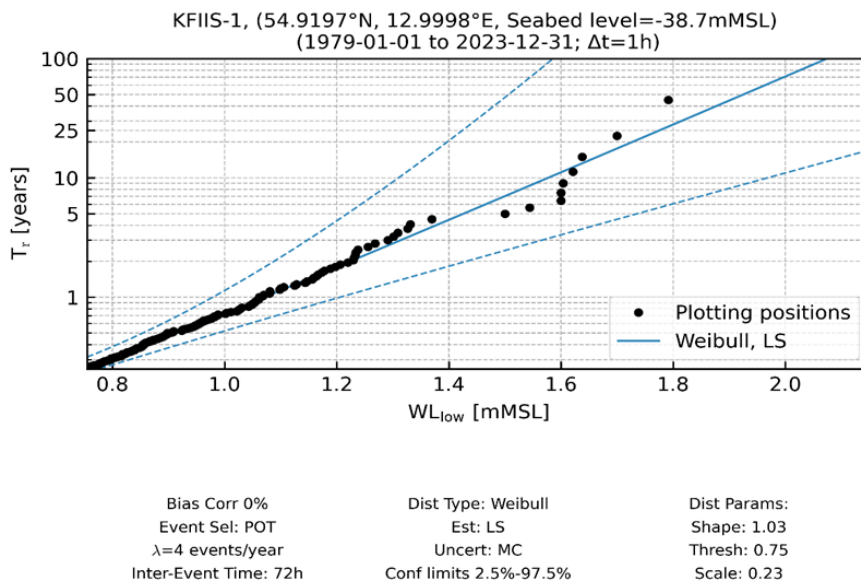


Figure 5-6 Marginal EVA of low-water level,  $WL_{low}$ , at KFIIS-1. Note that the low water levels are positive on the figure.

Table 5-6 Estimates of low water level,  $WL_{low}$ , at KFIIS-1.

	$WL_{low}$ [mMSL]					
	Quantile	$T_r$ 1	$T_r$ 5	$T_r$ 10	$T_r$ 25	$T_r$ 50
Omni	2.5%-tile	-1	-1.2	-1.3	-1.4	-1.4
	50%-tile	-1.1	-1.4	-1.6	-1.8	-1.9
	97.5%-tile	-1.2	-1.7	-2	-2.2	-2.6

### 5.2.4 Extreme residual low-water levels

The extreme residual low water level fit for the 45-year hindcast period is shown on Figure 5-7. Note that the low water levels are positive on the figure. Values for selected return periods are additionally shown in Table 5-6. The Weibull distribution fitted with the least squares method is shown along the upper 97.5% and lower 2.5% confidence interval. The fitted distribution aligns well to the hindcast data points, also at the tail, and all events are within the confidence levels. The 50-year residual low-water level is -1.8 m MSL.

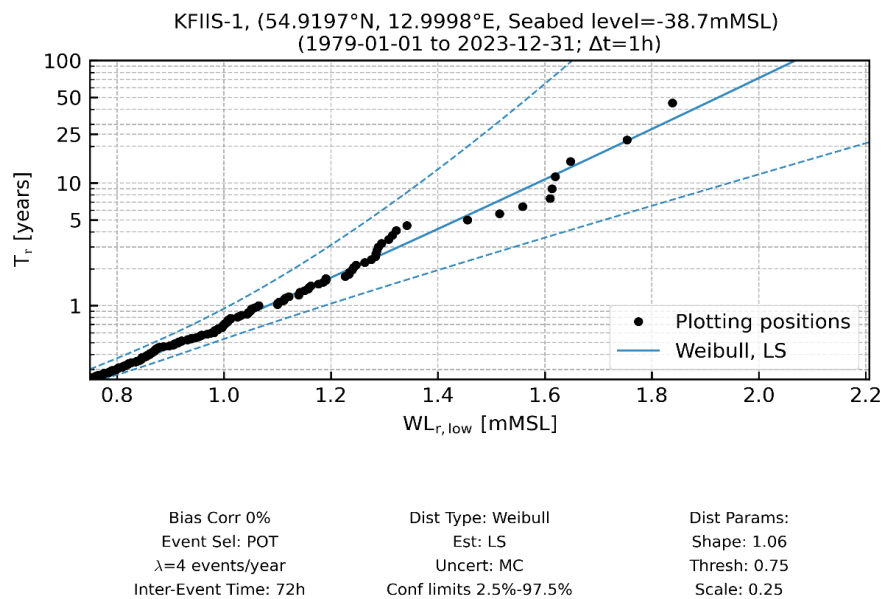


Figure 5-7 Marginal EVA of residual low-water level,  $WL_{r,low}$ , at KFIIS-1. Note that the low water levels are positive on the figure.

Table 5-7 Estimates of residual low water level,  $WL_{r,low}$ , at KFIIS-1.

		$WL_{r,low}$ [mMSL]					
		Quantile	$T_r 1$	$T_r 5$	$T_r 10$	$T_r 25$	$T_r 50$
Omni	2.5%-tile		-1	-1.2	-1.3	-1.4	-1.5
	50%-tile		-1.1	-1.4	-1.6	-1.8	-1.9
	97.5%-tile		-1.2	-1.8	-1.9	-2.4	-2.5

### 5.2.5 Maps of Extreme high-water levels

From Figure 5-8 to Figure 5-12 is shown the spatial variation of the total high water levels across the data delivery area of KFII for return periods of 1, 5, 10, 25 and 50 years based on individual extreme value analysis at each model grid point.



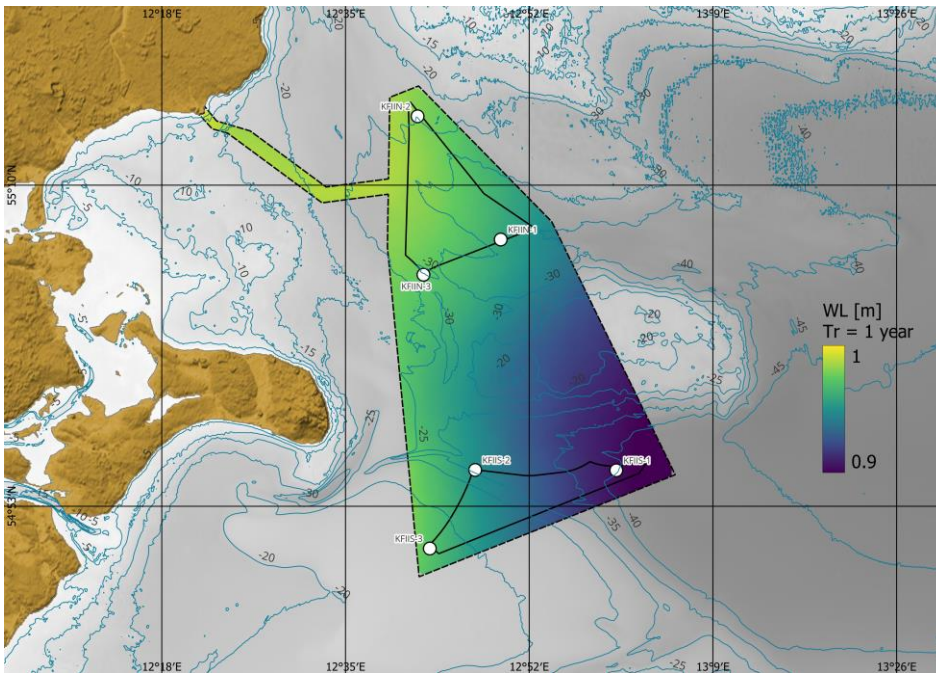


Figure 5-8 Spatial variation across the data delivery area of KFII of total water level, WL, for return periods of 1 years. The colour map shows the water level, and the contours show water depths.

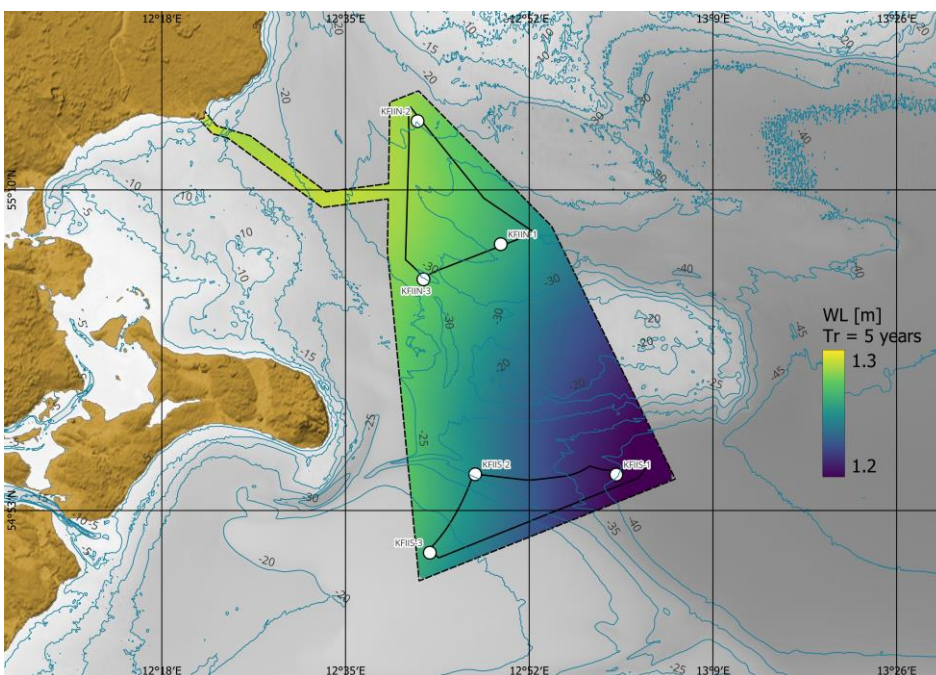


Figure 5-9 Spatial variation across the data delivery area of KFII of total water level, WL, for return periods of 5 years. The colour map shows the water level, and the contours show water depths.

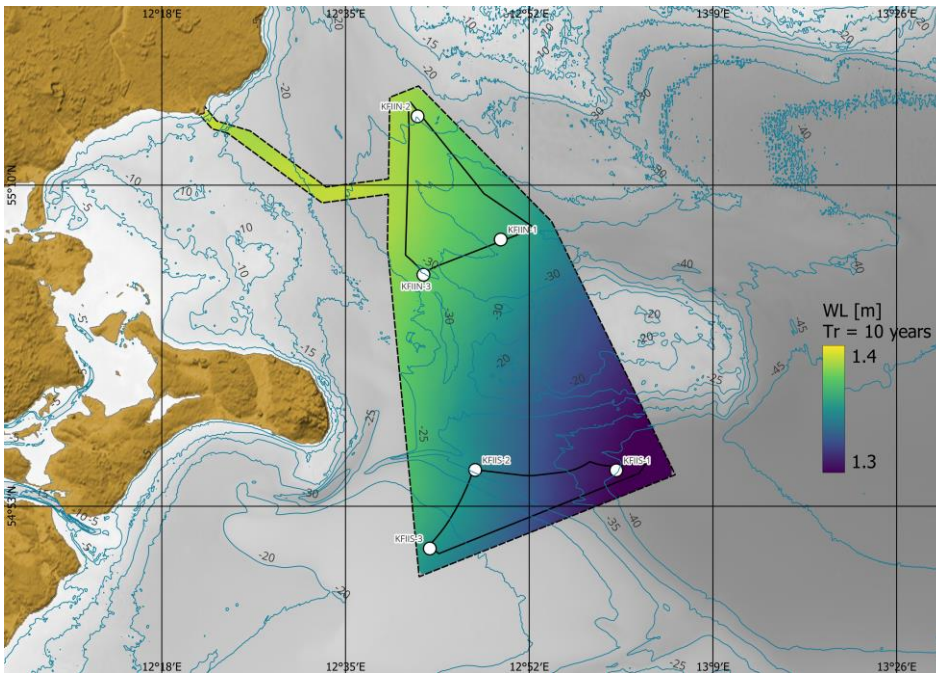


Figure 5-10 Spatial variation across the data delivery area of KFIIL of total water level, WL, for return periods of 10 years. The colour map shows the water level, and the contours show water depths.

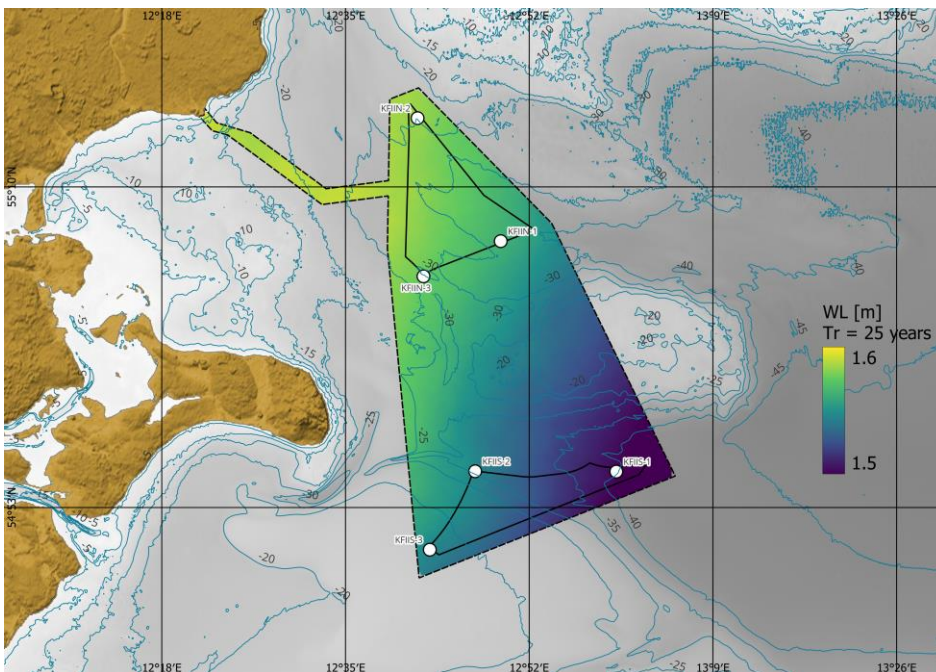


Figure 5-11 Spatial variation across the data delivery area of KFIIL of total water level, WL, for return periods of 25 years. The colour map shows the water level, and the contours show water depths.

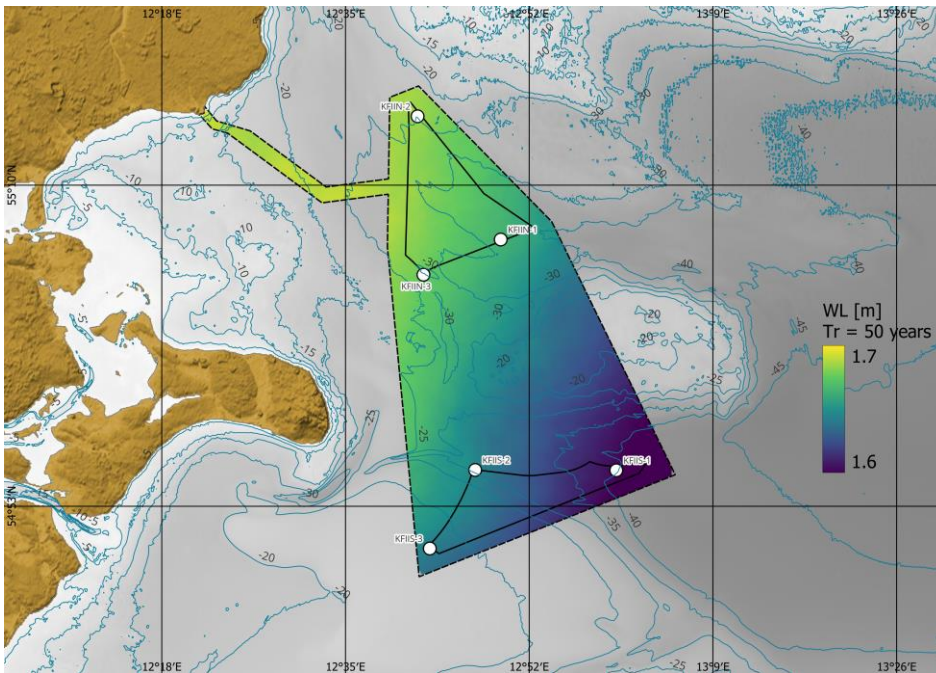


Figure 5-12 Spatial variation across the data delivery area of KFII of total water level, WL, for return periods of 50 years. The colour map shows the water level, and the contours show water depths.

### 5.2.6 Maps of Extreme low-water levels

From Figure 5-13 to Figure 5-17 is the spatial variation of the total low water levels across the data delivery area of KFII for return periods of 1, 5, 10, 25 and 50 years based on individual extreme value analysis on each model grid point.

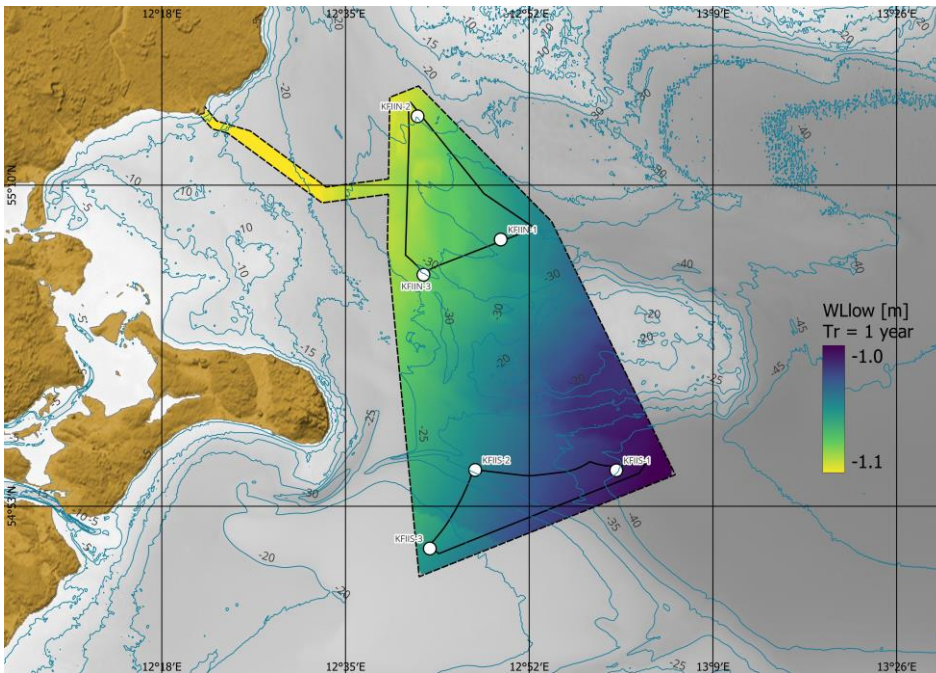


Figure 5-13 Spatial variation across the data delivery area of KFII of total water level,  $W_{Low}$ , for return periods of 1 years. The colour map shows the low water level, and the contours show water depths.

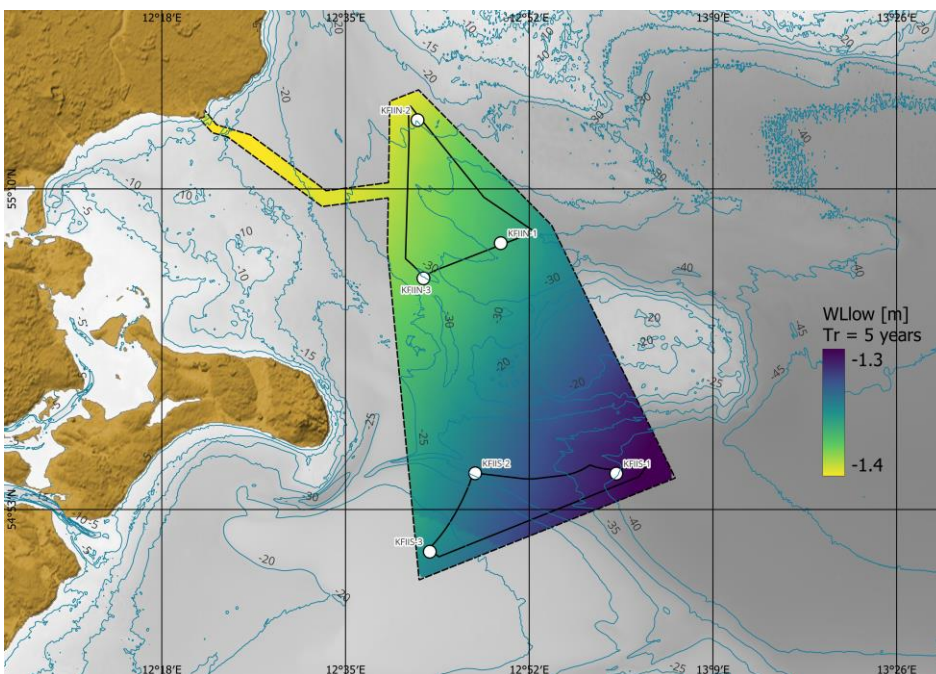


Figure 5-14 Spatial variation across the data delivery area of KFII of total water level,  $W_{Low}$ , for return periods of 5 years. The colour map shows the low water level, and the contours show water depths.

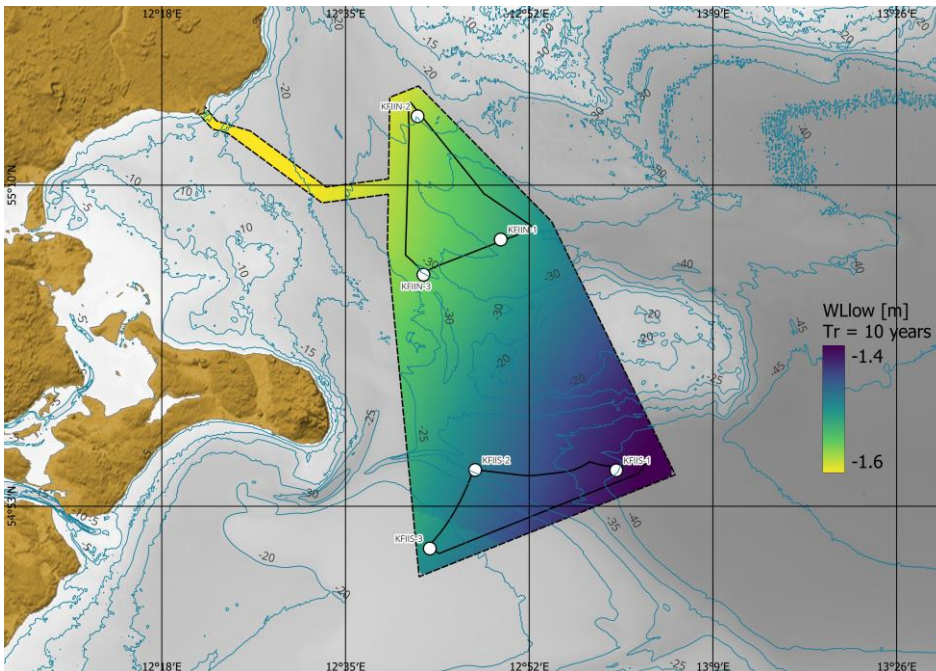


Figure 5-15 Spatial variation across the data delivery area of KFIIL of total water level,  $W_{Low}$ , for return periods of 10 years. The colour map shows the low water level, and the contours show water depths.

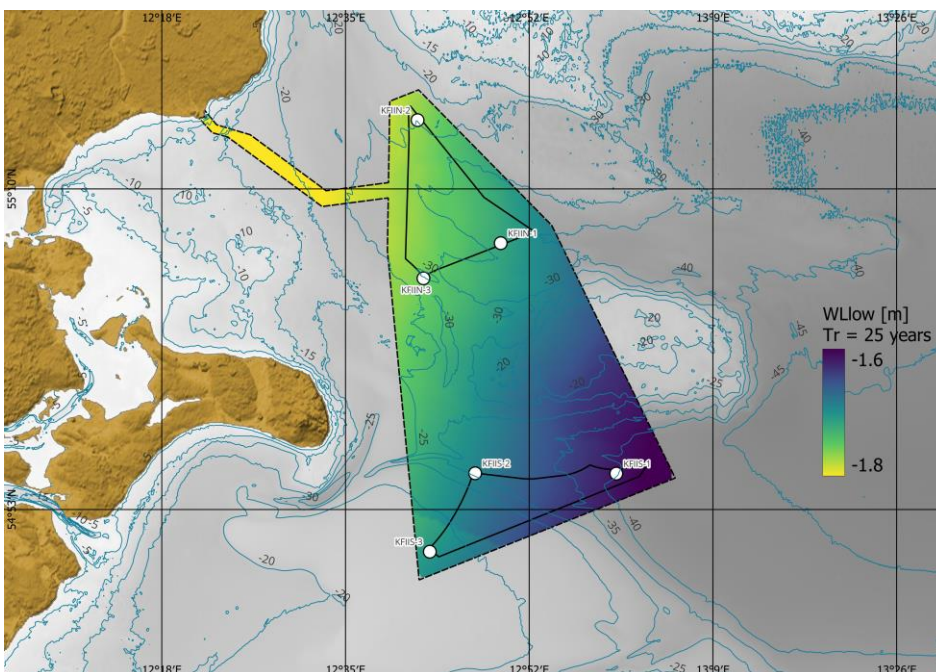


Figure 5-16 Spatial variation across the data delivery area of KFIIL of total water level,  $W_{Low}$ , for return periods of 25 years. The colour map shows the low water level, and the contours show water depths.

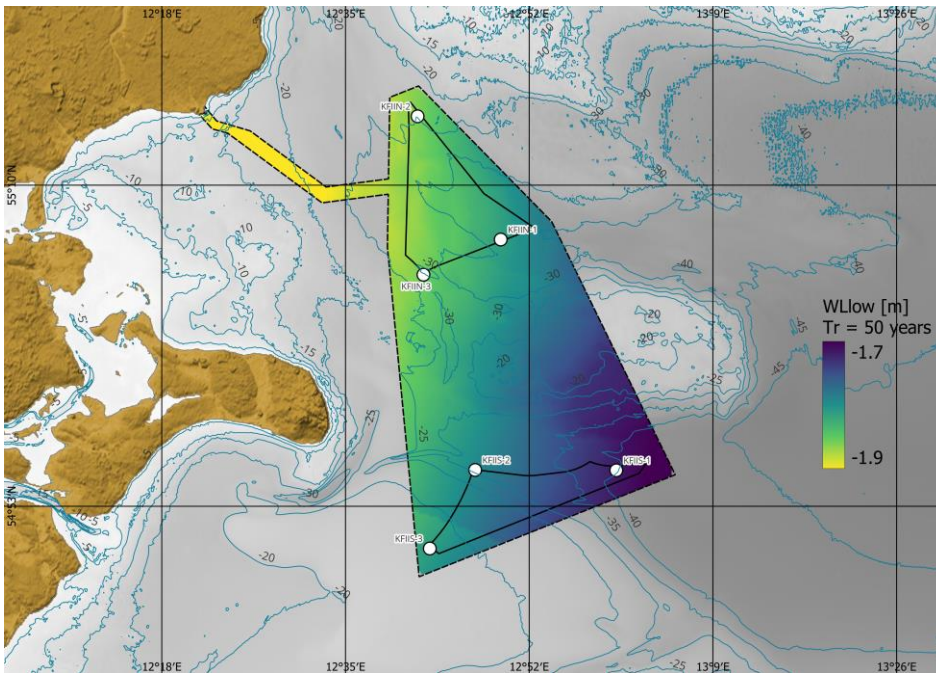


Figure 5-17 Spatial variation across the data delivery area of KFII of total water level,  $WL_{low}$ , for return periods of 50 years. The colour map shows the low water level, and the contours show water depths.

## 6 Current conditions

**This section presents a summary of the current data basis established in [6], followed by a presentation of normal and extreme current conditions at the KFII area.**

The current consists of a tidal and a residual component. Table 6-1 summarises the metadata of the dataset.

Table 6-1 Metadata of the wave dataset.

Name	Value
<b>Start Date [UTC]:</b>	1979-01-01 00:00:00
<b>End Date [UTC]:</b>	2023-12-31 23:00:00
<b>Time Step [s]</b>	3600

The current analyses are presented in bins of 0.1 m/s. Table 4.2 presents the current variables of the dataset, including the bin sizes applied in figures and tables throughout this report. For each variable in the table a derived variable for the tidal component and the residual component exists, denoted with suffix  $t$  and  $r$  respectively. This chapter presents the total current only, tidal and residual components can be found in the appendices.

Due to the method applied for extension of the 3D data, peak current speeds are in some points higher than what can be expected and is considered to be conservative. It is advisable to explore this further during the detailed design phase.

The data is presented at 3 depths throughout the water column, near surface, mid depth, and near-bed.

Table 6-2 Total current variables of the hydrodynamic dataset

Variable name	Abbrev.	Unit	Bin size
<b>Current speed – near surface</b>	CS <sub>stot</sub>	m/s	0.1
<b>Current speed – mid depth</b>	CS <sub>mtot</sub>	m/s	0.1
<b>Current speed – near bed</b>	CS <sub>btot</sub>	m/s	0.1
<b>Current direction – near surface</b>	CD <sub>stot</sub>	°N-going	22.5
<b>Current direction – mid depth</b>	CD <sub>mtot</sub>	°N-going	22.5
<b>Current direction – near bed</b>	CD <sub>btot</sub>	°N-going	22.5

### 6.1 Normal current conditions

The normal current conditions are presented in terms of:

- Time series
- Current roses
- Scatter plots
- Histograms
- Monthly statistics

- Directional statistics

### 6.1.1 Timeseries

Figure 6-1, Figure 6-2 and Figure 6-3 shows the time series of the total current speed at 3 levels at KFIIS-1 during the 45-year period. The lowest, mean, and highest current speed for each level is summarised in Table 6-3.

Table 6-3 Summary of current speed at 3 depths at KFIIS-1.

Current speed [m/s]	MIN	MEAN	MAX
<b>CS<sub>stot</sub> [m/s]</b>	0.0	0.2	1.7
<b>CS<sub>mtot</sub> [m/s]</b>	0.0	0.1	1.0
<b>CS<sub>btot</sub> [m/s]</b>	0.0	0.1	0.6

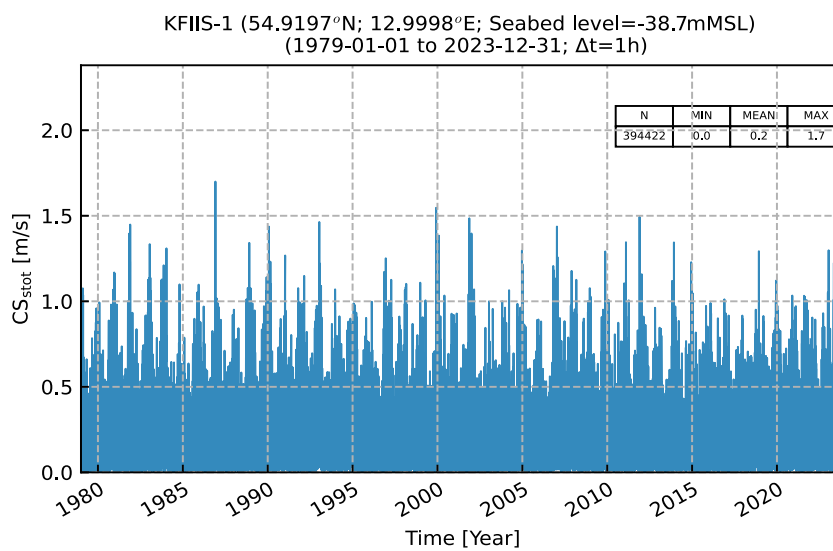


Figure 6-1 Time series of CS<sub>stot</sub> at KFIIS-1.



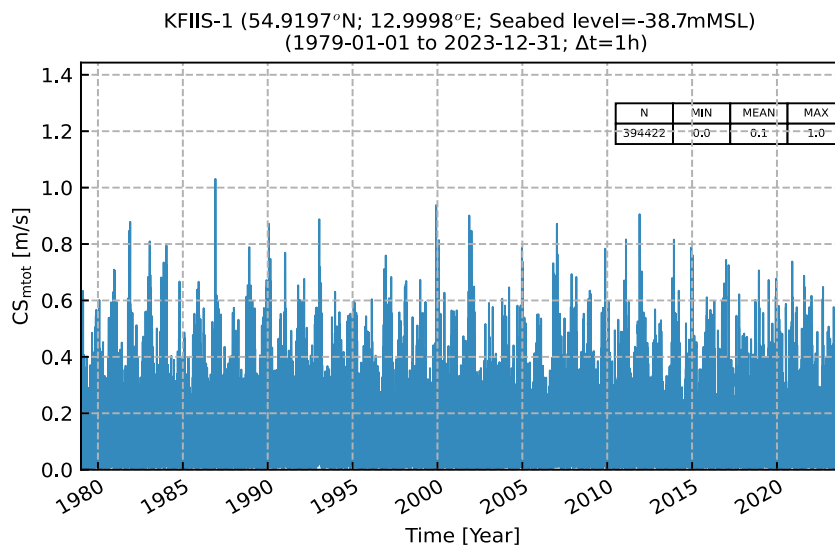


Figure 6-2 Time series of  $CS_{tot}$  at KFIIS-1.

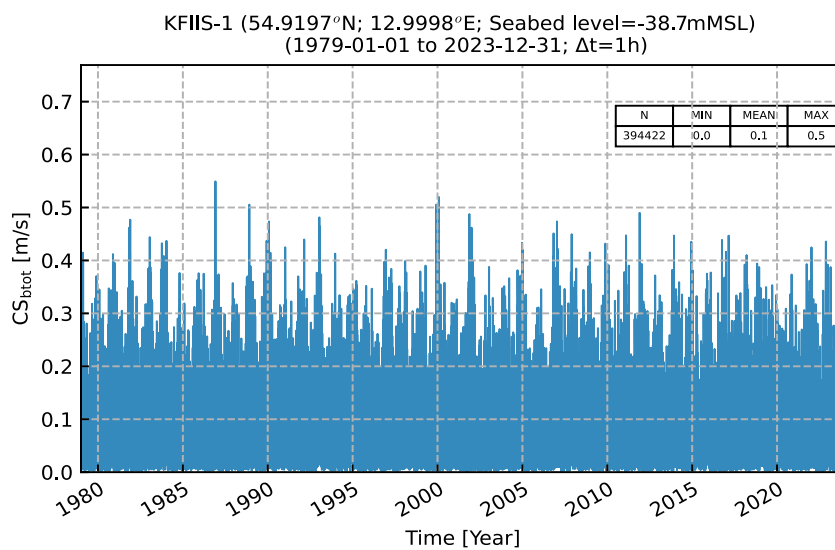


Figure 6-3 Time series of  $CS_{bot}$  at KFIIS-1.

### 6.1.2 Current roses

Figure 6-4, Figure 6-5 and Figure 6-6 shows roses of current speed at near-surface, mid-depth, and near-seabed at KFIIS-1. The near-surface and mid current shows currents predominantly going east and west. At near-seabed, the current is predominantly going southwest and northeast.

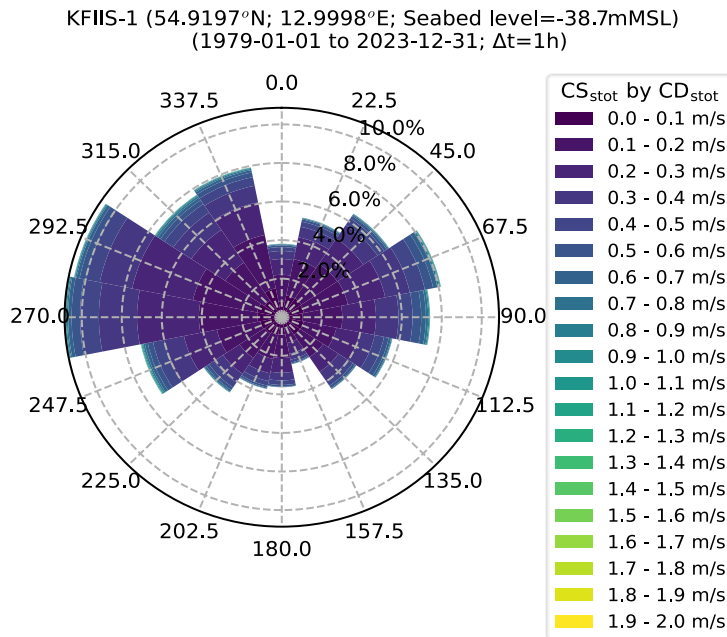


Figure 6-4 Rose plot of CS<sub>stot</sub> at KFIIS-1.

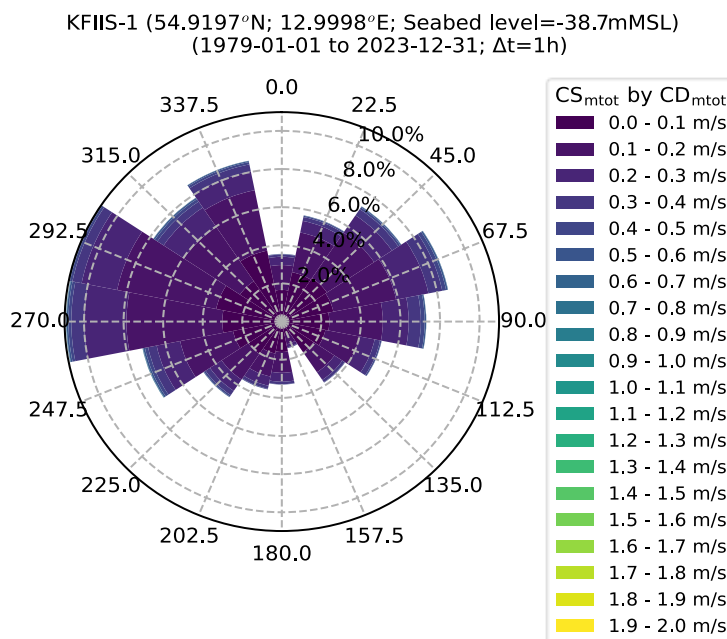


Figure 6-5 Rose plot of CS<sub>mt0t</sub> at KFIIS-1.

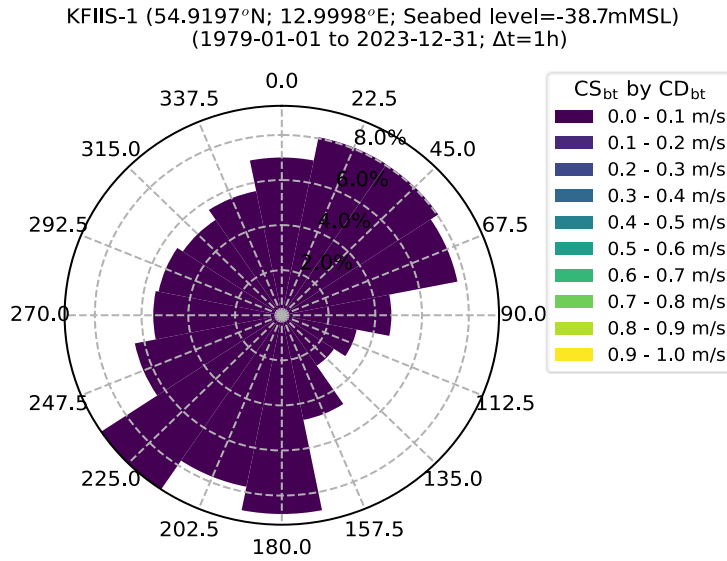


Figure 6-6 Rose plot of  $CS_{bt}$  at KFIIS-1.

### 6.1.3 Histogram

Figure 6-7, Figure 6-8 and Figure 6-9 show the histogram current speed at KFIIS-1, at near-surface, mid-depth, and near-seabed, respectively.

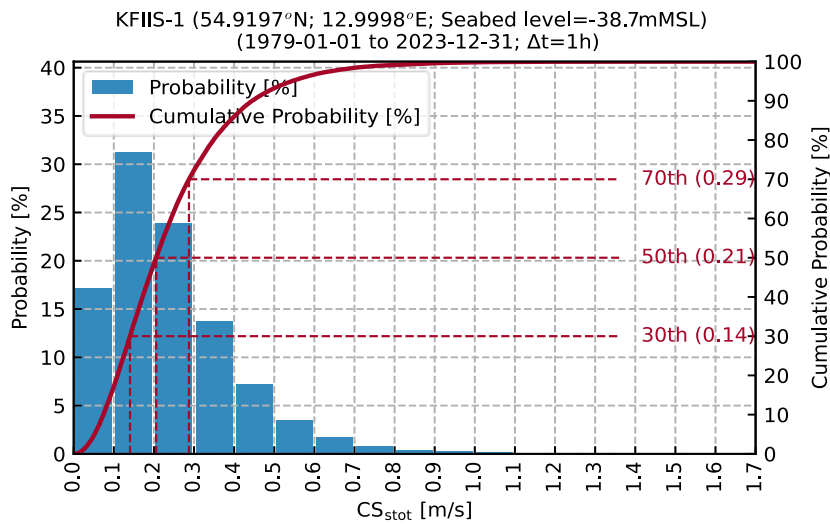


Figure 6-7 Probability plot of  $CS_{stot}$  at KFIIS-1.

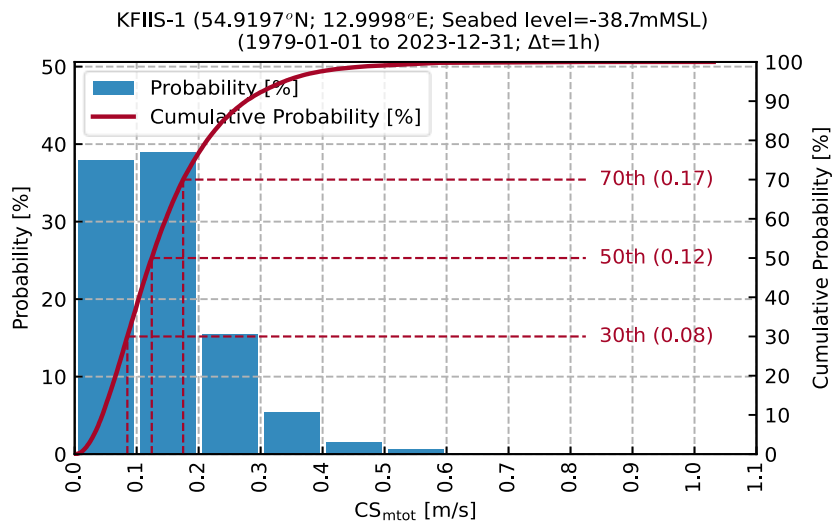


Figure 6-8 Probability plot of CS<sub>mtot</sub> at KFIIS-1.

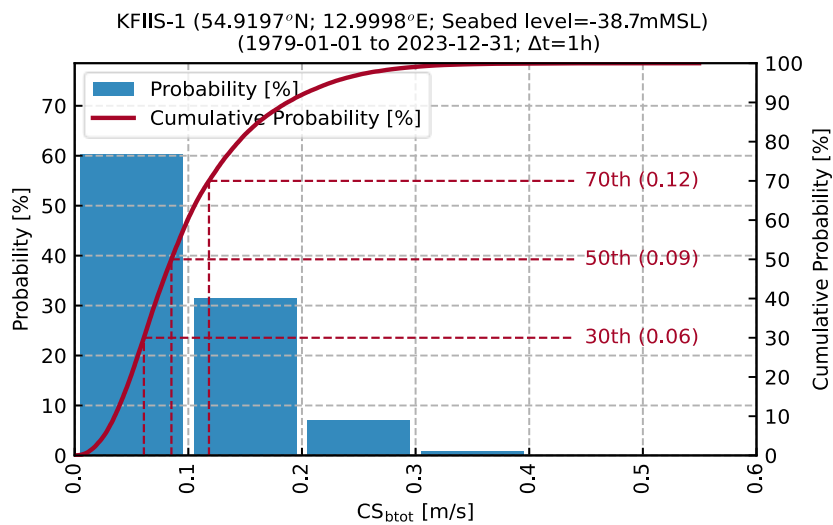


Figure 6-9 Probability plot of CS<sub>btot</sub> at KFIIS-1.

### 6.1.4 Monthly statistics

Figure 6-10, Figure 6-11 and Figure 6-12 show the monthly statistics of current speed at KFIIS-1, at near-surface, mid-depth, and near-seabed, respectively.

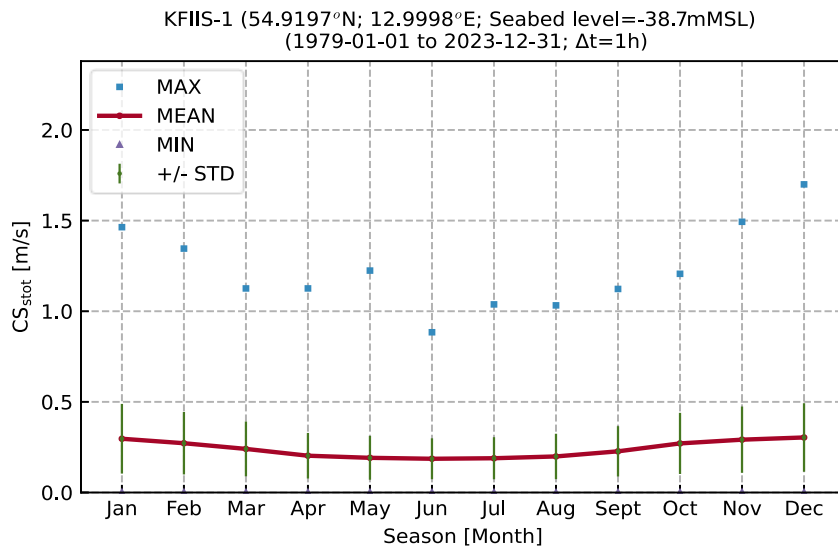


Figure 6-10 Monthly statistics of  $CS_{stot}$  at KFIIS-1.

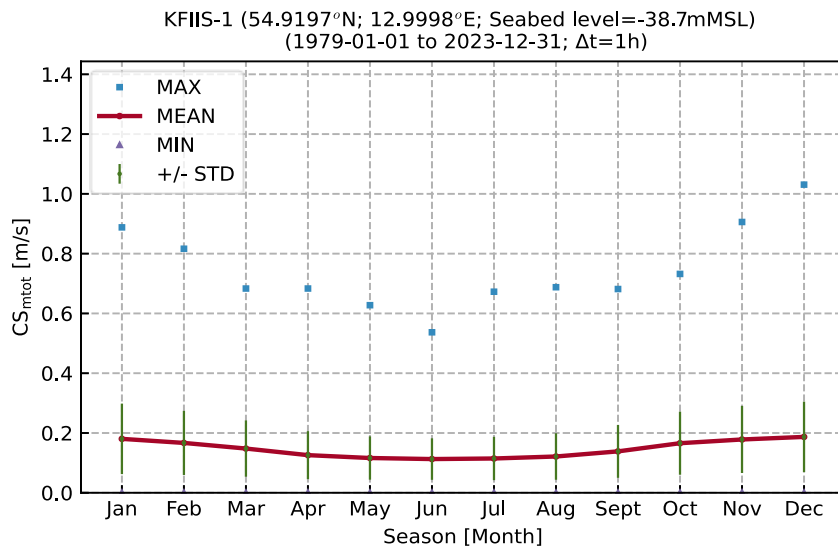


Figure 6-11 Monthly statistics of  $CS_{mtot}$  at KFIIS-1.

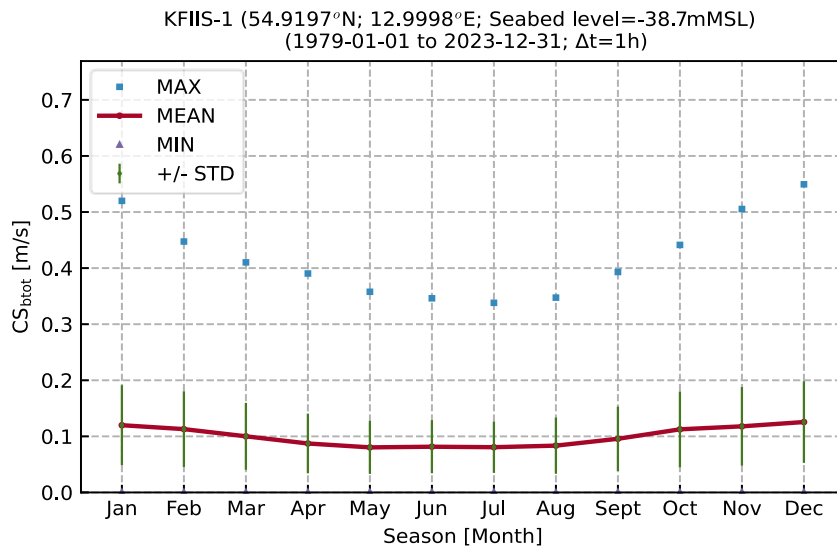


Figure 6-12 Monthly statistics of  $CS_{tot}$  at KFIIS-1.

### 6.1.5 Directional statistics

Figure 6-13, Figure 6-14 and Figure 6-15 show the directional statistics of current speed at KFIIS-1, at near-surface, mid-depth, and near-seabed, respectively.

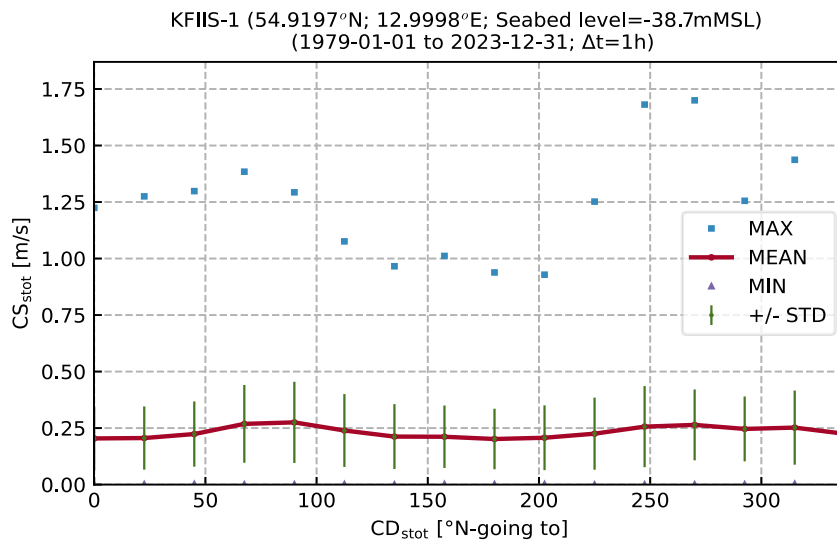


Figure 6-13 Directional statistics of  $CS_{tot}$ , sorted by  $CD_{tot}$ , at KFIIS-1.

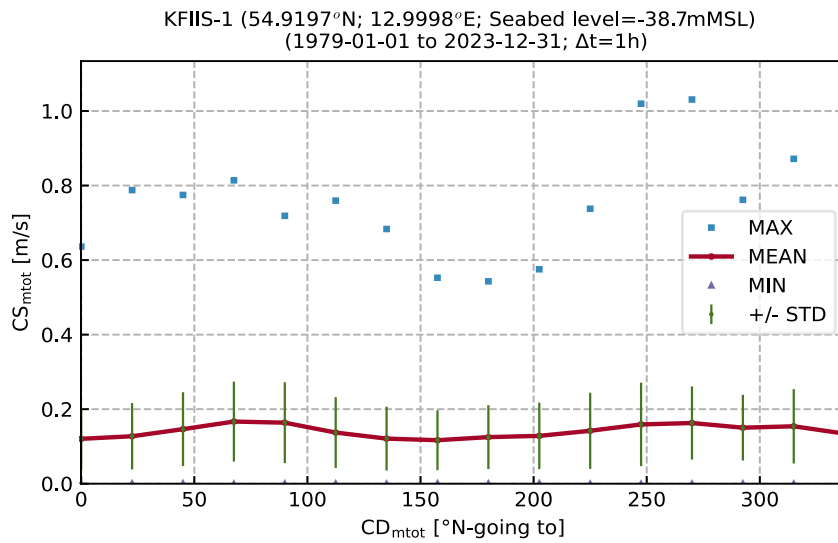


Figure 6-14 Directional statistics of  $CS_{tot}$ , sorted by  $CD_{tot}$ , at KFIIS-1.

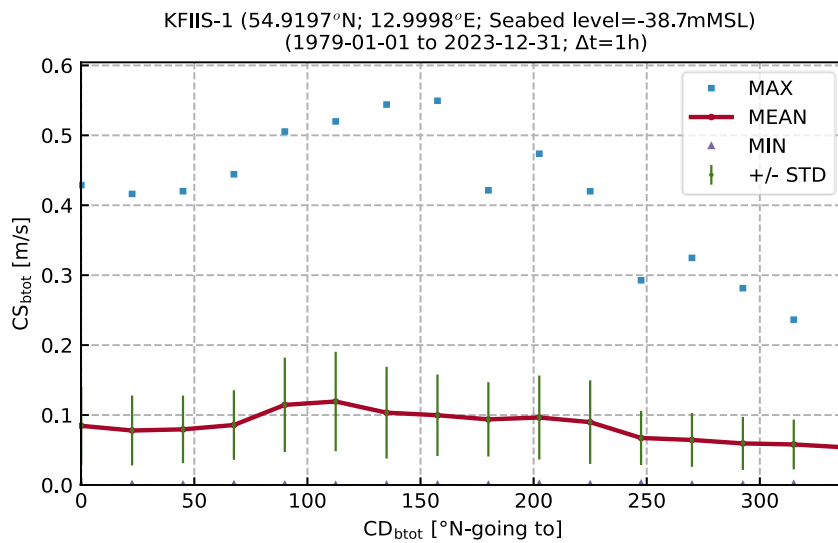


Figure 6-15 Directional statistics of  $CS_{bot}$ , sorted by  $CD_{bot}$ , at KFIIS-1.

### 6.1.6 Vertical profiles of current speed, temperature, and salinity

The hydrodynamic dataset also includes oceanographic variables, covering a 10-year period from 2014 to 2023. These variables are detailed in Table 6-4 and are available at all model levels throughout the water column. These levels are used for profiling.

Table 6-4 Oceanographic variables of the hydrodynamic dataset

Variable name	Abbrev.	Unit	Bin size
<b>Current speed</b>	CS	m/s	0.1
<b>Seawater temperature</b>	T <sub>sw</sub>	°C	1
<b>Salinity</b>	Sal	PSU	2

In Figure 6-16 is the seasonal division of the vertical profile presented across 3-month groups. Summer is Jun, Jul, Aug. Fall is Sep, Oct, Nov. Winter is Dec, Jan, Feb. Spring is Mar, Apr, May. Figure 6-17 includes each individual month.

The current speeds are largest in the winter and smallest in the summer. The upper body of the water is hottest in the summer and coldest in the winter. The lower water bodies are coldest in spring and hottest in fall. The thermocline is not distinct during winter, spring and fall. In the summer period the thermocline ranges from approximately -5 mMSL to -20 m MSL. The halocline is pronounced in all seasons and ranges from approximately -5 mMSL to seabed.

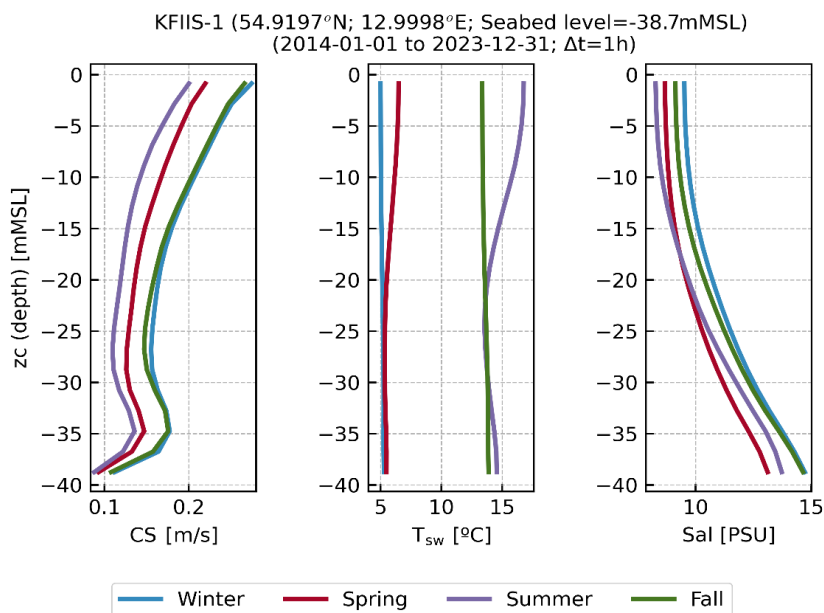


Figure 6-16 Profiles of current speed, Sea water temperature and salinity for each season winter, spring, summer, and fall.



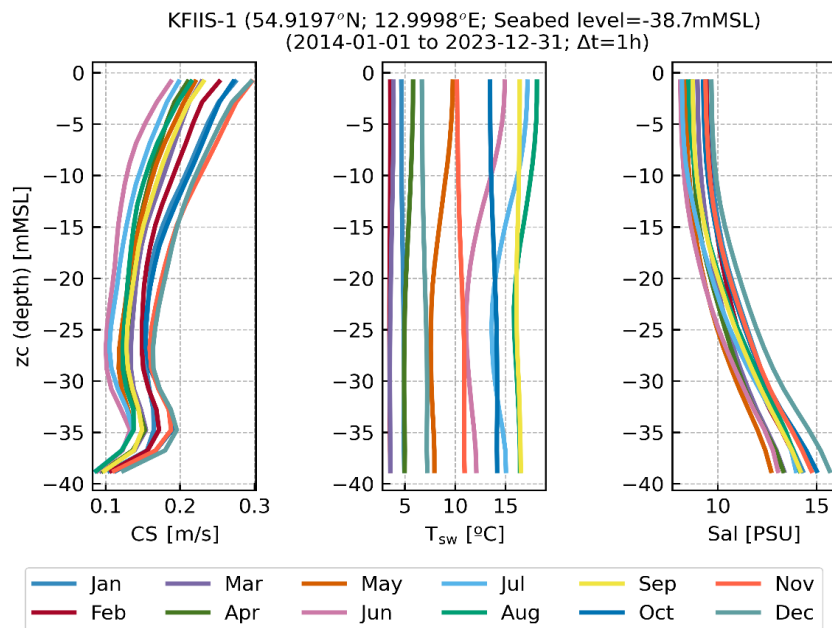


Figure 6-17 Profiles of current speed, Sea water temperature and salinity for each month.

### 6.1.7 Maps of $C_s$

Figure 6-18 to Figure 6-29 Figure 7-13 present maps across the data delivery area of the normalised moment of the current speed,  $C_s$ , calculated as follows.

$$\bar{C}_s = \left[ \frac{1}{N} \sum_{i=1}^N C_{s_i}^m \right]^{\frac{1}{m}}$$

where  $m = (1,2,4,5)$  is the power coefficient, and  $N$  is the total number of hindcast data points.  $m = 1$  is the mean  $C_s$  and  $m = 2$  is the root-mean-square of current speed.

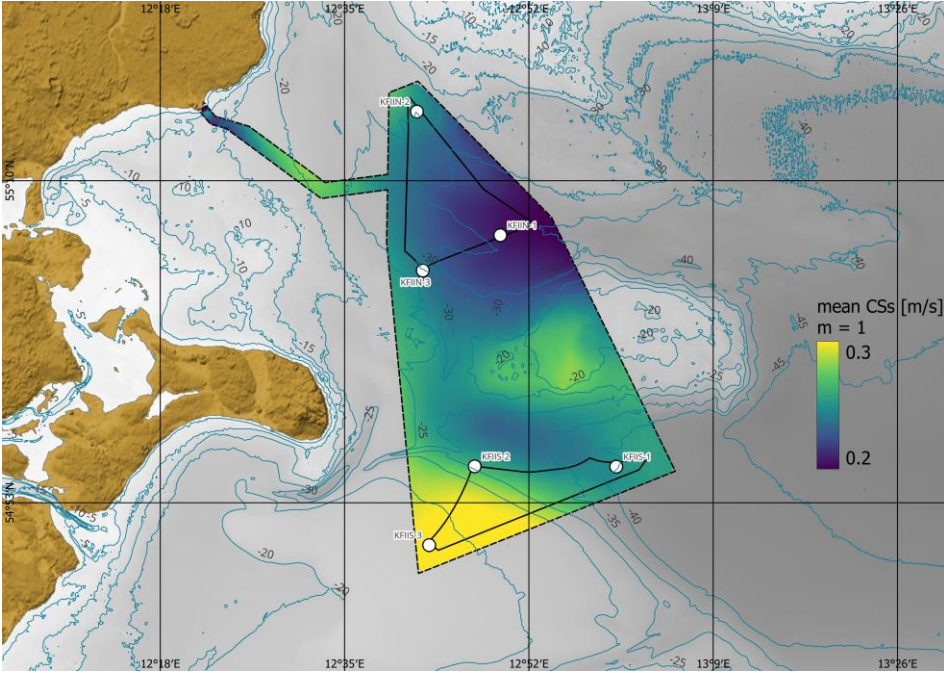


Figure 6-18 Spatial variation of moments of  $C_{Ss}$  across the data delivery area,  $m=1$

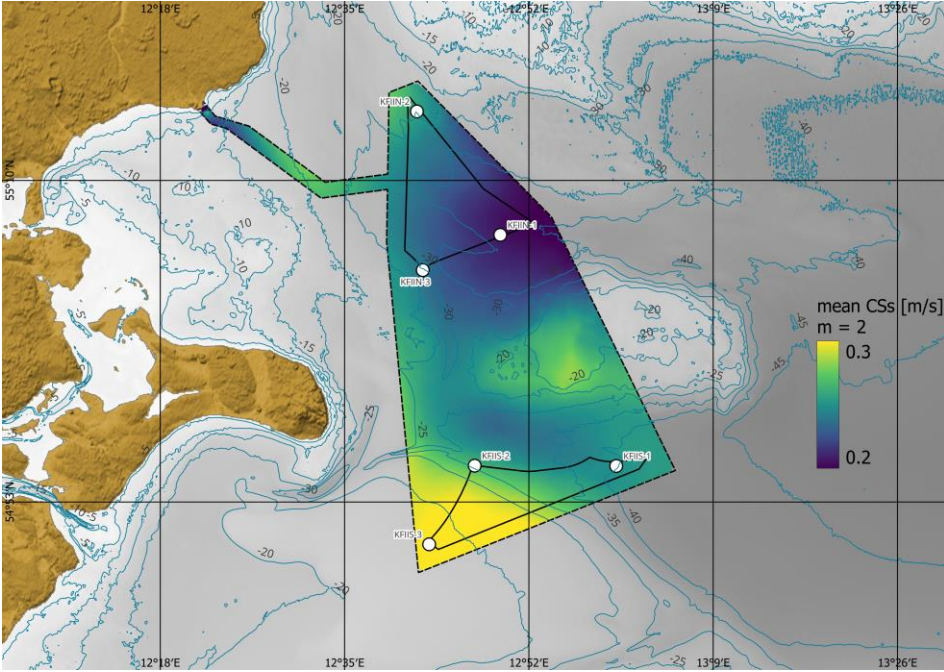


Figure 6-19 Spatial variation of moments of  $C_{Ss}$  across the data delivery area,  $m=2$

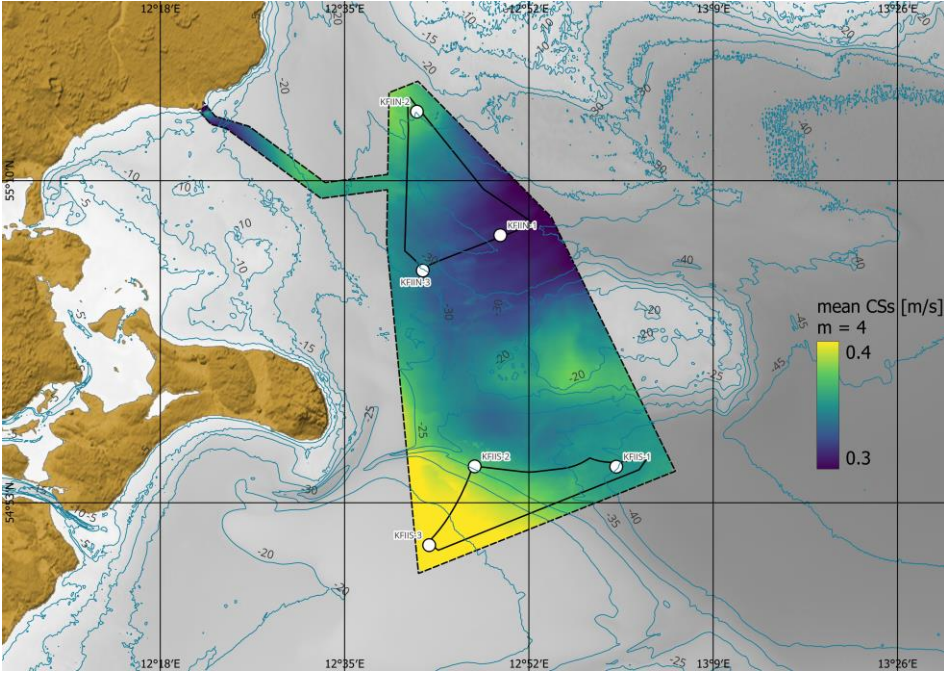


Figure 6-20 Spatial variation of moments of  $C_{Ss}$  across the data delivery area,  $m=4$

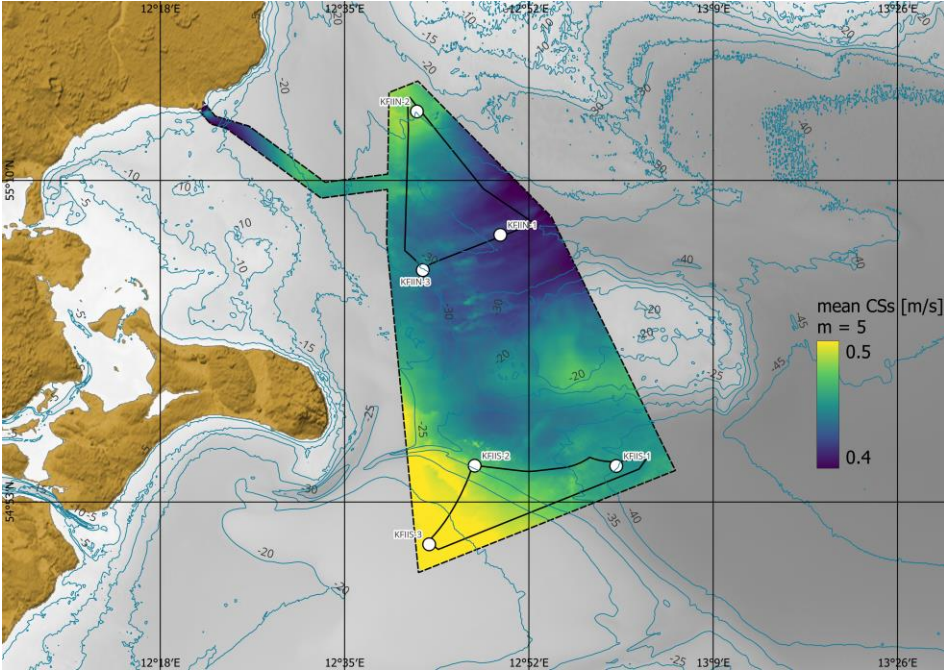


Figure 6-21 Spatial variation of moments of  $C_{Ss}$  across the data delivery area,  $m=5$

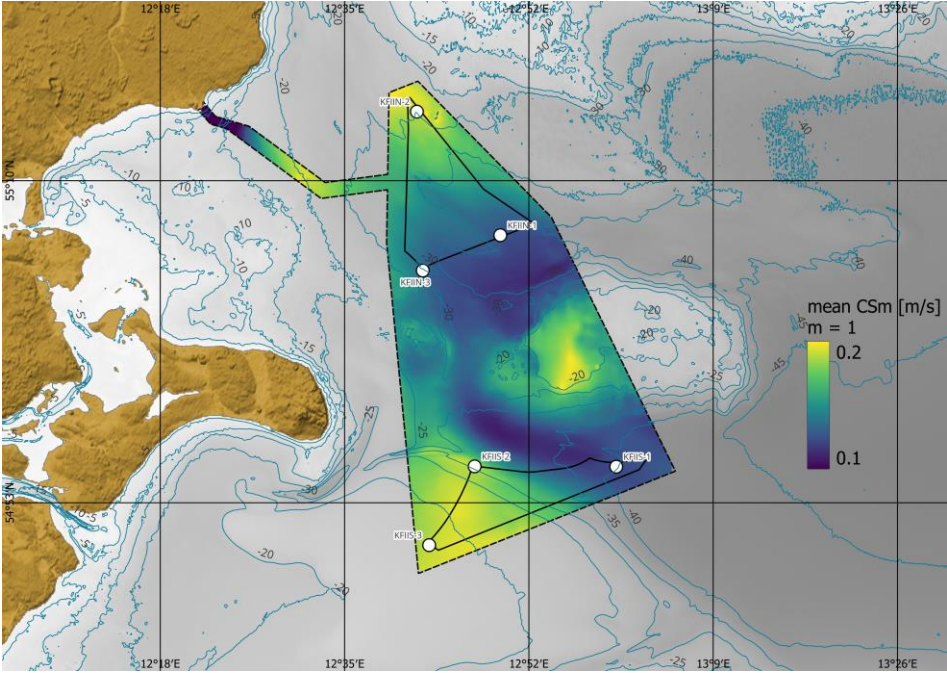


Figure 6-22 Spatial variation of moments of  $C_{Sm}$  across the data delivery area,  $m=1$ .

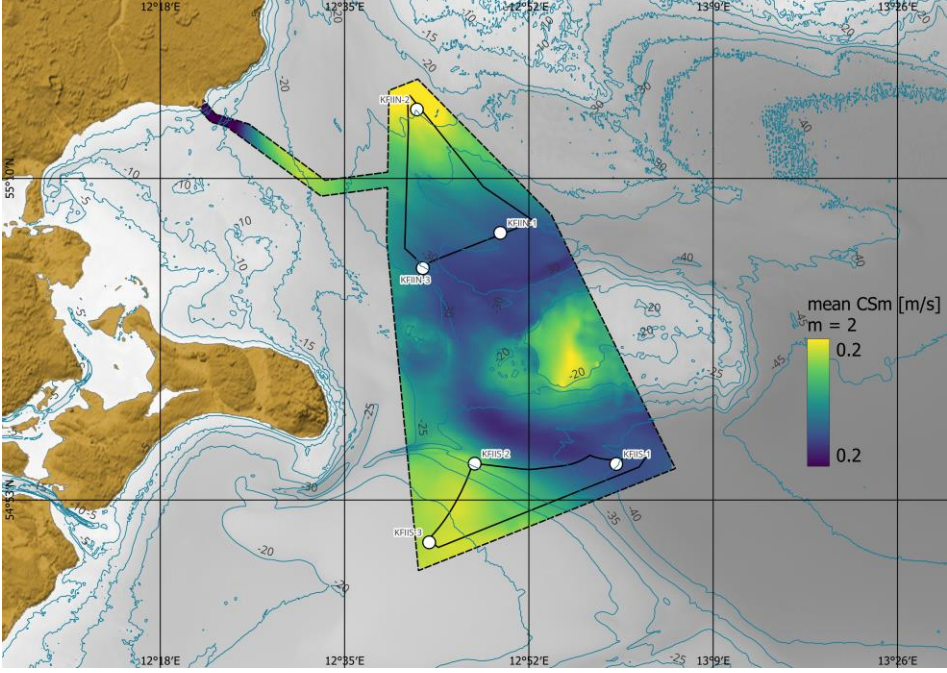


Figure 6-23 Spatial variation of moments of  $C_{Sm}$  across the data delivery area,  $m=2$ .

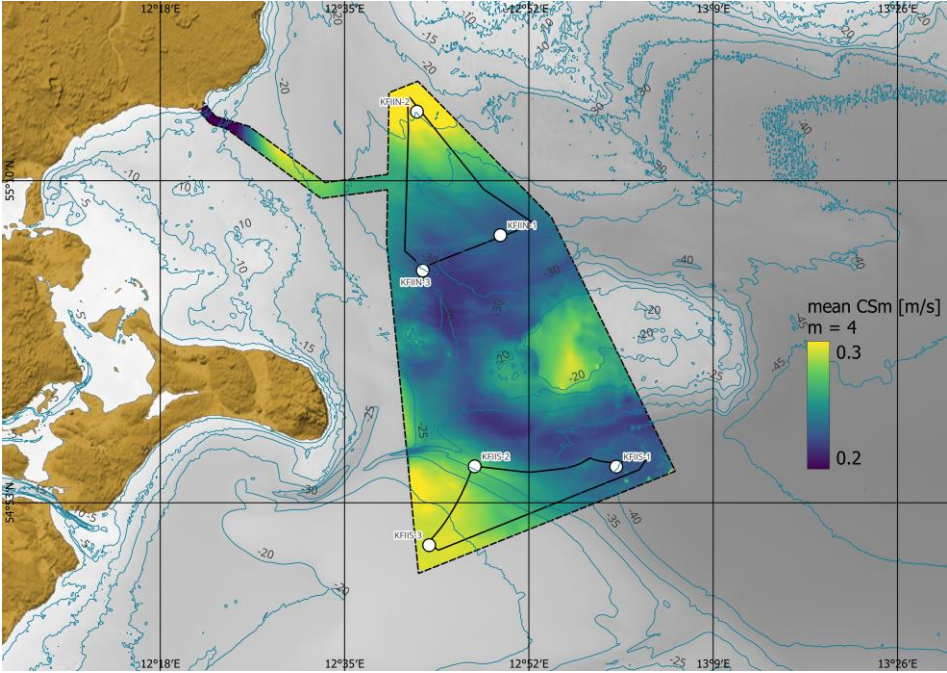


Figure 6-24 Spatial variation of moments of  $C_{Sm}$  across the data delivery area,  $m=4$

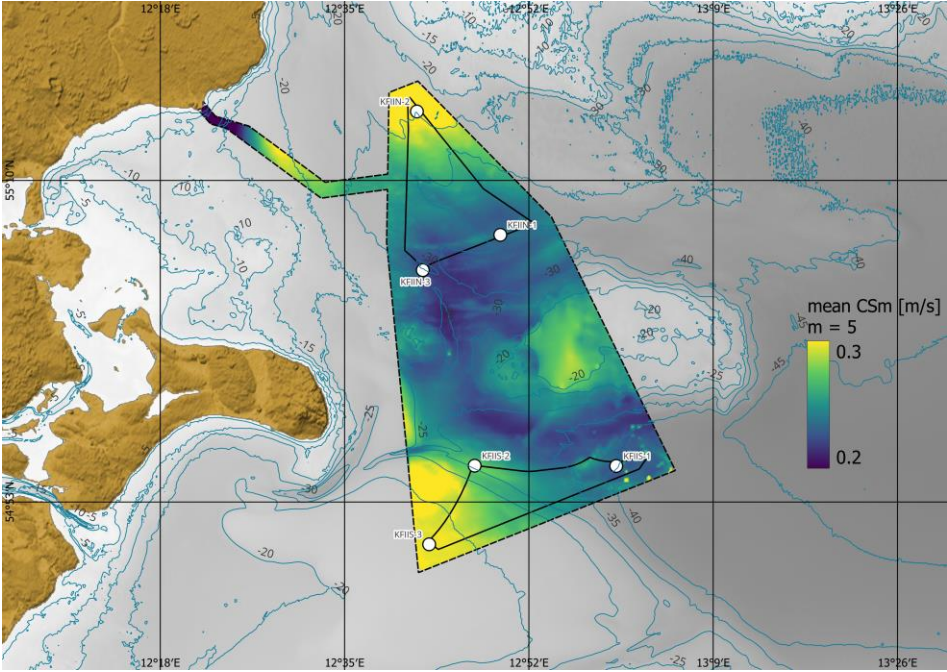


Figure 6-25 Spatial variation of moments of  $C_{Sm}$  across the data delivery area,  $m=5$

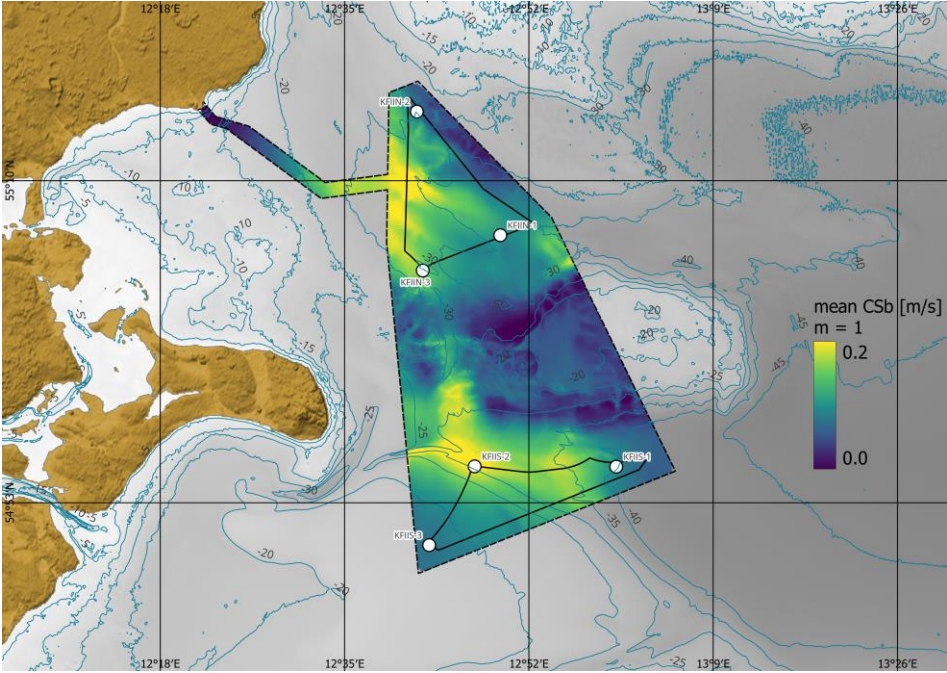


Figure 6-26 Spatial variation of moments of  $C_{sb}$  across the data delivery area,  $m=1$

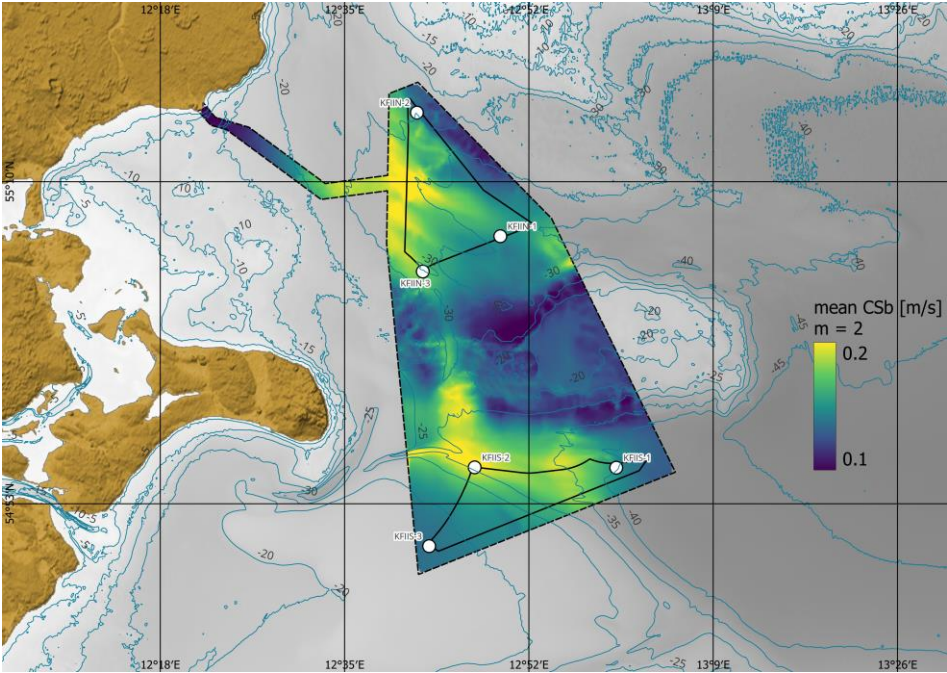


Figure 6-27 Spatial variation of moments of  $C_{sb}$  across the data delivery area,  $m=2$

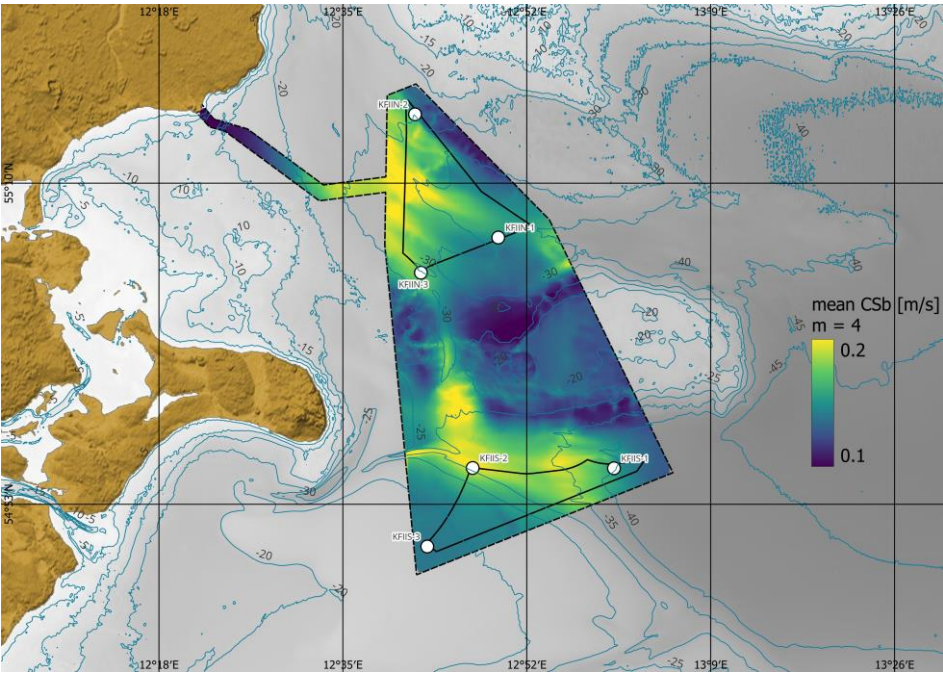


Figure 6-28 Spatial variation of moments of  $C_{sb}$  across the data delivery area,  $m=4$

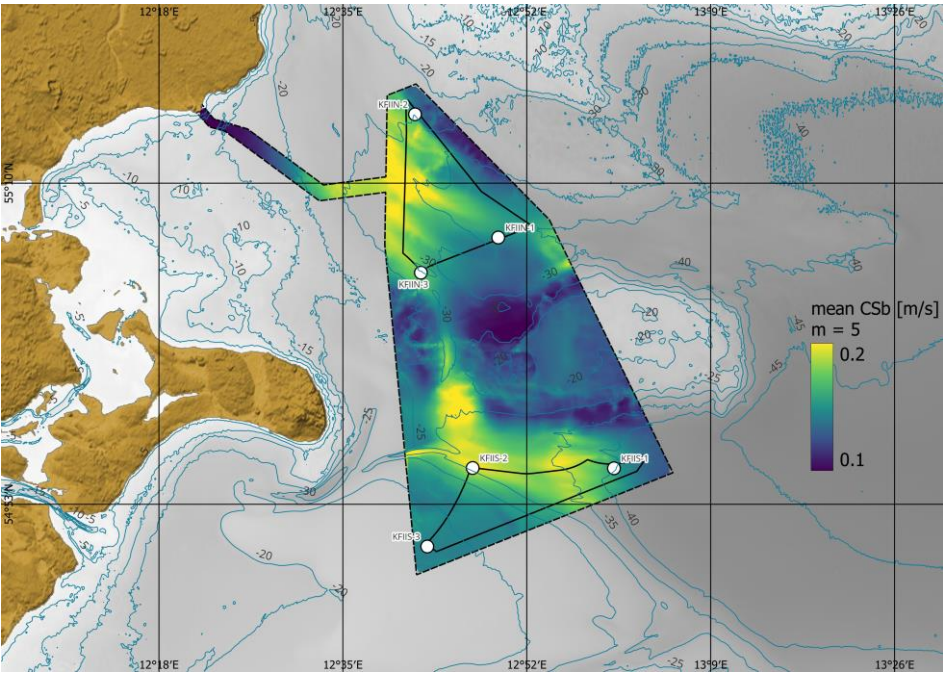


Figure 6-29 Spatial variation of moments of  $C_{sb}$  across the data delivery area,  $m=5$ .

## 6.2 Extreme current conditions unscaled

Extreme current conditions are established using Extreme Value analysis. The analysis is based on its performance and sensitivity to selection of distribution, threshold selection method,  $\lambda$ -value evaluation, and fitting estimator. A description of the methodology and the selection of settings is available in Appendix B.

For current speed, the 3-parameter Weibull distribution was fitted by the least square method to 45 peak events ( $\lambda=1$ ) separated by at least 72 hours.

It is noted that all Extreme Value Analysis results presented in this section are unscaled, in other words raw results from the EVA without scaling with regards to directionality. Scaled results according to DNV-RP-C205 where consistency between directional extremes and Omni for all return periods are ensured can be found in the appendices, see section 6.3 for details on the scaling.

### 6.2.1 Extreme total current speed at near surface

Figure 6-30 show the omni-directional EVA on current speed near surface. Figure 6-31 and Figure 6-32 shows the directional EVA on current speed near surface. Table 6-5 include the omni-directional EVA as well as the directional the directional extreme total near-surface current speed at KFIS-1.

The fitted distribution aligns well to the hindcast data points, also at the tail, and all events are within the confidence levels.

The 50-year total omni-directional near-surface current speed is 1.7 m/s.

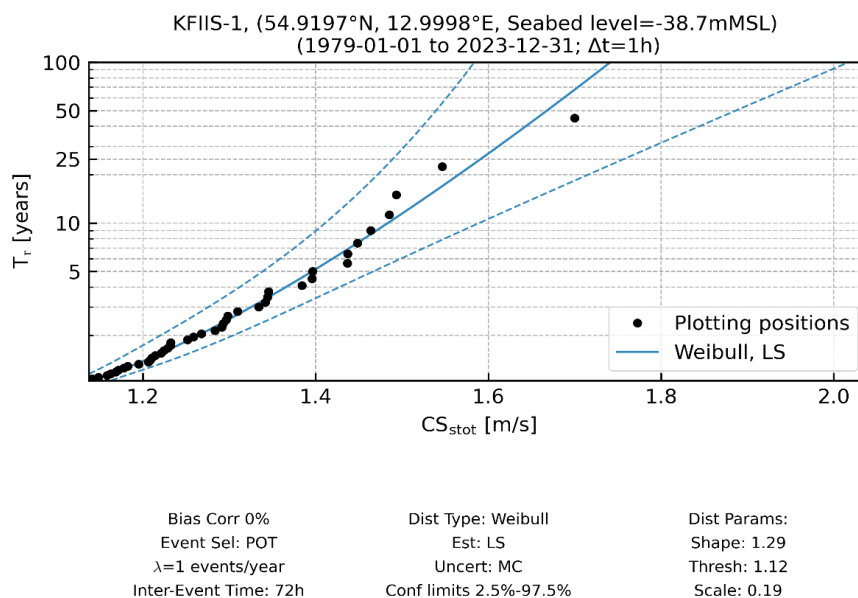


Figure 6-30 Marginal Omni-directional EVA estimates of  $CS_{stot}$  at KFIS-1.



Table 6-5 Marginal directional EVA estimates of  $CS_{stot}$  at KFIS-1.

Sector	$CS_{stot}$ [m/s]					
$CD_{stot}$ [°N-going to]	Quantile	$T_r$ 1	$T_r$ 5	$T_r$ 10	$T_r$ 25	$T_r$ 50
0.0	Central estimate	0.7	1	1	1.2	1.3
22.5		0.7	1	1.1	1.2	1.3
45.0		0.8	1	1.1	1.2	1.4
67.5		0.9	1.1	1.2	1.3	1.4
90.0		0.9	1.1	1.1	1.2	1.3
112.5		0.8	1	1	1.1	1.1
135.0		0.7	0.8	0.8	0.9	1
157.5		0.6	0.8	0.8	1	1
180.0		0.6	0.8	0.8	0.9	0.9
202.5		0.7	0.8	0.9	0.9	1
225.0		0.8	1	1.1	1.2	1.3
247.5		1	1.3	1.4	1.6	1.7
270.0		1	1.3	1.4	1.6	1.7
292.5		0.9	1.1	1.2	1.2	1.3
315.0		0.9	1.1	1.2	1.3	1.4
337.5		0.8	1	1.1	1.2	1.2
Omni		1.1	1.4	1.5	1.6	1.7

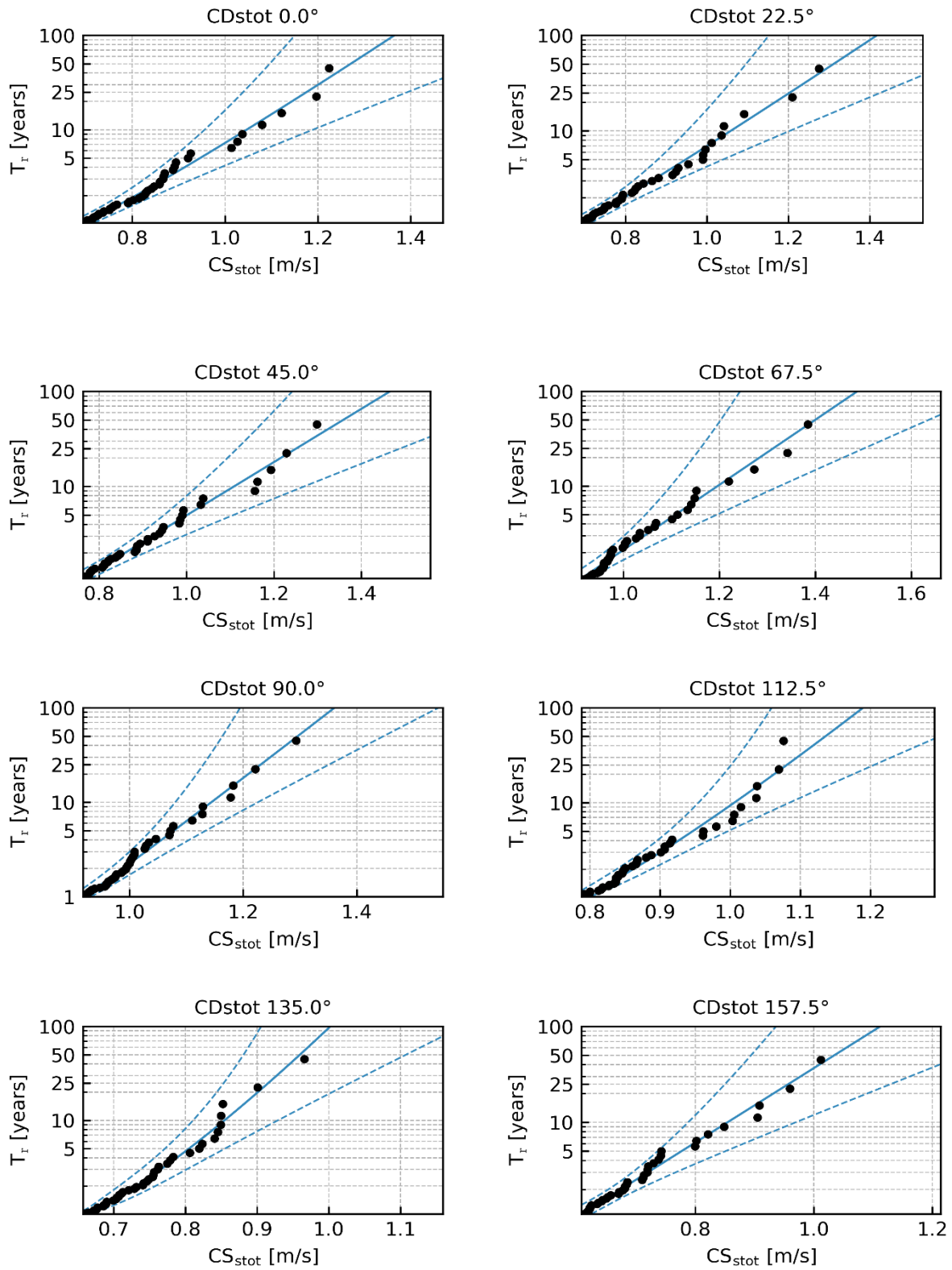


Figure 6-31 Marginal directional EVA estimates of  $CS_{stot}$  for  $CD_{stot}$  [°N-going to] sectors every 22.5° for KFIIS-1. Weibull LS,  $\lambda = 1$ . Confidence limits 2.5% -97.5%.

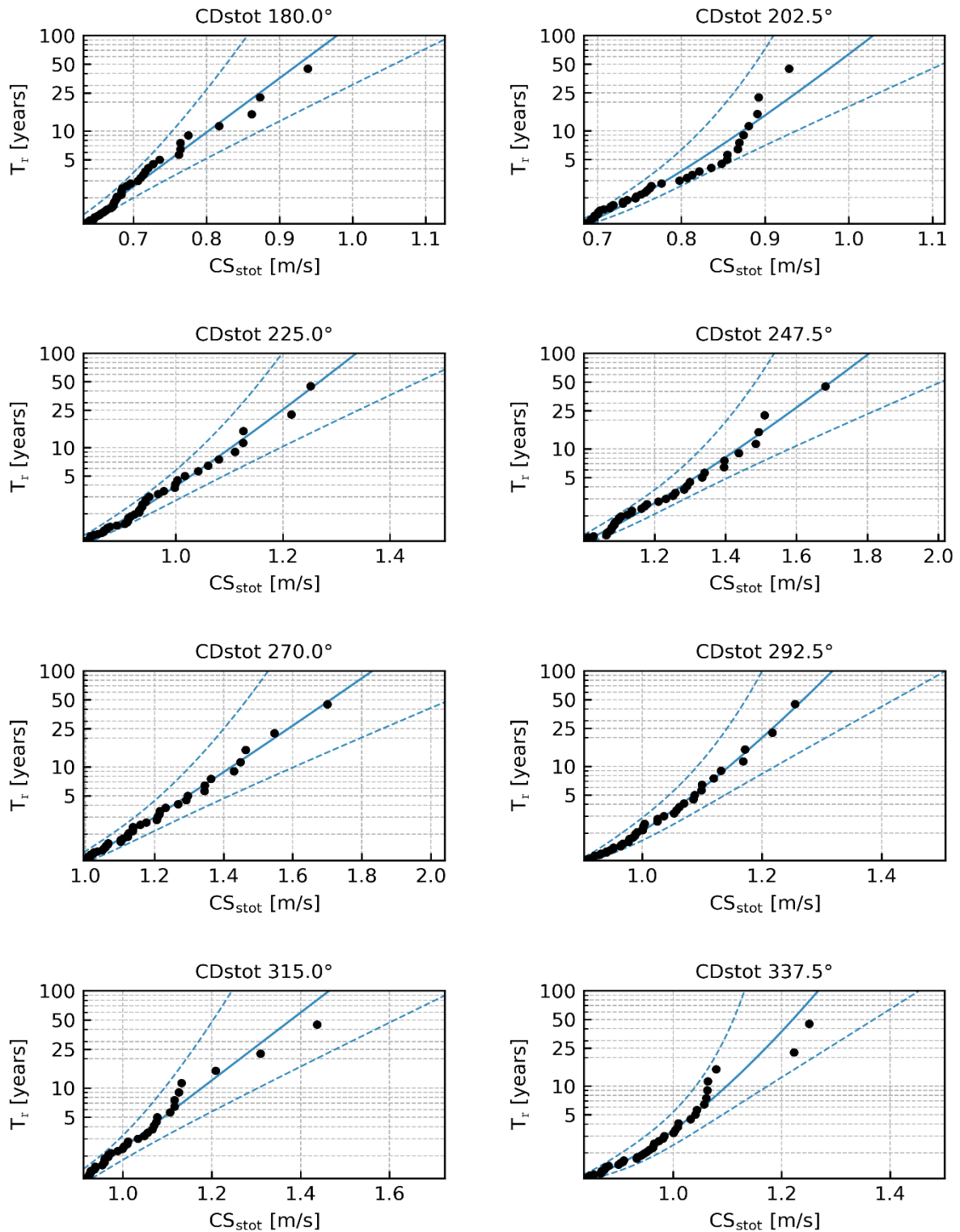


Figure 6-32 Marginal directional EVA estimates of  $CS_{stot}$  for  $CD_{stot}$  [°N-going to] sectors every 22.5° for KFIIS-1. Weibull LS,  $\lambda = 1$ . Confidence limits 2.5% -97.5%.

## 6.2.2 Extreme total current speed at mid-depth

Figure 6-33 show the omni-directional EVA on current speed mid-depth. Figure 6-34 and Figure 6-35 shows the directional EVA on current speed mid-depth. Table 6-6 include the omni-directional EVA as well as the directional the directional extreme mid-depth current speed at KFIIS-1

The fitted distribution aligns well to the hindcast data points, also at the tail, and all events are within the confidence levels.

The 50-year total omni-directional mid-depth current speed is 1.0 m/s.

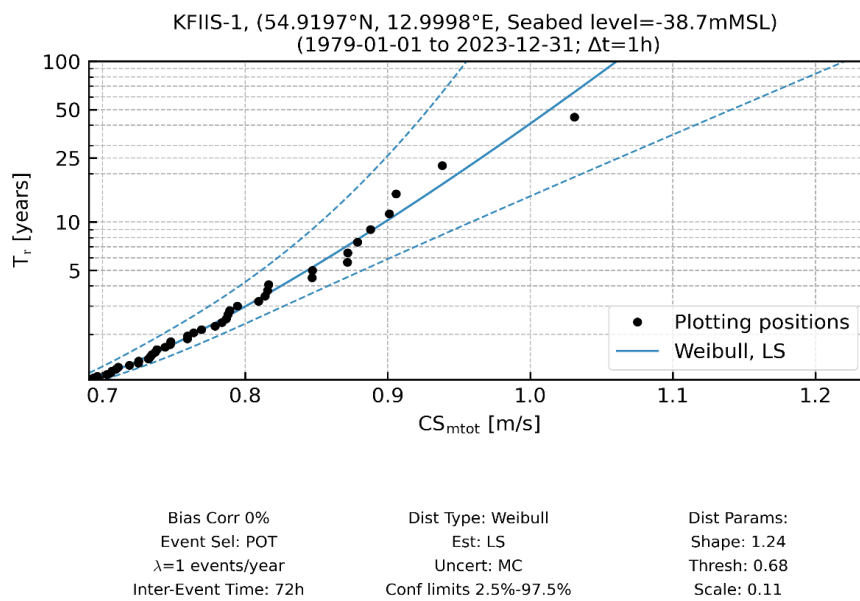
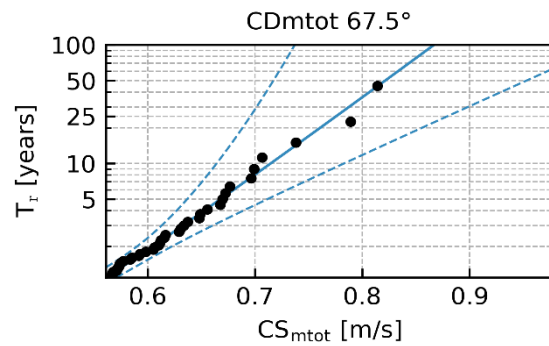
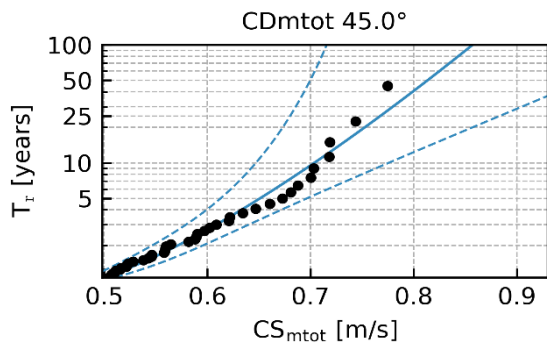
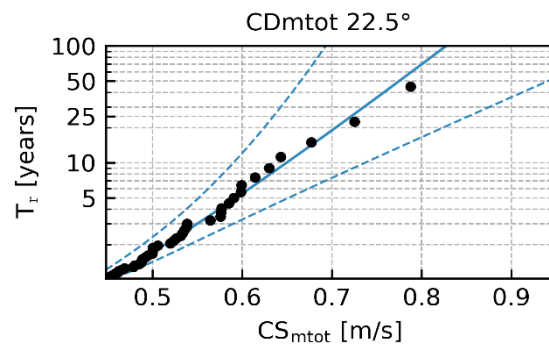
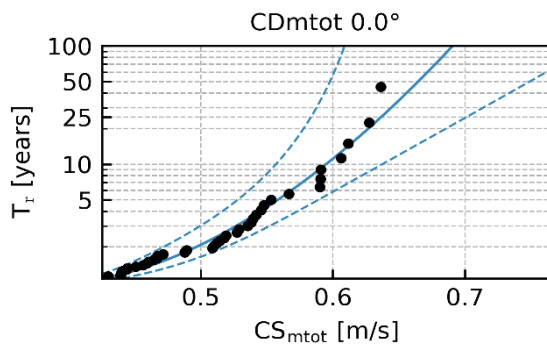


Figure 6-33 Marginal omni-directional EVA estimates of  $CS_{tot}$  at KFIIS-1.

Table 6-6 Marginal directional EVA estimates of  $CS_{mtot}$  at KFIIS-1.

Sector	$CS_{mtot}$ [m/s]					
$CD_{mtot}$ [°N-going to]	Quantile	$T_r$ 1	$T_r$ 5	$T_r$ 10	$T_r$ 25	$T_r$ 50
0.0	Central estimate	0.4	0.6	0.6	0.6	0.7
22.5		0.4	0.6	0.6	0.7	0.8
45.0		0.5	0.6	0.7	0.8	0.8
67.5		0.6	0.7	0.7	0.8	0.8
90.0		0.5	0.6	0.7	0.7	0.8
112.5		0.5	0.6	0.6	0.6	0.7
135.0		0.4	0.5	0.5	0.6	0.6
157.5		0.3	0.4	0.5	0.5	0.6
180.0		0.4	0.5	0.5	0.5	0.6
202.5		0.4	0.5	0.5	0.6	0.6
225.0		0.5	0.6	0.7	0.7	0.8
247.5		0.6	0.8	0.9	1	1
270.0		0.6	0.8	0.9	1	1
292.5		0.6	0.7	0.7	0.8	0.8
315.0		0.5	0.7	0.7	0.8	0.8
337.5		0.5	0.6	0.7	0.7	0.8
Omni		0.7	0.8	0.9	1	1



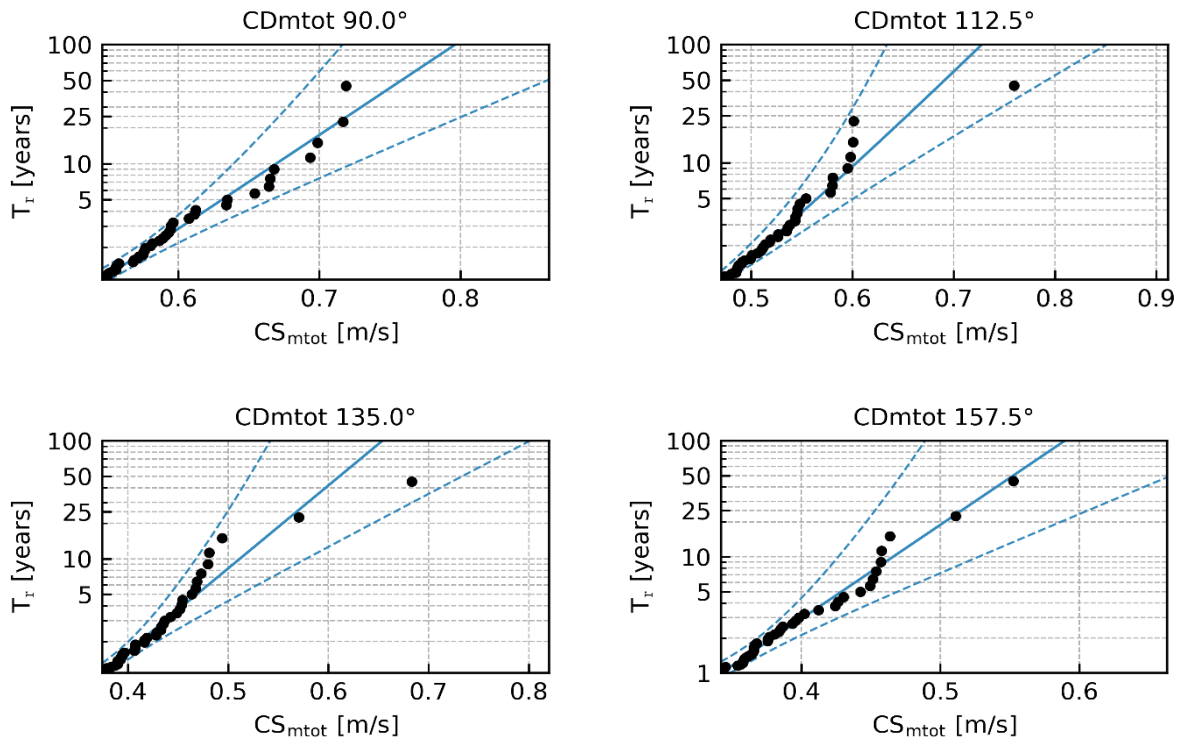
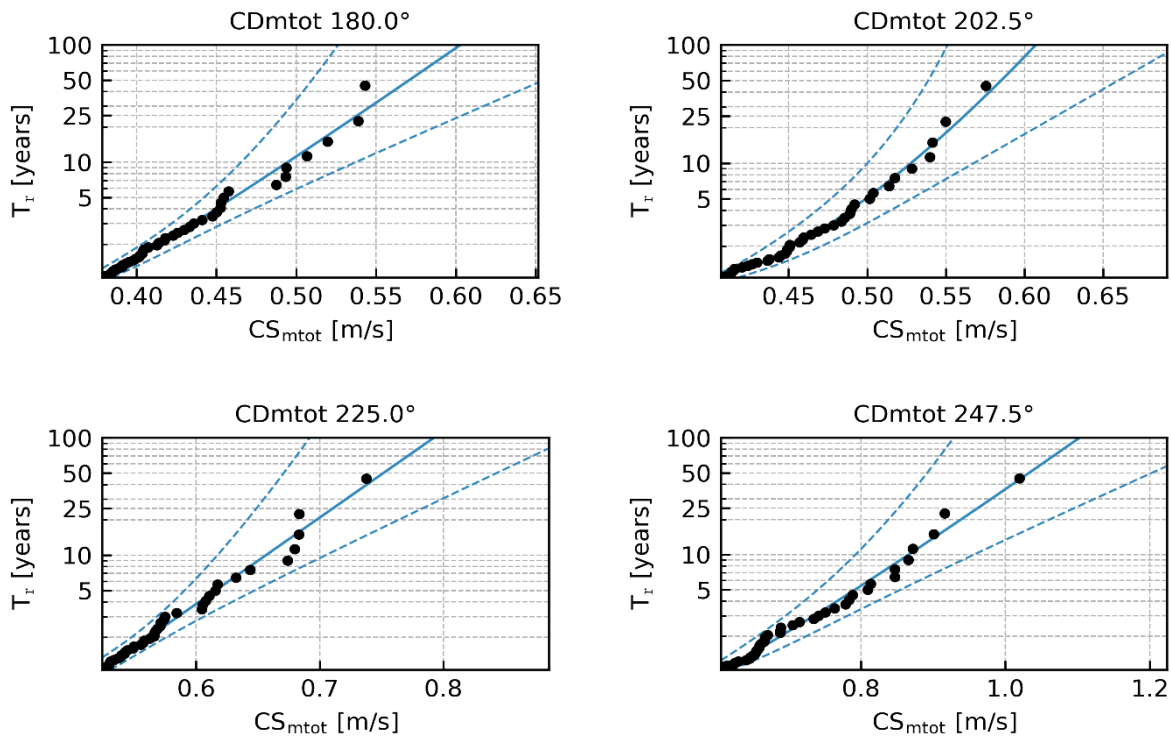


Figure 6-34 Marginal directional EVA estimates of  $CS_{mtot}$  for  $CD_{mtot}$  [ $^{\circ}$ N-going to] sectors every  $22.5^{\circ}$  for KFIIS-1. Weibull LS,  $\lambda = 1$ . Confidence limits 2.5% -97.5%.



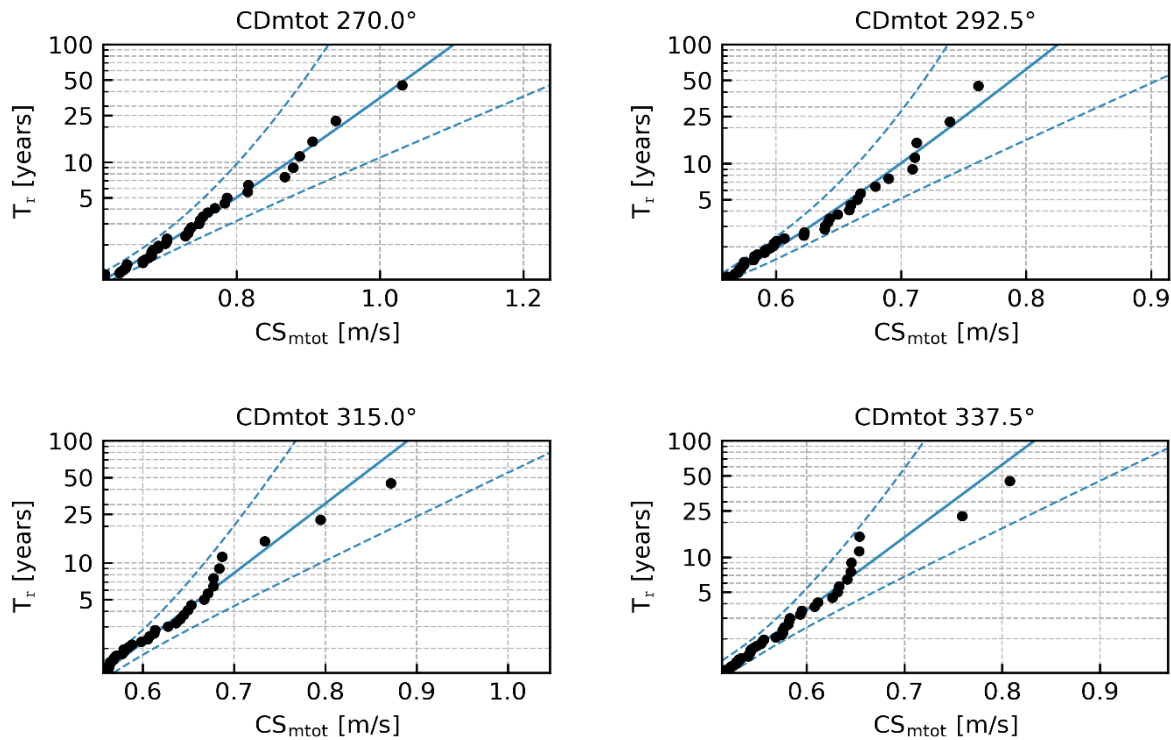


Figure 6-35 Marginal directional EVA estimates of  $CS_{mtot}$  for  $CD_{mtot}$  [ $^{\circ}$ N-going to] sectors every  $22.5^{\circ}$  for KFIIS-1. Weibull LS,  $\lambda = 1$ . Confidence limits 2.5% -97.5%.

### 6.2.3 Extreme total current speed at near bed

Figure 6-36 show the omni-directional EVA on current speed at near bed.

Figure 6-37 and Figure 6-38 shows the directional EVA on current speed at near bed.

Table 6-7 include the omni-directional EVA as well as the directional the directional extreme total near bed current speed at KFIIS-1

The fitted distribution aligns well to the hindcast data points, also at the tail, and all events are within the confidence levels.

The 50-year total omni-directional near-surface current speed is 0.6 m/s.

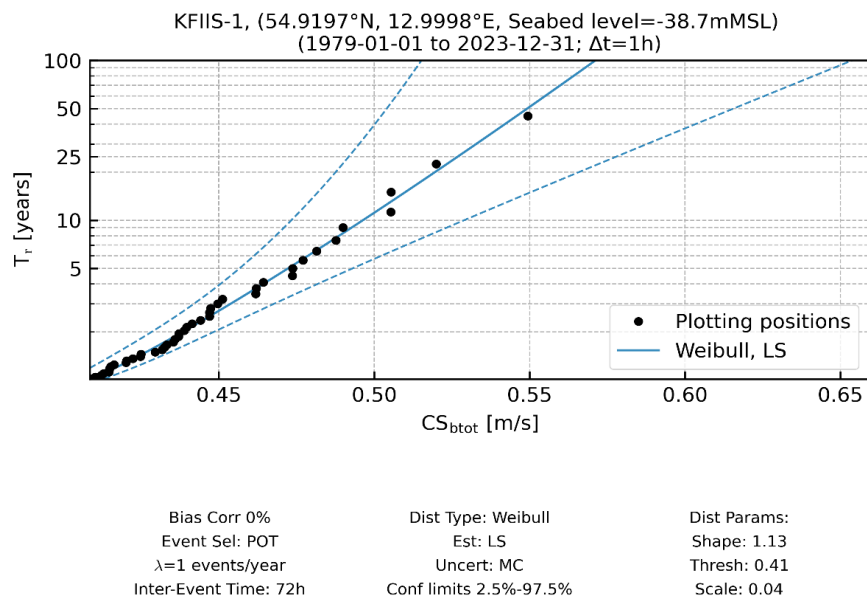


Figure 6-36 Marginal omni-directional EVA estimates of  $CS_{btot}$  at KFIS-1.

Table 6-7 Marginal directional EVA estimates of  $CS_{btot}$  at KFIS-1.

Sector	$CS_{btot}$ [m/s]					
	Quantile	$T_r$ 1	$T_r$ 5	$T_r$ 10	$T_r$ 25	$T_r$ 50
0.0	Central estimate	0.3	0.3	0.4	0.4	0.4
22.5		0.3	0.3	0.4	0.4	0.4
45.0		0.3	0.3	0.4	0.4	0.4
67.5		0.3	0.3	0.4	0.4	0.4
90.0		0.4	0.4	0.4	0.5	0.5
112.5		0.4	0.4	0.5	0.5	0.5
135.0		0.4	0.4	0.5	0.5	0.6
157.5		0.3	0.4	0.5	0.5	0.6
180.0		0.3	0.4	0.4	0.4	0.4
202.5		0.3	0.4	0.4	0.4	0.5
225.0		0.3	0.4	0.4	0.4	0.4
247.5		0.1	0.2	0.2	0.2	0.3
270.0		0.1	0.2	0.2	0.3	0.3
292.5		0.1	0.2	0.2	0.3	0.3
315.0		0.1	0.2	0.2	0.2	0.3
337.5		0.1	0.2	0.2	0.2	0.3
Omni		0.4	0.5	0.5	0.5	0.6



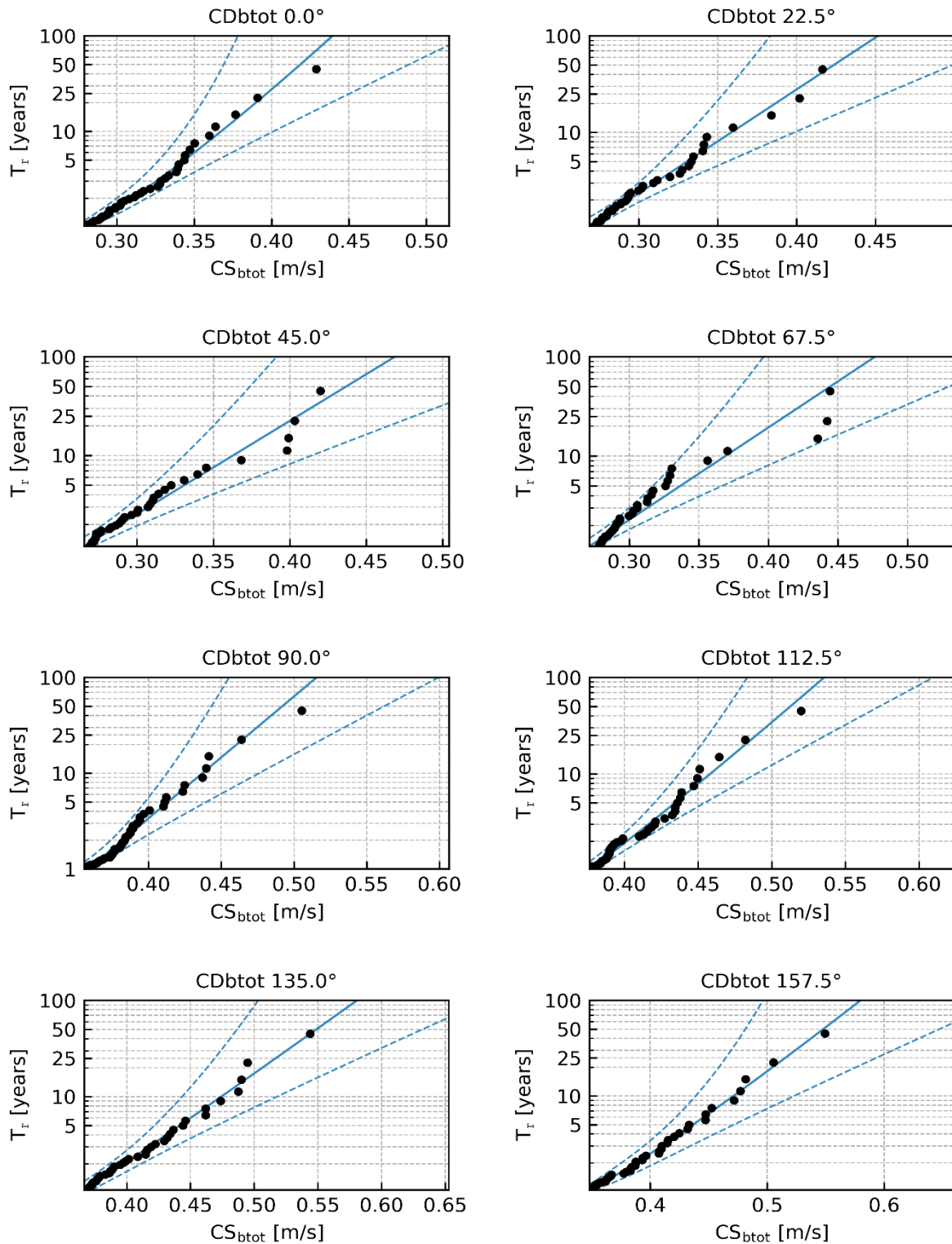


Figure 6-37 Marginal directional EVA estimates of  $CS_{btot}$  for  $CD_{btot}$  [ $^\circ$ N-going to] sectors every  $22.5^\circ$  for KFIIS-1. Weibull LS,  $\lambda = 1$ . Confidence limits 2.5% -97.5%.

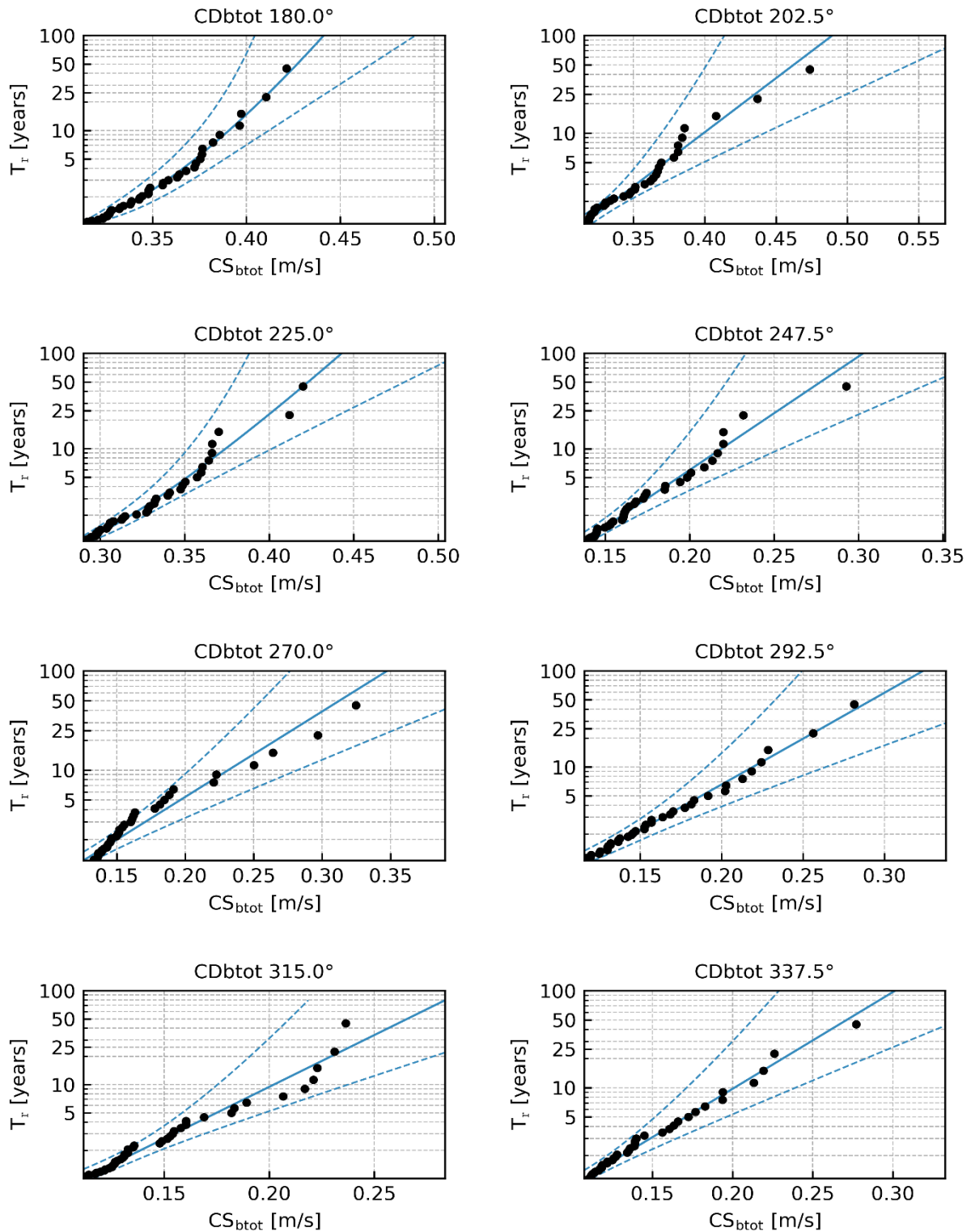


Figure 6-38 Marginal directional EVA estimates of  $CS_{btot}$  for  $CD_{btot}$  [°N-going to] sectors every 22.5° for KFIIS-1. Weibull LS,  $\lambda = 1$ . Confidence limits 2.5% -97.5%.

### 6.2.4 Maps of extreme current speed at 3 levels

From Figure 6-39 to Figure 6-53 is the spatial variation of the omni-directional total current speed across the data delivery area of KFII at 3 levels; near-surface, mid-depth and near-seabed, for return periods of 1, 5, 10, 25 and 50 years based on individual extreme value analysis on each model grid point.

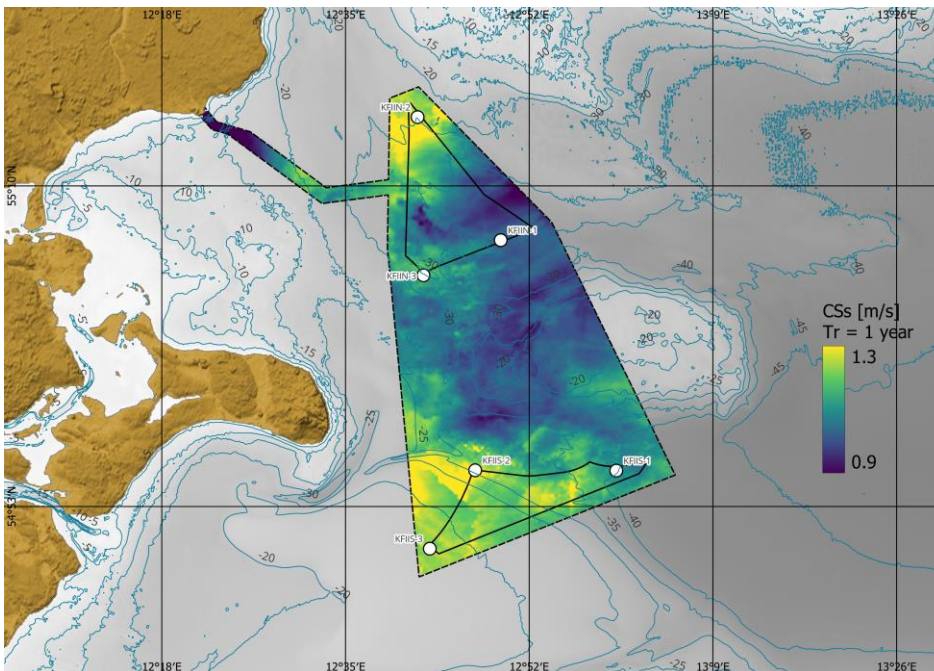


Figure 6-39 Spatial variation across the data delivery area of KFII of  $CS_{stat}$  for return periods of 1 years. The colour map shows the current speed, and the contours show water depths.

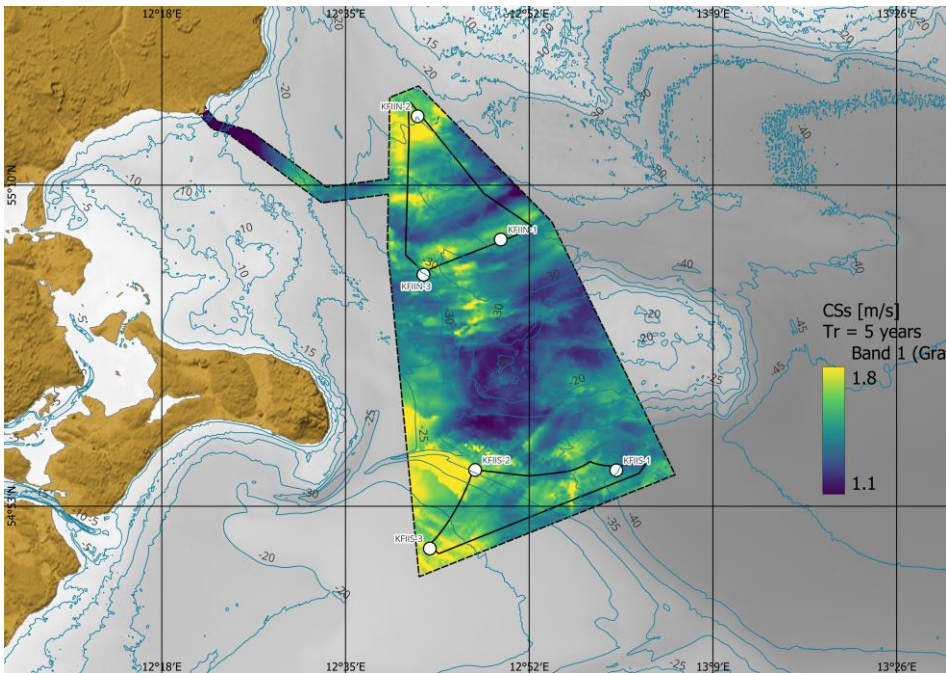


Figure 6-40 Spatial variation across the data delivery area of KFII of  $CS_{stot}$  for return periods of 5 years. The colour map shows the current speed, and the contours show water depths.

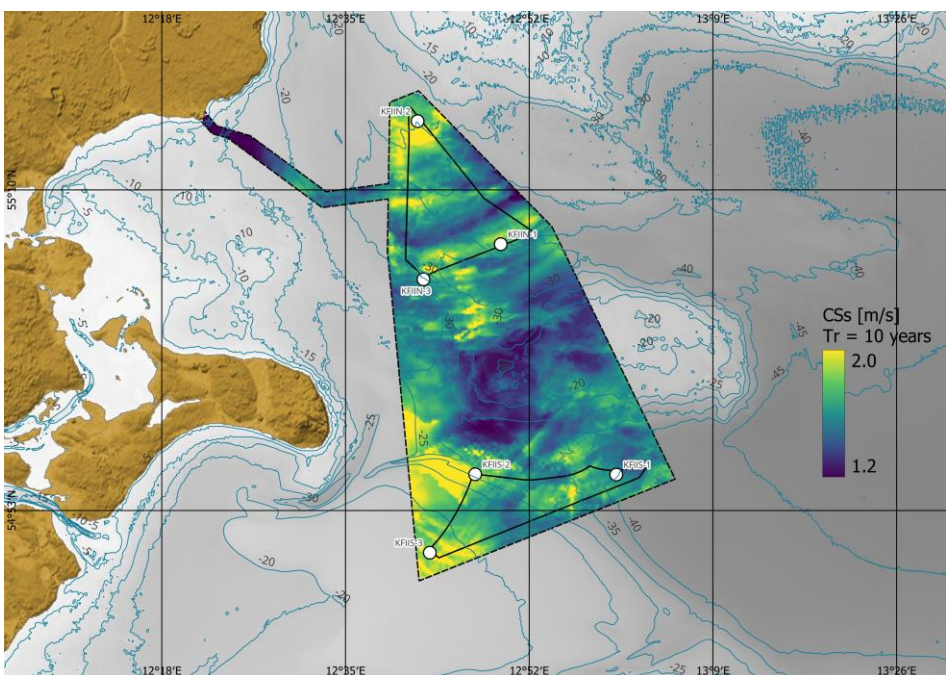


Figure 6-41 Spatial variation across the data delivery area of KFII of  $CS_{stot}$  for return periods of 10 years. The colour map shows the current speed, and the contours show water depths.

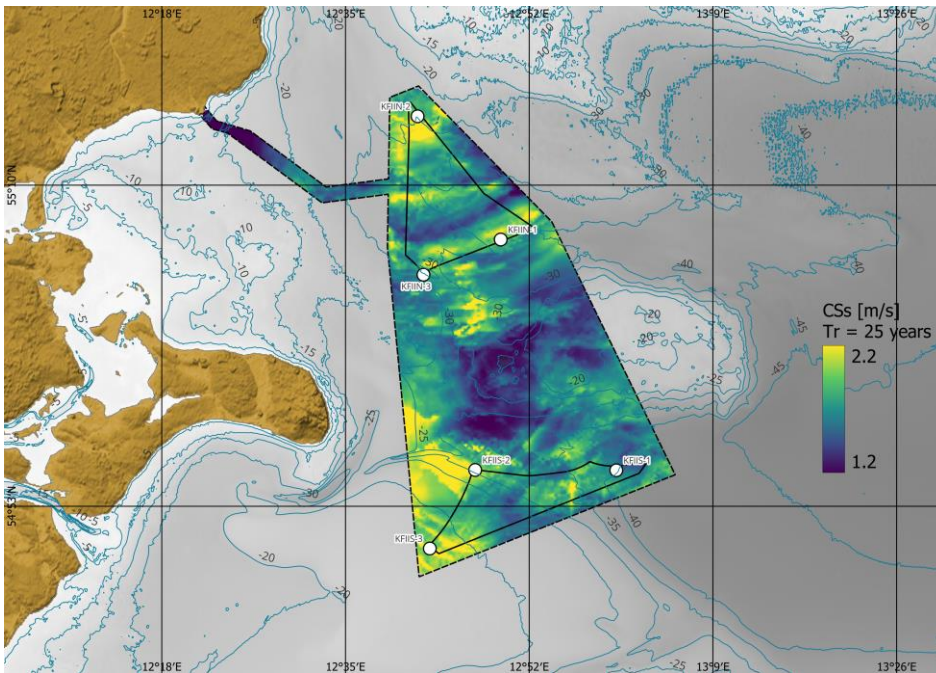


Figure 6-42 Spatial variation across the data delivery area of KFII of  $CS_{stot}$  for return periods of 25 years. The colour map shows the current speed, and the contours show water depths.

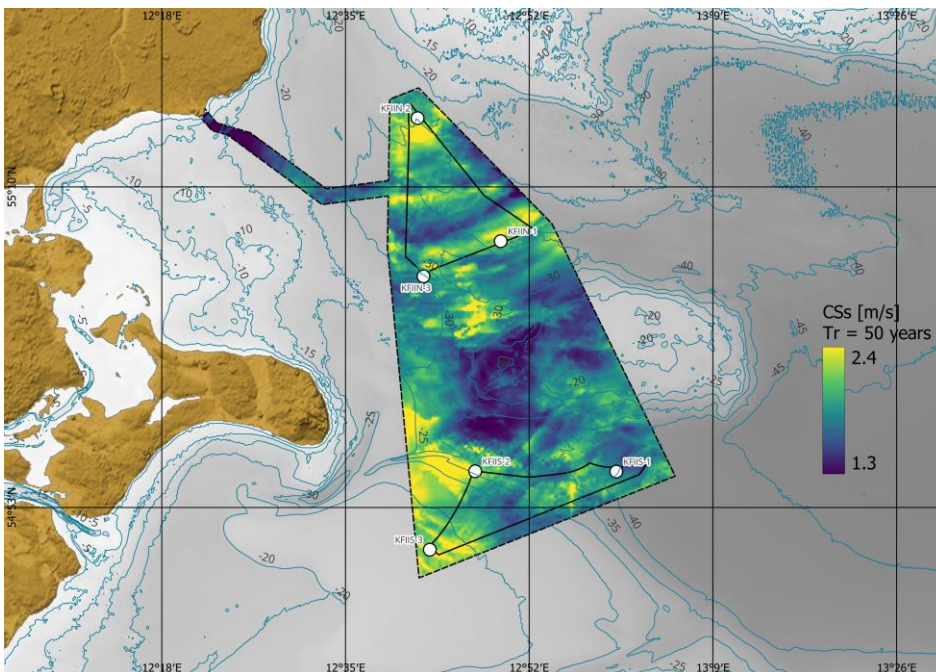


Figure 6-43 Spatial variation across the data delivery area of KFII of  $CS_{stot}$  for return periods of 50 years. The colour map shows the current speed, and the contours show water depths.

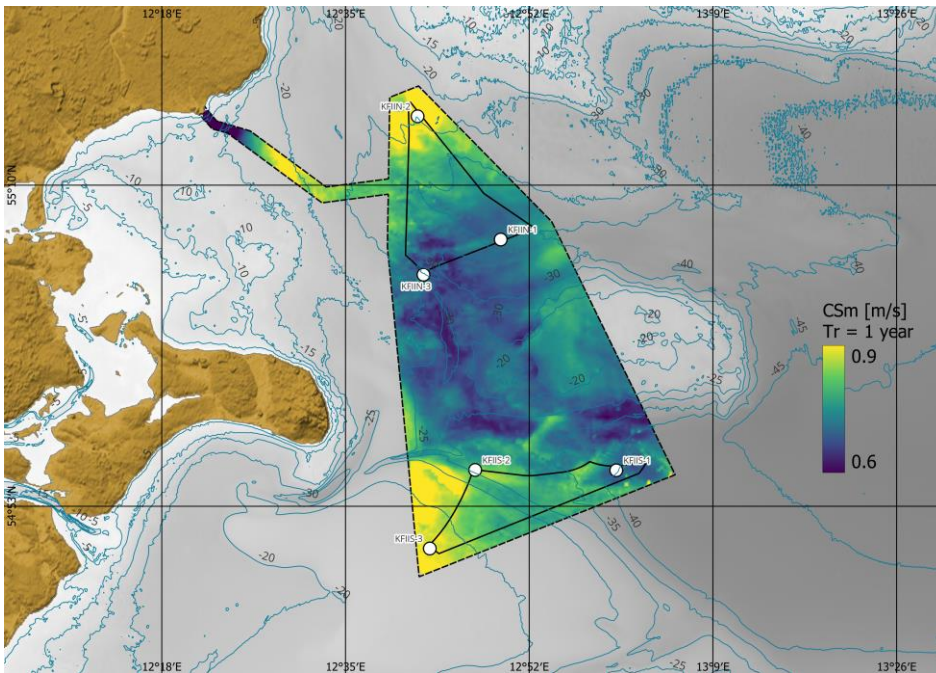


Figure 6-44 Spatial variation across the data delivery area of KFII of  $CS_{mtot}$  for return periods of 1 years. The colour map shows the current speed, and the contours show water depths.

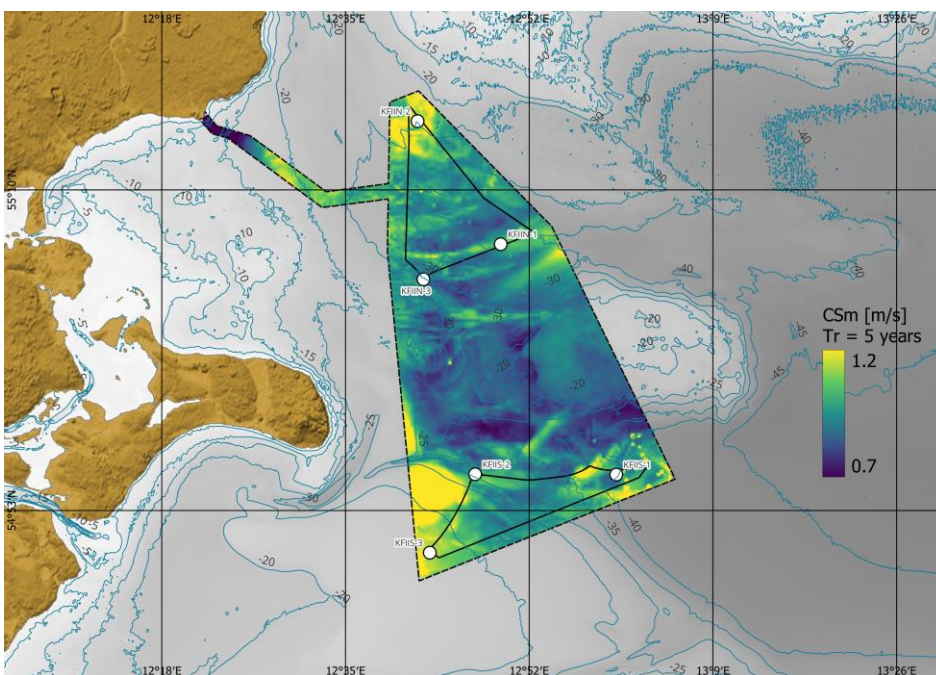


Figure 6-45 Spatial variation across the data delivery area of KFII of  $CS_{mtot}$  for return periods of 5 years. The colour map shows the current speed, and the contours show water depths.

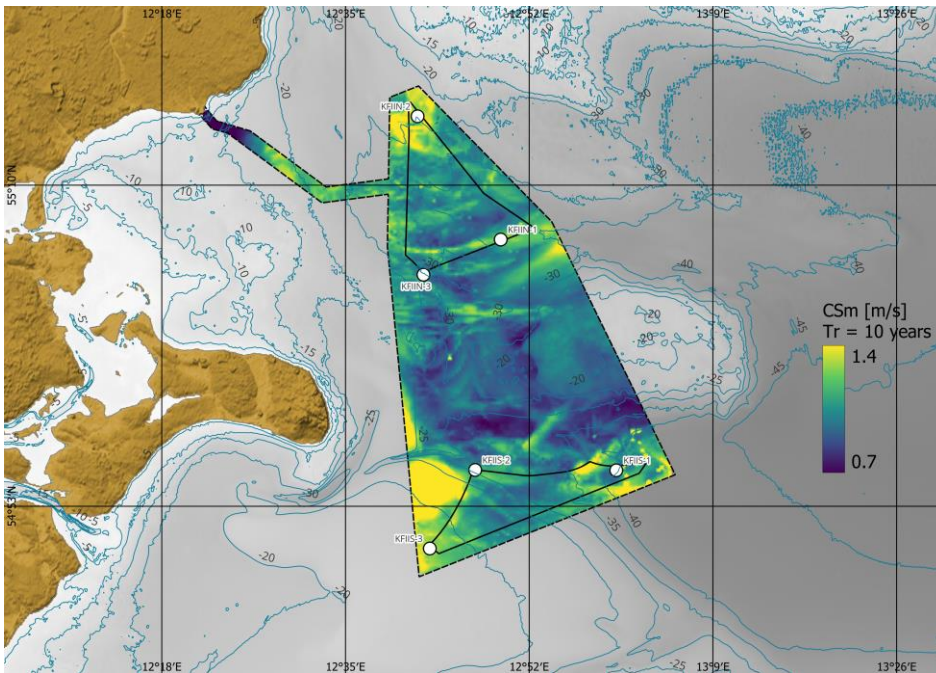


Figure 6-46 Spatial variation across the data delivery area of KFII of  $CS_{mtot}$  for return periods of 10 years. The colour map shows the current speed, and the contours show water depths.

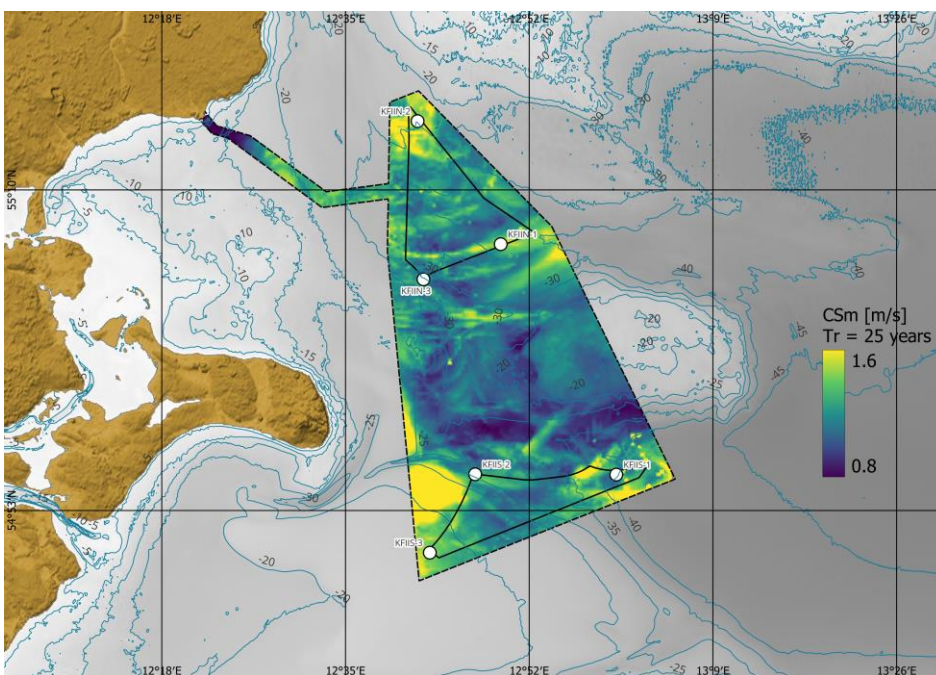


Figure 6-47 Spatial variation across the data delivery area of KFII of  $CS_{mtot}$  for return periods of 25 years. The colour map shows the current speed, and the contours show water depths.

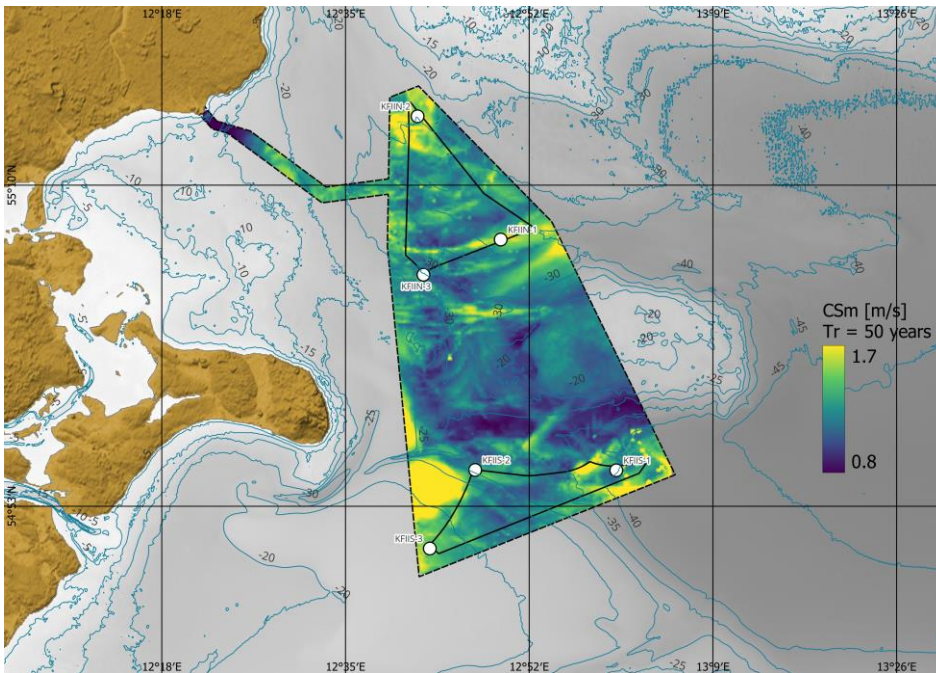


Figure 6-48 Spatial variation across the data delivery area of KFII of  $CS_{\text{tot}}$  for return periods of 50 years. The colour map shows the current speed, and the contours show water depths.

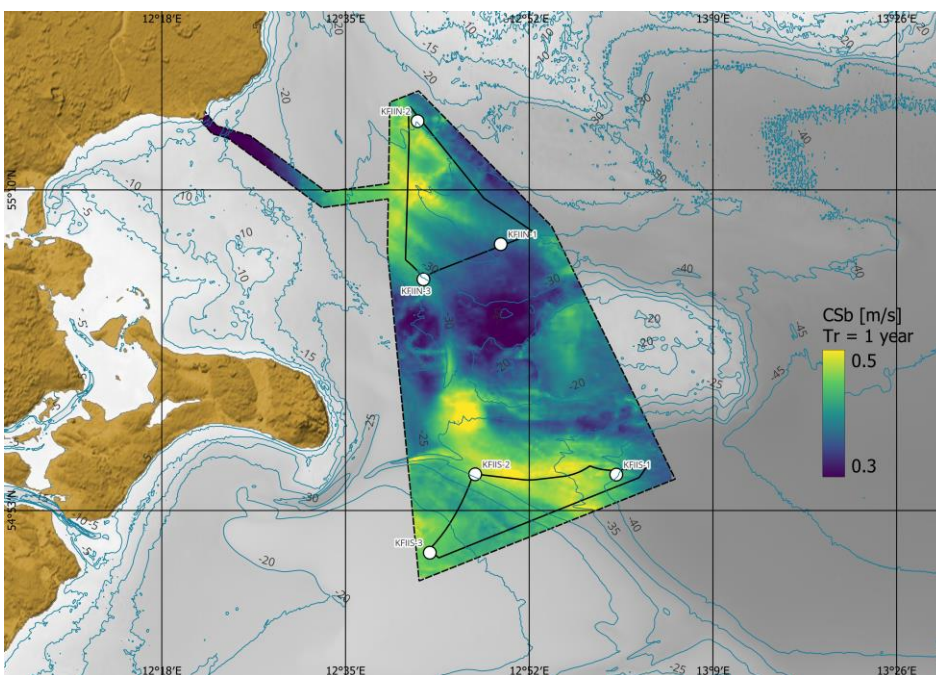


Figure 6-49 Spatial variation across the data delivery area of KFII of  $CS_{\text{tot}}$  for return periods of 1 years. The colour map shows the current speed, and the contours show water depths.



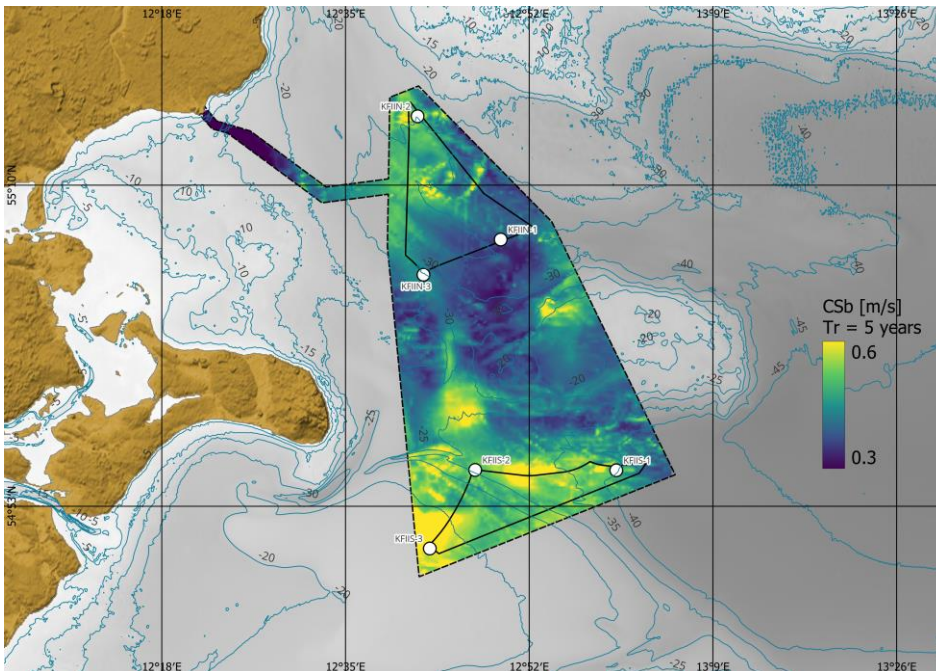


Figure 6-50 Spatial variation across the data delivery area of KFII of  $CS_{b_{tot}}$  for return periods of 5 years. The colour map shows the current speed, and the contours show water depths.

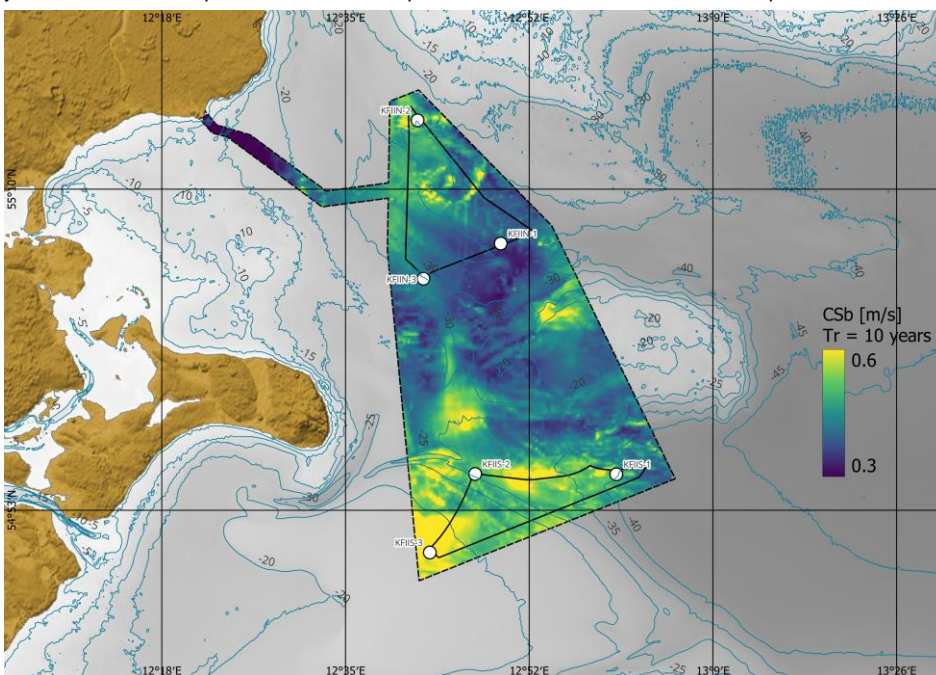


Figure 6-51 Spatial variation across the data delivery area of KFII of  $CS_{b_{tot}}$  for return periods of 10 years. The colour map shows the current speed, and the contours show water depths.

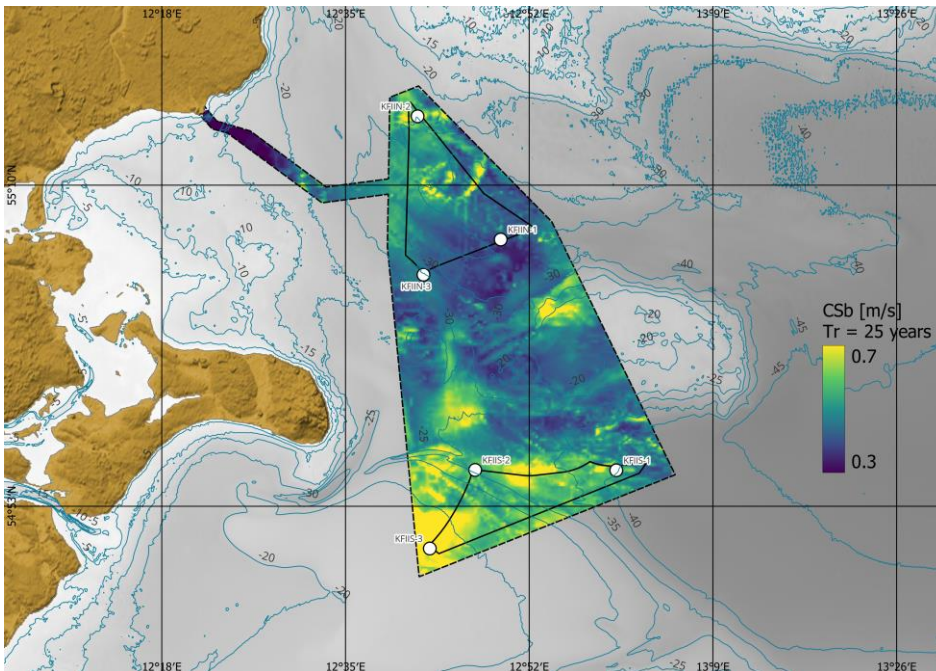


Figure 6-52 Spatial variation across the data delivery area of KFII of  $CS_{b\text{tot}}$  for return periods of 25 years. The colour map shows the current speed, and the contours show water depths.

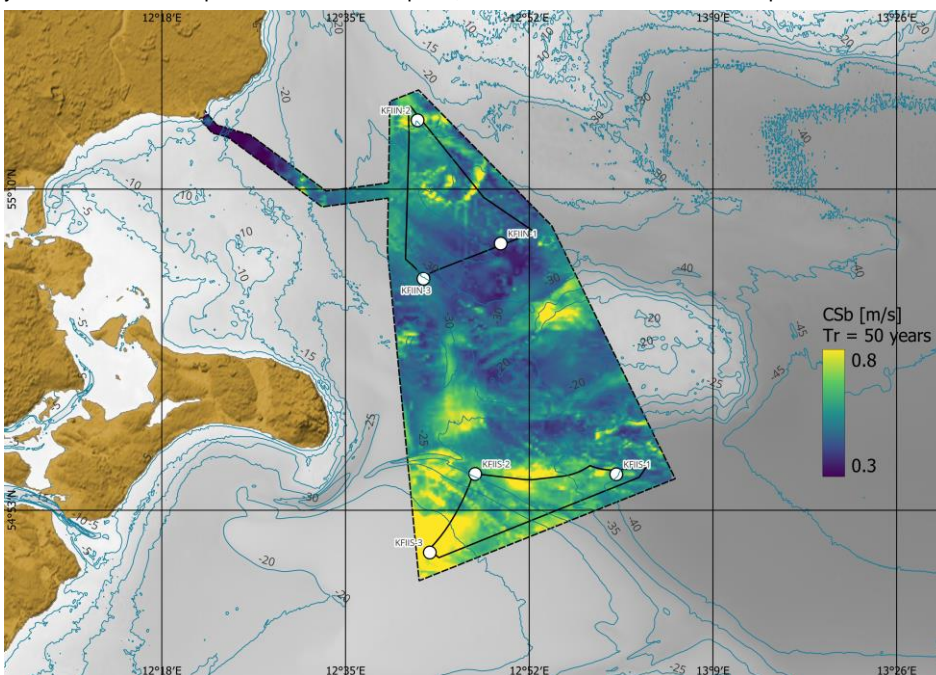


Figure 6-53 Spatial variation across the data delivery area of KFII of  $CS_{b\text{tot}}$  for return periods of 50 years. The colour map shows the current speed, and the contours show water depths.

### 6.3 Extreme current conditions scaled

Section 6.2 the results of the EVA analysis of the extreme current conditions. DNV-RP-C205 section 3.6.5.6 presents a method for scaling the results of the

EVA analysis. The applicability of the scaling method will not be discussed further here, but due care is advised when applying the results of the scaling.

Scaling according to DNV-RP-C205 section 3.6.5.6 has been performed for the extreme current conditions and is available in the Appendices.

## 7 Wave conditions

This section presents a summary of the wave data basis established in [1], followed by a presentation of normal and extreme wave conditions at the KFII area.

The wave dataset includes only the total wave component [1], without distinguishing between windsea and swell components. Table 7-1 summarises the metadata of the dataset.

Table 7-1 Metadata of the wave dataset.

Name	Value
<b>Start Date [UTC]:</b>	1979-01-01 00:00:00
<b>End Date [UTC]:</b>	2023-12-31 23:00:00
<b>Time Step [s]</b>	3600

The wave data is considered representative of 3-hour average sea state, assuming stationarity of the sea surface elevation for 3 hours as is standard practice, and is given at 1-hour interval. The wave analyses are presented in height bins of 0.5 m, period bins of 0.5 s, and directional bins of 22.5°.

Table 7-2 presents the variables of the wave dataset, incl. the bin sizes applied in analyses throughout this report.

Table 7-2 Wave variables of the wave dataset

Variable name	Abbrev.	Unit	Bin size
<b>Significant wave height</b>	$H_{m0}$	m	0.5
<b>Maximum wave height</b>	$H_{max}$	m	0.5
<b>Peak wave period</b>	$T_p$	s	0.5
<b>Mean wave period</b>	$T_{m01}$	s	0.5
<b>Zero-crossing wave period</b>	$T_{m02}$	s	0.5
<b>Mean energy period</b>	$T_{mm10}$	s	0.5
<b>Peak wave direction</b>	PWD	°N (clockwise from)	22.5
<b>Mean wave direction</b>	MWD	°N (clockwise from)	22.5
<b>Direction standard deviation</b>	DSD	°	22.5
<b>Maximum wave crest height</b>	$C_{max}$	m	0.5

The wave analyses cover the data period 1979-01-01 to 2023-12-31 (45 years).

### 7.1 Normal wave conditions

The normal wave conditions are presented in terms of:

- Time series
- Wave roses
- Histograms
- Monthly statistics
- Directional statistics
- Scatter diagrams for correlation
- Wind-wave misalignment
- Wave spectra
- Wave maps

### 7.1.1 Timeseries

Figure 7-1 and Figure 7-2 shows timeseries of  $H_{m0}$ ,  $T_p$ , and  $T_{m02}$ ,  $T_{mm10}$  and  $T_{m01}$  at KFIIS-1 during the 45-year hindcast period. An overview of simple statistics for the wave variables are given in Table 7-3.

Table 7-3 Overview of simple statistics for wave variables data period 1979-01-01 to 2023-12-31 at KFIIS-1.

Variable	MIN	MEAN	MAX
$H_{m0}$ [m]	0.0	1.0	6.0
$T_p$ [s]	1.1	4.4	9.5
$T_{m02}$ [s]	0.7	3.7	7.2
$T_{mm10}$ [s]	1.0	3.9	8.3
$T_{m01}$ [s]	0.8	3.5	7.6

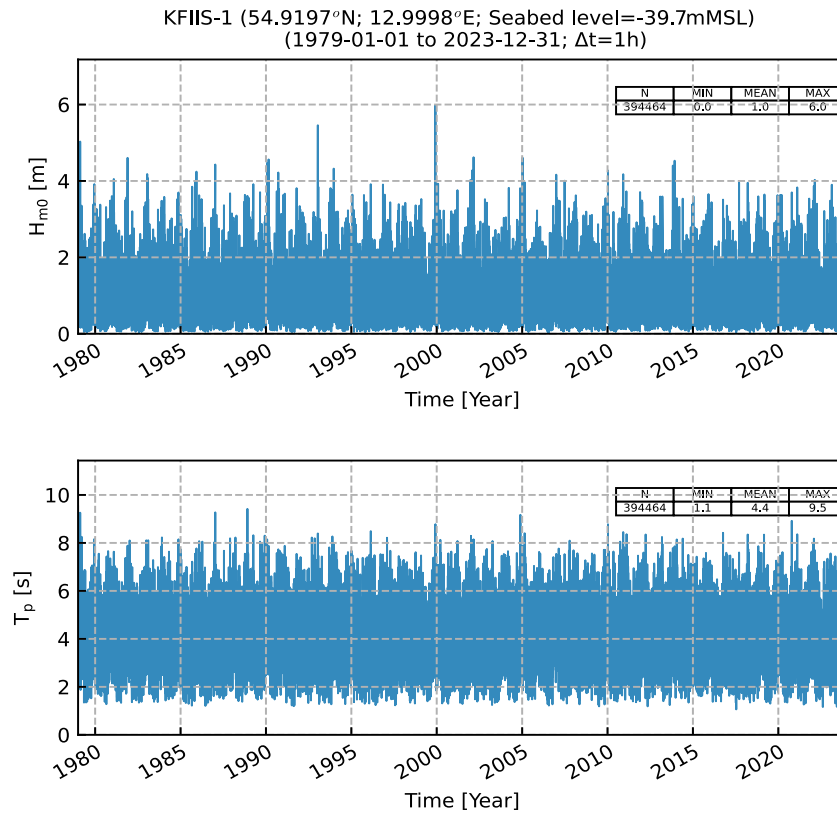


Figure 7-1 Timeseries of  $H_{m0}$  and  $T_p$  at KFIIS-1.

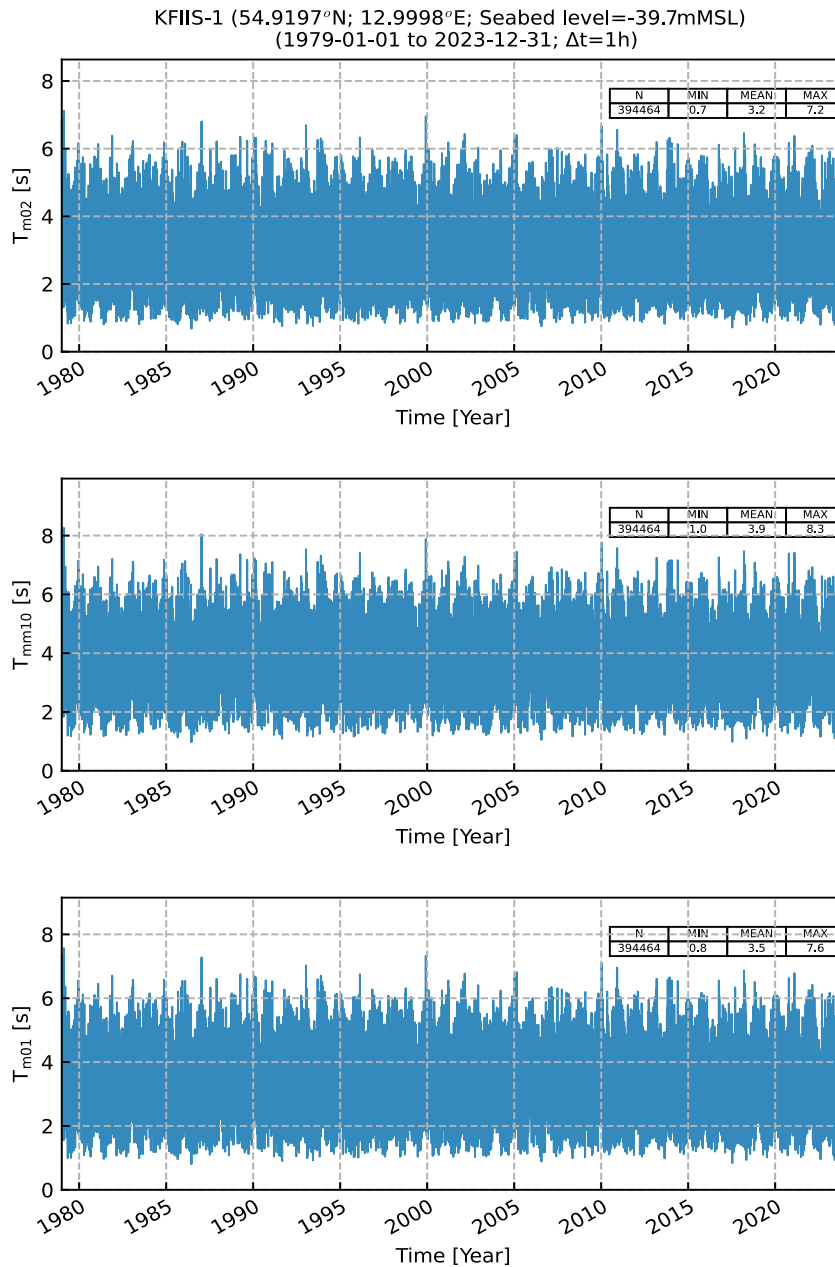


Figure 7-2 Timeseries of  $T_{m02}$ ,  $T_{m10}$ ,  $T_{m01}$  at KFIIS-1.

### 7.1.2 Wave roses

Figure 7-3 and Figure 7-4 shows wave roses at KFIIS-1 based on  $H_{m0}$ ,  $T_p$  and MWD for the total wave component. The wave rose indicate the predominance of waves coming from westerly sectors: W and WSW.

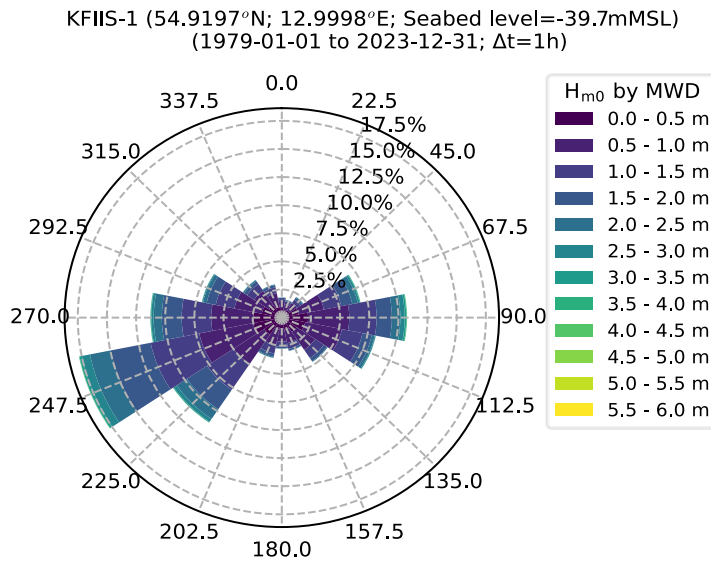


Figure 7-3 Rose plot of  $H_{m0}$ , sorted by MWD, at KFIIS-1.

Table 7-4 Table of  $H_{m0}$  and MWD in percentage, at KFIIS-1.

$H_{m0}$ [m]	MWD [°N-from]														Omni		
	0.0	22.5	45.0	67.5	90.0	112.5	135.0	157.5	180.0	202.5	225.0	247.5	270.0	292.5		315.0	337.5
0.0 - 0.5	0.77	0.69	0.79	1.47	2.25	2.05	1.53	1.11	0.96	1.08	1.82	2.52	2.44	1.75	1.32	1.08	23.6
0.5 - 1.0	0.63	0.53	0.78	2.20	3.53	3.21	1.92	1.20	1.17	1.45	3.16	4.69	3.62	2.39	1.54	1.14	33.2
1.0 - 1.5	0.26	0.26	0.36	1.52	2.35	1.80	0.88	0.53	0.48	0.73	2.73	4.26	2.53	1.63	0.74	0.53	21.6
1.5 - 2.0	0.11	0.11	0.20	0.96	1.31	0.81	0.34	0.15	0.14	0.30	2.09	3.50	1.70	0.80	0.30	0.20	13.0
2.0 - 2.5	0.03	0.03	0.07	0.47	0.73	0.26	0.06	0.04	0.03	0.09	1.03	1.81	0.70	0.31	0.11	0.06	5.8
2.5 - 3.0	0.00	0.01	0.02	0.16	0.38	0.08	0.00	0.00	0.01	0.02	0.31	0.70	0.21	0.08	0.03	0.01	2.0
3.0 - 3.5	0.00	0.00	0.00	0.06	0.13	0.02	0.00	0.00	0.00	0.00	0.07	0.21	0.05	0.02	0.01	0.00	0.6
3.5 - 4.0	0.00	0.00	0.00	0.02	0.06	0.00	0.00	0.00	0.00	0.00	0.01	0.04	0.02	0.00	0.00	0.00	0.2
4.0 - 4.5	0.00	0.00	0.00	0.01	0.01	0.00	0.00	0.00	0.00	0.00	0.01	0.01	0.00	0.00	0.00	0.00	0.0
4.5 - 5.0	0.00	0.00	0.00	0.00	0.01	0.00	0.00	0.00	0.00	0.00	0.00	0.00	0.00	0.00	0.00	0.00	0.0
5.0 - 5.5	0.00	0.00	0.00	0.00	0.00	0.00	0.00	0.00	0.00	0.00	0.00	0.00	0.00	0.00	0.00	0.00	0.0
5.5 - 6.0	0.00	0.00	0.00	0.00	0.00	0.00	0.00	0.00	0.00	0.00	0.00	0.00	0.00	0.00	0.00	0.00	0.0
All	1.8	1.6	2.2	6.9	10.7	8.2	4.7	3.0	2.8	3.7	11.2	17.7	11.3	7.0	4.0	3.0	100.0



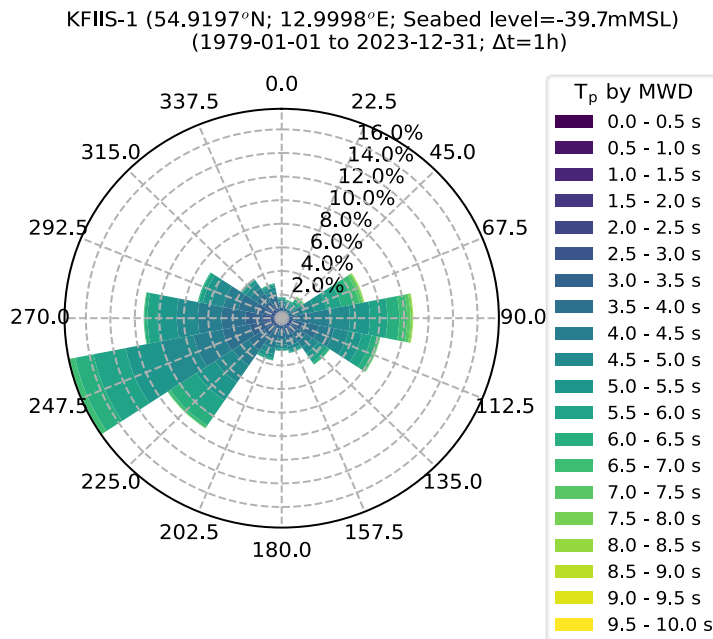


Figure 7-4 Rose plot of  $T_p$ , sorted by MWD, at KFIIS-1.

Table 7-5 Table of  $T_p$  and MWD in percentage, at KFIIS-1.

$T_p$ [s]	MWD [°N-from]															Omni	
	0.0	22.5	45.0	67.5	90.0	112.5	135.0	157.5	180.0	202.5	225.0	247.5	270.0	292.5	315.0		337.5
0.0 - 0.5	0.00	0.00	0.00	0.00	0.00	0.00	0.00	0.00	0.00	0.00	0.00	0.00	0.00	0.00	0.00	0.00	0.0
0.5 - 1.0	0.00	0.00	0.00	0.00	0.00	0.00	0.00	0.00	0.00	0.00	0.00	0.00	0.00	0.00	0.00	0.00	0.0
1.0 - 1.5	0.00	0.00	0.00	0.00	0.00	0.00	0.01	0.01	0.01	0.01	0.00	0.00	0.01	0.01	0.01	0.00	0.1
1.5 - 2.0	0.05	0.04	0.02	0.02	0.04	0.07	0.10	0.09	0.06	0.05	0.06	0.06	0.08	0.07	0.07	0.05	0.9
2.0 - 2.5	0.21	0.14	0.08	0.06	0.11	0.23	0.30	0.22	0.19	0.17	0.23	0.33	0.45	0.38	0.29	0.23	3.6
2.5 - 3.0	0.28	0.20	0.17	0.16	0.29	0.56	0.49	0.41	0.38	0.40	0.53	0.83	1.02	0.77	0.59	0.48	7.6
3.0 - 3.5	0.32	0.26	0.18	0.27	0.65	0.86	0.64	0.58	0.50	0.56	0.93	1.45	1.41	1.03	0.74	0.57	10.9
3.5 - 4.0	0.32	0.24	0.23	0.57	1.23	1.34	0.82	0.55	0.63	0.78	1.51	2.26	1.96	1.36	0.81	0.61	15.2
4.0 - 4.5	0.23	0.23	0.24	0.72	1.57	1.29	0.61	0.54	0.50	0.65	1.57	2.42	1.92	1.25	0.60	0.40	14.8
4.5 - 5.0	0.15	0.19	0.25	0.94	1.68	1.19	0.62	0.33	0.30	0.49	1.73	2.71	1.73	1.01	0.44	0.33	14.1
5.0 - 5.5	0.13	0.14	0.26	1.02	1.63	1.12	0.54	0.18	0.14	0.34	1.84	2.94	1.56	0.69	0.29	0.19	13.0
5.5 - 6.0	0.05	0.09	0.28	1.20	1.43	0.81	0.36	0.08	0.05	0.16	1.64	2.67	0.83	0.33	0.15	0.12	10.2
6.0 - 6.5	0.02	0.05	0.24	0.98	0.97	0.46	0.20	0.03	0.02	0.04	0.92	1.54	0.25	0.08	0.05	0.03	5.9
6.5 - 7.0	0.02	0.03	0.15	0.53	0.64	0.21	0.04	0.01	0.00	0.00	0.23	0.44	0.05	0.01	0.01	0.00	2.4
7.0 - 7.5	0.00	0.01	0.06	0.24	0.27	0.06	0.00	0.00	0.00	0.00	0.04	0.07	0.01	0.00	0.00	0.00	0.8
7.5 - 8.0	0.00	0.00	0.03	0.10	0.16	0.02	0.01	0.00	0.00	0.00	0.01	0.02	0.00	0.00	0.00	0.00	0.4
8.0 - 8.5	0.00	0.00	0.01	0.05	0.06	0.00	0.00	0.00	0.00	0.00	0.00	0.00	0.00	0.00	0.00	0.00	0.1
8.5 - 9.0	0.00	0.00	0.00	0.01	0.01	0.00	0.00	0.00	0.00	0.00	0.00	0.00	0.00	0.00	0.00	0.00	0.0
9.0 - 9.5	0.00	0.00	0.00	0.01	0.01	0.00	0.00	0.00	0.00	0.00	0.00	0.00	0.00	0.00	0.00	0.00	0.0
9.5 - 10.0	0.00	0.00	0.00	0.00	0.00	0.00	0.00	0.00	0.00	0.00	0.00	0.00	0.00	0.00	0.00	0.00	0.0
All	1.8	1.6	2.2	6.9	10.7	8.2	4.7	3.0	2.8	3.7	11.2	17.7	11.3	7.0	4.0	3.0	100.0

### 7.1.3 Histogram

The histogram on Figure 7-5 shows the significant wave height distribution with bins of 0.5 m. Additionally the cumulative probability distribution is also shown with the 30%, 50% and 70% quantile. The histogram for  $T_p$  is presented on Figure 7-6.

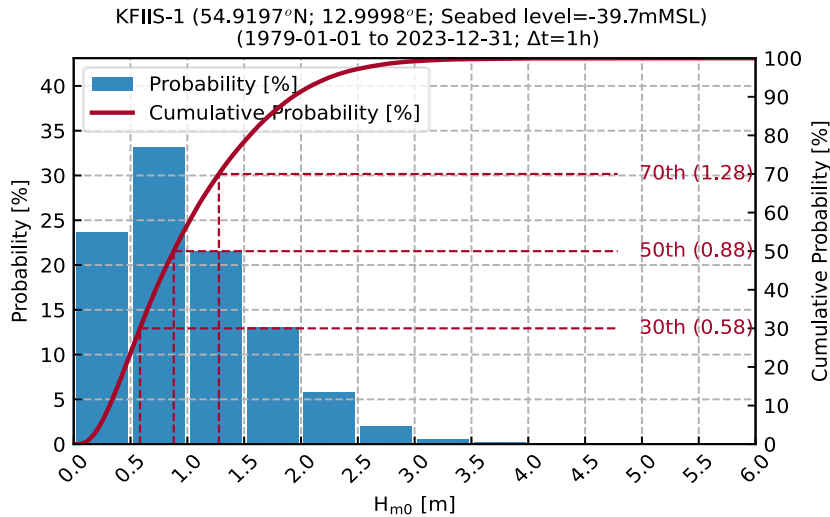


Figure 7-5 Probability plot of  $H_{m0}$  at KFIIS-1.

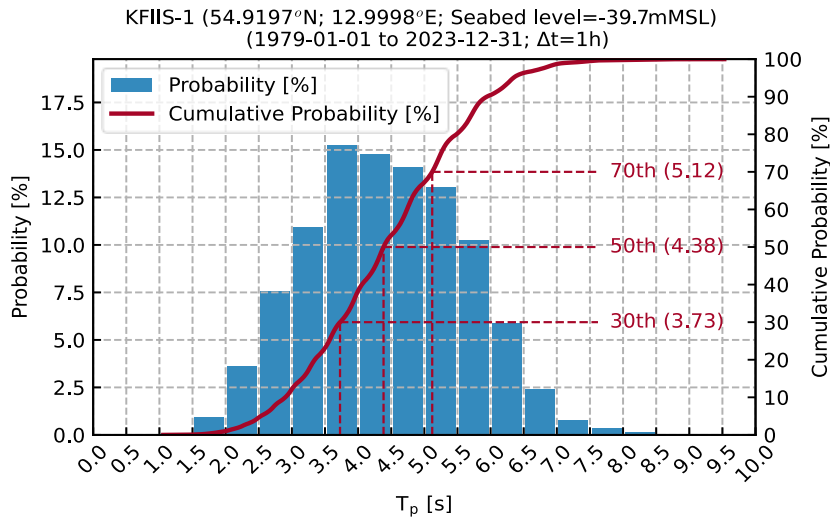


Figure 7-6 Probability plot of  $T_p$  at KFIIS-1.

### 7.1.4 Monthly statistics

Figure 7-7 shows monthly statistics for the significant wave height,  $H_{m0}$ , at KFIIS-1. The mean varies from 0.7m during summer to 1.2m during winter, with the highest mean waves occurring in January, while the maximum wave height occurs in December.  $T_p$  is shown on Figure 7-8.

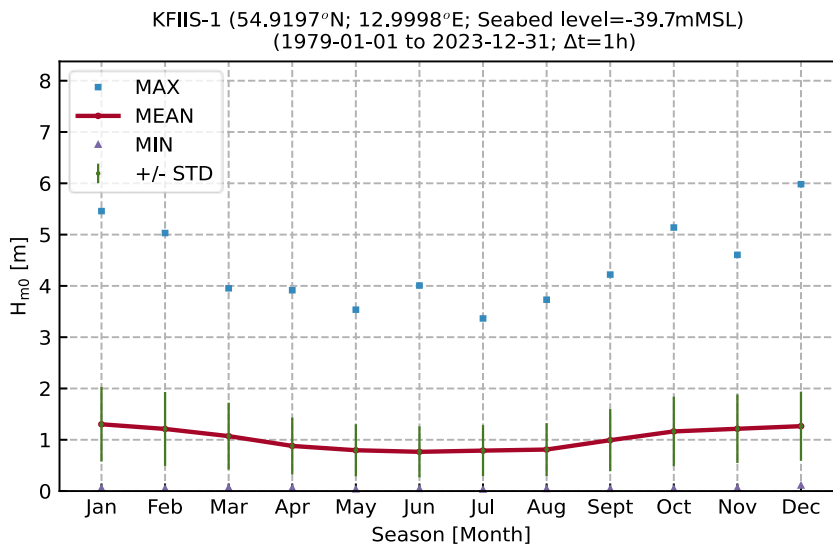


Figure 7-7 Monthly statistics of  $H_{m0}$  at KFIIS-1.

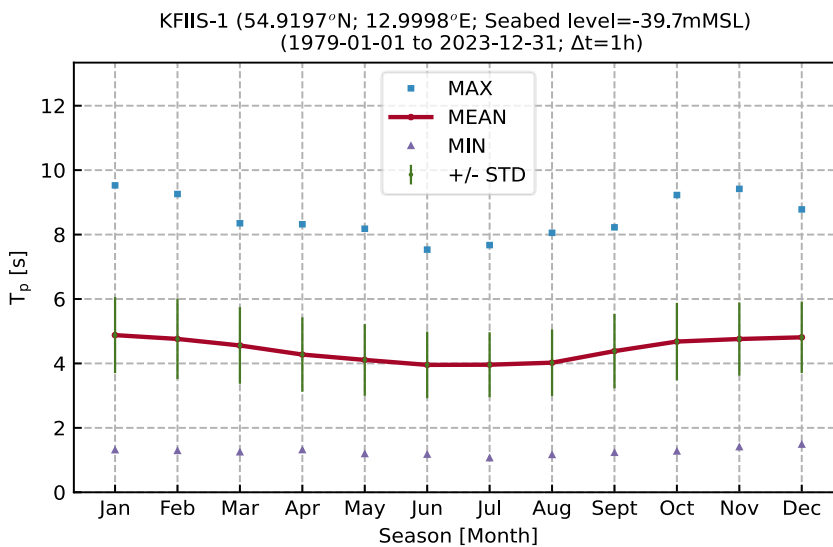


Figure 7-8 Monthly statistics of  $T_p$  at KFIIS-1.

### 7.1.5 Directional statistics

Figure 7-9 shows directional statistics for the significant wave height,  $H_{m0}$ , at KFIS-1. The mean and maximum significant wave height is highest from west-southwest.  $T_p$  is shown on Figure 7-10.

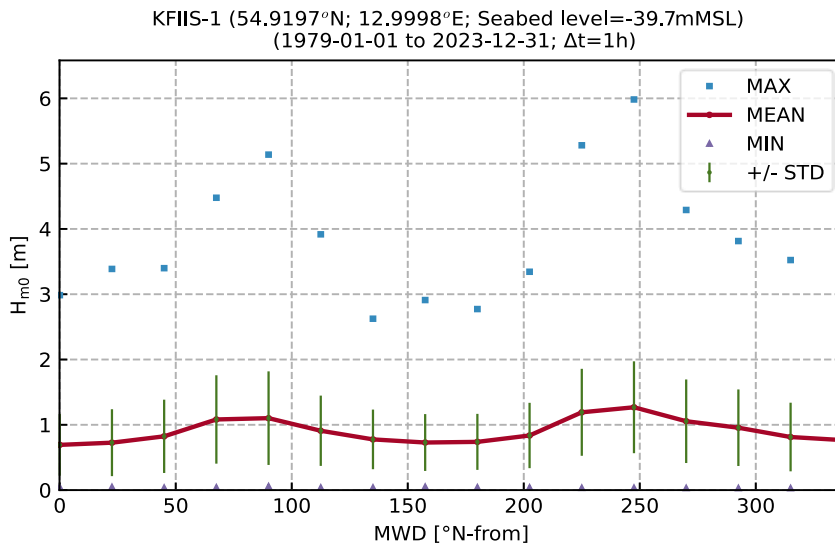


Figure 7-9 Directional statistics of  $H_{m0}$  sorted by MWD at KFIS-1.

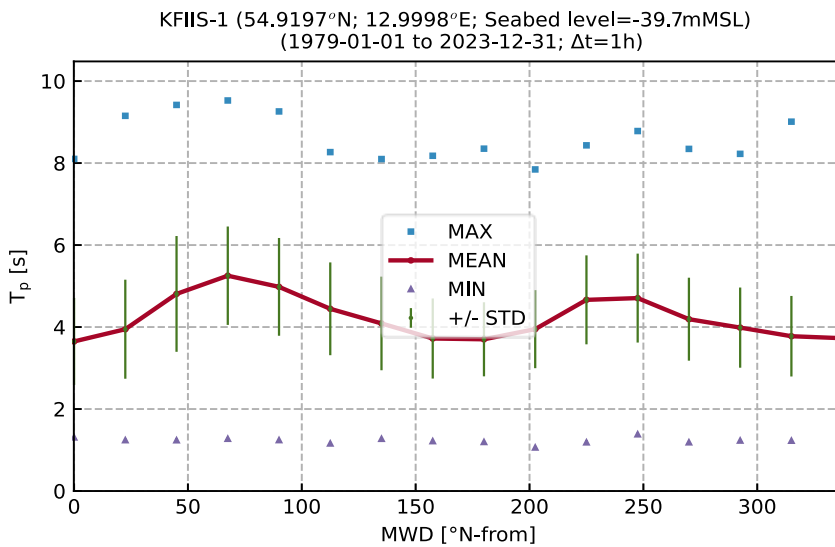


Figure 7-10 Directional statistics of  $T_p$  sorted by MWD at KFIS-1.

### 7.1.6 Correlation between wave height and period

On Figure 7-11 the correlation between  $H_{m0}$  and  $T_p$  at KFIIS-1 is presented for omni, similar plots are presented in the Appendices for all directions. The scatter shows the 2.5%, mean and 97.5% quantile. A power fit curve is fitted to the mean of  $H_{m0}$ .

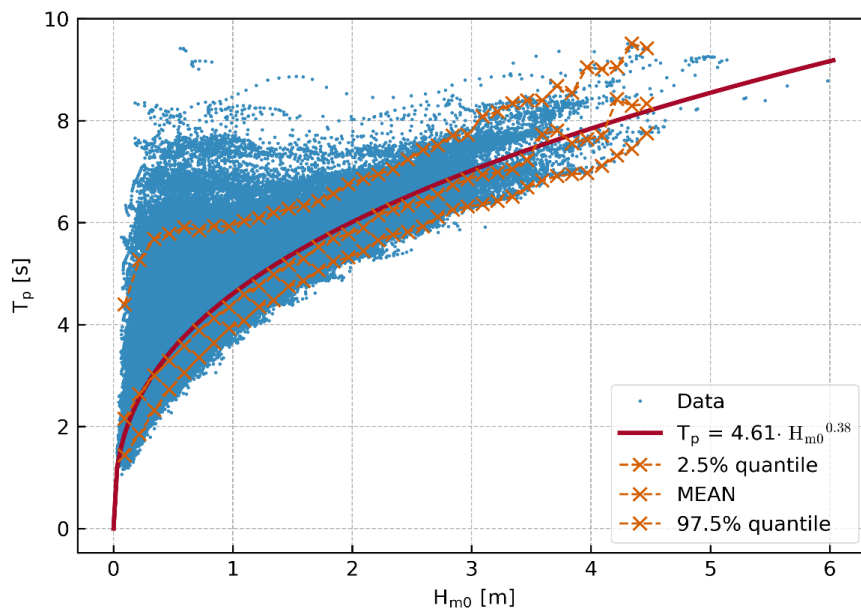


Figure 7-11  $T_p$  based on the mean of  $H_{m0}$  at KFIIS-1 for omni.

### 7.1.7 Maps of $H_{m0}$

Figure 7-12 and Figure 7-13 present maps across the data delivery area of the normalised moment of significant wave height,  $H_{m0}$ , calculated as follows.

$$\overline{H_{m0}} = \left[ \frac{1}{N} \sum_{i=1}^N H_{m0i}^m \right]^{\frac{1}{m}}$$

where  $m = (1,2,4,5)$  is the power coefficient, and  $N$  is the total number of hindcast data points.  $m = 1$  is the mean  $H_{m0}$  and  $m = 2$  is the root-mean-square wave energy.

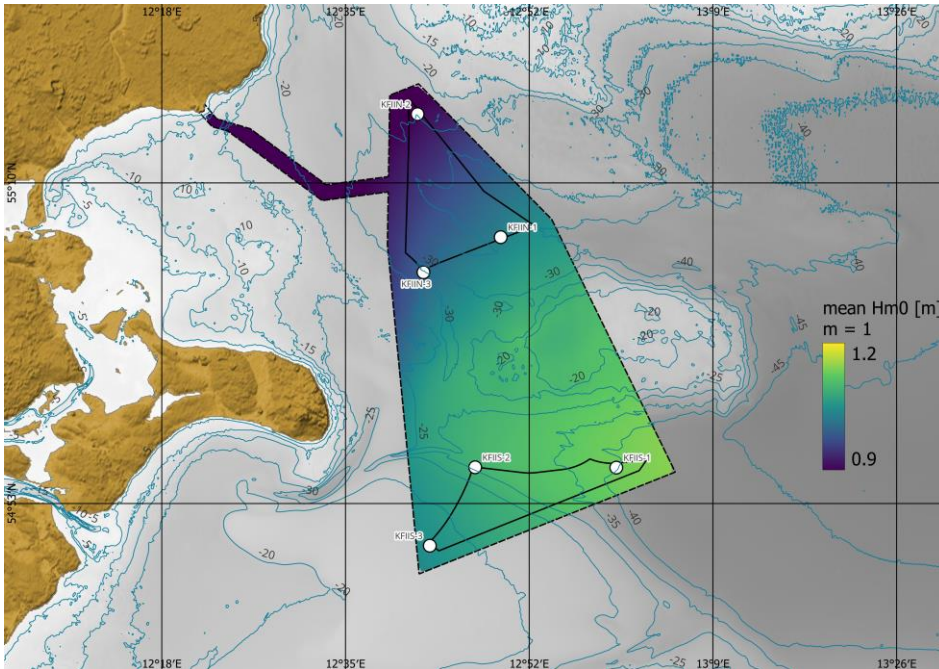


Figure 7-12 Spatial variation of moments of  $H_{m0}$  across the data delivery area,  $m=1$ .

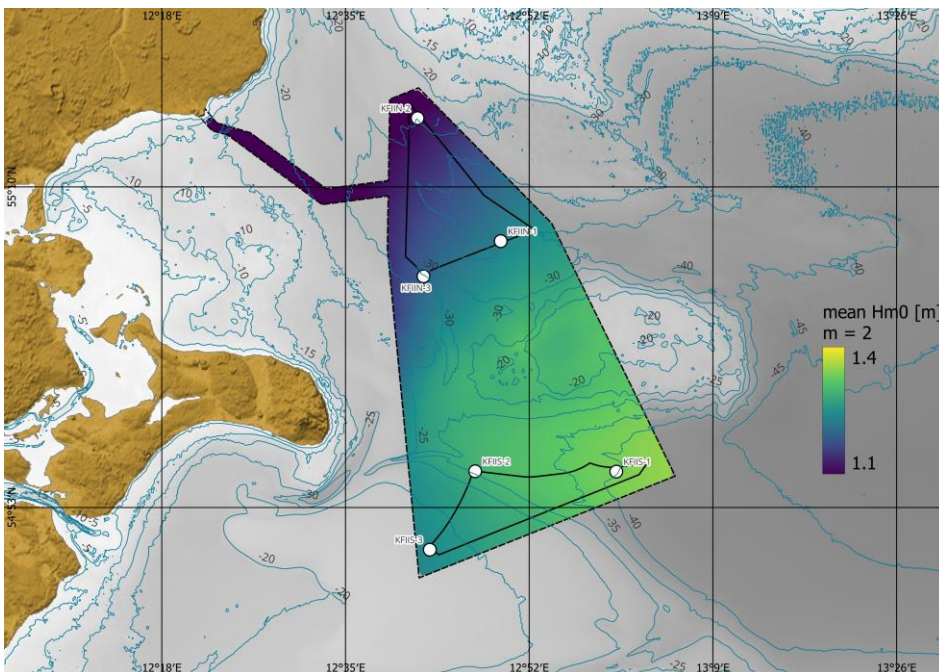


Figure 7-13 Spatial variation of moments of  $H_{m0}$  across the data delivery area,  $m=2$ .

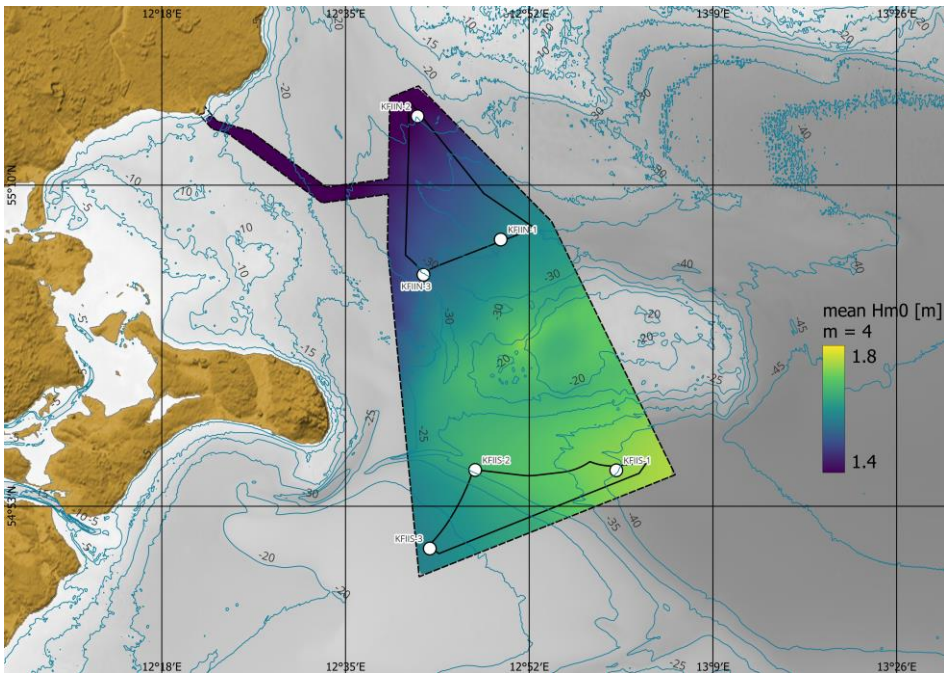


Figure 7-14 Spatial variation of moments of Hm0 across the data delivery area, m=4.

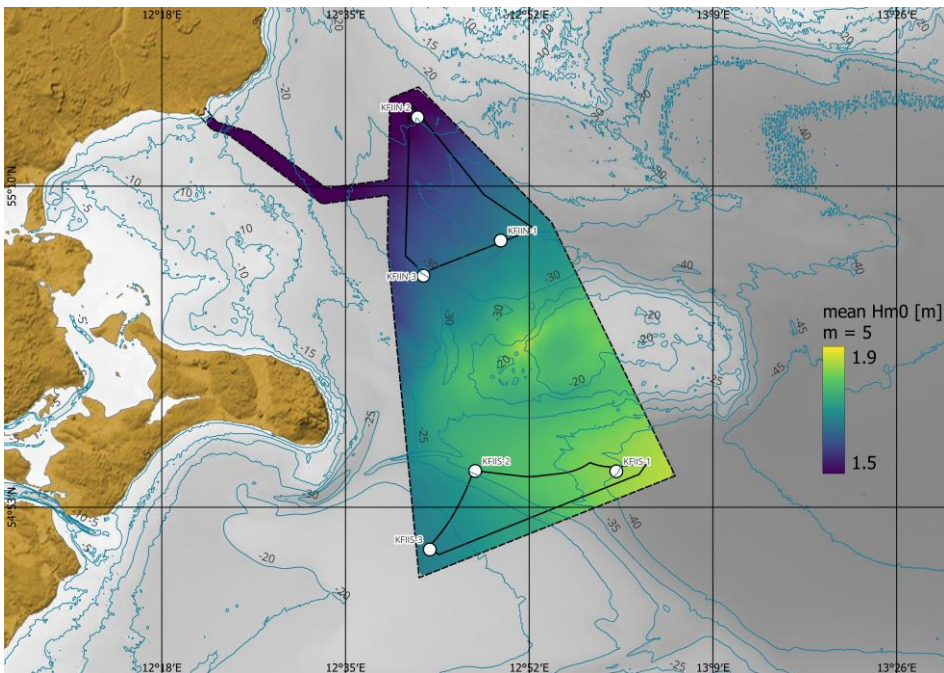


Figure 7-15 Spatial variation of moments of Hm0 across the data delivery area, m=5.

## 7.2 Extreme wave conditions unscaled

It is noted that all Extreme Value Analysis results presented in this section are unscaled, in other words raw results from the EVA without scaling with regards to directionality. Scaled results according to DNV-RP-C205 where consistency

between directional extremes and Omni for all return periods are ensured can be found in the appendices, see section 7.3 for details on the scaling.

### 7.2.1 Extreme $H_{m0}$

Extreme wave conditions are established using Extreme Value analysis. The analysis is based on its performance and sensitivity to selection of distribution, threshold selection method,  $\lambda$ -value evaluation and fitting estimator. A description of the methodology and the selection of settings is available in Appendix B.

For waves, the 3-parameter Weibull distribution was fitted by the least square method to 45 peak events ( $\lambda=1$ ) separated by at least 72 hours.

The omnidirectional extreme wave height,  $H_{m0}$ , fit for the 45-year hindcast period is shown on Figure 7-16. The Weibull distribution fitted with the least squares method is shown along the upper 97.5% and lower 2.5% confidence interval.

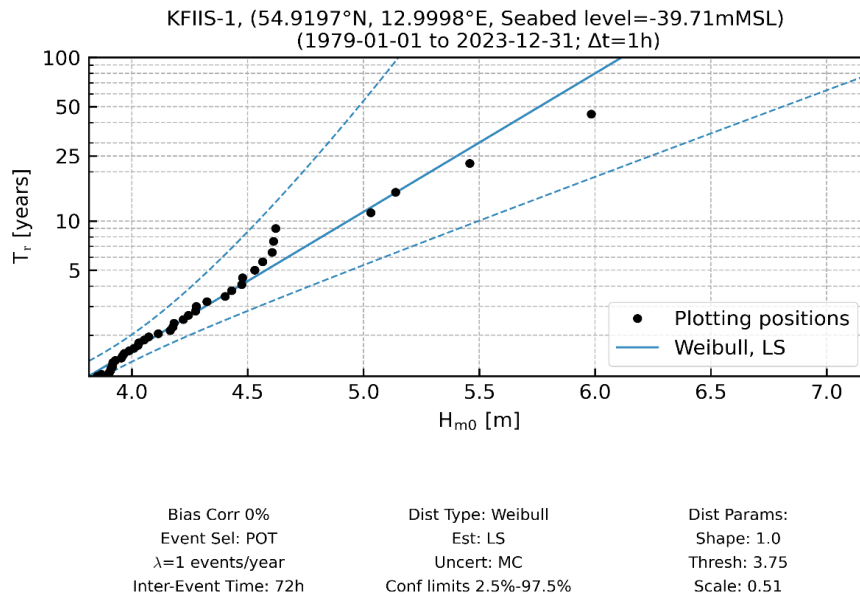


Figure 7-16 Extreme  $H_{m0}$  for omni at KFIS-1

The extreme wave fit for each direction is included in ( $H_{m0}$ ) and Table 7-7 (associated value of  $T_p$ ) as well as shown for each directional sector on Figure 7-17 ( $0^\circ$ - $157.5^\circ$ ) and Figure 7-18 ( $180^\circ$ - $337.5^\circ$ ).



Table 7-6 Marginal directional EVA estimates of  $H_{m0}$ , at KFIS-1.

Sector	$H_{m0}$ [m]					
MWD [°N-from]	Quantile	$T_r$ 1	$T_r$ 5	$T_r$ 10	$T_r$ 25	$T_r$ 50
0.0	Central estimate	1.8	2.3	2.5	2.8	3
22.5		1.8	2.4	2.6	2.9	3.1
45.0		2.1	2.7	2.9	3.3	3.5
67.5		2.8	3.6	3.9	4.3	4.6
90.0		3	3.9	4.2	4.7	5
112.5		2.4	3	3.3	3.6	3.8
135.0		2	2.3	2.4	2.6	2.6
157.5		1.9	2.3	2.4	2.6	2.8
180.0		2	2.4	2.6	2.8	3
202.5		2.3	2.8	2.9	3.2	3.3
225.0		3.3	4.1	4.4	4.8	5.2
247.5		3.5	4.4	4.8	5.2	5.6
270.0		3.2	3.8	4	4.2	4.4
292.5		2.7	3.4	3.6	3.8	3.9
315.0		2.4	3	3.2	3.5	3.7
337.5		2.1	2.5	2.7	3	3.1
Omni		3.8	4.6	4.9	5.4	5.8

Table 7-7 Peak wave period associated with the extreme  $H_{m0}$  at KFIS-1 based on mean correlation between  $H_{m0}$  and  $T_p$ .

Sector	$T_p$ [s]					
MWD [°N-from]	Quantile	$T_r$ 1	$T_r$ 5	$T_r$ 10	$T_r$ 25	$T_r$ 50
0.0	Mean estimate	5.2	5.7	5.8	6	6.2
22.5		5.2	5.6	5.8	6	6.1
45.0		6.7	7.2	7.4	7.6	7.8
67.5		7.4	8	8.2	8.4	8.6
90.0		7.4	8	8.3	8.6	8.8
112.5		6.7	7.3	7.5	7.8	7.9
135.0		6.1	6.5	6.6	6.7	6.8
157.5		5.4	5.7	5.8	6	6
180.0		5.4	5.9	6	6.2	6.3
202.5		6	6.4	6.5	6.7	6.8
225.0		7.1	7.6	7.8	8.1	8.3
247.5		7.1	7.7	8	8.2	8.5
270.0		6.5	7	7.1	7.3	7.4
292.5		6.1	6.6	6.8	6.9	7
315.0		6	6.5	6.6	6.9	7
337.5		5.7	6.2	6.3	6.5	6.7
Omni		7.6	8.3	8.5	8.8	9

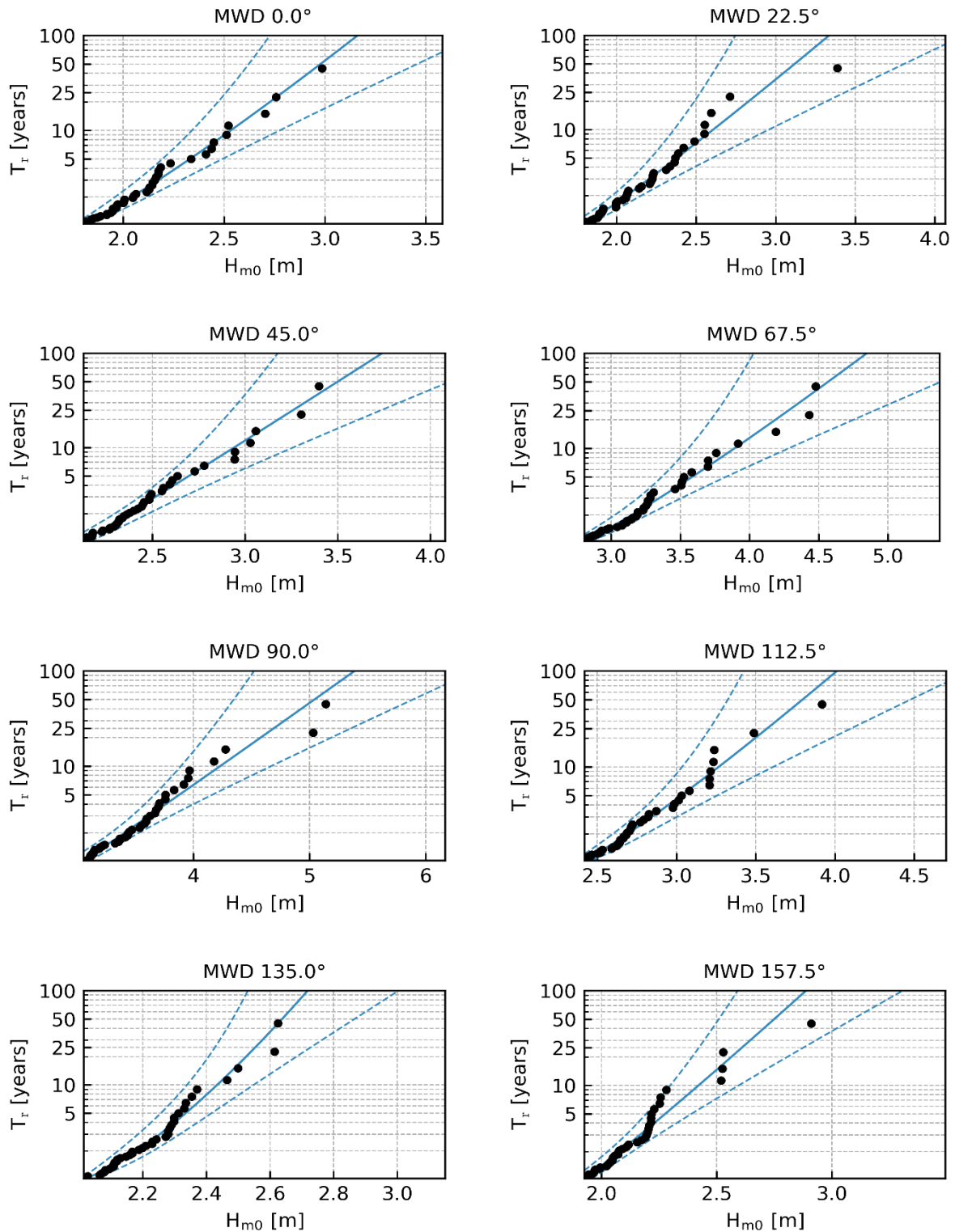


Figure 7-17 Extreme  $H_{m0}$  for MWD directional sectors at KFIS-1 (56.4251°E, 11.6797°N, Seabed level=-27.61mMSL, 1979-01-01 to 2023-12-31;  $\Delta t=1h$ ). Weibull LS,  $\lambda = 1$ . Confidence limits 2.5% - 97.5%.

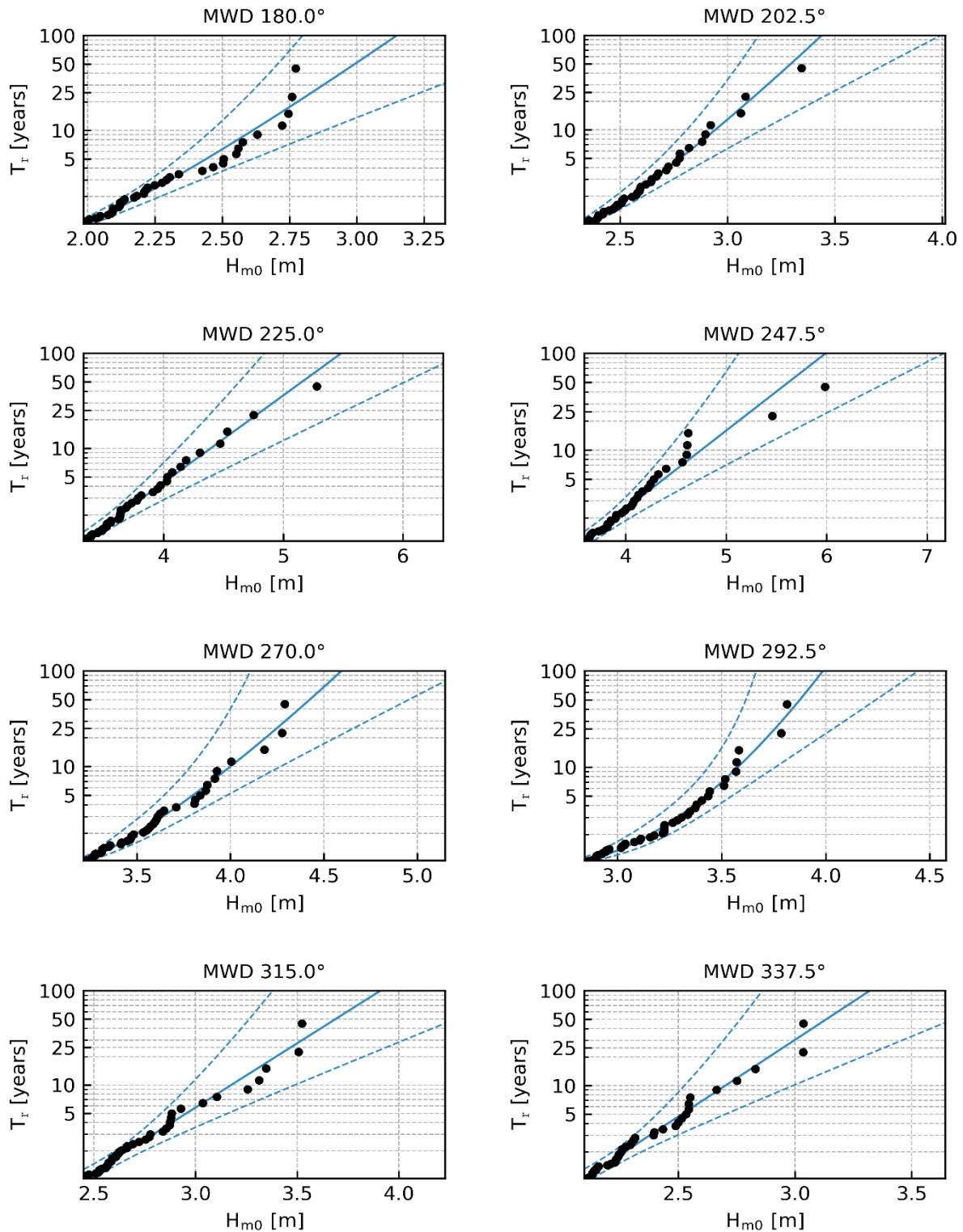


Figure 7-18 Extreme  $H_{m0}$  for MWD directional sectors at KFIS-1 (56.4251°E, 11.6797°N, Seabed level=-27.61mMSL, 1979-01-01 to 2023-12-31;  $\Delta t=1h$ ). Weibull LS,  $\lambda = 1$ . Confidence limits 2.5% - 97.5%.

### 7.2.1.1 Maps of extreme $H_{m0}$

Figure 7-19 presents the spatial variation of  $H_{m0}$  across the full data delivery area for return periods of 50-years. The wave height is based on extreme value analysis at each grid point in the data delivery area. The similar figures for return periods of 1, 5, 10 and 25 years return period can be found in Figure 7-20, Figure 7-21, Figure 7-22 and Figure 7-23 respectively. The highest extreme values in the KFII area can be found in the Centre and in the South-East part with relatively large and constant water depths.

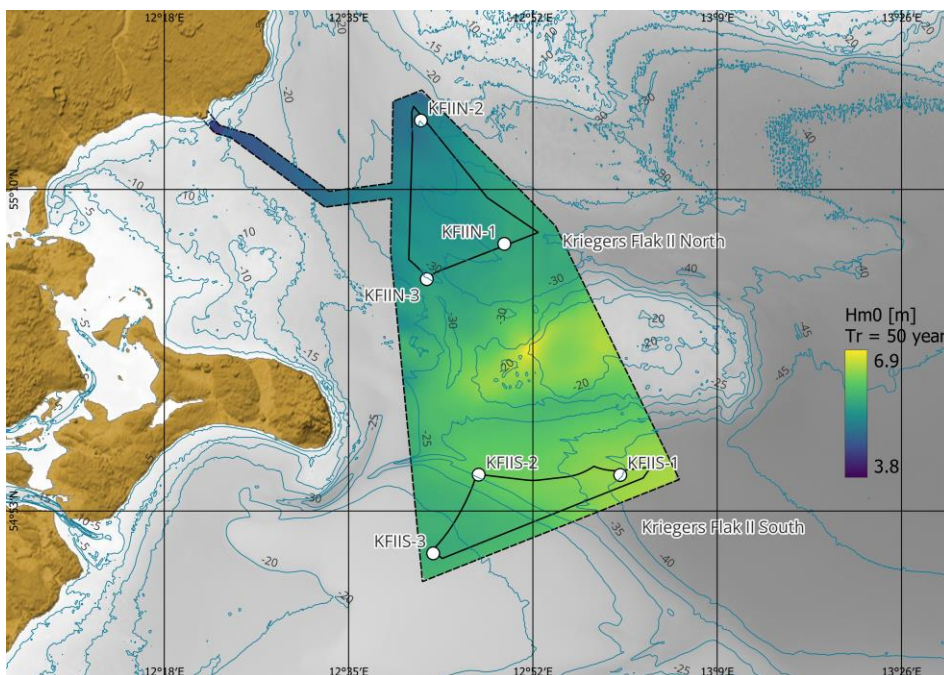


Figure 7-19 Spatial variation across the data delivery area of KFII of  $H_{m0}$  for return periods of 50 years. The colour map shows the wave height, and the contours show water depths.

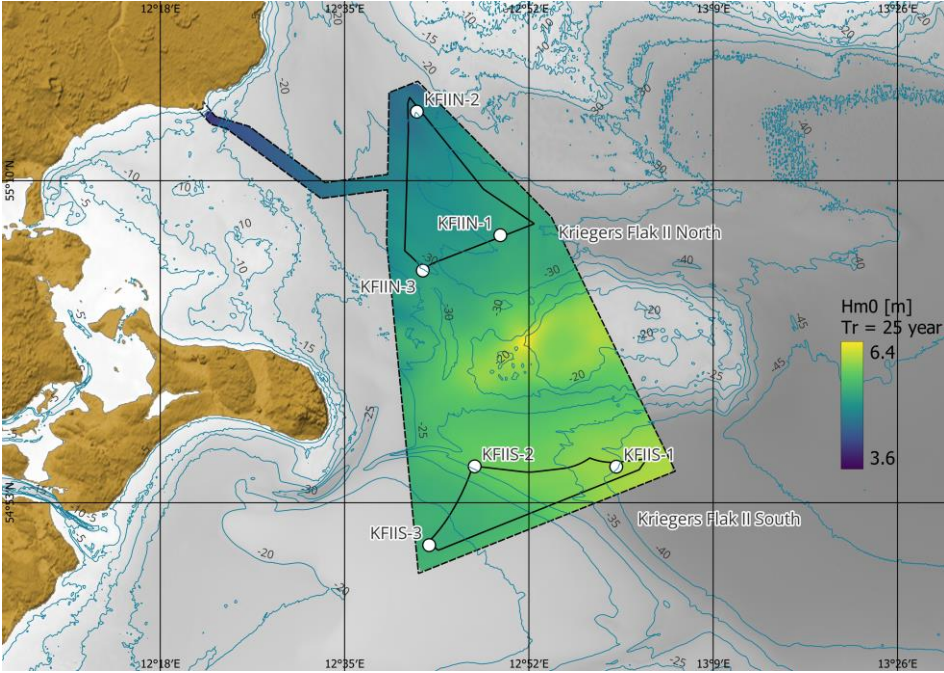


Figure 7-20 Spatial variation across the data delivery area of KFII of  $H_{m0}$  for return periods of 25 years. The colour map shows the wave height, and the contours show water depths.

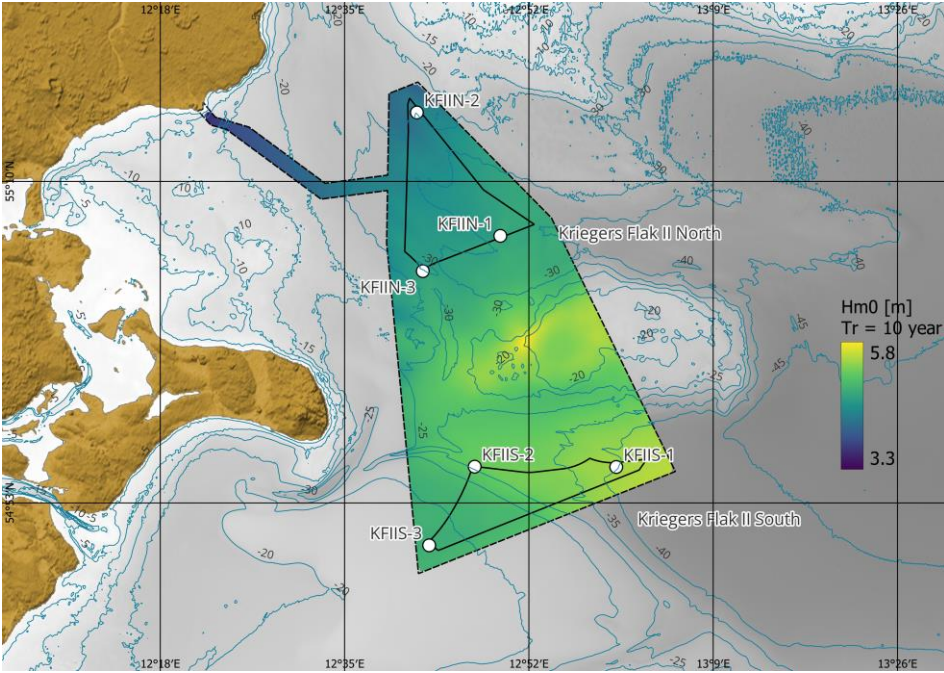


Figure 7-21 Spatial variation across the data delivery area of KFII of  $H_{m0}$  for return periods of 10 years. The colour map shows the wave height, and the contours show water depths.

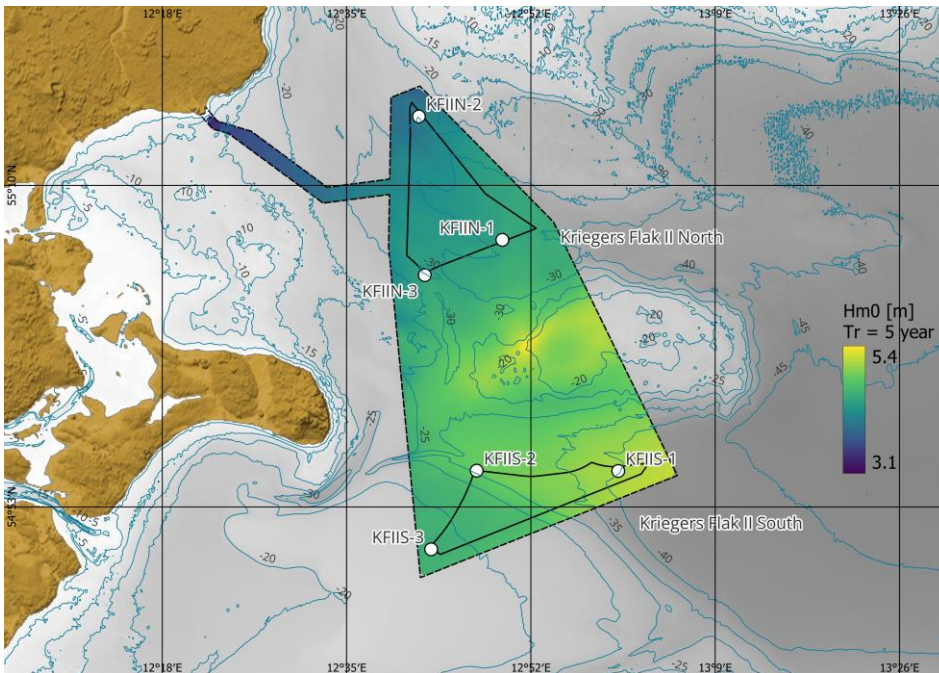


Figure 7-22 Spatial variation across the data delivery area of KFI of  $H_{m0}$  for return periods of 5 years. The colour map shows the wave height, and the contours show water depths.

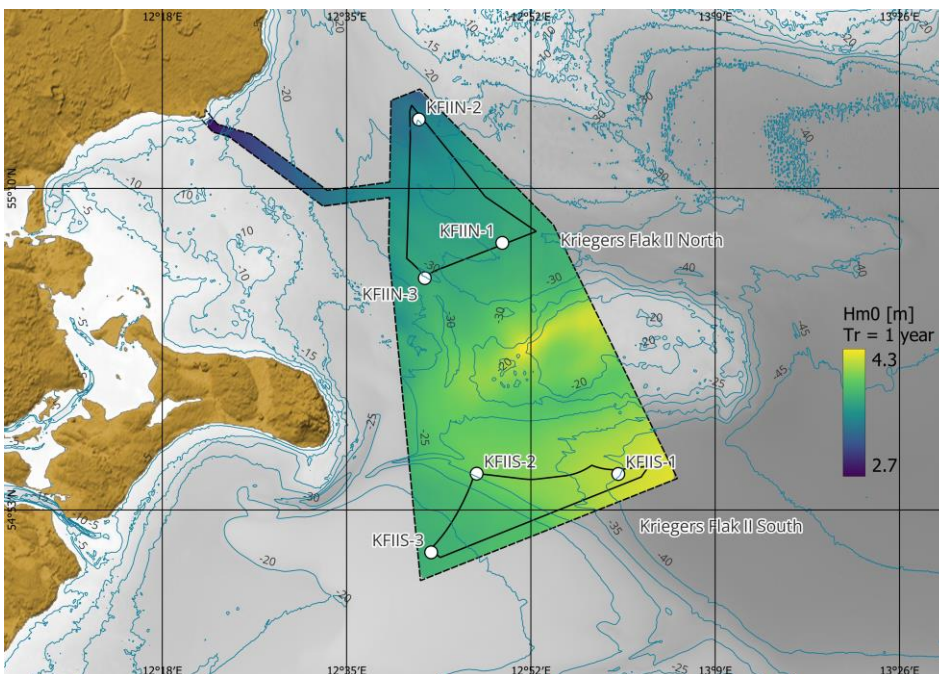


Figure 7-23 Spatial variation across the data delivery area of KFI of  $H_{m0}$  for return periods of 1 year. The colour map shows the wave height, and the contours show water depths.

### 7.2.1.2 Depth-limited significant wave height

A common approach to assess the validity of the extreme wave conditions is to consider the relationship between the wave height and the water depth. Waves are considered depth-limited when their height is constrained by the water depth. This usually occurs in shallow waters as waves approach the shore. Waves start to break when their height reaches a certain fraction of the water depth. For significant wave heights this fraction is typically around 0.5-0.6 for mildly sloping seabed, for steep sloping seabed this fraction can be higher.

When inspecting the area plot of the relationship between 50-year return period  $H_{m0}$  and water depth at MSL on Figure 7-24, the largest values are in the order of  $\approx 0.45$  in the full data delivery area, indicating that the extreme  $H_{m0}$  is realistic for the entire area.

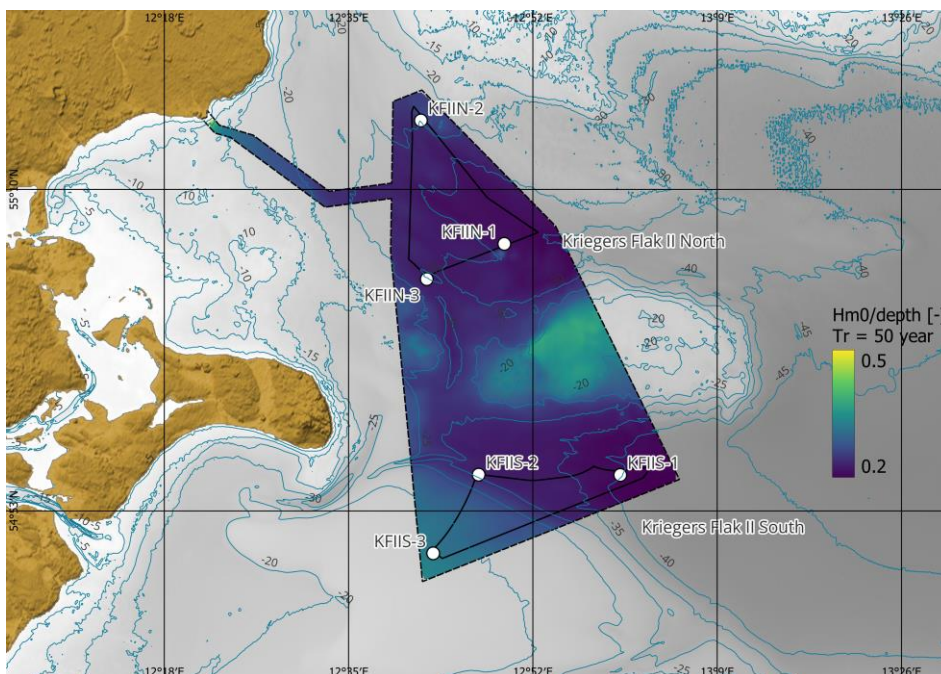


Figure 7-24 Relationship between the extreme wave height with a return period of 50 years and the depth at MSL at each model grid point in KFII.

### 7.2.2 Extreme $H_{max}$

The derivation of  $H_{max}$  for long return periods (long-term distribution) is based on a constant factor of  $H_{max}/H_{m0} = 1.95$ . This factor is higher than for example the short term Rayleigh or Forristall distribution  $H_{max}/H_{m0}$ , which by themselves only accounts for  $H_{max}$  of the individual seastate and therefore underestimates  $H_{max}$ .  $H_{max}/H_{m0} = 1.95$  is a common factor to assume to account for the long-term uncertainty and short-term uncertainty combined.

The maximum wave height,  $H_{max}$ , for each direction is included in Table 7-8 and the mode wave period associated with the maximum wave height,  $T_{Hmax}$  is presented in Table 7-9.  $T_{Hmax}$  is based on  $T_{Hmax} = 0.9 \times T_p$  as suggested in DNV-RP-C205:2021-09. The range of the wave period associated with  $H_{max}$  ( $T_{Hmax,ass}$ )

is based on equation (11) in IEC 61400-3-1:2019. The wave periods are presented in Table 7-9, Table 7-10 and Table 7-11.

It is noted that the 50 year omni  $H_{max} = 11.2\text{m}$  is far below the shallow water breaking limit ( $H/d=0.78$ , where  $H$  is the wave height and  $d$  is the water depth), indicating that the extreme maximum wave heights are realistic and the approach is reasonable.

Table 7-8 Marginal directional estimates of  $H_{max}$ , at KFIIS-1.

Sector	$H_{max}$ [m]					
MWD [°N-from]	Quantile	$T_r$ 1	$T_r$ 5	$T_r$ 10	$T_r$ 25	$T_r$ 50
0.0	Mean estimate	3.5	4.5	4.9	5.4	5.8
22.5		3.5	4.6	5.1	5.6	6.1
45.0		4.1	5.3	5.7	6.4	6.8
67.5		5.4	7	7.6	8.4	8.9
90.0		5.9	7.6	8.2	9.2	9.8
112.5		4.7	5.9	6.4	7	7.4
135.0		3.9	4.5	4.7	5	5.2
157.5		3.7	4.4	4.7	5.1	5.4
180.0		3.8	4.8	5.1	5.5	5.8
202.5		4.5	5.4	5.7	6.1	6.4
225.0		6.4	7.9	8.6	9.4	10.1
247.5		6.8	8.5	9.3	10.2	11
270.0		6.2	7.4	7.8	8.3	8.6
292.5		5.3	6.7	7	7.3	7.6
315.0		4.8	5.8	6.2	6.8	7.2
337.5		4.1	4.9	5.3	5.8	6.1
Omni		7.3	8.9	9.6	10.5	11.2



Table 7-9 Mode wave period associated with the maximum wave height at KFIS-1.

Sector	$T_{Hmax}$ [s]					
MWD [°N-from]	Quantile	$T_r$ 1	$T_r$ 5	$T_r$ 10	$T_r$ 25	$T_r$ 50
0.0	Mean estimate	4.7	5.1	5.3	5.4	5.6
22.5		4.7	5.1	5.2	5.4	5.5
45.0		6	6.5	6.6	6.8	7
67.5		6.6	7.2	7.4	7.6	7.7
90.0		6.6	7.2	7.4	7.7	7.9
112.5		6	6.6	6.8	7	7.2
135.0		5.5	5.8	5.9	6	6.1
157.5		4.8	5.1	5.2	5.4	5.4
180.0		4.9	5.3	5.4	5.6	5.7
202.5		5.4	5.7	5.8	6	6.1
225.0		6.4	6.8	7	7.3	7.5
247.5		6.4	7	7.2	7.4	7.6
270.0		5.9	6.3	6.4	6.5	6.6
292.5		5.5	6	6.1	6.2	6.3
315.0		5.4	5.8	6	6.2	6.3
337.5		5.2	5.5	5.7	5.9	6
Omni		6.9	7.4	7.6	7.9	8.1

Table 7-10 Wave period (low) associated with the maximum wave height at KFIS-1.

Sector	$T_{Hmax,ass,low}$ [s]					
MWD [°N-from]	Quantile	$T_r$ 1	$T_r$ 5	$T_r$ 10	$T_r$ 25	$T_r$ 50
0.0	Mean estimate	4.7	5.4	5.6	5.9	6.1
22.5		4.8	5.5	5.7	6	6.3
45.0		5.2	5.8	6.1	6.4	6.6
67.5		5.9	6.7	7	7.3	7.6
90.0		6.2	7	7.3	7.7	8
112.5		5.5	6.2	6.4	6.7	6.9
135.0		5	5.4	5.5	5.7	5.8
157.5		4.9	5.4	5.5	5.7	5.9
180.0		5	5.5	5.7	6	6.1
202.5		5.4	5.9	6.1	6.3	6.4
225.0		6.4	7.1	7.4	7.8	8.1
247.5		6.6	7.4	7.7	8.1	8.4
270.0		6.3	6.9	7.1	7.3	7.5
292.5		5.9	6.6	6.7	6.9	7
315.0		5.5	6.1	6.3	6.6	6.8
337.5		5.1	5.6	5.8	6.1	6.3
Omni		6.9	7.6	7.9	8.2	8.5

Table 7-11 Wave period (high) associated with the maximum wave height at KFIIS-1.

Sector	$T_{H_{max,ass,high}}$ [s]					
MWD [°N-from]	Quantile	$T_r 1$	$T_r 5$	$T_r 10$	$T_r 25$	$T_r 50$
0.0	Mean estimate	6.1	7	7.3	7.6	7.9
22.5		6.1	7	7.4	7.8	8.1
45.0		6.6	7.5	7.8	8.2	8.5
67.5		7.6	8.6	9	9.4	9.8
90.0		8	9	9.4	9.9	10.2
112.5		7.1	7.9	8.3	8.6	8.9
135.0		6.5	7	7.1	7.3	7.4
157.5		6.3	6.9	7.1	7.4	7.6
180.0		6.4	7.1	7.4	7.7	7.9
202.5		7	7.6	7.8	8.1	8.3
225.0		8.3	9.2	9.6	10	10.4
247.5		8.6	9.6	10	10.5	10.8
270.0		8.1	8.9	9.1	9.4	9.6
292.5		7.5	8.4	8.6	8.9	9
315.0		7.1	7.8	8.1	8.5	8.8
337.5		6.6	7.2	7.5	7.8	8.1
Omni		8.8	9.8	10.1	10.6	11

### 7.2.3 Extreme $C_{max}$

For  $C_{max}$ , the Stream Function theory is used based on the derived  $H_{max}$  and  $T_{H_{max,ass}}$  in section 7.2.2 and the water depth at MSL. This is a slightly conservative approach.  $C_{max}$  is based on MSL and does not include contribution from high/low water level.

The maximum wave crest height,  $C_{max}$ , for each direction is included in Table 7-12.

Table 7-12 Marginal directional extreme estimates of  $C_{max}$ , at KFIS-1.

Sector	$C_{max}$ [m AMSL]						
	MWD [°N-from]	Quantile	$T_r$ 1	$T_r$ 5	$T_r$ 10	$T_r$ 25	$T_r$ 50
	0.0	Mean estimate	2	2.6	2.9	3.2	3.4
	22.5		2	2.7	3	3.4	3.6
	45.0		2.3	2.9	3.2	3.6	3.8
	67.5		3	3.9	4.3	4.8	5.1
	90.0		3.3	4.3	4.7	5.3	5.7
	112.5		2.6	3.3	3.6	3.9	4.2
	135.0		2.2	2.5	2.6	2.8	2.9
	157.5		2.1	2.6	2.7	3	3.1
	180.0		2.2	2.8	3	3.2	3.4
	202.5		2.6	3.1	3.3	3.6	3.7
	225.0		3.7	4.6	5	5.5	6
	247.5		4	5	5.5	6.1	6.6
	270.0		3.6	4.4	4.6	4.9	5.1
	292.5		3.1	3.9	4.1	4.3	4.5
	315.0		2.7	3.3	3.6	3.9	4.2
	337.5		2.3	2.8	3	3.3	3.5
	Omni		4.2	5.2	5.6	6.2	6.7

## 7.3 Extreme wave conditions scaled

Section 7.2 presents the results of the EVA analysis of the extreme wave conditions. DNV-RP-C205 section 3.6.5.6 presents a method for scaling the results of the EVA analysis. The applicability of the scaling method will not be discussed further here, but due care is advised when applying the results of the scaling.

Scaling according to DNV-RP-C205 section 3.6.5.6 has been performed for the extreme wave conditions and is available in the Appendices.

## 7.4 Wave Spectrum

Full directional spectra are available in hindcast format, and a comparison with measured wave spectra has been performed in [1].

A comparison between hindcast wave spectra and JONSWAP spectra (as defined in DNV-RP-C205:2021-09) has been performed for a number of  $H_{m0}$  ranges. The comparison for several  $H_{m0}$  bins is presented in the appendices, and in Figure 7-25 an example is presented.

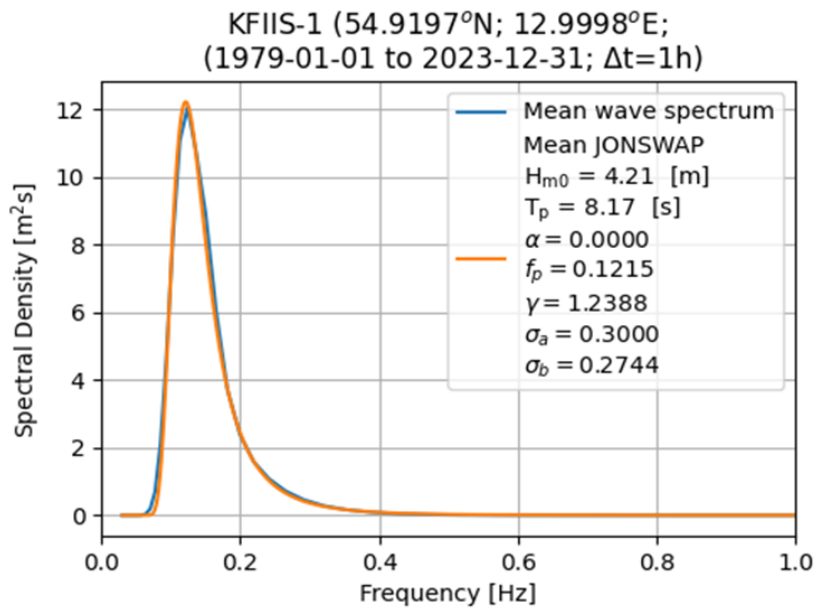


Figure 7-25 Comparison of hindcast (mean wave spectrum) and JONSWAP spectra for  $H_{m0} = 4.0$ - $4.5$  m at KFIS-1.

The analysis shows that the hindcast spectra cannot be represented precisely by the JONSWAP spectrum at the peak by the recommendations in DNV-RP-C205:2021-09, but that the overall fit is good. It is noted that in [1] the comparison between the hindcast spectrum and the measured spectrum is good, but the hindcast spectrum tends to undershoot the measured peak, thus the JONSWAP fit is closer to the measured spectrum. Therefore the JONSWAP wave spectrum is recommended for all stochastic wave series based on the recommendations in DNV-RP-C205:2021-09. The peak enhancement factor ( $\gamma$ ) can be determined using the following relationship:

$$\gamma = \begin{cases} 5 & \text{for } \frac{T_p}{\sqrt{H_s}} \leq 3.6 \\ \exp\left(5.75 - 1.15 \frac{T_p}{\sqrt{H_s}}\right) & \text{for } 3.6 < \frac{T_p}{\sqrt{H_s}} \leq 5 \\ 1 & \text{for } 5 < \frac{T_p}{\sqrt{H_s}} \end{cases}$$

### 7.4.1 Directional Spreading

The directional spreading factor is used to modify uni-directional regular wave theories. The directional spreading factor can be applied if no significant refraction is present.

Figure 7-26 shows the wave directional standard deviation as a function of the significant wave height.

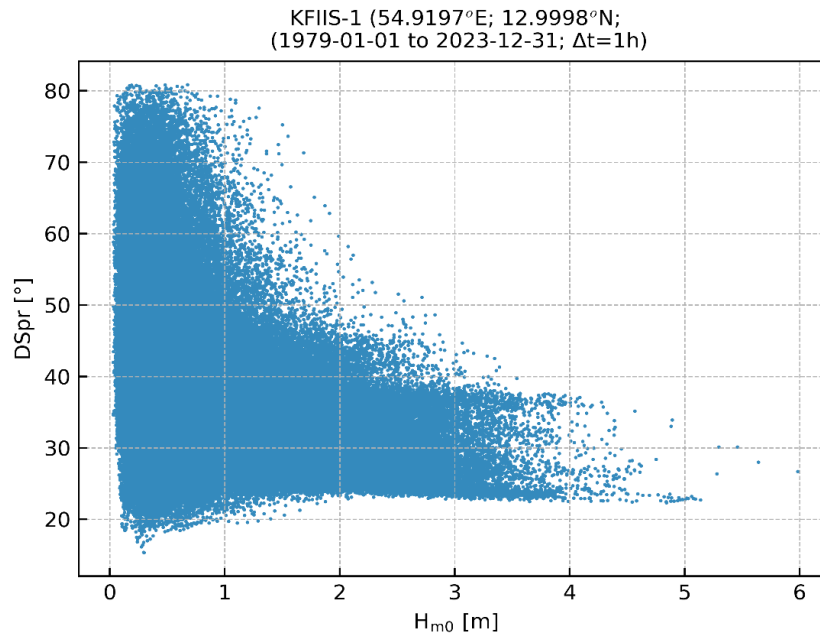


Figure 7-26 Wave directional standard deviation as a function H<sub>m0</sub>.

Based on Figure 7-26 a conservative estimate of the wave directional standard deviation for extreme conditions is found to be 21°.

In Figure 7-27 the spreading factor as a function of the directional standard deviation can be seen.

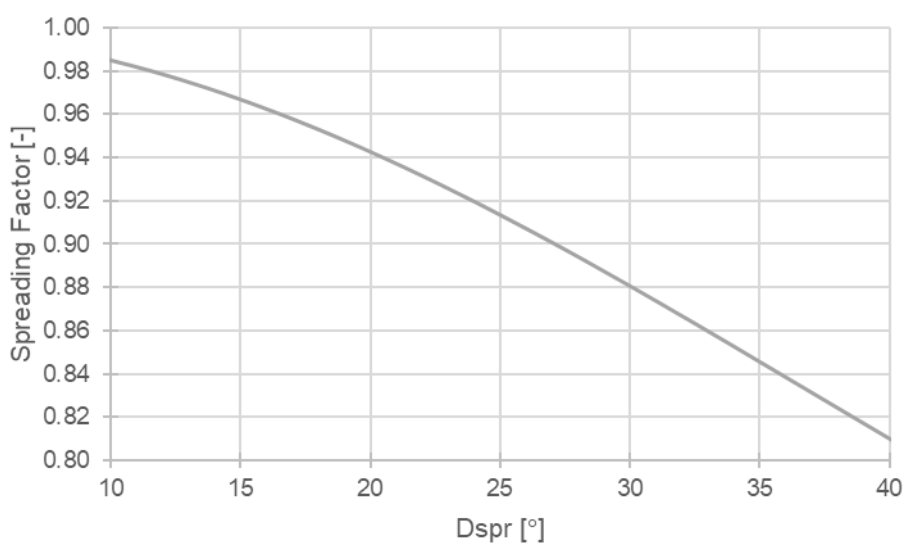


Figure 7-27 Relationship between directional standard deviation and Spreading factor applied in ISO 19901-1:2015.

In Figure 7-27 it is seen that the conservative estimate of a wave directional standard deviation of  $21^\circ$  yields a spreading factor of 0.94.

# 8 Scatter Distributions

This section presents a scatter diagrams and figures between various parameters.

## 8.1.1 Wind-wave misalignment

The scatter of MWD and  $U_{150dir}$  is presented on Figure 8-1 and Table 8-1. The scatter shows a clear trend along the 1:1 line with some scatter evenly spread across the range. The higher density areas opposite to the 1:1 line is due to the wrap around.

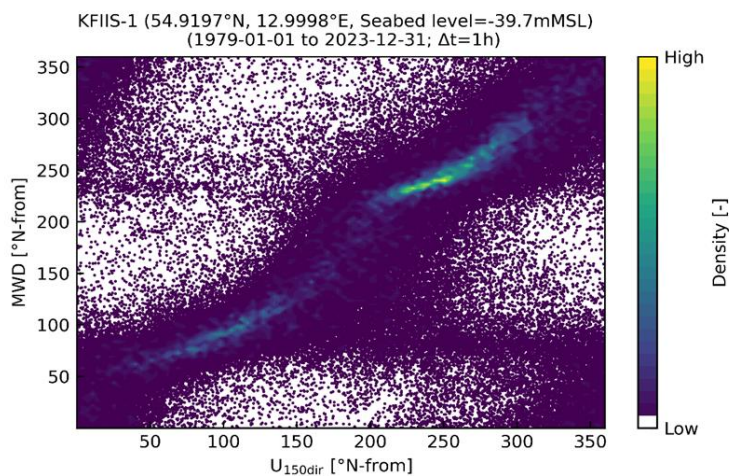


Figure 8-1 Scatter of MWD and  $U_{150dir}$  at KFIIS-1

Table 8-1 Table of  $U_{150dir}$  and MWD in percentage, at KFIIN-1. Total number of events=394464.

$U_{150dir}$ [°N- from]	MWD [°N-from]																Omni
	0.0	22.5	45.0	67.5	90.0	112.5	135.0	157.5	180.0	202.5	225.0	247.5	270.0	292.5	315.0	337.5	
0.0	0.71	0.30	0.08	0.03	0.02	0.01	0.01	0.01	0.01	0.01	0.02	0.03	0.04	0.07	0.12	0.33	1.8
22.5	0.48	0.48	0.15	0.05	0.02	0.01	0.01	0.01	0.01	0.01	0.02	0.03	0.03	0.05	0.09	0.17	1.6
45.0	0.32	0.75	0.46	0.14	0.05	0.02	0.02	0.01	0.02	0.03	0.02	0.04	0.04	0.06	0.09	0.13	2.2
67.5	0.22	0.53	1.57	2.15	1.29	0.24	0.09	0.07	0.07	0.08	0.08	0.08	0.08	0.09	0.10	0.16	6.9
90.0	0.11	0.11	0.23	1.06	3.84	3.41	0.77	0.28	0.17	0.14	0.13	0.13	0.10	0.08	0.08	0.09	10.7
112.5	0.03	0.03	0.03	0.09	0.31	2.52	3.52	0.89	0.28	0.16	0.12	0.09	0.05	0.04	0.04	0.03	8.2
135.0	0.01	0.01	0.01	0.02	0.04	0.14	1.23	2.06	0.64	0.25	0.12	0.08	0.04	0.03	0.02	0.01	4.7
157.5	0.01	0.01	0.01	0.01	0.02	0.04	0.16	0.95	1.14	0.37	0.16	0.08	0.04	0.02	0.02	0.01	3.0
180.0	0.01	0.01	0.01	0.01	0.01	0.02	0.06	0.31	1.18	0.72	0.26	0.11	0.05	0.02	0.01	0.01	2.8
202.5	0.01	0.01	0.01	0.01	0.01	0.01	0.03	0.12	0.82	1.66	0.63	0.20	0.07	0.03	0.01	0.01	3.7
225.0	0.03	0.03	0.03	0.02	0.02	0.02	0.04	0.07	0.27	2.36	5.84	2.01	0.31	0.10	0.06	0.03	11.2
247.5	0.06	0.04	0.03	0.02	0.02	0.02	0.03	0.04	0.08	0.21	1.68	8.22	6.02	0.95	0.23	0.09	17.7
270.0	0.09	0.04	0.03	0.02	0.02	0.01	0.02	0.03	0.04	0.08	0.17	0.70	4.49	4.48	0.83	0.23	11.3
292.5	0.14	0.06	0.03	0.01	0.01	0.01	0.02	0.02	0.02	0.04	0.05	0.13	0.59	3.45	1.96	0.47	7.0
315.0	0.24	0.08	0.03	0.02	0.01	0.01	0.01	0.01	0.02	0.02	0.03	0.05	0.13	0.61	1.76	1.02	4.0
337.5	0.77	0.16	0.05	0.02	0.01	0.01	0.01	0.01	0.01	0.01	0.02	0.03	0.06	0.14	0.43	1.29	3.0
Omni	3.2	2.6	2.8	3.7	5.7	6.5	6.0	4.9	4.8	6.2	9.3	12.0	12.1	10.2	5.9	4.1	100

The wind-wave misalignment is calculated as  $U_{10\text{mag}}$  minus MWD. Figure 8-2 and Table 8-2 presents the misalignment vs.  $U_{150\text{mag}}$  at KFIIS-1. The misalignment shows a high scatter for wind speeds less than  $\sim 5$  m/s, while the scatter (misalignment) is relatively low for higher wind speeds.

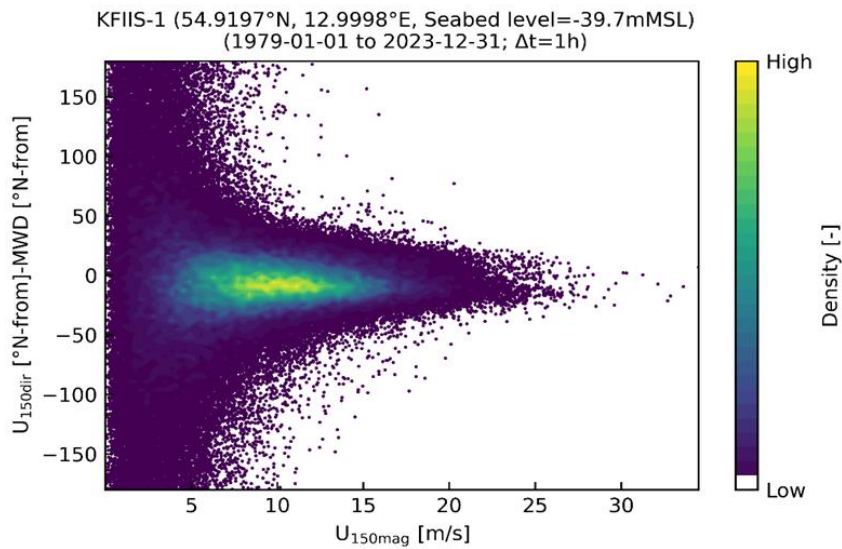


Figure 8-2 Scatter of  $U_{150\text{mag}}$  and  $U_{150\text{dir}} - \text{MWD}$



Table 8-2 Table of  $U_{150mag}$  and  $U_{150dir}$ -MWD in percentage, at KFIS-1.

$U_{150mag}$ [m/s]	$U_{150dir}$ [°N-from] - MWD															Sum	
	180.0	157.5	135.0	112.5	90.0	67.5	45.0	22.5	0.0	22.5	45.0	67.5	90.0	112.5	135.0		157.5
0.0 - 1.0	0.05	0.04	0.05	0.05	0.05	0.05	0.07	0.07	0.07	0.06	0.06	0.06	0.06	0.05	0.05	0.05	0.9
1.0 - 2.0	0.09	0.10	0.12	0.13	0.15	0.19	0.24	0.28	0.27	0.22	0.18	0.15	0.13	0.11	0.10	0.09	2.5
2.0 - 3.0	0.10	0.10	0.12	0.17	0.23	0.35	0.51	0.64	0.54	0.40	0.31	0.20	0.14	0.12	0.10	0.09	4.1
3.0 - 4.0	0.07	0.09	0.11	0.15	0.25	0.47	0.86	1.21	0.94	0.60	0.30	0.18	0.12	0.09	0.07	0.07	5.6
4.0 - 5.0	0.06	0.06	0.09	0.12	0.23	0.52	1.16	1.82	1.45	0.68	0.26	0.14	0.08	0.05	0.05	0.05	6.8
5.0 - 6.0	0.04	0.05	0.05	0.09	0.19	0.48	1.38	2.59	1.96	0.64	0.19	0.08	0.04	0.03	0.02	0.03	7.9
6.0 - 7.0	0.02	0.02	0.04	0.05	0.13	0.40	1.53	3.41	2.37	0.62	0.12	0.04	0.02	0.01	0.01	0.01	8.8
7.0 - 8.0	0.01	0.01	0.02	0.04	0.08	0.29	1.49	4.15	2.60	0.48	0.07	0.02	0.01	0.01	0.01	0.01	9.3
8.0 - 9.0	0.00	0.01	0.01	0.02	0.04	0.20	1.31	4.69	2.55	0.34	0.04	0.01	0.00	0.00	0.00	0.00	9.2
9.0 - 10.0	0.00	0.00	0.01	0.01	0.03	0.13	1.10	4.92	2.38	0.26	0.02	0.00	0.00	0.00	0.00	0.00	8.9
10.0 - 11.0	0.00	0.00	0.00	0.01	0.02	0.07	0.87	4.68	2.12	0.21	0.01	0.00	0.00	0.00	0.00	0.00	8.0
11.0 - 12.0	0.00	0.00	0.00	0.00	0.01	0.04	0.67	4.32	1.82	0.16	0.00	0.00	0.00	0.00	0.00	0.00	7.0
12.0 - 13.0	0.00	0.00	0.00	0.00	0.00	0.02	0.48	3.68	1.43	0.12	0.00	0.00	0.00	0.00	0.00	0.00	5.7
13.0 - 14.0	0.00	0.00	0.00	0.00	0.00	0.02	0.36	3.03	1.15	0.08	0.00	0.00	0.00	0.00	0.00	0.00	4.6
14.0 - 15.0	0.00	0.00	0.00	0.00	0.00	0.01	0.23	2.31	0.87	0.06	0.00	0.00	0.00	0.00	0.00	0.00	3.5
15.0 - 16.0	0.00	0.00	0.00	0.00	0.00	0.01	0.17	1.68	0.62	0.03	0.00	0.00	0.00	0.00	0.00	0.00	2.5
16.0 - 17.0	0.00	0.00	0.00	0.00	0.00	0.00	0.10	1.11	0.46	0.02	0.00	0.00	0.00	0.00	0.00	0.00	1.7
17.0 - 18.0	0.00	0.00	0.00	0.00	0.00	0.00	0.05	0.72	0.35	0.02	0.00	0.00	0.00	0.00	0.00	0.00	1.1
18.0 - 19.0	0.00	0.00	0.00	0.00	0.00	0.00	0.03	0.46	0.21	0.01	0.00	0.00	0.00	0.00	0.00	0.00	0.7
19.0 - 20.0	0.00	0.00	0.00	0.00	0.00	0.00	0.02	0.28	0.12	0.00	0.00	0.00	0.00	0.00	0.00	0.00	0.4
20.0 - 21.0	0.00	0.00	0.00	0.00	0.00	0.00	0.01	0.18	0.07	0.00	0.00	0.00	0.00	0.00	0.00	0.00	0.3
21.0 - 22.0	0.00	0.00	0.00	0.00	0.00	0.00	0.01	0.08	0.04	0.00	0.00	0.00	0.00	0.00	0.00	0.00	0.1
22.0 - 23.0	0.00	0.00	0.00	0.00	0.00	0.00	0.00	0.05	0.02	0.00	0.00	0.00	0.00	0.00	0.00	0.00	0.1
23.0 - 24.0	0.00	0.00	0.00	0.00	0.00	0.00	0.00	0.03	0.01	0.00	0.00	0.00	0.00	0.00	0.00	0.00	0.0
24.0 - 25.0	0.00	0.00	0.00	0.00	0.00	0.00	0.00	0.02	0.01	0.00	0.00	0.00	0.00	0.00	0.00	0.00	0.0
25.0 - 26.0	0.00	0.00	0.00	0.00	0.00	0.00	0.00	0.01	0.01	0.00	0.00	0.00	0.00	0.00	0.00	0.00	0.0
26.0 - 27.0	0.00	0.00	0.00	0.00	0.00	0.00	0.00	0.01	0.00	0.00	0.00	0.00	0.00	0.00	0.00	0.00	0.0
27.0 - 28.0	0.00	0.00	0.00	0.00	0.00	0.00	0.00	0.00	0.00	0.00	0.00	0.00	0.00	0.00	0.00	0.00	0.0
28.0 - 29.0	0.00	0.00	0.00	0.00	0.00	0.00	0.00	0.00	0.00	0.00	0.00	0.00	0.00	0.00	0.00	0.00	0.0
29.0 - 30.0	0.00	0.00	0.00	0.00	0.00	0.00	0.00	0.00	0.00	0.00	0.00	0.00	0.00	0.00	0.00	0.00	0.0
30.0 - 31.0	0.00	0.00	0.00	0.00	0.00	0.00	0.00	0.00	0.00	0.00	0.00	0.00	0.00	0.00	0.00	0.00	0.0
31.0 - 32.0	0.00	0.00	0.00	0.00	0.00	0.00	0.00	0.00	0.00	0.00	0.00	0.00	0.00	0.00	0.00	0.00	0.0
32.0 - 33.0	0.00	0.00	0.00	0.00	0.00	0.00	0.00	0.00	0.00	0.00	0.00	0.00	0.00	0.00	0.00	0.00	0.0
33.0 - 34.0	0.00	0.00	0.00	0.00	0.00	0.00	0.00	0.00	0.00	0.00	0.00	0.00	0.00	0.00	0.00	0.00	0.0
34.0 - 35.0	0.00	0.00	0.00	0.00	0.00	0.00	0.00	0.00	0.00	0.00	0.00	0.00	0.00	0.00	0.00	0.00	0.0
Sum	0.5	0.5	0.6	0.8	1.4	3.3	12.7	46.4	24.5	5.0	1.6	0.9	0.6	0.5	0.4	0.4	100

### 8.1.2 Scatter distribution of wave height and water level

The scatter of  $H_{m0}$  and WL is presented on Figure 8-3 and in Table 8-3. In the appendices figures for all directions of MWD can be found.

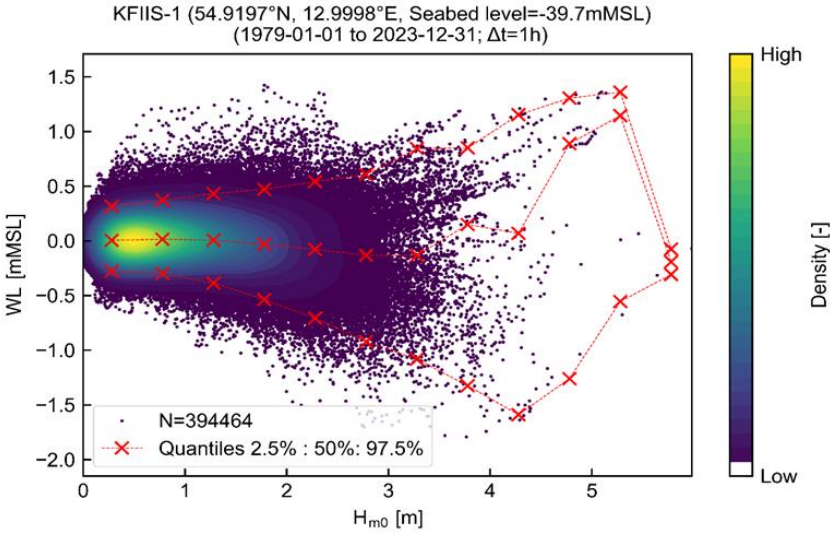


Figure 8-3 Scatter of  $H_{m0}$  and WL at KFIIS-1. Plots for all directions of MWD are in the appendices.

Table 8-3 Table of  $H_{m0}$  and WL in percentage, at KFIIS-1.

WL [mMSL]	$H_{m0}$ [m]												Sum	
	0.0-0.5	0.5-1.0	1.0-1.5	1.5-2.0	2.0-2.5	2.5-3.0	3.0-3.5	3.5-4.0	4.0-4.5	4.5-5.0	5.0-5.5	5.5-6.0		
-1.7--1.6	0.00	0.00	0.00	0.00	0.00	0.00	0.00	0.00	0.00	0.00	0.00	0.00	0.00	0.0
-1.6--1.5	0.00	0.00	0.00	0.00	0.00	0.00	0.00	0.00	0.00	0.00	0.00	0.00	0.00	0.0
-1.5--1.4	0.00	0.00	0.00	0.00	0.00	0.00	0.00	0.00	0.00	0.00	0.00	0.00	0.00	0.0
-1.4--1.3	0.00	0.00	0.00	0.00	0.00	0.00	0.00	0.00	0.00	0.00	0.00	0.00	0.00	0.0
-1.3--1.2	0.00	0.00	0.00	0.00	0.00	0.00	0.00	0.00	0.00	0.00	0.00	0.00	0.00	0.0
-1.2--1.1	0.00	0.00	0.00	0.00	0.00	0.00	0.00	0.00	0.00	0.00	0.00	0.00	0.00	0.0
-1.1--1.0	0.00	0.00	0.00	0.00	0.00	0.01	0.00	0.00	0.00	0.00	0.00	0.00	0.00	0.0
-1.0--0.9	0.00	0.00	0.00	0.00	0.01	0.02	0.01	0.01	0.00	0.00	0.00	0.00	0.00	0.0
-0.9--0.8	0.00	0.00	0.00	0.01	0.01	0.02	0.01	0.00	0.00	0.00	0.00	0.00	0.00	0.1
-0.8--0.7	0.00	0.00	0.01	0.02	0.04	0.03	0.02	0.01	0.00	0.00	0.00	0.00	0.00	0.1
-0.7--0.6	0.00	0.00	0.01	0.05	0.07	0.05	0.02	0.00	0.00	0.00	0.00	0.00	0.00	0.2
-0.6--0.5	0.00	0.01	0.04	0.10	0.13	0.08	0.03	0.01	0.00	0.00	0.00	0.00	0.00	0.4
-0.5--0.4	0.02	0.03	0.10	0.21	0.21	0.12	0.05	0.01	0.00	0.00	0.00	0.00	0.00	0.8
-0.4--0.3	0.08	0.16	0.27	0.41	0.35	0.16	0.05	0.01	0.00	0.00	0.00	0.00	0.00	1.5
-0.3--0.2	0.31	0.61	0.66	0.76	0.50	0.18	0.04	0.01	0.00	0.00	0.00	0.00	0.00	3.1
-0.2--0.1	1.40	2.01	1.55	1.28	0.66	0.19	0.04	0.01	0.00	0.00	0.00	0.00	0.00	7.1
-0.1--0.0	3.64	4.83	3.07	1.94	0.75	0.19	0.03	0.01	0.00	0.00	0.00	0.00	0.00	14.4
0.0--0.1	6.00	7.76	4.64	2.37	0.71	0.17	0.02	0.00	0.00	0.00	0.00	0.00	0.00	21.7
0.1--0.2	6.24	8.01	4.48	2.19	0.68	0.15	0.02	0.00	0.00	0.00	0.00	0.00	0.00	21.8
0.2--0.3	3.86	5.42	3.30	1.61	0.63	0.18	0.05	0.01	0.00	0.00	0.00	0.00	0.00	15.1
0.3--0.4	1.38	2.64	1.88	1.02	0.44	0.15	0.05	0.01	0.00	0.00	0.00	0.00	0.00	7.6
0.4--0.5	0.47	1.06	0.87	0.51	0.26	0.13	0.03	0.01	0.00	0.00	0.00	0.00	0.00	3.3
0.5--0.6	0.16	0.39	0.42	0.24	0.17	0.09	0.04	0.02	0.00	0.00	0.00	0.00	0.00	1.5
0.6--0.7	0.04	0.14	0.18	0.13	0.10	0.05	0.02	0.01	0.00	0.00	0.00	0.00	0.00	0.7
0.7--0.8	0.01	0.05	0.06	0.06	0.04	0.03	0.02	0.01	0.00	0.00	0.00	0.00	0.00	0.3
0.8--0.9	0.00	0.02	0.02	0.04	0.02	0.01	0.01	0.00	0.00	0.00	0.00	0.00	0.00	0.1
0.9--1.0	0.00	0.00	0.01	0.01	0.01	0.01	0.01	0.00	0.00	0.00	0.00	0.00	0.00	0.1
1.0--1.1	0.00	0.00	0.00	0.01	0.01	0.00	0.00	0.00	0.00	0.00	0.00	0.00	0.00	0.0
1.1--1.2	0.00	0.00	0.00	0.01	0.01	0.00	0.00	0.00	0.00	0.00	0.00	0.00	0.00	0.0
1.2--1.3	0.00	0.00	0.00	0.00	0.00	0.00	0.00	0.00	0.00	0.00	0.00	0.00	0.00	0.0
1.3--1.4	0.00	0.00	0.00	0.00	0.00	0.00	0.00	0.00	0.00	0.00	0.00	0.00	0.00	0.0
1.4--1.5	0.00	0.00	0.00	0.00	0.00	0.00	0.00	0.00	0.00	0.00	0.00	0.00	0.00	0.0
1.5--1.6	0.00	0.00	0.00	0.00	0.00	0.00	0.00	0.00	0.00	0.00	0.00	0.00	0.00	0.0
Sum	23.6	33.2	21.6	13.0	5.8	2.0	0.6	0.2	0.0	0.0	0.0	0.0	0.0	100.0

## 9 Reference Sea States

**This section presents the reference seastates; Normal Sea State, Severe Sea State and Extreme Sea State in line with IEC 61400-3-1:2019.**

The NSS and SSS are conditioned on the 10-minute average wind speed at hub height as required by the client. The conversion from 1 hour averaging to 10-minute averaging has been obtained by the conversion factor in IEC 61400-3-1:2019 of 1/0.95.

The wave hindcast data has a resolution of 1 hour but is considered representative of a 3-hour reference period as is standard practice.

### 9.1 Normal Sea State

NSS, characterized by a significant wave height and peak wave period, is defined as the expected significant wave height conditioned on the average wind speed at hub height.

NSS is given as a table with significant wave height and peak wave periods for different ranges of wind speeds and different directional sectors of MWD in the Appendices, Figure 9-1 presents an example for the omnidirectional description. Note that  $H_{m0}$  is capped with the 50-year return period value of  $H_{m0}$  from section 7.2.1 and the peak period is derived from the analysis in 7.1.6.

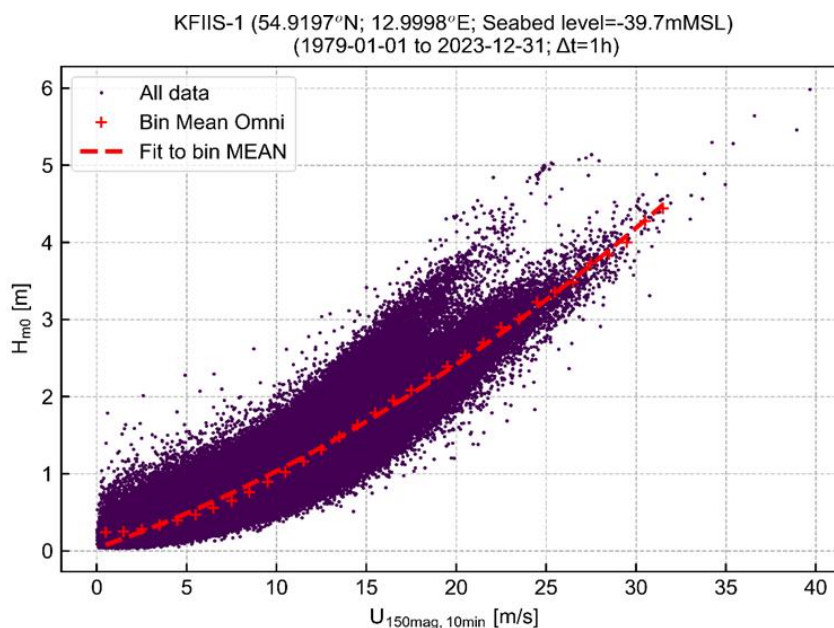


Figure 9-1 NSS for omni with fit. Fits and coefficients for all directional sectors are presented in the appendices.

## 9.2 Severe sea state

SSS is modelled as a sea state described by a combination of normal wind conditions and the significant wave height used for calculation of the ultimate loading of an offshore wind turbine during power production. SSS associates a severe sea state with each mean wind speed in the range corresponding to power production from cut-in to cut-out. The combination of wind speed and height is used to determine the 50-year return period contour to derive the individual significant wave height for each wind speed. The IFORM (IEC 61400-3-1:2019) and joint distribution is described by a global hierarchical model. In this model, one variable is taken as independent, and the other variables are modelled to be conditional on this variable using dependence functions.

The wind speed is here taken as the independent variable and the wave height is used the dependent variable. The method revolves around the description of the two variables in their joint distribution. Both variables are described by and fitted to the Exponentiated Weibull Distribution (EWD). The EWD is a generalization of the Weibull distribution. The fitted and observed data in the separate bins are shown on Figure 9-3 and Figure 9-4 and show a good approximation of the Weibull distribution to the data.

The result is shown on Figure 9-2. In the graph shows both the scatter data colored by the density and the IFORM contour with a 50-year return period. The contour follows along the density of the data. The light blue scatter data represents the marginal extreme values of  $H_{m0}$ .

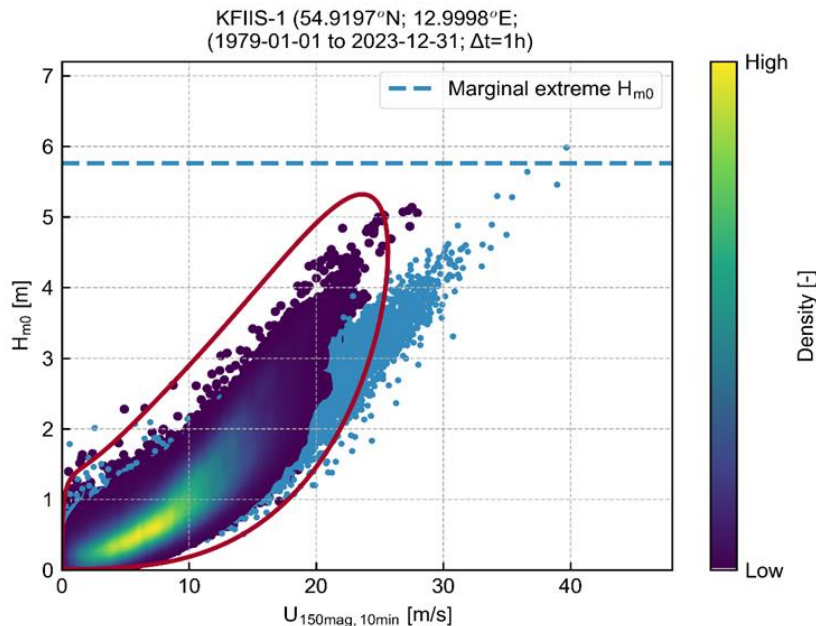
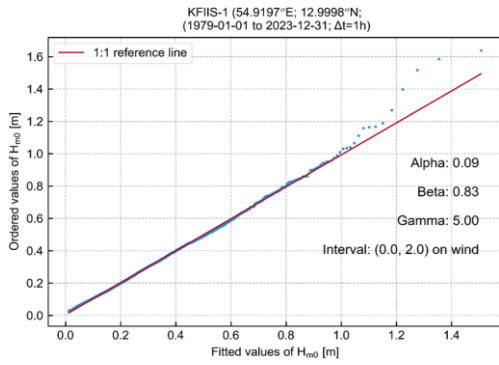


Figure 9-2 IFORM contour for SSS with a 50-year return period for  $H_{m0}$  and  $U_{150mag}$  at KFIIS-1. The blue line shows the marginal 50-year return period  $H_{m0}$ .

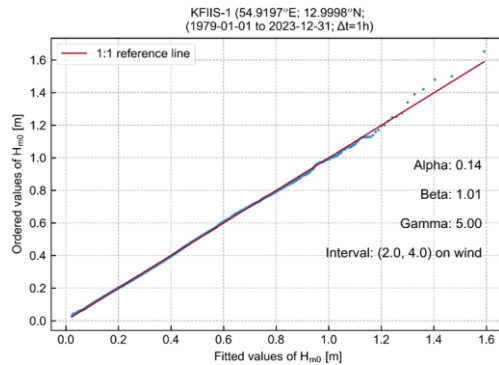
Associated parameters for the sea state is presented in Table 9-1.  $T_p$  is based on section 7.1.6,  $H_{max}$  is based on section 7.2.2,  $T_{Hmax}$  is  $0.9 \times T_p$  and  $T_{Hmax,ass}$  is based on equation (11) in IEC 61400-3-1:2019.

Table 9-1 SSS from the 50-year return period environmental contour for  $H_{m0}$  and  $U_{150mag,10min}$ .

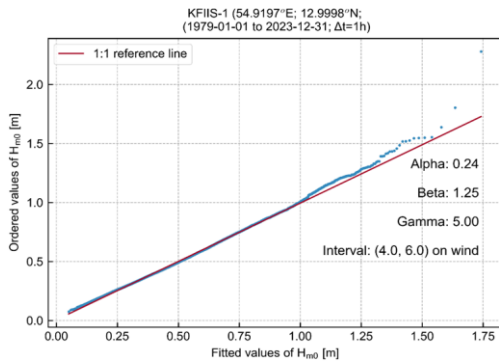
$U_{150mag,10min}$ [m/s]	$H_{m0}$ [m]	$T_p$ [s]	$H_{max}$ [m]	$T_{Hmax,ass,low}$ [s]	$T_{Hmax,ass,high}$ [s]	$T_{Hmax}$ [s]
0-2.5	1.4	5.1	2.7	5.4	4.6	1.4
2.5-3.5	1.6	5.4	3.2	5.9	4.8	1.6
3.5-4.5	1.8	5.5	3.5	6.1	5.0	1.8
4.5-5.5	2.0	5.7	3.8	6.4	5.2	2.0
5.5-6.5	2.1	5.9	4.2	6.7	5.3	2.1
6.5-7.5	2.3	6.1	4.5	7.0	5.5	2.3
7.5-8.5	2.5	6.3	4.9	7.2	5.6	2.5
8.5-9.5	2.7	6.4	5.3	7.5	5.8	2.7
9.5-10.5	2.9	6.6	5.7	7.8	6.0	2.9
10.5-11.5	3.1	6.8	6.0	8.0	6.1	3.1
11.5-12.5	3.3	6.9	6.4	8.3	6.2	3.3
12.5-13.5	3.5	7.1	6.8	8.5	6.4	3.5
13.5-14.5	3.7	7.2	7.2	8.8	6.5	3.7
14.5-15.5	3.9	7.4	7.6	9.0	6.6	3.9
15.5-16.5	4.1	7.5	8.0	9.3	6.8	4.1
16.5-17.5	4.3	7.7	8.4	9.5	6.9	4.3
17.5-18.5	4.5	7.8	8.8	9.7	7.0	4.5
18.5-19.5	4.7	7.9	9.2	9.9	7.1	4.7
19.5-20.5	4.9	8.0	9.6	10.1	7.2	4.9
20.5-21.5	5.1	8.1	9.9	10.3	7.3	5.1
21.5-22.5	5.2	8.2	10.2	10.4	7.4	5.2
22.5-23.5	5.3	8.3	10.3	10.5	7.4	5.3
23.5-24.5	5.3	8.3	10.4	10.5	7.4	5.3
24.5-25.5	5.8	8.5	11.2	11.0	7.7	5.8
25.5-26.5	5.8	8.5	11.2	11.0	7.7	5.8
26.5-27.5	5.8	8.5	11.2	11.0	7.7	5.8
27.5-28.5	5.8	8.5	11.2	11.0	7.7	5.8
28.5-29.5	5.8	8.5	11.2	11.0	7.7	5.8
29.5-30.5	5.8	8.5	11.2	11.0	7.7	5.8
30.5-31.5	5.8	8.5	11.2	11.0	7.7	5.8
31.5-32.5	5.8	8.5	11.2	11.0	7.7	5.8
32.5-33.5	5.8	8.5	11.2	11.0	7.7	5.8



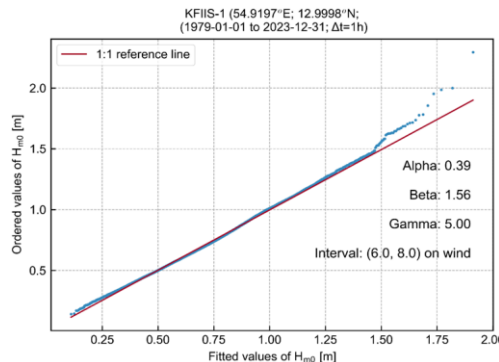
Probability plot of the Weibull parameter fit for wind bin Interval: (0.0, 2.0)



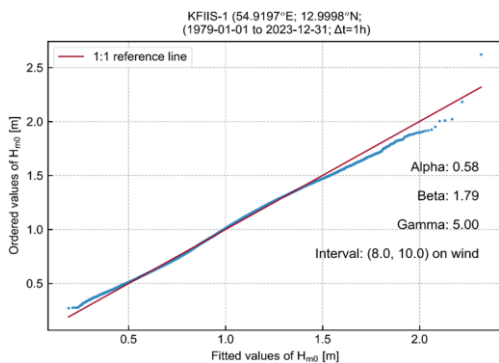
Probability plot of the Weibull parameter fit for wind bin Interval: (2.0, 4.0)



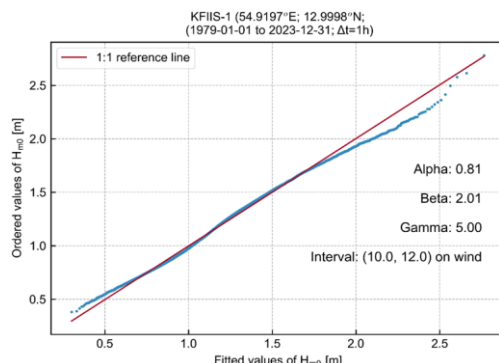
Probability plot of the Weibull parameter fit for wind bin Interval: (4.0, 6.0)



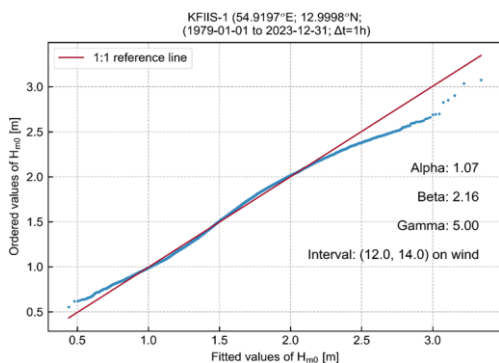
Probability plot of the Weibull parameter fit for wind bin Interval: (6.0, 8.0)



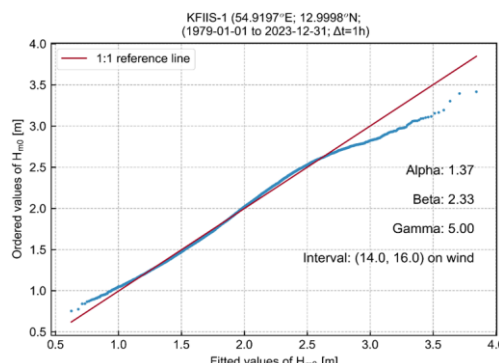
Probability plot of the Weibull parameter fit for wind bin Interval: (8.0, 10.0)



Probability plot of the Weibull parameter fit for wind bin Interval: (10.0, 12.0)

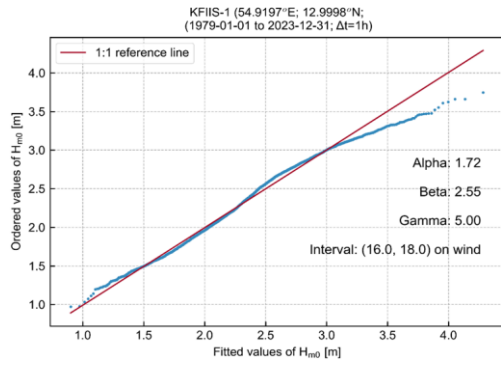


Probability plot of the Weibull parameter fit for wind bin Interval: (12.0, 14.0)

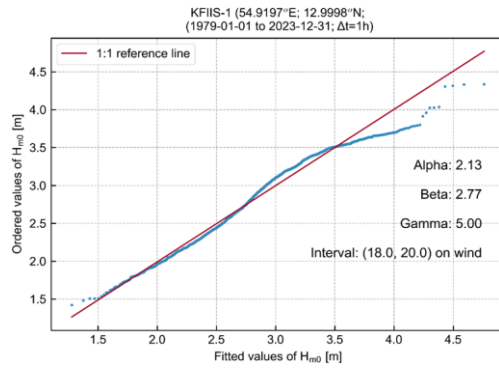


Probability plot of the Weibull parameter fit for wind bin Interval: (14.0, 16.0)

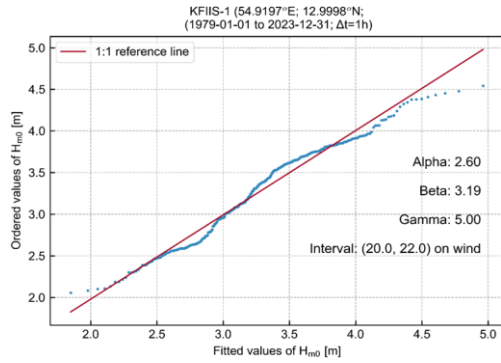
Figure 9-3 Exponentiated Weibull fit for sections of  $H_{m0}$  data binned by 2 m/s intervals of  $U_{150mag,10min}$ .



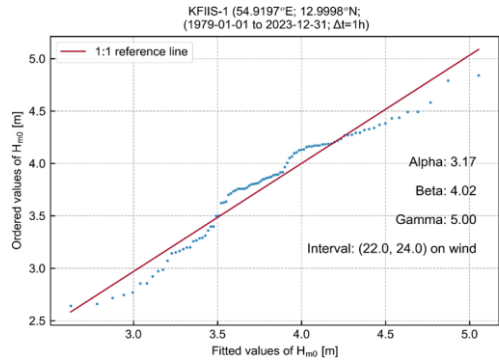
Probability plot of the Weibull parameter fit for wind bin Interval: (16.0, 18.0)



Probability plot of the Weibull parameter fit for wind bin Interval: (18.0, 20.0)



Probability plot of the Weibull parameter fit for wind bin Interval: (20.0, 22.0)



Probability plot of the Weibull parameter fit for wind bin Interval: (22.0, 24.0)

Figure 9-4 Exponentiated Weibull fit for sections of  $H_{m0}$  data binned by 2 m/s intervals of  $U_{150mag,10min}$ .



## 9.3 Extreme sea state

ESS characterised by a significant wave height, a peak wave period and a wave direction, is given by the unconditional significant wave height with estimated average recurrence periods of 1 year and 50 years.

ESS, based on section 7.2, is given as tables with significant wave height for different directional sectors of MWD in Table 9-2 and Table 9-3. Associated parameters for the sea state are also presented. Results presented below are unscaled. Results scaled according to DNV-RPC205 can be found in the appendices, i.e. section 7.3.

Table 9-2 ESS for 50-year return period at KFIIS-1 (unscaled).

Parameter	MWD [°N-from]																
	0.0	22.5	45.0	67.5	90.0	112.5	135.0	157.5	180.0	202.5	225.0	247.5	270.0	292.5	315.0	337.5	Omni
$H_{m0}$ [m]	3.0	3.1	3.5	4.6	5.0	3.8	2.6	2.8	3.0	3.3	5.2	5.6	4.4	3.9	3.7	3.1	5.8
$T_p$ [s]	6.2	6.1	7.8	8.6	8.8	7.9	6.8	6.1	6.3	6.8	8.3	8.5	7.4	7.0	7.0	6.7	9.0
$H_{max}$ [m]	5.8	6.1	6.8	8.9	9.8	7.4	5.2	5.4	5.8	6.4	10.1	11.0	8.6	7.6	7.2	6.1	11.2
$T_{Hmax,ass,low}$ [s]	6.1	6.3	6.6	7.6	8.0	6.9	5.8	5.9	6.1	6.4	8.1	8.4	7.5	7.0	6.8	6.3	8.5
$T_{Hmax,ass,high}$ [s]	7.9	8.1	8.5	9.8	10.3	8.9	7.4	7.6	7.9	8.3	10.4	10.8	9.6	9.0	8.8	8.1	11.0
$C_{max}$ [m]	3.4	3.6	3.8	5.1	5.7	4.2	2.9	3.1	3.4	3.7	6	6.6	5.1	4.5	4.2	3.5	6.7

Table 9-3 ESS for 1-year return period at KFIIS-1 (unscaled).

Parameter	MWD [°N-from]																
	0.0	22.5	45.0	67.5	90.0	112.5	135.0	157.5	180.0	202.5	225.0	247.5	270.0	292.5	315.0	337.5	Omni
$H_{m0}$ [m]	1.8	1.8	2.1	2.8	3.0	2.4	2.0	1.9	2.0	2.3	3.3	3.5	3.2	2.7	2.4	2.1	3.8
$T_p$ [s]	5.2	5.2	6.7	7.4	7.4	6.7	6.1	5.4	5.4	6.0	7.1	7.1	6.5	6.1	6.0	5.7	7.7
$H_{max}$ [m]	3.5	3.5	4.1	5.4	5.9	4.7	3.9	3.7	3.8	4.5	6.4	6.8	6.2	5.3	4.8	4.1	7.3
$T_{Hmax,ass,low}$ [s]	4.7	4.8	5.2	5.9	6.2	5.5	5.0	4.9	5.0	5.4	6.4	6.6	6.3	5.9	5.5	5.1	6.9
$T_{Hmax,ass,high}$ [s]	6.1	6.1	6.7	7.6	8.0	7.1	6.5	6.3	6.4	7.0	8.3	8.6	8.1	7.5	7.1	6.6	8.8
$C_{max}$ [m]	2.0	2.1	2.7	2.3	4.2	2.3	3.0	3.3	2.6	2.2	2.2	2.6	3.7	4.0	3.6	3.1	2.0

# 10 Other atmospheric and oceanographic conditions

This section presents analyses of other atmospheric- and oceanographic conditions. The atmospheric conditions are air temperature, humidity, solar radiation and lightning and the oceanographic conditions are seawater temperature and salinity as well as the marine growth.

## 10.1 Air temperature, pressure, humidity, and solar radiation

Modelled air temperature at 2 m above sea level, air pressure at 2 m above sea level, relative humidity and solar radiation are based on ERA5 (1979-01-15 to 2023-12-31), The results are presented in Figure 10-1, Figure 10-2, Figure 10-3, and Figure 10-4, and summarised on Table 10-1, Table 10-2, Table 10-3 and Table 10-4.

There is a clear seasonal variation for all four variables. Air temperature, relative humidity and solar radiation are larger during the summer months and lower during the winter months.

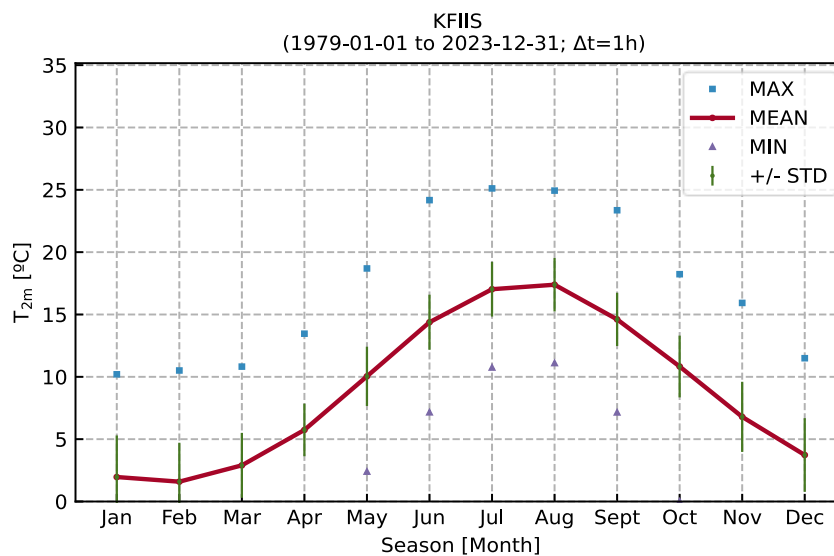


Figure 10-1 Monthly statistics of air temperature at 2 m above sea level.

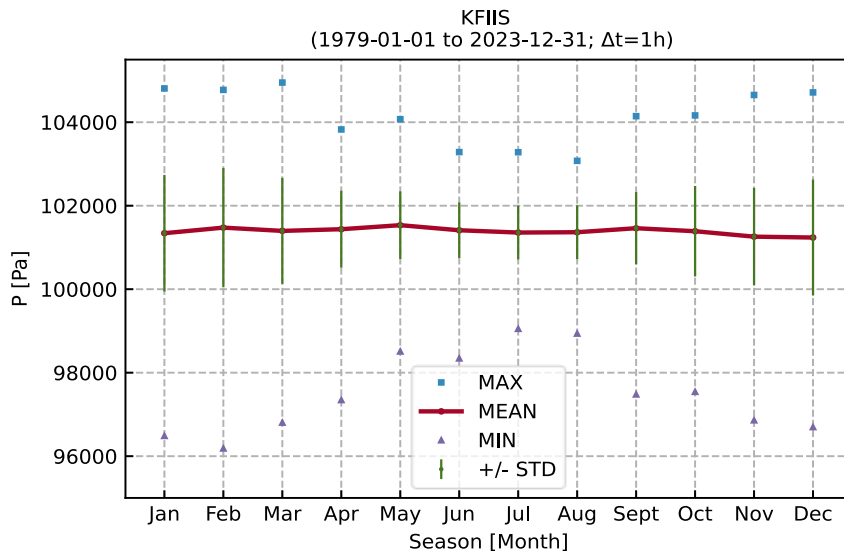


Figure 10-2 Monthly statistics of pressure at 2 m above sea level.

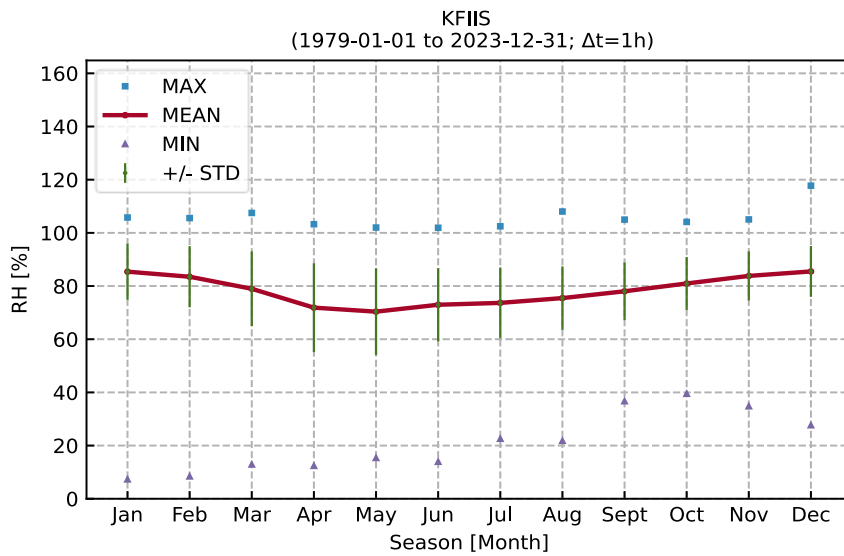


Figure 10-3 Monthly statistics of relative humidity at 2 m above sea level.

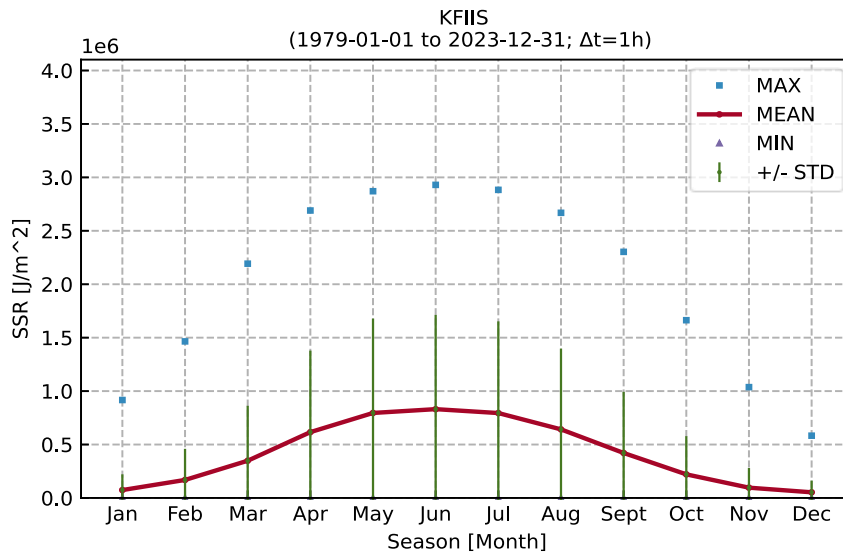


Figure 10-4 Monthly statistics of downward solar radiation.

Table 10-1 Monthly statistics for air temperature at 2 m above sea level at KFIIS-1

Season	T <sub>2m</sub> [°C]							
	N [-]	MEAN	STD	MIN	P05	P50	P95	MAX
Jan	33,480.0	2.0	3.3	-13.8	-4.0	2.4	6.6	10.2
Feb	30,504.0	1.6	3.1	-14.1	-3.9	1.8	6.1	10.5
Mar	33,480.0	2.9	2.6	-12.5	-1.5	3.1	6.6	10.8
Apr	32,400.0	5.7	2.1	-1.8	2.3	5.7	9.3	13.5
May	33,480.0	10.0	2.4	2.4	6.2	10.0	13.9	18.7
Jun	32,400.0	14.4	2.2	7.2	10.9	14.3	18.1	24.2
Jul	33,480.0	17.0	2.2	10.7	13.6	16.9	20.9	25.1
Aug	33,480.0	17.4	2.2	11.1	14.0	17.3	21.2	24.9
Sept	32,400.0	14.6	2.1	7.1	11.1	14.6	18.1	23.4
Oct	33,480.0	10.8	2.5	0.0	6.4	11.0	14.5	18.2
Nov	32,400.0	6.8	2.8	-4.2	1.8	7.1	11.0	15.9
Dec	33,480.0	3.7	3.0	-9.0	-1.7	4.0	8.0	11.5

Table 10-2 Monthly statistics for pressure at KFIIS-1 at 2 m above sea level at KFIIS-1

Season	P [Pa]							
Month	N [-]	MEAN	STD	MIN	P05	P50	P95	MAX
Jan	33,480	101,342	1,397	96,485	98,952	101,413	103,478	104,809
Feb	30,504	101,475	1,428	96,185	99,021	101,593	103,662	104,774
Mar	33,480	101,397	1,269	96,804	99,277	101,437	103,339	104,950
Apr	32,400	101,437	922	97,344	99,861	101,486	102,868	103,827
May	33,480	101,534	810	98,508	100,173	101,548	102,830	104,072
Jun	32,400	101,412	666	98,342	100,298	101,440	102,453	103,285
Jul	33,480	101,357	643	99,050	100,234	101,402	102,313	103,281
Aug	33,480	101,365	644	98,936	100,241	101,408	102,322	103,075
Sept	32,400	101,461	866	97,479	99,912	101,539	102,752	104,145
Oct	33,480	101,389	1,084	97,541	99,494	101,463	103,073	104,163
Nov	32,400	101,259	1,168	96,859	99,265	101,316	103,078	104,653
Dec	33,480	101,238	1,389	96,697	98,885	101,287	103,494	104,714

Table 10-3 Monthly statistics for relative humidity at KFIIS-1

Season	RH [%]							
Month	N [-]	MEAN	STD	MIN	P05	P50	P95	MAX
Jan	33,480	85	11	7	67	87	99	106
Feb	30,504	84	12	8	63	85	99	106
Mar	33,480	79	14	13	52	82	97	107
Apr	32,400	72	17	12	40	75	94	103
May	33,480	70	16	15	41	72	93	102
Jun	32,400	73	14	14	48	75	92	102
Jul	33,480	74	13	23	49	76	92	102
Aug	33,480	75	12	22	54	77	92	108
Sept	32,400	78	11	37	58	79	94	105
Oct	33,480	81	10	39	62	82	95	104
Nov	32,400	84	9	35	67	85	97	105
Dec	33,480	85	10	28	68	87	99	118

Table 10-4 Annual and monthly statistics for downward solar radiation at KFIIS-1

Season	SSR [J/m <sup>2</sup> ]							
Month	N [-]	MEAN	STD	MIN	P05	P50	P95	MAX
Jan	33,480	73,983	147,385	0	0	0	426,351	916,554
Feb	30,504	168,672	291,180	0	0	0	846,093	1,465,224
Mar	33,480	348,489	514,128	0	0	6,313	1,504,941	2,192,301
Apr	32,400	616,128	762,899	0	0	183,805	2,143,390	2,690,011
May	33,480	795,485	883,098	0	0	407,683	2,478,855	2,870,522
Jun	32,400	831,056	881,857	0	0	504,709	2,484,889	2,929,900
Jul	33,480	794,619	858,270	0	0	456,585	2,412,264	2,883,240
Aug	33,480	641,778	756,246	0	0	254,116	2,108,313	2,668,511
Sept	32,400	420,942	571,919	0	0	44,190	1,620,576	2,303,005
Oct	33,480	220,970	357,136	0	0	0	1,042,176	1,663,485
Nov	32,400	96,307	183,933	0	0	0	543,730	1,037,231
Dec	33,480	53,007	109,869	0	0	0	327,811	582,796

## 10.2 Lightning

This section presents the occurrence and frequency of lightning in the KFII area (data delivery area). By using measurement data from the Danish Meteorological Institute (DMI) [7], a comprehensive time series for lightning strikes is established. The frequency and the intensity of lightning strikes over time is analysed by aggregating the data into hourly values. The timeseries consist of both cloud to ground (positive and negative) and cloud to cloud lightning. Lightning strikes are registered with an accuracy of 500-2000 meters.

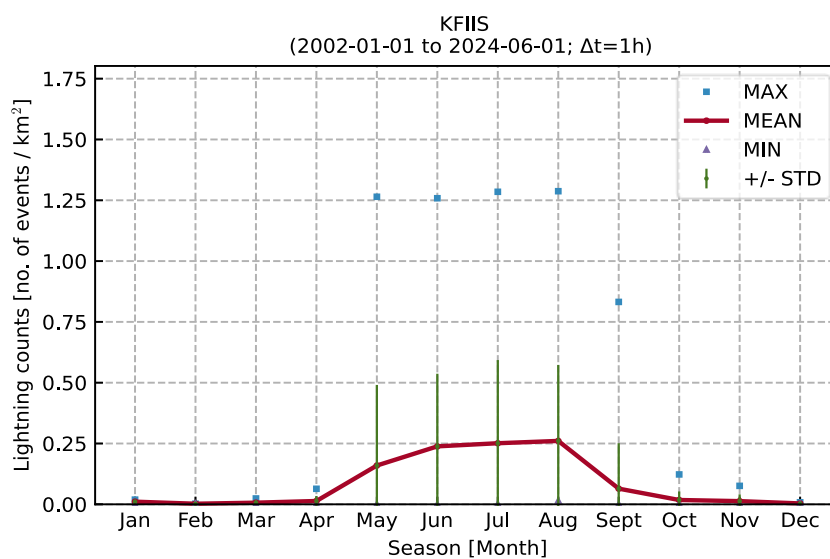


Figure 10-5 Monthly statistics of lightning counts at the data delivery area.

During the full 22-year period a total amount of 17,665 lightning strikes was observed within the data delivery area. This amounts to an average during that full period of 0.94 LTG/km<sup>2</sup>/year. This average provides a baseline understanding of lightning activity in the KFII, illustrating that while intense thunderstorms can occur, the overall frequency of lightning strikes is relatively low.

The values correspond well with the general rule that in Denmark with a value of 1 LTG/km<sup>2</sup>/year across landmasses and less across water bodies. The expected seasonal variation expects ~75% of lightning strikes observed from June to August. and this area agrees with those findings.

Table 10-5 Seasonal variation of lightning strike across the data delivery area.

Season	Lightning counts [no. of events / year / km <sup>2</sup> ]							
Month	N [-]	MEAN	STD	MIN	P05	P50	P95	MAX
Jan	27.0	0.0	0.0	0.0	0.0	0.0	0.0	0.0
Feb	2.0	0.0	0.0	0.0	0.0	0.0	0.0	0.0
Mar	28.0	0.0	0.0	0.0	0.0	0.0	0.0	0.0
Apr	102.0	0.0	0.0	0.0	0.0	0.0	0.1	0.1
May	2,516.0	0.2	0.3	0.0	0.0	0.0	0.9	1.3
Jun	4,352.0	0.2	0.3	0.0	0.0	0.2	0.7	1.3
Jul	4,588.0	0.3	0.3	0.0	0.0	0.1	0.8	1.3
Aug	4,762.0	0.3	0.3	0.0	0.0	0.2	0.9	1.3
Sept	1,016.0	0.1	0.2	0.0	0.0	0.0	0.1	0.8
Oct	162.0	0.0	0.0	0.0	0.0	0.0	0.1	0.1
Nov	76.0	0.0	0.0	0.0	0.0	0.0	0.1	0.1
Dec	24.0	0.0	0.0	0.0	0.0	0.0	0.0	0.0

## 10.3 Salinity, seawater temperature and density

The oceanographic properties were derived from the hydrodynamic dataset. Time series data for density, seawater temperature and salinity were extracted at three depth levels: near-surface, mid-depth, and near-seabed. This part of the dataset spans a 10-year period (2014 to 2023) with a temporal resolution of one hour. The analysis presents the monthly variations in seawater temperature, density, and salinity across the three layers. Oceanographic variables of the hydrodynamic dataset presented in this section is listed in Table 10-6. The following sections are split into variables name and levels.

Table 10-6 Oceanographic variables of the hydrodynamic dataset

Variable name	Abbrev.	Unit	Bin size
<b>Seawater temperature</b>	T <sub>sw</sub>	°C	1
<b>Salinity</b>	Sal	PSU	2
<b>Water density</b>	D <sub>sw</sub>	kg/m <sup>3</sup>	2

### 10.3.1 Salinity

Figure 10-6, Figure 10-7, Figure 10-8, Table 10-7, Table 10-8 and Table 10-9 show the monthly salinity at KFIIS-1, at near-surface, mid-depth, and near-seabed, respectively.

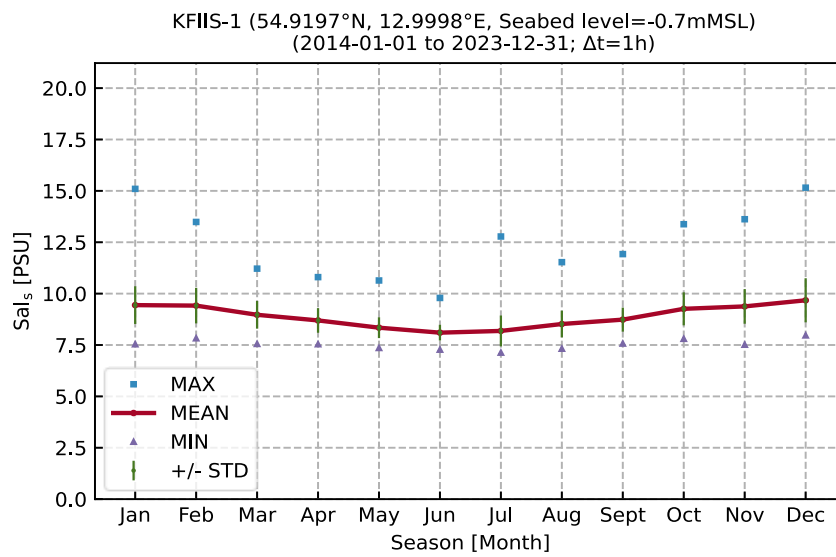


Figure 10-6 Plot of monthly statistics of Sal<sub>s</sub>, at KFIIS-1.

Table 10-7 Table with monthly statistics of Sal<sub>s</sub>, at KFIIS-1.

Season	Sal <sub>s</sub> [PSU]							
Month	N [-]	MEAN	STD	MIN	P05	P50	P95	MAX
Jan	7,423.0	9.4	0.9	7.5	8.2	9.4	11.0	15.1
Feb	6,760.0	9.4	0.9	7.8	8.3	9.3	11.1	13.5
Mar	7,416.0	9.0	0.7	7.6	7.9	8.9	10.3	11.2
Apr	7,189.0	8.7	0.6	7.5	7.8	8.6	9.9	10.8
May	7,426.0	8.3	0.5	7.4	7.6	8.3	9.3	10.6
Jun	7,180.0	8.1	0.4	7.3	7.6	8.0	8.8	9.8
Jul	7,412.0	8.2	0.8	7.1	7.3	8.0	9.3	12.8
Aug	7,410.0	8.5	0.7	7.3	7.7	8.4	9.8	11.5
Sept	7,176.0	8.7	0.6	7.6	7.9	8.7	10.0	11.9
Oct	7,425.0	9.3	0.8	7.8	8.2	9.1	10.9	13.4
Nov	7,183.0	9.4	0.8	7.5	8.1	9.2	10.9	13.6
Dec	7,415.0	9.7	1.1	8.0	8.4	9.5	11.9	15.2



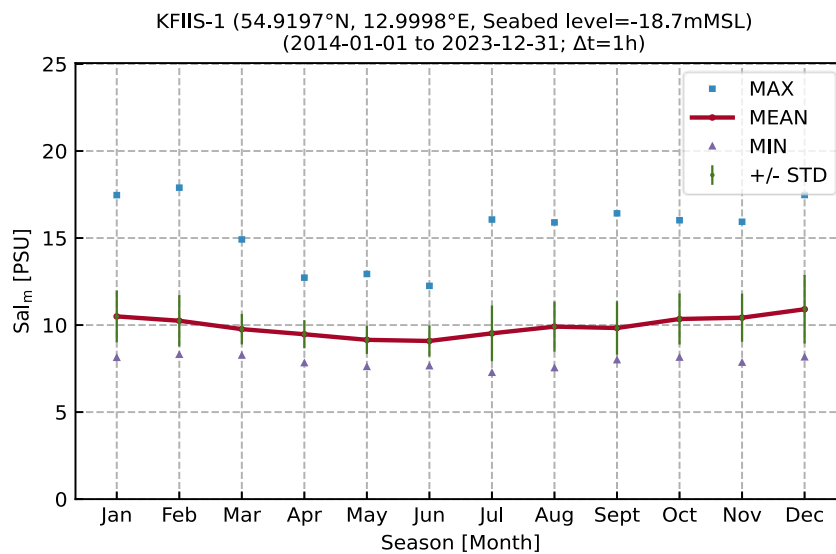


Figure 10-7 Plot of monthly statistics of  $Sal_m$ , at KFIS-1.

Table 10-8 Table with monthly statistics of  $Sal_m$ , at KFIS-1.

Season	$Sal_m$ [PSU]							
Month	N [-]	MEAN	STD	MIN	P05	P50	P95	MAX
Jan	7,440.0	10.5	1.5	8.1	8.6	10.2	13.5	17.5
Feb	6,768.0	10.3	1.5	8.3	8.9	9.9	13.4	17.9
Mar	7,440.0	9.8	0.9	8.3	8.7	9.6	11.4	14.9
Apr	7,200.0	9.5	0.8	7.8	8.5	9.3	11.1	12.7
May	7,440.0	9.2	0.8	7.6	8.1	9.0	10.9	12.9
Jun	7,198.0	9.1	0.9	7.6	7.9	9.0	10.8	12.3
Jul	7,439.0	9.5	1.6	7.3	7.7	9.2	13.0	16.1
Aug	7,440.0	9.9	1.4	7.5	8.1	9.7	12.5	15.9
Sept	7,198.0	9.8	1.5	8.0	8.3	9.4	13.6	16.4
Oct	7,439.0	10.4	1.5	8.1	8.7	9.8	13.3	16.0
Nov	7,200.0	10.4	1.4	7.8	8.9	10.1	13.3	15.9
Dec	7,428.0	10.9	2.0	8.2	8.6	10.3	15.2	17.5

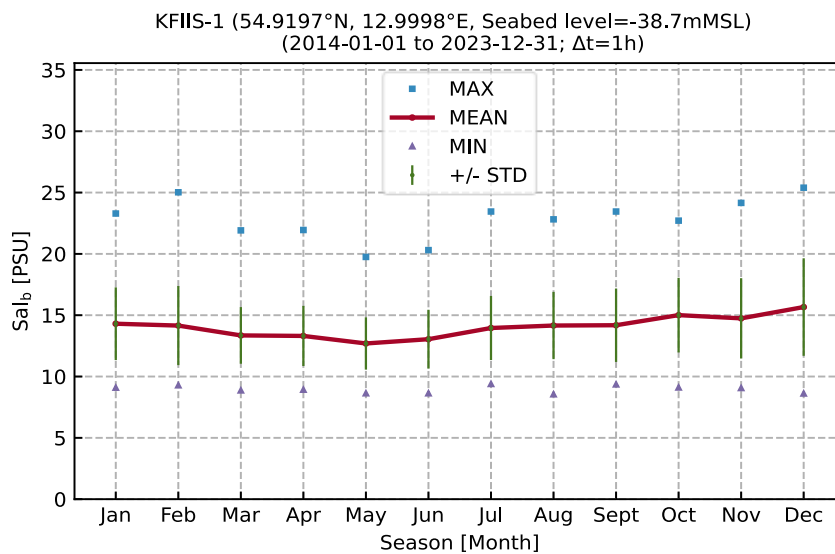


Figure 10-8 Plot of monthly statistics of Sal<sub>b</sub>, at KFIS-1.

Table 10-9 Table with monthly statistics of Sal<sub>b</sub>, at KFIS-1.

Season	Sal <sub>b</sub> [PSU]							
Month	N [-]	MEAN	STD	MIN	P05	P50	P95	MAX
Jan	7,440.0	14.3	3.0	9.1	10.2	13.9	20.2	23.3
Feb	6,768.0	14.2	3.2	9.3	9.7	14.1	20.3	25.0
Mar	7,440.0	13.4	2.3	8.9	10.2	13.0	18.2	21.9
Apr	7,200.0	13.3	2.5	8.9	9.8	13.0	17.6	22.0
May	7,440.0	12.7	2.1	8.6	10.1	12.3	17.5	19.8
Jun	7,198.0	13.0	2.4	8.6	9.7	12.8	17.4	20.3
Jul	7,439.0	14.0	2.6	9.4	10.7	13.3	19.5	23.5
Aug	7,440.0	14.2	2.7	8.6	10.6	13.7	19.7	22.8
Sept	7,198.0	14.2	3.0	9.4	10.7	13.3	20.3	23.5
Oct	7,439.0	15.0	3.1	9.1	9.9	14.6	20.4	22.7
Nov	7,200.0	14.7	3.3	9.1	9.9	14.4	21.1	24.2
Dec	7,428.0	15.7	4.0	8.6	10.1	14.9	22.9	25.4

### 10.3.2 Seawater temperature

Figure 10-9, Figure 10-10, Figure 10-11, Table 10-10, Table 10-11 and Table 10-12 show the monthly seawater temperature at KFIS-1, at near-surface, mid-depth, and near-seabed, respectively.

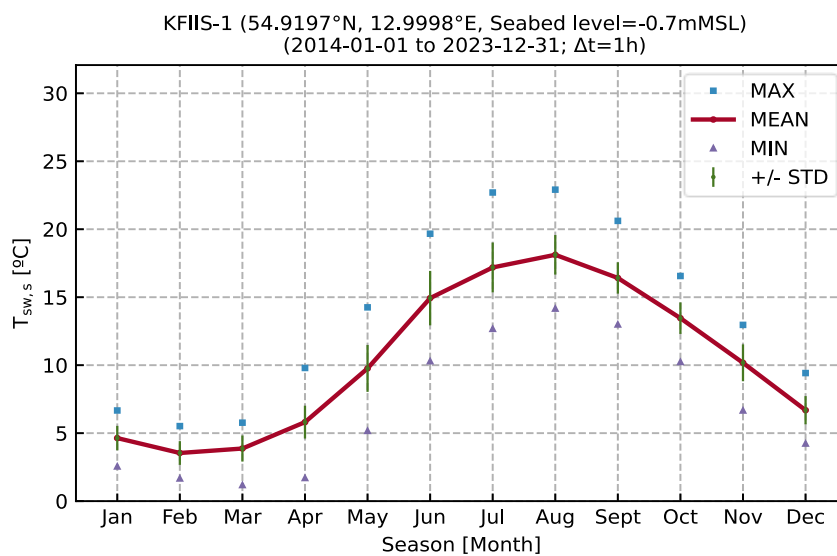


Figure 10-9 Plot of monthly statistics of T<sub>sw,s</sub> at KFIIS-1.

Table 10-10 Table with monthly statistics of T<sub>sw,s</sub> at KFIIS-1.

Season	T <sub>sw,s</sub> [°C]							
	Month	N [-]	MEAN	STD	MIN	P05	P50	P95
Jan	7,423.0	4.6	0.9	2.6	3.1	4.7	6.0	6.7
Feb	6,760.0	3.5	0.9	1.7	2.2	3.5	5.2	5.5
Mar	7,416.0	3.9	1.0	1.2	1.8	4.0	5.3	5.8
Apr	7,189.0	5.8	1.2	1.7	4.1	5.8	7.8	9.8
May	7,426.0	9.8	1.7	5.2	7.1	9.7	13.0	14.3
Jun	7,180.0	14.9	2.0	10.3	11.9	14.8	18.2	19.7
Jul	7,412.0	17.2	1.8	12.7	14.4	17.0	20.4	22.7
Aug	7,410.0	18.1	1.5	14.2	16.0	18.0	20.8	22.9
Sept	7,176.0	16.4	1.2	13.0	14.4	16.5	18.4	20.6
Oct	7,425.0	13.5	1.2	10.2	11.8	13.3	15.6	16.6
Nov	7,183.0	10.2	1.4	6.7	7.9	10.3	12.3	13.0
Dec	7,415.0	6.7	1.0	4.2	5.0	6.7	8.5	9.4

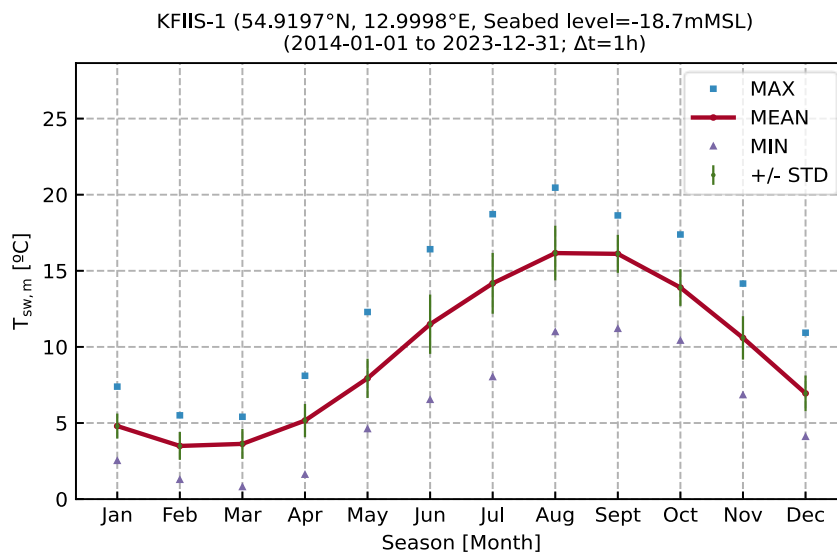


Figure 10-10 Plot of monthly statistics of  $T_{sw,m}$ , at KFIIS-1.

Table 10-11 Table with monthly statistics of  $T_{sw,m}$ , at KFIIS-1.

Season	$T_{sw,m}$ [°C]							
Month	N [-]	MEAN	STD	MIN	P05	P50	P95	MAX
Jan	7,440.0	4.8	0.8	2.5	3.4	4.9	6.1	7.4
Feb	6,768.0	3.5	0.9	1.3	2.0	3.5	5.1	5.5
Mar	7,440.0	3.6	1.0	0.8	1.6	3.8	5.2	5.4
Apr	7,200.0	5.2	1.1	1.6	3.3	5.2	6.9	8.1
May	7,440.0	7.9	1.3	4.6	5.9	7.9	10.1	12.3
Jun	7,198.0	11.5	2.0	6.5	8.2	11.5	14.7	16.4
Jul	7,439.0	14.2	2.0	8.0	10.7	14.4	16.9	18.7
Aug	7,440.0	16.2	1.8	11.0	13.4	16.3	19.2	20.5
Sept	7,198.0	16.1	1.3	11.2	13.7	16.3	17.7	18.6
Oct	7,439.0	13.9	1.2	10.4	12.0	13.8	16.0	17.4
Nov	7,200.0	10.6	1.4	6.8	8.0	10.8	12.7	14.2
Dec	7,428.0	7.0	1.2	4.1	5.1	7.0	8.9	10.9

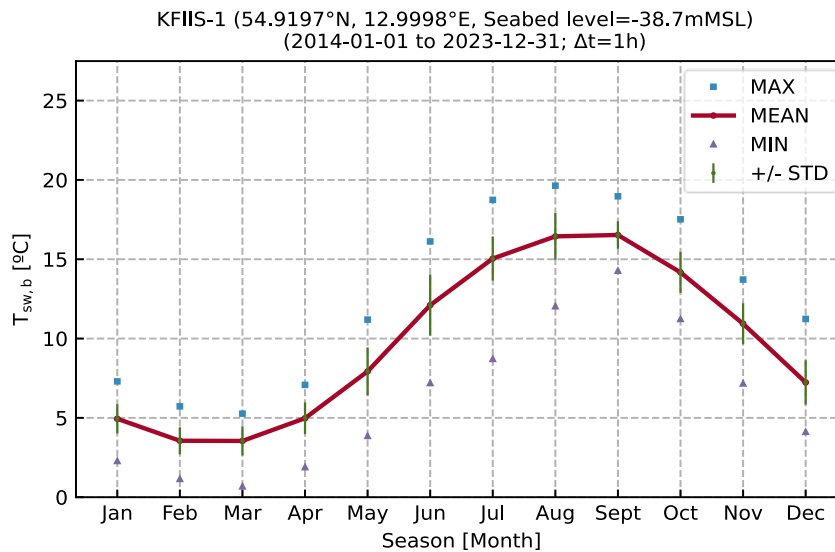


Figure 10-11 Plot of monthly statistics of  $T_{sw,b}$ , at KFIS-1.

Table 10-12 Table with monthly statistics of  $T_{sw,b}$ , at KFIS-1.

Season	$T_{sw,b}$ [°C]							
Month	N [-]	MEAN	STD	MIN	P05	P50	P95	MAX
Jan	7,440.0	4.9	0.9	2.3	3.3	5.1	6.3	7.3
Feb	6,768.0	3.6	0.9	1.2	2.0	3.6	5.0	5.7
Mar	7,440.0	3.6	0.9	0.7	1.7	3.7	5.0	5.3
Apr	7,200.0	5.0	1.0	1.9	3.4	4.9	6.7	7.1
May	7,440.0	7.9	1.5	3.9	5.4	7.9	10.2	11.2
Jun	7,198.0	12.1	1.9	7.2	8.9	12.0	15.1	16.1
Jul	7,439.0	15.0	1.4	8.7	12.6	15.2	17.2	18.7
Aug	7,440.0	16.4	1.5	12.0	14.0	16.5	19.0	19.6
Sept	7,198.0	16.5	0.9	14.3	15.1	16.6	18.0	19.0
Oct	7,439.0	14.2	1.3	11.2	12.0	14.2	16.5	17.5
Nov	7,200.0	10.9	1.3	7.2	8.5	11.2	12.8	13.7
Dec	7,428.0	7.2	1.4	4.1	5.3	7.0	10.0	11.2

### 10.3.3 Density

Figure 10-12, Figure 10-13, Figure 10-14, Table 10-13, Table 10-14 and Table 10-15 show the monthly seawater density at KFIS-1, at near-surface, mid-depth, and near-seabed, respectively.

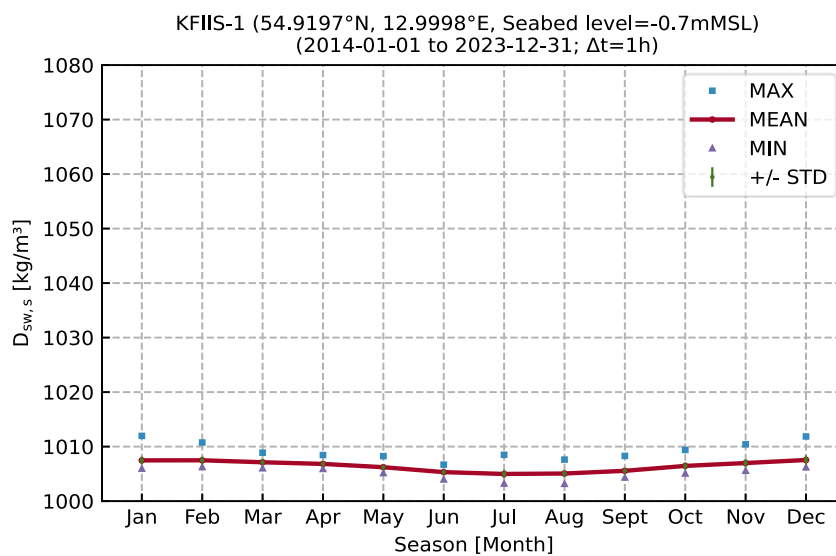


Figure 10-12 Plot of monthly statistics of  $D_{sw,s}$  at KFIS-1.

Table 10-13 Table with monthly statistics of  $D_{sw,s}$  at KFIS-1.

Season	$D_{sw,s}$ [kg/m <sup>3</sup> ]							
Month	N [-]	MEAN	STD	MIN	P05	P50	P95	MAX
Jan	7,423.0	1,007.5	0.7	1,006.0	1,006.5	1,007.4	1,008.7	1,012.0
Feb	6,760.0	1,007.5	0.7	1,006.2	1,006.6	1,007.4	1,008.8	1,010.8
Mar	7,416.0	1,007.1	0.5	1,006.0	1,006.3	1,007.1	1,008.1	1,008.9
Apr	7,189.0	1,006.8	0.5	1,005.9	1,006.1	1,006.8	1,007.8	1,008.5
May	7,426.0	1,006.2	0.5	1,005.1	1,005.5	1,006.2	1,007.0	1,008.3
Jun	7,180.0	1,005.3	0.5	1,004.0	1,004.6	1,005.3	1,006.2	1,006.7
Jul	7,412.0	1,005.0	0.7	1,003.2	1,003.8	1,004.9	1,006.1	1,008.5
Aug	7,410.0	1,005.1	0.7	1,003.2	1,003.9	1,005.0	1,006.3	1,007.6
Sept	7,176.0	1,005.6	0.5	1,004.3	1,004.9	1,005.5	1,006.6	1,008.3
Oct	7,425.0	1,006.5	0.7	1,005.1	1,005.6	1,006.3	1,007.7	1,009.4
Nov	7,183.0	1,007.0	0.7	1,005.6	1,006.0	1,006.9	1,008.2	1,010.4
Dec	7,415.0	1,007.5	0.8	1,006.2	1,006.5	1,007.4	1,009.3	1,011.9

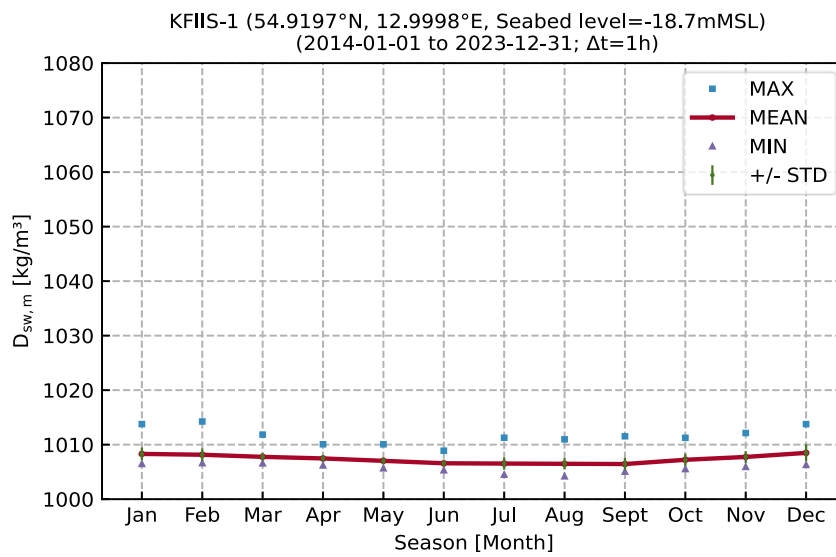


Figure 10-13 Plot of monthly statistics of  $D_{sw,m}$ , at KFIS-1.

Table 10-14 Table with monthly statistics of  $D_{sw,m}$ , at KFIS-1.

Season	$D_{sw,m}$ [kg/m <sup>3</sup> ]							
Month	N [-]	MEAN	STD	MIN	P05	P50	P95	MAX
Jan	7,440.0	1,008.3	1.2	1,006.5	1,006.8	1,008.1	1,010.7	1,013.8
Feb	6,768.0	1,008.2	1.2	1,006.6	1,007.1	1,007.8	1,010.7	1,014.3
Mar	7,440.0	1,007.8	0.7	1,006.6	1,007.0	1,007.6	1,009.0	1,011.9
Apr	7,200.0	1,007.5	0.6	1,006.2	1,006.7	1,007.4	1,008.7	1,010.1
May	7,440.0	1,007.0	0.6	1,005.7	1,006.3	1,006.9	1,008.4	1,010.1
Jun	7,198.0	1,006.6	0.7	1,005.3	1,005.7	1,006.5	1,007.7	1,008.9
Jul	7,439.0	1,006.5	1.1	1,004.5	1,005.1	1,006.4	1,008.8	1,011.3
Aug	7,440.0	1,006.5	1.0	1,004.2	1,005.0	1,006.4	1,008.3	1,011.0
Sept	7,198.0	1,006.5	1.1	1,005.1	1,005.4	1,006.1	1,009.3	1,011.5
Oct	7,439.0	1,007.2	1.1	1,005.5	1,005.9	1,006.9	1,009.4	1,011.3
Nov	7,200.0	1,007.8	1.1	1,005.9	1,006.6	1,007.5	1,009.9	1,012.1
Dec	7,428.0	1,008.5	1.6	1,006.3	1,006.7	1,008.0	1,011.8	1,013.8

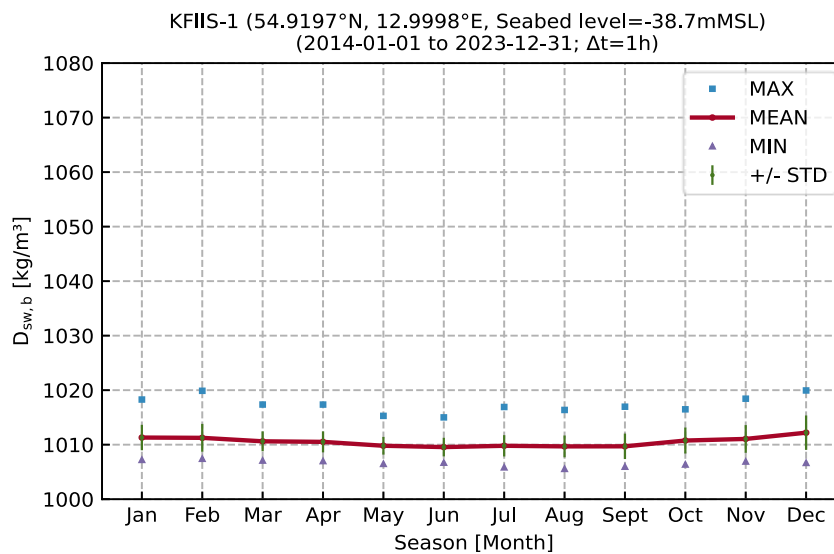


Figure 10-14 Plot of monthly statistics of  $D_{sw,b}$ , at KFIIS-1.

Table 10-15 Table with monthly statistics of  $D_{sw,b}$ , at KFIIS-1.

Season	$D_{sw,b}$ [kg/m <sup>3</sup> ]							
	Month	N [-]	MEAN	STD	MIN	P05	P50	P95
Jan	7,440.0	1,011.3	2.3	1,007.2	1,008.1	1,011.0	1,015.9	1,018.3
Feb	6,768.0	1,011.3	2.6	1,007.4	1,007.8	1,011.2	1,016.2	1,019.9
Mar	7,440.0	1,010.6	1.8	1,007.1	1,008.1	1,010.4	1,014.4	1,017.4
Apr	7,200.0	1,010.5	1.9	1,007.0	1,007.7	1,010.3	1,013.9	1,017.4
May	7,440.0	1,009.8	1.6	1,006.5	1,007.8	1,009.5	1,013.5	1,015.3
Jun	7,198.0	1,009.6	1.7	1,006.7	1,007.1	1,009.4	1,012.8	1,015.0
Jul	7,439.0	1,009.8	2.0	1,005.8	1,007.3	1,009.3	1,014.0	1,016.9
Aug	7,440.0	1,009.7	2.0	1,005.6	1,007.3	1,009.3	1,013.9	1,016.4
Sept	7,198.0	1,009.7	2.3	1,006.0	1,007.0	1,009.0	1,014.5	1,017.0
Oct	7,439.0	1,010.8	2.4	1,006.4	1,006.9	1,010.5	1,015.0	1,016.5
Nov	7,200.0	1,011.1	2.5	1,006.9	1,007.4	1,010.8	1,016.0	1,018.4
Dec	7,428.0	1,012.2	3.2	1,006.7	1,007.7	1,011.6	1,018.0	1,019.9

## 10.4 Marine growth

Marine growth, also known as biofouling, refers to the growth or establishment of marine organisms, such as algae, marine animals, and bacteria, on submerged surfaces like piers, buoys, ship hulls, and offshore structures. It is crucial to consider marine growth on offshore structures, like wind farms, to minimize its impact on the hydrodynamic efficiency and structural integrity of these structures [8].

The composition and structure of marine growth vary depending on various physical and environmental factors, including temperature, salinity, currents, wave exposure, and food availability [9]. These factors play a significant role in shaping the community and abundance of species inhabiting these structures,



resulting in geographical variations in species composition and biomass. For example, protected structures tend to have more seaweed and kelp, while turbid environments favor mussels. The colonization of marine structures typically occurs over a relatively short period of 2 to 3 years, with a succession of species, where early colonizers are eventually replaced by others [10].

In the western Baltic Sea, where Kriegers Flak II is situated, there is an increase in the number of marine species compared to the rest of the Baltic Sea, due to increased salinity. Previous investigations have documented 90 different benthos species in this area, with crustaceans and mussels being the dominating taxa [11]. However, species richness is still lower than in fully marine nearby areas, for example in Kattegat. The specific composition and density of marine growth near Kriegers Flak II is not extensively studied, but investigations in other areas of the Baltic Sea have provided valuable insights. These investigations have shown that mussels, barnacles, other crustacean species, large seaweed, and kelp are the dominant groups colonizing these structures [12, 13]. For instance, after the establishment of a wind park in Fehmarn Belt (Nysted, Denmark), mussels and barnacles were the main colonizers on the vertical structures, accompanied by other crustaceans and algae. *Mytilus edulis* and *Balanus spp.* were the most abundant and contributed significantly to the biomass, with biomass decreasing in deeper layers.

Similarly, in a study conducted at Darss Sill, it was found that mussels, mainly *Mytilus edulis*, and crustaceans, mainly *Balanus spp.*, were the dominant species in terms of abundance and biomass on established test structures at depths ranging from 4 to 20 meters [13]. After 143 days of exposure, *Mytilus edulis* had obtained a biomass ranging from 1.7 to 22.3 g afdw/m<sup>2</sup>, while *Balanus spp.* had a biomass ranging from 8.8 to 146 g afdw/m<sup>2</sup>, with the biomass continuing to increase by day 246 and 470. The study also observed a decrease in the abundance and biomass of marine growth in deeper layers, indicating vertical differentiation. The colonization of these structures followed a succession pattern, where barnacles, initially dominant, were subsequently replaced by mussels.

Kriegers Flak II is located in close proximity to the previously mentioned sites in the western Baltic, with similar salinity and temperature regimes. Furthermore, considering the direction and intensity of prevalent currents in this area, it is expected that there would be a similar composition of species and colonization history between the above mentioned sites and Kriegers Flak II. The dominant species in terms of abundance and biomass in marine growth are expected to be mussels, barnacles, other crustacean species, and algae. *Mytilus edulis* and *Balanus spp.* are prevalent in this area and, given their life-history patterns and colonization ability [14, 15], they are expected to be the primary colonizers on new structures established in Kriegers Flak II, constituting the majority of the biomass.

The thickness of marine growth also depends on project specific conditions such as the position of the structural component relative to the sea level, the orientation of the component relative to the sea level and relative to the dominant current, the age of the component, and the maintenance strategy for the component, apart from salinity, oxygen content, pH value, current and temperature (DNV-ST-0437:2024-05).

A marine growth density of 1325 kg/m<sup>3</sup> and a marine growth thickness of 100 mm from the seafloor to -2 mMSL is recommended in DNV-ST-0437:2024-05 for the central North Sea and the Baltic Sea.

Since project specific conditions, and composition and biomass data for the KFII area, are not available, and since data from the North Sea and Baltic Sea does not indicate otherwise, it is recommended to use an standard (DNV-ST-0437:2024-05) density of 1325 kg/m<sup>3</sup> and a marine growth thickness of 100 mm from the seafloor to -2 mMSL.

## 11 Bibliography

- [1] Sweco/Deltares, "41011329A\_KFII\_PartA\_Measurements\_and\_Hindcast\_Data\_Basis," 2024.
- [2] DMI, Storms in Denmark since 1981, March 4th, 2024.
- [3] DMI, Stormens ABC, January 28th, 2022.
- [4] Kystdirektoratet, Højvandsstatistikker 2024, Kystdirektoratet, Miljøministeriet, 2024.
- [5] ECMWF, "ERA5," [Online]. Available: <https://cds.climate.copernicus.eu/cdsapp#!/dataset/reanalysis-era5-single-levels?tab=form>.
- [6] Sweco/Deltares, "41011328A\_KG-HS\_PartA\_Measurements\_and\_Hindcast\_Data\_Basis," 2024.
- [7] DMI, "Frie Data," [Online]. Available: <https://www.dmi.dk/frie-data/>.
- [8] W. Shi, H.-C. Park, J.-H. Baek, C.-W. Kim, Y.-C. Kim and H.-K. Shin, "Study on the marine growth effect on the dynamic response of offshore wind turbines," *International Journal of Precision Engineering and Manufacturing*, vol. 13, pp. 1167-1176, 2012.
- [9] E. C. O. Renewable, "Marine growth mapping and monitoring," 2016.
- [10] J. K. Petersen, E. Stenalt and W. B. Hansen, "Invertebrate re-colonisation in Mariager Fjord (Denmar) after severe hypoxia. II. Blue mussels (*Mytilus edulis* L.)," *Ophelia*, vol. 56, pp. 215-225, 2002.
- [11] M. Goggina, H. Nygård, M. Blomqvist, D. Daunys, A. B. Josefson, J. Kotta, A. Maximov, J. Warzocha, V. Yermakov, U. Gräwe and M. L. Zettler, "The Baltic Sea scale inventory of benthic faunal communities," pp. 1196-1213, 2016.
- [12] E. E. A/S, "Development of the fouling community of turbine foundations and scour protections in Nysted offshore wind farm, 2003," 2003.
- [13] M. L. Zettler and F. Pollehne, "The impact of wind engine constructions on benthic growth patterns in the western Baltic," in *Offshore wind energy: Research on environmental impacts*, 2006, pp. 201-222.
- [14] A.-L. Wrangé, C. André, T. Lundh, U. Lind, A. Blomberg and P. J. Jonsson, "Importance of plasticity and local adaptation for coping with changing salinity in coastal areas: a test case with barnacles in the Baltic Sea," *BMC Evolutionary Biology*, vol. 14, pp. 1-15, 2014.

- [15] P. Strelkov, M. Katolikova and R. Väinölä, "Temporal change of the Baltic Sea-North Sea blue mussel hybrid zone over two decades," *Marine Biology*, vol. 164, p. 214, 2017.

## Appendix A

A number of excel workbooks (and PDF versions of the workbooks) accompany this report. A list of these Data Reports and a brief description of their content is provided below. X in the list below denotes North or South and the reference location number 1-3.

- **Normal\_KFIIX-X**
  - Contains presentation of data for individual parameters of wind, waves, current and water level in the form figures and tables of timeseries, roses, statistics (monthly and directional) and probabilities for operational conditions.
- **Spectra\_KFIIX-X**
  - Contains a comparison between hindcast wave spectra and JONSWAP spectra (as defined in DNV-RP-C205:2021-09) a number of  $H_{m0}$  ranges.
- **Sensitivity\_KFIIX-X**
  - Contains presentation of sensitivity analyses of marginal EVA to determine the suitable distribution, threshold (POT), and fitting methods for individual parameters of waves, current and water level.
- **EVA\_KFIIX-X**
  - Contains presentation of marginal EVA results for individual parameters of waves, current and water level.
- **Scatter\_KFIIX**
  - Contains presentation of scatter diagrams and figures between various parameters such as: wind-waves (incl. misalignment and water level-waves).
- **Sea\_State\_KFIIX-X**
  - Contains a presentation of NSS, SSS and ESS.
- **Atmospheric\_KFII**
  - Contains a presentation of air temperature, humidity, solar radiation, and lightning.
- **Oceanographic\_KFIIX**
  - Contains a presentation of seawater temperature, salinity and density.
- **Oceanographic\_profile\_KFIIX-X**
  - Contains a presentation of current speed, seawater temperature, and salinity profiles across the water depth.

## Appendix B

This section presents a sensitivity analysis of marginal EVA to determine the suitable distribution, threshold (POT), and fitting methods for the setup of EVA. Statistical independence is ensured by the inter-event time, and identical distribution is ensured as only windsea components are present for waves, for water level and current these are completely dominated by the residual component thereby ensuring identical distribution.

The figures below show the sensitivity of the 50-year return period for the respective parameters against different events per year. On each figure, different common fitting methods (Maximum likelihood (MLE), Least-Squares (LS) and Method of Moments (MM)) have been used to fit different common long-term extreme value distributions (Weibull, Gumbel, Generalized Pareto and Frechet). More details on average relative error and the actual fits are presented in the appendices. The data and fits have been evaluated considering the visual fit, the average relative error and stability for the various distributions, thresholds (POT), and fitting methods.

Based on the approach outlined above, the selected EVA settings are as follows:

- Waves: 3-parameter Weibull distribution fitted with Least-Squares to the 44 peak events with an inter-event time of 72 hours.
- Water level (high): 3-parameter Weibull distribution fitted with Least-Squares to the 180 peak events with an inter-event time of 72 hours.
- Water level (low): 3-parameter Weibull distribution fitted with Least-Squares to the 45 peak events with an inter-event time of 72 hours.
- Current speed: 3-parameter Weibull distribution fitted with Least-Squares to the 45 peak events with an inter-event time of 72 hours.

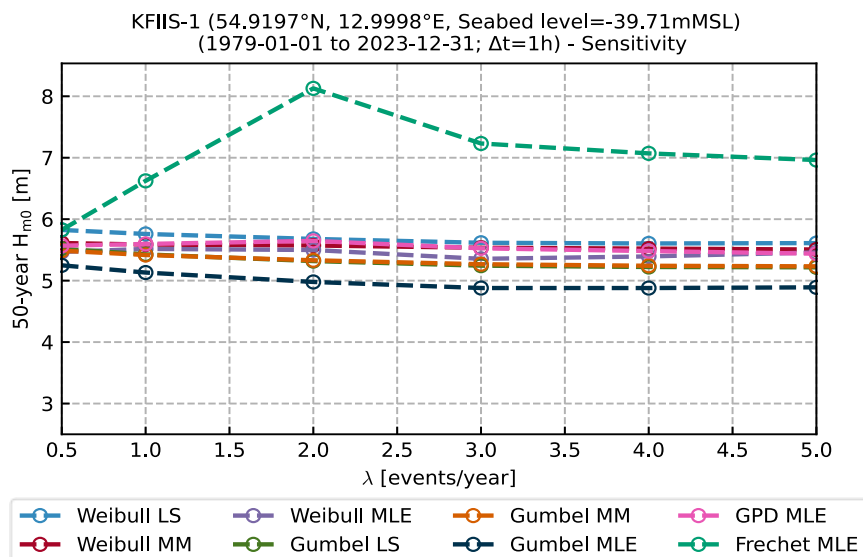


Figure 11-1 Sensitivity of 50 year marginal  $H_{m0}$  EVA to distribution, threshold, and fitting. Inter-event time 72h.

Together with our clients and the collective knowledge of our 22,000 architects, engineers and other specialists, we co-create solutions that address urbanisation, capture the power of digitalisation, and make our societies more sustainable.

Sweco – Transforming society together